IMMUNE CELL MIGRATION IN COMPLEX ENVIRONMENTS

Connie Shen

Department of Microbiology and Immunology

McGill University

Montréal, QC, Canada

August 2024

A thesis submitted to McGill University in partial fulfillment of the requirements of the degree of Doctor of Philosophy

TABLE OF CONTENTS

ABSTRACT

Cell migration is fundamental to immune responses, enabling leukocytes to traffic throughout the body, transmigrate out of vessels, and traverse diverse tissues with distinct architectures, topologies, and mechanical properties. How immune cells are able to navigate such a broad range of complex 3-dimensional (3D) microenvironments – from lymph nodes, to collagen-rich skin, or dense tumours – and the specific cytoskeletal processes that enable them to do so while keeping their cell integrity intact, remains incompletely understood. This work examines the cytoskeletal mechanisms that enable immune cell cohesion during migration and explores the role of nuclear structure.

We examine Dedicator of Cytokinesis 8 (Dock8), a gene associated with immunodeficiency when mutated. In the absence of Dock8, cells become entangled during migration through confined environments, leading to catastrophic cell rupturing, while their migration on 2D surfaces remains intact. We investigated the specific cytoskeletal defect of Dock8-deficient activated T cells, showing that even prior to entanglement they display a striking difference in actin distribution compared to wild type (WT) cells. We describe a central pool of F-actin in WT murine and human T cells which is absent in Dock8 KO T cells, and determine that this central F-actin pool is mechanoresponsive, emerging only when cells are very confined. Our works shows that the central actin pool is nucleo-protective, reducing nuclear deformation and DNA damage during confined migration. We identify the Hippo-pathway kinase MST1 as a co-mediator of this mechanosensitive pathway in conjunction with DOCK8, allowing for cell cohesion and survival during migration through complex environments.

Neutrophils, another immune cell type, have a naturally lobulated nuclear shape. These cells are among the fastest-moving immune cells, and their speed is critical to their function as 'first responder' cells at sites of damage or infection and it has been postulated that the neutrophils' unique segmented nucleus functions to assist their

rapid migration. We tested this hypothesis by imaging primary human neutrophils traversing narrow channels using custom-designed microfluidic devices. Individuals were given intravenous low-dose endotoxin to elicit the recruitment of neutrophils into the blood with a high diversity of nuclear phenotypes, ranging from hypo- to hyper-segmented. Both by sorting on neutrophils from the blood using markers that correlate with lobularity, and by directly quantifying the migration of neutrophils with distinct lobe numbers, we found that neutrophils with 1-2 nuclear lobes were significantly slower to traverse narrower channels, compared to neutrophils with >2 nuclear lobes. Thus, our data show that in primary human neutrophils nuclear segmentation provides a speed advantage during migration through confined spaces.

Overall, this work describes critical cytoskeletal and nuclear mechanisms underpinning immune cell migration, providing insights into how these cells maintain integrity in confined environments. Furthermore, it highlights the heterogeneity amongst immune cell types in the regulation of migration, where immune cell differ in their form and function. We identified that where dendritic cells and T cells utilize a dock8-dependent method of mechanosensing during migration, this pathway was dispensable for neutrophils. Instead, neutrophils have a more flexible nucleus which confers greater ability to pass through small pores, and the mechanisms of cell integrity maintenance for these cell may differ. These findings underscore the diverse strategies employed by immune cells to migrate effectively, providing novel insights into the regulation of immune cell migration.

RÉSUMÉ

Migration des cellules immunitaires dans des environnements complexes

La migration cellulaire est fondamentale pour les réponses immunitaires. Elle permet aux leucocytes de circuler dans tout le corps, de transmigrer hors des vaisseaux, et de traverser divers tissus aux architectures, topologies et propriétés mécaniques distinctes. La manière dont les cellules immunitaires parviennent à naviguer dans une si grande variété de microenvironnements tridimensionnels (3D) complexes, par exemple des ganglions lymphatiques à la peau riche en collagène ou aux tumeurs denses, et les éléments du cytosquelette qui leur permettent de le faire, tout en conservant leur intégrité cellulaire, restent encore mal compris à ce jour. Cette thèse examine les mécanismes dépendant du cytosquelette qui permettent la cohésion des cellules immunitaires pendant leur migration et explore le rôle de la structure du noyau dans ce processus.

Ici nous étudions le gène Dedicator of Cytokinesis 8 (Dock8), associé à une immunodéficience lorsqu'il est dysfonctionnel. En l'absence de Dock8, les cellules immunitaires migrant en 3D sous confinement s'emmêlent pendant leur migration, ce qui conduit à une rupture cellulaire catastrophique, alors que les cellules migrant sur des surfaces en 2D restent intactes. Les cellules T activées déficientes en Dock8 présentent une différence frappante dans la distribution de leur actine filamenteuse (actine-F) par rapport aux cellules de type sauvage (WT), même avant leur l'enchevêtrement, un phénomène que nous avons investigué en détail. Nous décrivons l'existence d'un pool central d'actine-F dans les cellules T murines et humaines WT, absent dans les cellules T déficientes en Dock8, et démontrons que ce pool central d'actine-F est mécanosensible et qu'il apparaît que lorsque les cellules sont en milieux confinées. Nos travaux montrent que le pool central d'actine-F est nucléoprotecteur, réduisant la déformation nucléaire et les dommages à l'ADN intervenant pendant la migration sous confinement. Nous identifions la kinase MST1 de la voie Hippo comme co-médiateur de cette voie mécanosensible, en conjonction avec DOCK8, permettant

la cohésion et la survie des cellules pendant la migration dans des environnements complexes.

Les neutrophiles, un autre type de cellules immunitaires, ont un noyau naturellement lobulé. Ces cellules sont parmi les cellules immunitaires les plus rapides, et leur vitesse élevée est essentielle à leur fonction de premiers répondants sur les sites inflammatoires. Il a été postulé que la segmentation unique de leur noyau facilite leur migration rapide. Nous avons testé cette hypothèse en imageant la migration de neutrophiles humains primaires traversant des microcanaux conçus à l'aide méthodes de microfluidiques. Des individus ont reçu une faible dose intraveineuse d'endotoxine pour induire la mobilisation de neutrophiles dans le sang possédant une grande diversité de phénotypes nucléaires, allant de l'hypo- à l'hyper-segmentation. Tant par l'analyse différentielle des neutrophiles du sang à l'aide de marqueurs corrélant avec leur lobularité, que par la quantification directe de leur nombre de lobes, nous avons constaté que les neutrophiles avec 1 ou 2 lobes nucléaires étaient significativement plus lents à traverser des canaux étroits, par rapport aux neutrophiles avec 3 lobes nucléaires ou plus. Ainsi, nos données montrent que chez les neutrophiles humains primaires, la segmentation nucléaire confère un avantage de vitesse pendant la migration à travers des espaces confinés.

Dans l'ensemble, ces travaux décrivent des mécanismes dépendant du cytosquelette et du noyau qui soutiennent et régulent la migration des cellules immunitaires, fournissant des informations sur la manière dont ces cellules maintiennent leur intégrité dans des environnements confinés. En outre, ils mettent en lumière l'hétérogénéité entre les types de cellules immunitaires dans la régulation de leur migration, où les cellules immunitaires diffèrent par leur forme et leur fonction. Nous avons identifié que les cellules dendritiques et les cellules T intègrent des signaux mécaniques, dépendamment de la présence de Dock8, au contraire des neutrophiles qui ne se servent pas de ce mécanisme. Au lieu de cela, ces derniers utilisent un noyau plus flexible, ce qui leur confère une plus grande capacité à passer par de petits pores. Les mécanismes de maintien de l'intégrité cellulaire pour ces cellules peuvent donc

différer. Ces découvertes soulignent les diverses stratégies employées par les cellules immunitaires pour migrer efficacement, offrant de nouvelles perspectives sur la régulation de la migration des cellules immunitaires.

ACKNOWLEDGEMENTS

I spent much of the last few years in a dark place— the microscope room. Sometimes, surrounded by only the soft whir of the lasers, the rhythmic hum of mechanical motors, and a single unabashedly bright screen, the room would start to feel otherworldly. I am grateful to have experienced the joy of losing myself in those moments when the outside world would fade from consciousness and I would simply revel in discovery. Science has proven to be massively laborious and laden with failures, but it's those moments that have made this entire undertaking worthwhile.

Judith, thank you for making those experiences possible. You believed in me before the idea even crossed my mind. Years ago, when you pitched to me a PhD, knowing how to make a hard sell, you promised that science was an opportunity to see the world. Now reporting from the other side, this degree has brought me views of the world from both 10,000 meters up and at 1 micron across. Thank you for giving me the space to find my own scientific path, while never leaving me stranded and alone. Your enthusiasm for science is infectious (pun intended).

To my lab mates past and present, official and honorary, you are the ones who have made this journey memorable. Thank you for all the hearty laughs, endless coffee breaks, and general tomfoolery that carried me through even the longest of experiment days.

To my family, thank you for providing me with infinite support and whimsy. I am deeply appreciative of the sacrifices you have made to bring me to where I am today.

Finally, Tanner, it is hard to believe that it has been a decade since we first met. Sitting outside Molson Hall together as freshmen, neither of us could have imagined just how deeply Montreal would shape our lives. Four degrees, two cats, one pandemic, and one wedding later– we are finally moving on to our next chapter. Thank you for sticking by my side through it all.

RESEARCH PUBLICATIONS

This is a manuscript-based thesis. The works presented here is or will be published as detailed below. Unpublished chapters may change based on revisions for publication.

Chapter 2

C Shen, E Mulder, W Buitenwerf, J Postat, A Jansen, M Kox, JN Mandl, N Vrisekoop. "**Nuclear segmentation facilitates neutrophil migration**". *Journal of Cell Science*, 2023. (*1*)

https://doi.org/10.1242/jcs.260768

Chapter 3

The data presented in this chapter are from an unpublished manuscript; pre-print of this manuscript can be found on BioRxiv.

C Shen, J Postat, A Cerf, A Bhagrath, D Rogers, M Merino, D Patel, V Luo, C Schneider, A Sharma, W-K Suh, JN Mandl. "**DOCK8 regulates mechanosensitive actin redistribution that maintains cell cohesion and protects the nucleus during T cell migration**." *BioRxiv*, 2024. (*2*)

https://doi.org/10.1101/2024.07.26.605273.

Other research contributions

Manuscripts I have contributed to but are not included in this thesis:

J Postat, A Bhagrath, C Shen, J Brodbeck, PT Bahnamiri, A Cerf, D Rogers, T Jeyakumar, AR Mingarelli, C Schneider, J Textor, A Sharma, A Ehrlicher, R Sharif-Naeni, JN Mandl. "**Stiffness sensing by T cells promotes tissue-resident memory T cell differentiation**." *In Revision.*

VM Luo, C Shen, S Worme, A Bhagrath, E Simo-Cheyou, S Findlay, S Hebert, WL Poon, T Zhang, R Zahedi, J Boulais, C Borchers, J-F Cote, C Kleinman, JN Mandl, A Orthwein. "**The deubiquitylase Otub1 regulates the chemotactic response of splenic B cells by modulating the stability of the γ-subunit Gng2**" *Molecular and Cellular Biology*, 2023. (*3*)

D Rogers, A Sood, H Wang, JJP van Beek, TJ Rademaker, P Artusa, C Schneider, C Shen, DC Wong, A Bhagrath, M-È Lebel, SA Condotta, MJ Richer, AJ Martins, JS Tsang, LB Barreiro, P François, D Langlais, HJ Melichar, J Textor, JN Mandl. "**Pre-existing chromatin accessibility and gene expression differences among naive CD4+ T cells influence effector potential**." *Cell Reports*, 2021. (*4*)

C Schneider, C Shen, A Gopal, T Douglas, B Forestell, K Kauffmann, P Artusa, D Rogers, Q Zhang, H Jing, DL Barber, M Saleh, P Wiseman, H Su, J N Mandl. "**Migration-induced cell shattering due to DOCK8-deficiency causes a type-2 biased helper T cell response**." *Nature Immunology*, 2020. (*5*)

AA Tong, B Forestell, DV Murphy, A Nair, F Allen, J Myers, F Klauschen, C Shen, AA Gopal, AY Huang, JN Mandl. "**Regulatory T cells differ from conventional CD4 + T cells in their recirculatory behavior and lymph node transit times**." *Immunology & Cell Biology*, 2019. (*6*)

CONTRIBUTION OF AUTHORS

Chapter 2

The project idea for the work in Chapter 2 was conceived by J.N.M and N.V. I performed most of the experiments and analysis with critical help from E.M and W.B at the University Medical Center Utrecht. A.J and M.K at the Radboud University Medical Center coordinated the clinical samples from the human endotoxemia trial. J.P designed the microfluidic devices. Manuscript figures were put together by myself and J.N.M. The manuscript was written by J.N.M and myself, with all authors contributing and providing feedback.

Chapter 3

J.N.M. conceived and supervised the project. J.N.M. and I designed the research. I performed most of the experiments with critical help from J.P., M.M., D.P., A.B., V.L., A.A., and C.S.. J.P. contributed the RNA sequencing experiment and analysis, and established the microfluidic assays. M.M. contributed the neutrophil migration data; A.C. performed the PCA analyses of cell shape parameters and generated the F-actin heatmap summaries. Data analysis was led by myself and J.P. with key contributions from A.C., M.M., D.P., and A.B.. At the McGill University Health Centre, A.S. coordinated the human ethics protocol with help from D.P. and oversaw the collection of human blood samples. Critical reagents and intellectual input were provided by V.L., A.A., W-K.S, A.S., A.E., and J-F.C. Manuscript figures were put together by myself, J.P., and J.N.M. The manuscript was written by J.N.M and I, with all authors contributing and providing feedback.

CONTRIBUTION TO ORIGINAL KNOWLEDGE

This work contributes to our understanding of how immune cells migrate through mechanically challenging environments.

Chapter 2

Prior to our study, the dogma was that neutrophils evolved a segmented nucleus to support their role as first responders to a site of infection. We provide experimental evidence for the long-held hypothesis that the uniquely lobulated neutrophil nucleus serves to facilitate migration through small pores, allowing for fast migration. We show this using a physiologically relevant model, a phenotypically heterogeneous population of human neutrophils.

Chapter 3

Prior to this study, we and others observed a loss of cell cohesion in Dock8-deficient T cells and BMDCs. In both murine and human T cells, we demonstrate a mechanosensitive function for Dock8 in mediating the production of a central actin structure that appears only under confinement. We further implicate Hippo pathway MST1 as a co-mediator of this mechanosensitive circuit. We find that this actin structure serves to protect the nucleus, as without it the nucleus becomes more deformed and accrues more DNA damage. This adds to the body of literature describing lymphocyte survival defects in Dock8-immunodeficiency.

LIST OF FIGURES

Chapter 3

Figure 1. Loss of cell cohesion and death of migrating *Dock8* KO T cells is collagen-density dependent.

Figure 2. *Dock8* KO T cells navigate simple environments and small constrictions with no impairment

Figure 3. Confinement-induced redistribution of F-actin is absent in *Dock8* KO T cells.

Figure 4. The confinement-induced central actin pool is located at the nucleus front in migrating human and murine T cells.

Figure 5. The DOCK8-dependent F-actin redistribution in migrating T cells is nucleo-protective.

Figure 6. Mst1 is required for the nucleo-protective central actin pool during migration.

Figure S1. *Dock8* KO T cells are chemotactic but lose cell cohesion in collagen matrices

Figure S2. Perturbed nuclei of entangled *Dock8* KO T cells are stretched but do not rupture

Figure S3. *Dock8* KO T cells display normal cell cytoskeleton, organelle organization, total F-actin, and cell division under confinement.

Figure S4. Confinement-dependent central actin pool is present in dendritic cells, but not in entanglement-resistant neutrophils

LIST OF ABBREVIATIONS

ADP	adenosine diphosphate
APC	antigen-presenting cell
ARHGEF	Rho/Rac guanine nucleotide exchange factor
Arp2/3	actin-related protein 2/3
ATP	adenosine triphosphate
BMDC	bone marrow-derived dendritic cell
CCL	C-C motif chemokine ligand
CCR	C-C chemokine receptor
CD	cluster of differentiation
CDC42	cell division cycle 42
cPLA2	cytosolic phospholipase A2
CXCL	C-X-C chemokine ligand
CXCR	C-X-C chemokine receptor
DC	dendritic cell
DOCK	dedicator of cytokinesis
ECM	extracellular matrix
ERM	ezrin, radixin, moesin
F-actin	filamentous actin
FRC	fibroblastic reticular cell
fMLF	N-Formylmethionine-leucyl-phenylalanine
G-actin	globular actin
GDP	guanosine diphosphate
GEF	guanine exchange factor
GM-CSF	granulocyte-macrophage colony-stimulating factor
GPCR	G protein-coupled receptor

GTP	guanosine triphosphate
HEV	high endothelial venule
ICAM	intracellular adhesion molecule
IL	interleukin
IS	immunological synapse
KO	knockout
LBR	lamin B receptor
LFA	lymphocyte function-associated antigen
LINC	linker of nucleoskeleton and cytoskeleton
LPS	lipopolysaccharide
MHC	major histocompatibility complex
MLC	myosin light chain
MST	mammalian STE20-like protein kinase
MTOC	microtubule organizing center
NF-κB	nuclear factor kappa B
NK	natural killer
NKT	natural killer T cell
NPC	nuclear pore complex
PAK	p21-activated kinase
PDMS	polydimethylsiloxane
PI3K	phosphatidylinositol 3-kinase
PIP_2	phosphatidylinositol 4,5-bisphosphate
PIP_3	phosphatidylinositol 3,4,5-triphosphate
RHO	Ras homology
ROCK	Rho-associated kinase
ROS	reactive oxygen species

S1P	sphingosine-1-phosphate
SLO	secondary lymphoid organ
TAZ	transcriptional co-activator with PDZ-binding motif
T_{CM}	central memory T cell
TCR	T cell receptor
T_{EM}	effector memory T cell
TEM	transendothelial migration
TIRF	total internal reflection fluorescence
T_{RM}	tissue-resident memory T cell
VCAM	vascular cell adhesion protein
WASP	Wiskott-Aldrich syndrome protein
WAVE	WASP-family verprolin-homologous protein
WIP	Wiskott-Aldrich syndrome protein-interacting protein
WT	wildtype
YAP	yes-associated protein

CHAPTER 1: INTRODUCTION

1.1 SCOPE

And you may ask yourself, "Well, how did I get here?"

—Talking Heads, *Once in a Lifetime*

The crux of this thesis is: *How do immune cells get anywhere?*

It is a simple question, but it is one that has changed my entire view of the immune system. I spent three years obtaining an undergraduate degree in immunology prior to this research. A standard course in immunology alludes to the importance of cell migration, but leaves much of the inner workings to the imagination. Immune cell migration is hidden in descriptions of 'trafficking' or 'recruitment' or 'patrolling'. I more or less appreciated cells to be membranous spheres covered in receptors, the true stars of fundamental immunology. Not *another* Cluster of Differentiation, as the joke often goes.

At a surface level, how a cell gets anywhere is largely via chemoattractants (and aforementioned receptors). This is the level of understanding I started my graduate degree with. I was then presented with the question of why there were migration defects in Dock8 immunodeficiency. Chemotactically, these cells were fine. Their migration defect was much stranger– they would rip themselves apart and die. Suddenly, I found myself trying to understand how cells could actually generate forward momentum, and the physical laws which governed their motion. Immune cells move by growing and building, akin to a human moving forward not by putting one foot in front of the other, but rather by disassembling the bones of the rear leg and re-attaching them to the front to produce a new leg[1]. And all this happens at an

[1] I acknowledge this is a grotesque analogy, but it illustrates how foreign these concepts were to me at the time.

incredible speed. In time, I did come to understand not only how the cell cytoskeleton generates motion, but also how effective motion relies on immune cells sensing their environment to move properly, especially when the environment is challenging. I tell the story of what we learned from studying Dock8-deficiency in Chapter 3. While observing the migration defects of Dock8-deficient T cells, we would occasionally marvel at their incredibly stretched nuclei. Typically, the nucleus of a cell is relatively rigid and large. When cells migrate, lugging around this bulky organelle can be cumbersome. Neutrophils bypass this problem by having a nucleus that is segmented and flexible. In Chapter 2, we examine exactly how their unique nuclei impacts their migration. Throughout this thesis, I focus on the immune cells I have spent most of my time studying: neutrophils, T cells, and for comparison's sake, dendritic cells.

Chapter 1 is a literature review encompassing the fundamentals of cell migration as well as emerging concepts arising over the time in which this research took place. Chapter 1.2 provides an overview of the general principles and biomechanics which underlie cell migration. Chapter 1.3 outlines the role of locomotion in the life course of various immune cells and the immunodeficiencies arising from dysregulated motility. Chapter 1.4 highlights our rapidly expanding understanding of immune cell mechanosensing and how it drives immune cell migration and function.

Chapter 2 asks how migration is constrained by the physical properties of a cell. Specifically, we test the hypothesis that the lobulated nuclear morphology of the neutrophil nucleus facilitates rapid migration through small constrictions. Using a phenotypically heterogeneous population of human neutrophils released upon endotoxin administration, we show that greater nuclear lobulation confers a greater ability to pass through narrow channels. Furthermore, we demonstrate that the greater migration capacity of neutrophils is more strongly correlated to nuclear phenotype, rather than functional subtype.

Chapter 3 investigates how immune cells integrate mechanical information about the environment into effective locomotion. Studying Dock8-deficiency, we describe a

novel circuit employed by T cells to integrate information about the environment and protect the nucleus while migrating through challenging terrain. Specifically, we find that Dock8 is required for T cells to produce a mechanosensitive actin structure at the mid-body of the cell. We further implicate Mst1 in this pathway that maintains cellular and nuclear cohesion during three-dimensional migration.

This thesis concludes with Chapter 4, which is a discussion of the findings from Chapters 2 and 3 placed into the greater context of immune cell migration and mechanosensing research. I will highlight some avenues for further investigation arising from our research and the questions outstanding in this field.

Through the ups and downs of research, I now appreciate the dynamism of immune cell migration. The immune system at its core is really just a motley crew of roaming cells, not contained but omnipresent and ever-changing, for better or for worse. This thesis is my answer to the opening question and my small contribution to it.

1.2 PHYSICAL BASIS OF MIGRATION

Cellular movement is the bedrock of the immune system. Where there is no cell movement, there is no immunity. Uniquely, immune cells possess the ability to enter and traverse nearly any tissue in the body. Immune cells are intrepid explorers, adept at navigating the diverse and challenging landscapes of the body. Just as an explorer would traverse various terrains, from bustling cities, to remote mountains, and dense forests; immune cells migrate through an array of bodily environments, including cell-rich lymph nodes, collagen-rich skin, and dense tumors, adapting to different conditions and overcoming obstacles to reach their destinations. Immune cells each have a distinct form and function, and differentially utilize a shared set of cytoskeletal machinery to produce forward motion. In this section, I will provide an overview of the main molecular players of the cytoskeleton and explain how they work in concert to produce motility.

THE CYTOSKELETON & FORCE GENERATION

The cell's cytoskeleton determines its shape and structure, but also drives cellular function and motion. The cytoskeleton is comprised of three main polymers: actin, microtubules, and intermediate filaments. In this section, I describe the dynamics and regulation of each of these polymers individually and highlight their role in cell movement.

ACTIN

Actin is the workhorse of cell migration. The ancestral gene encoding for actin was present in a common ancestor nearly 3 billion years ago (*7*). Actin-dependent motility, common to a diverse range of eukaryotic organisms, is driven by polymer network dynamics (*8*). Evolved alongside actin are over 100 accessory proteins that modulate actin filament dynamics such as polymerization, assembly, crosslinking, capping, and severing (*7*). Actin filaments are highly dynamic, with an average half-life of just one minute (*9*). Together, hundreds of actin regulators integrate intracellular and

extracellular signals to mediate the structure of the actin network at any given moment.

The building block of all actin structures is the actin monomer (G-actin), which must be assembled into actin filaments (F-actin), and then into higher-order structures such as bundles and networks. G-actin concentration in the cellular cytoplasm is in excess, though its distribution is not necessarily homogenous, but rather regulated and sequestered by a number of actin-binding proteins (*10*). G-actin monomers first form into dimers and trimers, the nucleation step, before polymerizing into filaments by the addition of monomers primarily to the plus end (barbed end). Rapid network growth requires actin nucleators, as spontaneously assembled dimers and trimers are highly unstable (*11*). Arp2/3, the first- and best-described actin nucleator, is a seven-protein complex that promotes actin nucleation on the sides of existing filaments at a characteristic 70° angle (*12*). The 1988 characterization of Arp2/3 by Pollard and colleagues led to the classic dendritic nucleation model of actin polymerization, which has since been greatly expanded upon (**Figure 1**). As actin filaments grow at the cell front, the filaments will physically push the cell membrane, thereby moving the cell forward (*11*). Besides Arp2/3, another major class of actin nucleators are formins. Formins are a family of proteins that nucleate actin tips for filament extension. There are the namesake formins (FMN1, FMN2), diaphanous formins (mDia1, mDia2, mDia3), formin-related proteins identified in FMNL1, FMNL2, FMNL3), formin homology domain-containing proteins (FHOD1, FHOD2), among others– totaling 15 formin proteins identified in vertebrates (*13*). Associating with barbed ends of actin filaments, formins act as both nucleation and elongation factors, and emerging research suggests that some may possess an even greater range of activities beyond actin assembly (*14*). Spire, a third class of actin nucleator, can bind the sides of existing filaments similar to Arp2/3, but do not result in a similarly branched network (*15*). Together, these three nucleators act to overcome the kinetically unfavourable first step of actin nucleation.

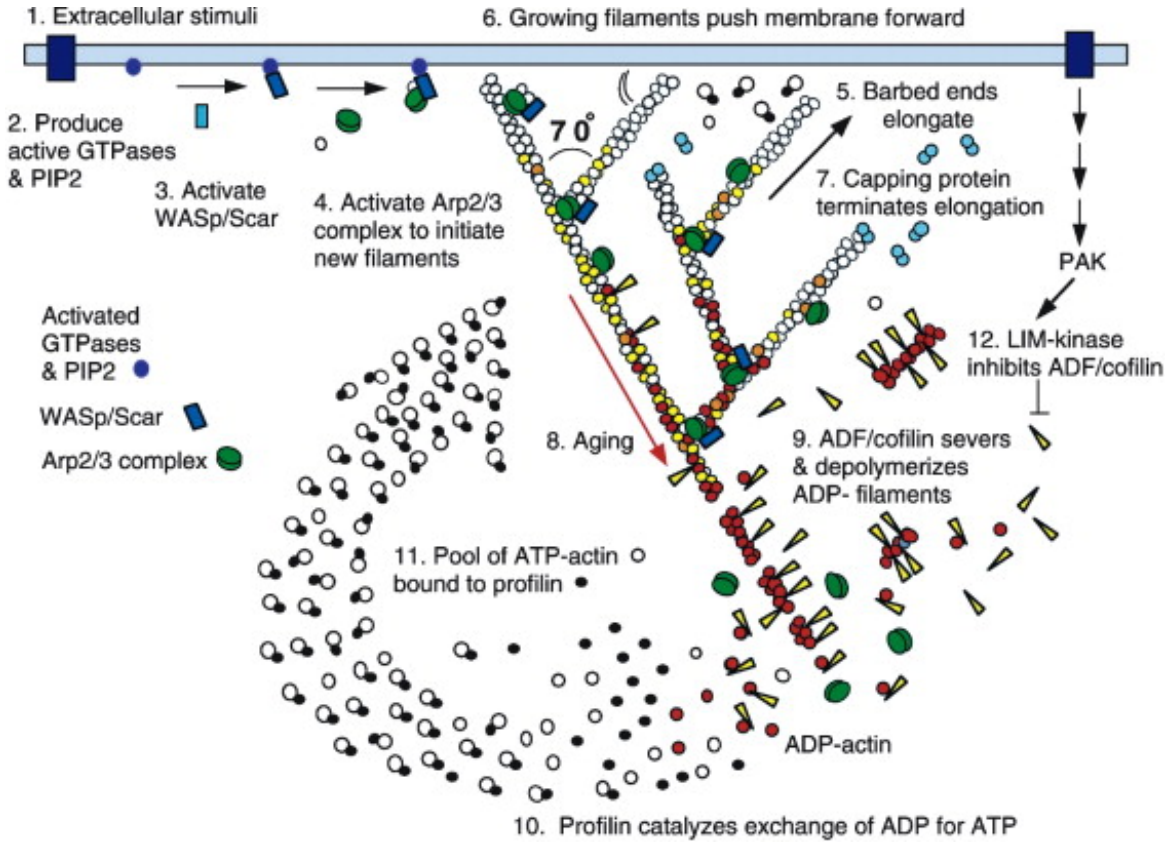

Figure 1. Model of actin force generation at the leading edge. This model represents an expanded view of the original dendritic nucleation model of actin polymerization proposed by Mullins, Heuser, and Pollard in 1988 (*12*). Extracellular signals activate receptors **(1)** that activate Rho-family GTPases (such as CDC42, Rac, and Rho) and PIP2 **(2)** which activate nucleation promoting factors such as WASP/Scar **(3)**. WASP/Scar proteins bring Arp2/3 and an actin monomer to a preexisting filament **(4)**. Barbed ends elongate **(5)**, which pushes forward the cell membrane **(6)**, until capping proteins terminate growth **(7)**. Actin filaments age by ATP hydrolysis **(8)**, and ADF-cofilin promotes the dissociation of ADP-actin **(9)**. Profilin catalyses ADP for ATP **(10)** to return subunits to the free actin pool **(11)**. Rho-family GTPases may also activate PAK and LIM kinases which phosphorylate cofilin to slow the turnover of filaments **(12)**. Adapted from (*11*).

Nucleators require help from nucleation promoting factors (NPFs) to become activated. NPFs, such as WASP and WAVE/Scar, bind both Arp2/3 and actin monomers to bring them together and activate Arp2/3. The binding of two NPFs to Arp2/3 will cause a conformational change that brings the complex to the side of a pre-existing mother filament to start a new branch. Profilin-actin favours elongation, so NPFs must compete for actin monomers, creating a balance within the cell of elongation- vs nucleation-competent monomers (*16*). NPFs are bound to the lipid membrane and activated upstream by GTPases.

Rho GTPases can switch between their inactive GDP-bound and active GTP-bound phases. The most well-described are CDC42, Rac, and Rho. In active conformation, Rho GTPases induce the polymerization of actin filaments. However, not all actin polymerization is the same, and different Rho GTPases were found to promote different cytoskeletal structures (*17*). In immune cells, CDC42 and its effector WASP mediate cell polarity and actin polymerization at the cell front. Rac1 and Rac2 via effectors PAK1 and WAVE/Scar, also promote actin polymerization at the cell front as well as the immunological synapse. RhoA and its effectors mDia1, ROCK1, and ROCK2, exert activity primarily at the cell rear, engaging with the actin cortex, myosin, microtubules, and intermediate filaments (*18*). The localized activation of the Rho GTPases is critical to directed cell migration, where Rac and CDC42 accumulate at front, and Rho at the back, creating a spatially distinct front-rear axis (*19*). Classical Rho GTPases are activated by GEFs which I discuss in greater detail in section 1.3.

Effective cell locomotion requires tight regulation of not only actin polymerization dynamics, but also turnover. Unencumbered, actin filaments continue to grow, pushing the membrane forwards until something terminates the process. Capping proteins terminate growth. Filament capping is an important process for leading edge dynamics to keep filaments short and with high branch density, which is thought to provide the mechanical stiffness required for force generation at the membrane (*20*). Capping proteins regulate branching, and the loss of capping protein results in the

loss of lamellipodial structures and a switch to filopodial structures (*21*). Actin polymerization is an ATP-intensive process, as ATP-bound actin more readily polymerizes. Following filament assembly, ATP is hydrolyzed, leading to filament aging as ADP-actin is less stable. Actin depolymerizing factor (ADF)/cofilin binding to ADP-actin results in filament severing and full subunit disassociation. Profilin binds and catalyzes the ADP-ATP exchange on actin, recycling actin monomers for the process to begin anew (*11*). As a counter-regulatory mechanism, Rho family GTPases may also activate PAK and LIM kinases that can phosphorylate ADF/cofilin to slow actin filament turnover (**Figure 1**). The rate of actin polymerization and turnover has been directly linked to cell speed and persistence (*22*). This cycle is the physical basis for actin treadmilling, where the formation of new filaments at the front and disassembly of filaments in the rear creates a network that pushes forward.

Actin treadmilling at the cell front generates forward motion, however, other structures in addition to the lamellipodia are present. The edge of a cell typically consists of four protrusive structures: lamellipodia, filopodia, blebs, and invadopodia/podosomes (*23*). Lamellipodia are thin sheet-like regions at the leading edge described in the classic model of actin nucleation. Usually occupying about 2-4 μm at the cell front, lamellipodia are formed by a cross-linked F-actin array, mediated primarily by Arp2/3 and cofilin (*24*). Filopodia are sharp finger-like projections that contain parallel actin bundles. Bundling proteins such as fascin mediate the bundle formation. Invadopodia and podosomes are related actin-based protrusions of the plasma membrane. Invadosomes are specific to cancer cells, and have matrix-degrading capability. In contrast, podosomes are present in non-transformed cells, and exist on a much shorter time-scale (minutes, compared to hours for invadopodia) (*25*, *26*). Podosomes are comprised of branched actin and bundled actin mediated by actin-bundling proteins such as α-actinin, fascin, and T- and L-plastin (*27*). Finally, blebs occur when the plasma membrane detaches from the actin cortex, allowing the cytoplasm to flow into the space, pushing the membrane outwards. Actin filaments fill within the bleb to reform the actin cortex (*28*). Cortical actin below the plasma

membrane forms a non-aligned network connected by crosslinkers such as filamin (*29*). Leading edge dynamics are largely driven by actin, and the cell front is mostly free of microtubules, IFs, and membranous organelles (*24*). These various actin structures can be present in some combination at the leading edge of a migrating cell.

Leukocytes have many actin protrusions which facilitate their roles in immunity such as environmental exploration, antigen sampling, and phagocytosis. Pseudopodia are unique protrusions that are characteristic of migrating leukocytes. These actin-rich structures are actually comprised of thin lamellipodial sheets, dependent on Arp2/3. In three-dimensional migration, multiple sheets can interweave and form rosettes, giving pseudopods their dynamic and complex morphologies (*8*). Treatment of these cells with Arp2/3 inhibitor CK666 results in the collapse of pseudopods into long, tubular protrusions, but no loss of motility in 3D. Though they do migrate a bit slower without pseudopods in 3D, the pseudopods primarily serve to promote directional changes and environmental exploration (*8*). The lamellar sheets are driven by the WAVE complex, and the deletion of *Hem1*, a subunit of the WAVE complex, results in the loss of lamellipodia in favour of spiky filopodia (*30*). Actin protrusive forces must be regulated to promote either pseudopodial or filopodial structures. Leukocytes may also exhibit transient blebbing at the cell front during migration due to high contractility detaching the plasma membrane from the actin cortex. While immune cells have been shown to exhibit bleb-like protrusions *in vitro*, there is yet no evidence of their presence *in vivo* (*28*). Leading edge dynamics are highly fluid so the contribution of blebs to the more well-established lamellipodial protrusions remains to be confirmed, as these regimes may cooperate spatially or temporally.

The linkage of the actin cortex to the plasma membrane is important in cell shape and motility. Breakdown of the membrane-to-cortex attachment can lead to a loss of directed migration (*31*). This attachment is not uniform around a cell. Cortical actin varies in density, changing the local membrane tension and thus cellular protrusion dynamics and migration (*32*, *33*). Actin cortex architecture is regulated by actin filament length, where longer actin filaments form a thicker cortex and more rigid

network (*34*). Mechanical forces on the actin cortex will elicit rapid propagation of membrane tension across the cell, allowing for the integration of short local signals to coordinate cell-wide behaviours such as migration (*35*, *36*). Active migration doubles membrane tension, and this increase in tension is an important signal for localizing leading edge protrusion to the cell front (*37*). The actin cortex is anchored to the plasma membrane via ERM proteins. All three ERM proteins share a common domain mediating their association with the membrane and F-actin binding, though they differ in their specific expression patterns and function (*38*, *39*). Lymphocytes express two of the ERM proteins: ezrin and moesin (*40*). In T cells, ERM proteins are enriched in the rear (*41*). Increasing constitutively active ezrin in T cells boosts membrane tension which results in slower migration, and defective homing *in vivo* (*40*). Conversely, ERM-deficient T cells display impaired trafficking to lymphoid organs due to reduced entry across HEVs and defective S1P-mediated egress (*42*). Membrane tension and cortical actin must be linked for optimal migration.

Actin is one of the most abundant proteins in the cell, it is important in cellular motility and nearly every physical process. The actin cytoskeleton also facilitates phagocytic activity, immune synapse formation, and transmigration (**Figure 2**). There are even emerging roles for actin in the nucleus, where it has been implicated in nuclear architecture, DNA repair, and transcriptional control (*43*, *44*). Other regulators, such as inner nuclear envelope protein emerin, may enhance nuclear stiffness by promoting actin polymerization (*45*). Whether actin in the nucleus participates canonically in regulating nuclear shape or stiffness has remained elusive, but may be answered as further research into the nucleoskeleton is now possible due to recent technological advancements in visualizing nucleoplasmic processes (*46*, *47*). Ultimately, actin is the single cytoskeletal component that is present in nearly every physical aspect of cell function. Understanding its regulation and how it operates together with all the other cytoskeletal components is key to understanding how cells produce motility.

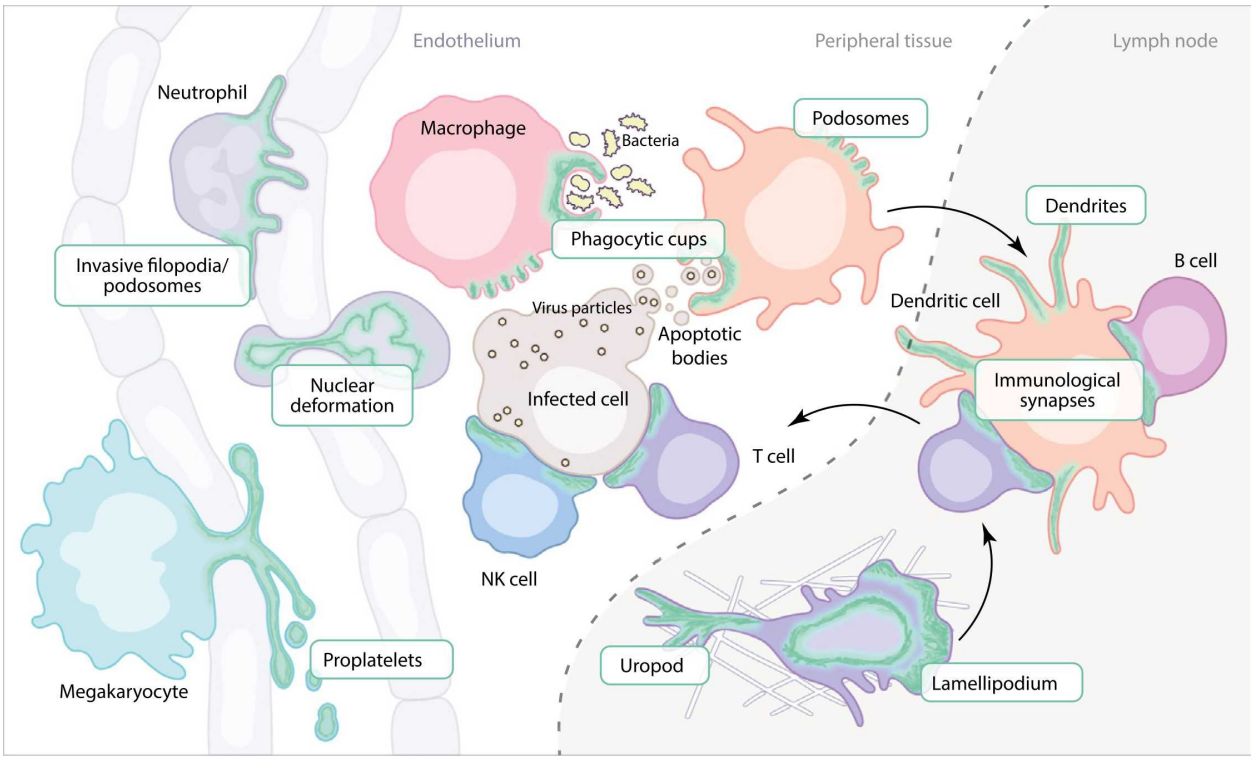

Figure 2. Actin-rich structures in immune cells. Actin structures are represented in green. Highlighted actin-based functions include in transendothelial migration, nuclear squeezing, podosomal structures, phagocytosis, immunological synapse formation, and migration. Adapted from (*48*).

MICROTUBULES

Microtubules carry out a wide range of cellular functions. Though they have been perhaps most well described in the context of cell division, they are also critically important to cell migration. Of the three main cytoskeletal filaments, microtubules are the widest and most rigid. Comprised of α- and ß-tubulin heterodimers, microtubules form a long hollow polymer tube of typically 13 linear protofilaments (*49*). These filaments are polarized into a plus and minus end. Another isoform, γ-tubulin, facilitates the nucleation of new actin filaments and is associated with the minus end of the microtubule filament. Uniquely amongst the cytoskeletal filaments, microtubules are centrally organized by a microtubule organizing center (MTOC). The canonical MTOC is the centrosome, comprised of a centriole pair and several other components, though other organelles and cellular structures can also serve as MTOCs (*50*). Microtubule filaments extend radially from the MTOC and can grow as long as the entire length of the cell. Broadly, the microtubule network is shaped by the intrinsic property of dynamic instability. Both α- and ß-tubulin subunits are bound to GTP, but only the ß-tubulin bound GTP is hydrolyzed, resulting in destabilization. Tubulin rapidly hydrolyzes GTP upon polymerization, so a microtubule filament is comprised primarily of GDP-tubulin, with only the tip of newly-bound dimers being GTP-bound to stabilize the entire filament (*51*). When the rate of GTP hydrolysis is greater than the addition of new subunits, catastrophe occurs. The term catastrophe refers to the rapid depolymerization and shrinking of a microtubule. True to the dramatic name of this phenomenon, the microtubule will continue to disassemble until the filament has been completely disassociated unless it is rescued (*52*). Thus, regulation of the microtubule network as a whole occurs primarily through proteins that promote catastrophe or rescue at the plus end of the filament. Another means of microtubule regulation is through post-translational modifications including detyrosination, acetylation, glutamylation, and glycylation (*53*). Acetylation increases microtubule stability and resilience to mechanical force (*54*). In migrating cells, the microtubule network becomes highly polarized, and microtubule stability is regulated through post-translational modifications and

microtubule-associated proteins (MAPs) to maintain the asymmetric spatial distribution of the network (*55*).

In immune cells, the microtubule network is a critical regulator of motility. In leukocytes, the microtubule networks are centrosome-anchored and relatively short and sparse, allowing for rapid reorientation (*56*). The centrosome-anchored MTOC in T cells is highly dynamic– it is located at the cell rear during migration and rapidly swings past the nucleus to anchor the immune synapse (*57*). Lymphocyte polarization induces a complete retraction of microtubules into the uropod (*41*). Compared to other cell types, immune cell microtubule density is far lower, and consequently, microtubules do not provide as much structural support (*50*). Instead, the primary role of microtubules in leukocytes is rather for locomotion, cell shape, and polarity maintenance. At the uropod, the microtubule network pushes the nucleus forward during migration (*57*). Nucleus-first configuration allows for pore-size discrimination. The MTOC is tethered to the rear of the nucleus, and long-reaching microtubules mediate the retraction of protrusions for productive decision-making and path-finding (*58*). Migrating DCs typically have multiple protrusions while exploring complex environments. The MTOC serves as the cellular structure which prescribes the cell path, and protrusion retraction is driven by microtubule catastrophe. Local microtubule collapse leads to the release of microtubule-bound RhoA GEF Lfc (murine homologue of ARHGEF2/GEF-H1), which triggers actomyosin contractility and full retraction of distal protrusions to mediate directional migration. Microtubule destabilization leads to DC migration that is uncoordinated, multipolar, and often leads to cell entanglement in complex environments (*59*). In amoeboid cells, the MTOC is typically located behind the nucleus, but MTOC positioning in neutrophils and DCs can be plastic depending on the context (*57*). For migrating leukocytes, microtubules are not necessary for the generation of movement, but are essential for cell cohesion and *directed* movement, particularly towards a chemoattractant.

INTERMEDIATE FILAMENTS

Intermediate filaments form complex networks in both the cytoplasm and nucleus of cells. Compared to actin filaments or microtubules, intermediate filaments have slower filament dynamics and very high tensile strength, making them resistant to compression, twisting, and bending forces. Of the major cytoskeletal polymers, intermediate filaments are distinct in several ways. Intermediate filaments are apolar and have no associated motor proteins (*60*, *61*). In humans, intermediate filaments are encoded by >70 genes, organized into 5 types: Types I and II are acidic and basic keratins respectively, and are found exclusively in the epithelium. Type III are variably expressed in various cell types and includes vimentin, desmin, GFAP, and peripherin. Type IV are primarily expressed in progenitors and neural cells, and includes neurofilaments, internexin, nestin, and synemin. Type V are ubiquitously expressed, and consists of the nuclear lamins (*62*). Filaments assemble as coiled homodimers that aggregate into mature filaments through a polymerization process that differs depending on the particular filament, though this process is not thought to require cofactors (*63*). In general, intermediate filaments have been more difficult to study due to a relative lack of small molecule inhibitors and redundancies in function. However, evidence suggests that intermediate filaments are critical to the mechanical integrity of cells, shape determination, cytoskeletal stability, and motility.

Vimentin is expressed in nearly all mesenchymal cells, especially during migration, and is one of the better-studied intermediate filaments. Most notably, vimentin expression is associated with high motility, where it promotes epithelial to mesenchymal transition, and higher expression is associated with higher cancer cell metastatic potential (*64*). To promote migration, the vimentin network must be positioned away from the leading edge, as its presence inhibits lamellipodial formation. Thus, vimentin assembly and disassembly is necessary to establish cell polarity. When a cell is not in motion, vimentin is present throughout the cytoplasm and appears to be a cell surface stabilizer that can promote mechanical resilience

(*65*). Vimentins contribute to the mechanical properties of the cell depending on the cell state. In mesenchymal cells, vimentin creates a filamentous perinuclear cage which protects the nucleus against deformation and rupture during migration (*66*). Vimentin is the only cytoplasmic intermediate filament in leukocytes, though its function in lowly-adhesive immune cells has been sparsely studied. In circulating T cells, vimentin forms a spherical cage that is the primary source of cellular rigidity (*67*). This is hypothesized to protect the circulating cell from damage by forces from fluid flow. Unlike in mesenchymal cells, vimentin in migrating leukocytes is localized to the uropod and does not form a perinuclear cage (*41*). Upon polarization, as with the microtubule network, the intermediate filaments also collapse into the uropod (*67*). Loss of vimentin in T cells leads to loss of integrin-β1, and accordingly less adhesion and diapedesis during TEM. This finding suggests a role of vimentin in dynamically anchoring and localizing surface adhesion molecules (*68*). Similarly, vimentin in DCs contributes to their stiffness. Vimentin-deficient DCs migrate slower, with less search efficiency, and less well to lymph nodes *in vivo* (*69*). In sum, vimentins provide mechanical protection for non-polarized cells and mediate polarization during leukocyte migration.

Nuclear lamins are a primary component of nuclear architecture, forming a dense ring at the edge of the nucleus. There are A-type and B-type lamins. A-type lamins are encoded by the *LMNA* gene and alternatively spliced into Lamin A and Lamin C isoforms. B-type lamins include Lamin B1 and Lamin B2, encoded by *LMNB1* and *LMNB2* respectively. All nucleated cells express B-type lamins, but expression of A-type lamins is profoundly asynchronous (*70*). Lamins form an interconnected meshwork under the nuclear envelope to provide structural support to the nucleus. Lamin A/C is a primary determinant of nuclear stiffness, whereas B-type lamins are negligible in this regard. Cells lacking Lamin A/C have reduced nuclear stiffness, more misshapen nuclei, and decreased viability under strain (*71*). Lamin B1 may contribute to stiffness in cells with low Lamin A/C. The mechanics of these lamins are different however, as Lamin A contributes to viscous resistance and Lamin B1 to

elastic resistance (*72*). Together, nuclear lamins and chromatin are the primary determinants of nuclear stiffness (*45*, *73*). Chromatin provides resistance against small deformations, whereas Lamin A resists larger nuclear deformations with a nuclear strain stiffening response (*74*). DNA is organized into heterochromatin and euchromatin. Euchromatin is easily accessible and transcriptionally active. Heterochromatin is tightly bound and transcriptionally silent. Compacted heterochromatin increases the nuclear stiffness and is typically anchored at the nuclear periphery (*75*). Nuclear lamins play a major role in spatial genome organization, primarily through Lamin Associated Domains (LADs), which can sequester genes at the lamina to silence them (*76*). LADS are organized and tethered to the lamina through Lamin B1, LBR, LEM proteins (LAP2, emerin, and MAN1) (*77*). Nuclear lamins in addition to being a major structural protein, also participate in signal transduction and genomic regulation. I'll expand further on the extra regulatory roles of lamin in Chapter 1.4.

The rigid nucleus is often a challenge in migration, as it is the largest and stiffest organelle. In leukocytes, elevated Lamin A will impede passage through small pores and motility in 3D collagen barriers (*78*, *79*). This may partly explain the relatively low levels of Lamin A present in granulocytes and lymphocytes, cells for which rapid migration is critically important for function. Neutrophils have uniquely lobulated nuclei, dependent on Lamin A/C and Lamin B1 downregulation alongside Lamin B2 and Lamin B receptor upregulation during maturation (*80*). T cells too, maintain low Lamin A/C levels, which only transiently upregulate during T cell activation to enhance actin polymerization and synaptic formation (*81*). An overly stiff nucleus will limit migration, but an overly soft nucleus will result in migration-induced stress and reduced survival (*82*). Failure to protect the nucleus can result in nuclear rupture or genomic damage (*83*, *84*). It has been shown that in both cancer cells and DCs, the nucleus does actually rupture during passage through constrictions. Nuclear envelope ruptures occurred at the tip, an area of low lamin and high nuclear pressure (*85*–*87*). Nuclear rupture results in the leakage of nuclear components into the

cytosol, exposing DNA to damage from nucleases, ROS, and cytosolic DNA sensors (*88*). Surprisingly, even repeated nuclear ruptures are not a death knell, and cells can repair the nuclear envelope with ESCRT-III machinery (*85*, *86*). Barrier-to-autointegration factor (BAF) recognizes chromatin exposed to the cytosol after nuclear envelope rupture, acting independently and upstream of ESCRT-III mediated membrane repair (*89*). *In vivo*, alveolar macrophages in the lung reside in a confined and mechanically active environment, and Lamin A/C is necessary to protect against nuclear envelope rupture and DNA damage (*90*). Even short of full nuclear rupture, deformation of the nucleus is sufficient to induce DNA damage (*91*). Lamins therefore are key regulators of nuclear mechanics during migration.

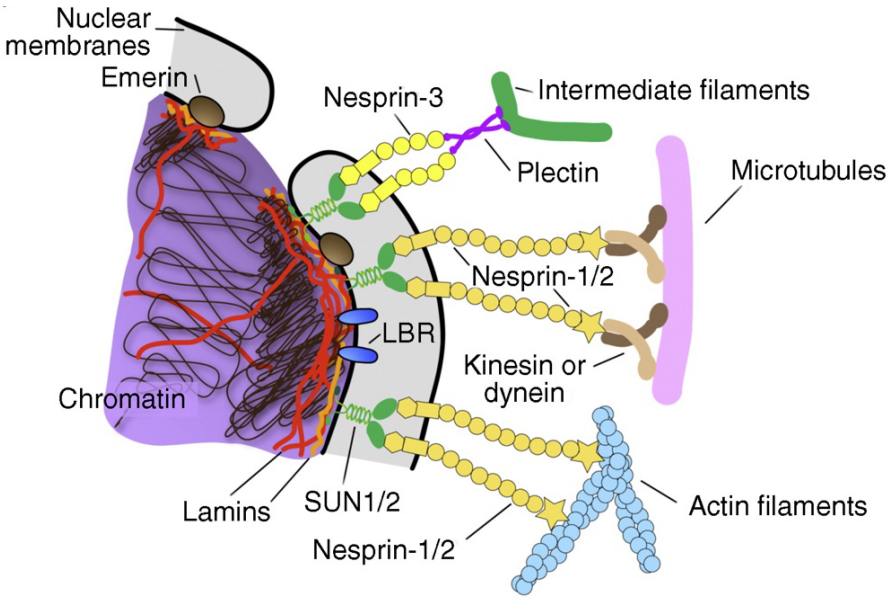

Figure 3. Structural proteins link the nucleus to the cytoskeleton. Lamins form a network beneath the nuclear membrane. LINC complex SUN proteins are embedded at the inner membrane and nesprin proteins at the outer membrane. SUN and nesprin proteins bind each other in the perinuclear space. Nesprins bind the cytoskeleton via plectins to intermediate filaments, kinesins or dyenins to microtubules, and direct interactions with actin. Chromatin is bound to the inner nuclear envelope through interaction with lamins, emerin, LBR, and SUN proteins. Adapted from (*45*).

CYTOSKELETAL CROSSTALK

Collectively, the cytoskeletal elements create a deeply entangled network. The three filaments have distinct physical properties that each contribute to cellular function. Actin filaments are the thinnest of the three, and microtubules are the thickest. Both of these filaments are relatively stiff and brittle, and exist on the timescale of seconds to minutes. In contrast, intermediate filaments, named such due to their intermediate size between actin and tubulin, are highly flexible and persist on the time scale of hours. Actin and intermediate filaments are generally considered to be the main determinants of cell stiffness, with vimentin contributing to cytoplasmic stiffness, and actin dominating cortical stiffness (*9*, *92*). Because the three networks are enmeshed, there can be unexpected emergent mechanical behaviour compared to what might be expected from the properties of isolated filaments. Intracellular microtubule networks are supported by both actin and intermediate filaments, which stabilize microtubule filaments from buckling (*93*). Conversely, microtubules are absolutely essential for intermediate filament organization, as intermediate filaments tend to follow and wrap around the microtubule network, a configuration that is dependent on kinesin-dependent transport of the intermediate filaments along the microtubule (*94*). Kinesin and dynein are microtubule-associated motors that move unidirectionally along the filament. Myosin is the main motor protein associated with actin. These motors allow cytoskeletal connections to be dynamically remodelled alongside migration. The cytoskeletal networks are also physically connected by passive cross-linkers such as plectins (*9*). High connectivity means dysregulation in one cytoskeletal component often influences the entire system.

Rho GTPases are master regulators of the cytoskeleton and possess the ability to modulate the activity of all three major cytoskeletal networks simultaneously. Rho GTPase activities have been mainly characterized with respect to actin regulation, though increasing data suggests their downstream signaling also regulates microtubules and intermediate filaments. For example, vimentin can be phosphorylated by ROCK, a downstream effector of Rho, a well-established mediator

of actomyosin contractility (*95*). Another Rho GTPase, Rac1, is highly active at the lamellipodia. Rac activity will stimulate actin polymerization via WAVE/Scar to form the lamellipodia. Rac activation will also stimulate the local disassembly of vimentin via phosphorylation to promote protrusive lamellipodia assembly (*65*). Microtubules at the leading edge can also actively drive lamellipodial protrusion via Rac activation (*96*). Together, these regulatory mechanisms form a unified feed-forward loop in the production of lamellipodia and front-rear polarity more generally.

The nucleus is tethered to the cytoskeletal network, primarily through the linker of nucleoskeleton and cytoskeleton (LINC) complex (**Figure 3**). The complex is comprised of SUN proteins (SUN1/2) in the inner membrane, and KASH (Nesprin-1/-2/-3) proteins in the outer membrane. SUN proteins are anchored to the nuclear interior primarily by lamins. Nesprins-1/2 bind F-actin directly, and microtubules indirectly through dyenins and kinesins. Nesprin-3 binds intermediate filaments via plectins. SUN and KASH proteins are bound to each other in the luminal space (*97*, *98*). The nuclear-cytoskeletal linkage is critical to facilitate migration in 3D. Disruption of the LINC complex can result in the collapse of protrusions and impaired migration in mesenchymal-type cells (*99*). The role of the LINC complex in migration and nuclear positioning of leukocytes is less clear. The nucleus in immune cells is located at the cell front, ahead of the centrosome, though precise positioning depends on the cell type (*100*, *101*). It has been proposed that a structural link exists between the nucleus and the centrosome (*102*). The LINC complex associates with a cloud of centrosomal F-actin that attaches the centrosome to the nucleus, and this pool is depleted during lymphocyte polarization allowing for centrosomal detachment for synaptic formation (*103*). During immune cell migration, nucleokinesis does not depend on microtubules, but primarily on actomyosin contractility, particularly to facilitate polarity switching during path-finding (*104*). The nucleus, and organelles more generally, are not free-floating in the cell, but are attached to the cytoskeletal network as a whole (*100*). Proper migration requires full coordination of the

cytoskeletal network and the organelles contained within. In Chapter 2, we examine how nuclear shape influences neutrophil motility.

MODES OF MIGRATION

The default mechanisms cells use to migrate have been classified into 'modes' of migration. The most well-described of these modes are the mesenchymal and amoeboid, which are prototypically represented by fibroblasts and immune cells respectively. In this section, I will describe the defining features of these two modes, and then discuss the plasticity between them.

MESENCHYMAL

Mesenchymal cell migration is the most-studied migration modality. Many of our most fundamental insights into the biomechanics of motion were gleaned from studying these cells. Mesenchymal migration proceeds in several steps which happen concurrently. First, leading edge extension occurs at the cell front facilitated by actin protrusions. Focal adhesions form at the leading edge. Stress fibers are anchored to the focal adhesions, and actomyosin forces contract the cell body. Finally, mature focal adhesions in the rear disassemble allowing for rear retraction and forward movement (*95*). These steps comprise the classical 2D stepwise migration model of protrusion, adhesion, and contraction. Mesenchymal cells migrating in 3D follow roughly the same steps, with the added function of proteolysis to digest and remodel ECM (*105*). Conventionally, mesenchymal cells position their nuclei in the rear with the centrosome in front to pull their nuclei forward (*98*). Numerous focal adhesions promote stability and allow mesenchymal cells to pull on the surrounding matrix (**Figure 4**). The adhesive and protrusive front results in a 'front-wheel drive' locomotion strategy. Mesenchymal migration is highly adhesive, adhesive, lowly contractile, and slow.

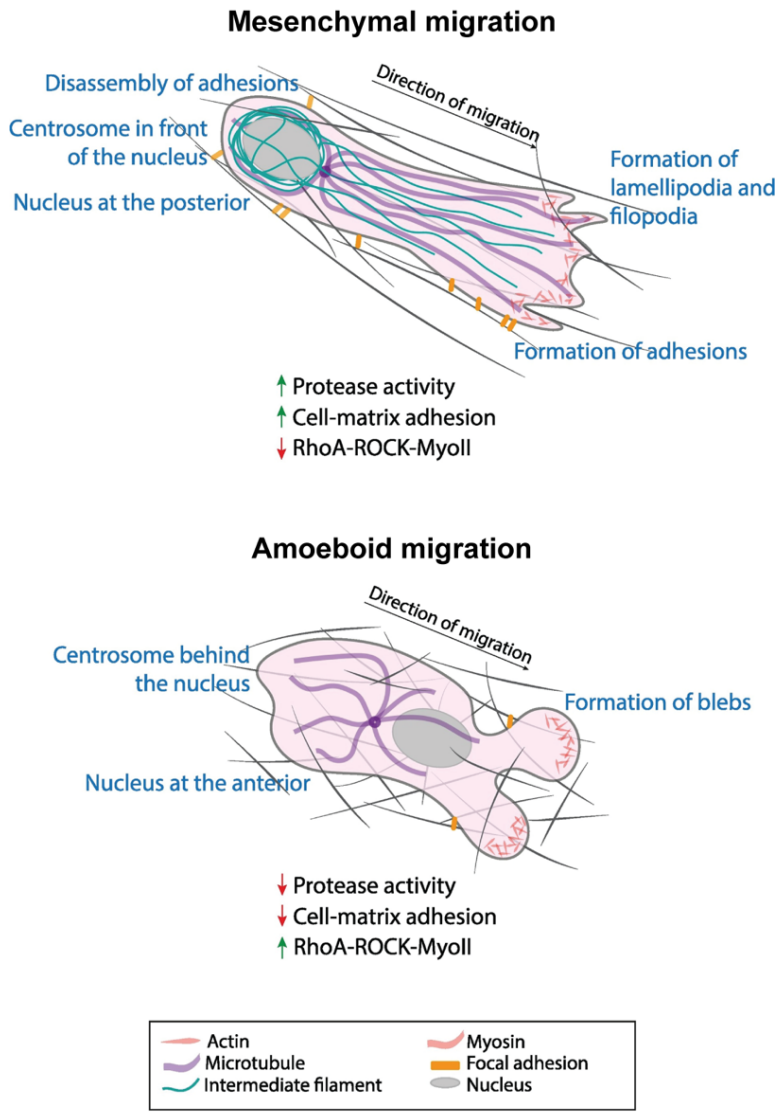

Figure 4. Spatial organization of mesenchymal and amoeboid migration modes. In mesenchymal migration, focal adhesions attach to the ECM and stress fibers, and the centrosome is positioned in front of the nucleus. In amoeboid migration, adhesions are minimal, and the nucleus is typically positioned ahead of the centrosome. Cells can switch between these modes depending on the environment. Adapted from (*95*).

AMOEBOID

Compared to mesenchymal cells, amoeboid moving cells can migrate nearly 100 times faster (*106*). Amoeboid cells completely lack mature focal adhesions and stress fibers. Instead, amoeboid migrating cells typically have low adhesion and adapt to the shape of the environment rather than digesting a path. Commonly, amoeboid cells have nuclei positioned at the front of the cell and in front of the centrosome (**Figure 4**). Also unlike mesenchymal cells, amoeboid cell migration strategies differ more in 2D and 3D (*105*).

In two-dimensional migration, the cell front of leukocytes is not bound to the surface but is rather a freely undulating lamellipodial structure in space (*8*, *30*). This is in direct contrast to the mesenchymal cells, where adhesions are strongest in the cell front and disassociate in the back. In immune cells, the leading edge is rich with chemoattractant (ex. fMLP, C5a, chemokine, LTB4, S1P, LPS) and surface (ex. TCR, FcR) receptors (*107*). The uropod is the site of an adhesive and contractile rear, containing MTOC, mitochondria, Golgi, ERM proteins, and mediators of extracellular interactions (ex.CD44, ICAM-1, ICAM-3, β1 integrins) (*107*). On 2D surfaces, integrin-mediated adhesion is absolutely essential for motility. Movement is generated by actin protrusion in the front and Myosin II contractility in the rear (*108*). Biomechanically, one of the largest distinctions between these two migration modes is reliance on adhesive structures. In three-dimensional migration, leukocytes can migrate absent all integrins and focal adhesions (*109*, *110*). Adhesion-free migration can achieved through frictional forces generated by cells pushing laterally against the environment (*111*, *112*). Even when adhesive structures are available, Myosin IIA activity modulates the level of binding. Loss of myosin IIA, the only class II myosin in T cells, results in diminished intra-lymph node migration and reduced trafficking due to over-adherence (*113*, *114*). The efficiency of amoeboid motility increases with actomyosin contractility and decreases with adhesive interactions.

Actomyosin contractility is a critical driver of amoeboid migration. Myosin motor proteins bind to actin filaments, generating force between filaments to produce

contractions and bundling them together as filaments reach the rear of the cell. High myosin II activity is required for actin network disassembly at the rear of the cell where contractile forces can mechanically rip apart actin filaments, facilitating actin network treadmilling (*115*). As the actin at the leading edge protrudes, the rear retracts on a several-second lag, indicating that the myosin activity is responsive to motion initiated by the cell front. As a cell's leading edge turns, myosin II rapidly re-orients to the outside of the turn, to facilitate the direction change (*116*). Rear contractility is important for pushing the nucleus to facilitate nuclear transit, particularly through constrictive environments (*110*). Together, these dynamics where actin at the leading edge dictates the direction and myosin II forces fuel uropod retraction results in a 'rear-wheel drive' mechanism of motion that propels amoeboid cells.

PLASTICITY BETWEEN MIGRATION MODES

Migration mode usage depends on the context in which the migration takes place. For example, mesenchymal cells can be induced to migrate in a fast-amoeboid like manner when placed in conditions of low adhesion and strong confinement (*117*). Similarly, a migrating fibroblast can switch from the stereotypical actin-driven lamellipodial protrusion in 2D to a completely different mode of migration in confined 3D environments where they employ the nucleus as a piston to generate a pressure differential across the cell, driving lobopodial protrusions. In this mode of migration, nuclear passage through confined spaces is achieved through actin, myosin, and vimentin at the cell front pulling the nucleus forwards, tethered by the LINC complex (*118*). Embryonic progenitor cells can be induced to migrate in an amoeboid-like stable bleb migration mode by modulating contractility (*119*). Other cells, such as certain cancer cells, when faced with a confined 3D environment can switch from mesenchymal-like non-cortex-driven migration to an amoeboid-like contractile rear cortex-driven mechanism of nuclear transit (*120*). Together, these examples demonstrate the plasticity that cells possess to modify their migration strategy based on the environment, and that the range of plasticity is cell-type specific. Cells tune

their migration mode depending on a number of cell-intrinsic and -extrinsic factors. Two primary factors that can account for nearly the full range of migration plasticity are adhesiveness and contractility (*121*, *122*). Importantly, migration strategies exist on a continuum rather than a definitive amoeboid and mesenchymal binary.

Immune cells can adapt their migratory strategy to the environment. DCs, for example can use adhesive structures when available and rapidly switch mechanisms in environments where substrates are non-adhesive. In a beautiful demonstration of this, DCs confined under agarose migrate towards a chemokine gradient at a similar velocity regardless of substrate adhesiveness. On non-adhesive substrates, actin polymerization is sped up to compensate for the lack of molecular clutch, allowing migration speed to remain remarkably consistent over these different environments (*123*). Similarly, T cells on a flat surface are able to switch from a more mesenchymal-like migration mode to an amoeboid walking mode depending on integrin availability (*124*). Substrate rigidity of flat surfaces also influences T cells to adopt a more mesenchymal-like migration mode compared to on softer substrates, a plasticity that is mediated by microtubules (*125*). T cells can change migration mode based on environmental cues such as chemoattractant availability. Chemokines such as CCL19 drive lamellipodial-based migration but S1P promotes increased intracellular pressure and bleb-based motility. CCR7 is associated with long-distance migration within lymph nodes, whereas S1PR1 elicits T cell transmigration through lymphatic endothelium. These biochemical signals are associated with specific environments, and these signals may serve to promote migration strategies best suited for that environment (*42*). Confinement is a key contextual difference in migration studies, and is particular poignant when comparing two-dimensional vs three-dimensional contexts. T cells can toggle between adhesive and non-adhesive migration modes depending on environmental geometry. Leukocytes in 3D can migrate completely independently of integrins. Protrusive F-actin flow is sufficient to propel the cell forwards (*110*). Critically, 3D environments provide topological features against which cells can produce forward motion by generating retrograde shear forces, even

when Talin is completely ablated and transmembrane force coupling is lost. Nonetheless, the same basic mechanisms of retrograde actin flow power both adhesion-dependent and adhesion-independent migration (*112*).

Finally, while leukocytes generally share the same basic features of amoeboid migration, there are some differences depending on the immune cell type. For amoeboid cells, migration modules can be refined into three defining parameters: actin polymerization, myosin II-dependent contraction, and adhesion (*106*, *108*). Leukocytes differ in the balance of these forces. DCs uniquely have a leading edge with multiple dendrites. Monocytes are slow, and lack a bona fide uropod. Tissue-resident macrophages take on a more mesenchymal migration mode and adhesive fibroblast-like appearance and they are poorly motile. Several immune cells such as neutrophils and macrophages are capable of producing MMPs, though their migration is not strictly dependent on its secretion (*107*). The next section will cover some cell-specific mechanisms of migration for the immune cells studied in this thesis.

CONCLUSION

In this section, I detailed how the molecular building blocks of the cytoskeleton are assembled to facilitate cell locomotion. Using the same cytoskeletal building blocks, immune cells can generate a smorgasbord of different structures to carry out an even greater array of functions. In the next section, I will outline how these processes are regulated during migration, and why they must be tightly controlled for effective immunity.

Migration is a defining feature of immune cells. Max Schultze in the 1960's pioneered a warm stage microscopy technique allowing for the first visualizations of immune cell migration (*126*). Schultze observed the movements of a 'finely granular' white blood cell, most likely a neutrophil, to be highly dynamic (**Figure 5**). He was struck by the lively and amoeba-like movements.

Figure 5. Early observations of immune cell migration. Drawings from Max Schultze's 1865 paper showing examples of a "finely granular" white blood cell moving on a glass slide. Images are from the same cell demonstrating a series of rapid shape changes and "lively creeping movement". Translation from (*127*). Figures from (*128*).

As suggested by those early observations, immune cells demonstrate an incredible range of adaptability and versatility. There is also great heterogeneity amongst immune cells, varying based on size, morphology, location, and function. Different types of immune cells employ unique strategies suited to their functions. In this section, I will provide an overview of where immune cells need to go, broken down by cell type, to highlight the differences in their migratory lives. I will focus specifically on the cell types studied in this work: neutrophils, T cells, and DCs. I will then detail the consequences of the dysregulation of these processes by reporting on primary

immunodeficiencies arising from failed immune cell migration. Finally, I will outline in detail one of those immunodeficiencies, Dock8-deficiency, the focus of much of the research in this thesis.

IMMUNE CELL MIGRATION AT HOMEOSTASIS AND INFLAMMATION

GENERAL MEDIATORS

Effective immunity necessitates that the right cells be at the right place at the right time. Much of the directed motility is regulated by G protein-coupled receptors (GPCRs), a superfamily of proteins comprised of over 800 members (*129*). GPCRs are transmembrane proteins with an N-terminus extracellular domain and a C-terminus intracellular domain. These domains mediate the binding of ligands in the extracellular environment to trigger intracellular signalling cascades. G-proteins consist of three subunits comprising an αβγ membrane-bound trimer. Activated GPCR leads to conformational change, activating GEF activity to facilitate the exchange of GDP for GTP on the Gα subunit, and dissociation of the Gα-GTP from the Gβγ subunit. Both of these active subunits mediate signal transduction downstream (*130*). GPCRs mediate directional movement by facilitating an asymmetry, or polarization within a cell. Polarity is primarily established through PI3K and Rho GTPases that stimulate actin polymerization at the leading edge (*131*).

Chemoattractants can be soluble or surface-bound and are present in every tissue where immune cells reside or infiltrate. Leukocyte chemoattractants span a diverse range of molecules including lipids, peptides, and small proteins. One of the best-studied drivers of leukocyte motility is chemokines, a group of nearly 50 small molecules (*132*, *133*). Chemotactic signals operate at a long range attracting immune cells to specific organs during steady state and inflammation, as well as at a local scale to mediate directional migration towards a site of injury or even a single bacterium. GPCRs activate PI3K to convert PIP_2 to PIP_3 in the membrane, which recruits downstream small GTPases Rac and CDC42 to the leading edge of the membrane to promote actin polymerization (*134*). In a uniform chemotactic

environment, GPCR signalling can elicit polarization and increased motility in an undirected manner in a migration pattern termed chemokinesis. Chemotaxis occurs when the motion becomes directional due to a chemotactic gradient. Gradients can be generated from simple diffusion (*131*). Gradients can also be self-generated by local attractant depletion, occurring when cells degrade chemoattractant upon binding (*135*, *136*). Chemoattractants that are not soluble but rather surface-bound encourage motion that is termed haptotaxis or haptokinetic. With the presence of multiple chemoattractants and many GPCRs expressed on a cell at any given time, GPCRs themselves must synergize or compete (*130*). GPCR signaling networks are highly complex and multiple GPCR signals must consolidate into one locomotion strategy.

NEUTROPHILS

Neutrophils are perhaps the most impressive example of immune cell motility, and exhibit some of the highest migration speeds even amongst leukocytes (*80*, *107*). Fast migration is core to their function. Generally, neutrophils develop in the bone marrow, and are released into the circulation upon maturation. When an inflammatory insult occurs, neutrophils are recruited into peripheral tissues (*137*). Once at the site of infection, neutrophils exert anti-microbial functions such as phagocytosis, production of reactive oxygen species, and expulsion of extracellular traps (*138*). Optimal pathogen control necessitates rapid motility.

To enter endothelial tissues, neutrophils, and leukocytes more generally, must undergo transendothelial migration. The well described leukocyte-adhesion cascade is a multi-step process that begins with selectin-driven rolling on the vasculature, followed by integrin-dependent arrest and adhesion which allows for leukocyte crawling on the luminal side of the endothelium and scanning for a permissible place through which to transmigrate (*139*). To initiate the cascade, cytokines are released at the site of inflammation. Endothelial cells sense these cytokines and upregulate a buffet of adhesion molecules to allow for cellular attachment. Selectins allow for weak transient interactions. Firm attachment occurs when LFA-1 binds ICAM-1. In neutrophils, crawling is facilitated by the integrin Mac-1, and this crawling

surprisingly occurs either perpendicular to or against the direction of flow (*140*). Finally, extravasation of the cell occurs through either a paracellular or transcellular route, through the junctions of adjacent cells or through the body of an endothelial cell, respectively. The degree to which leukocytes will use the either route has been debated in the literature, and likely depends on the particular experimental conditions (*139*, *141*). Transcellular transmigration relies on WASP-dependent invasive podosomes that probe for permissive routes (*142*). One major challenge of TEM is the nucleus, which must squeeze through micron-sized gaps in the endothelial barrier. Leukocytes actively insert either a pre-existing or de novo nuclear lobe into a pore to facilitate passage (*143*). Once extravasated, neutrophils will follow a hierarchy of chemoattractant gradients away from the endothelium and towards the inflammatory site. Neutrophils sort through the noise of chemotactic molecules with preferential migration towards 'end-target' chemoattractant (*144*). Neutrophil recruitment is a process that is carefully regulated through a cascade of steps.

One unique dynamic of neutrophil migration *in vivo* is swarming behavior. Occurring in response to tissue damage or microbial invasion, neutrophil swarms were first observed in the lymphoid tissues (*145*) and skin (*146*), and have since been described in various other organs. Swarms initiate when tissue damage or infection is detected. The swarms amplify through secondary cell death and long-distance signal relay. Accumulating neutrophils aggregate into tight clusters that seal the wound. Specific swarming behaviours are also dependent on the local tissue architecture, bystander cells, and the chemoattractant environment (*147*). Extravascular swarming in fibrillar skin or cell-rich lymph nodes is integrin-independent, compared to intravascular swarming which relies on integrin-mediated crawling. Ultimately, the containment of microbes or tissue damage is important for host protection, however swarms must also be resolved to control excessive harm from tissue remodeling or destruction of tissue-resident cells (*147*). Swarming can resolve in a neutrophil intrinsic manner via GPCR sensitization (*148*). For minor cell injuries, tissue-resident macrophages can sequester damage by "cloaking" to prevent the swarming

altogether (*149*). Swarming requires layers of signalling and regulation to deploy neutrophils while limiting destruction to mediate optimal immune protection.

Recent work expands our understanding of neutrophil functions and where they need to go. Neutrophils recruited to inflammatory sites in peripheral tissues may even undergo reverse transmigration to re-enter the circulation and enter other organs (*150*, *151*). Neutrophils are functional at steady state as well, where it is now understood that neutrophils infiltrate healthy peripheral tissues (*152*). Neutrophils participate in homeostatic immune surveillance by delivering antigens to the lymph node (*153*). Lymph node neutrophils modulate adaptive immunity by presenting antigens and promoting or suppressing the activation of T cells (*144*, *154*). Often, these additional functions are carried out by specific subsets of neutrophils located in specific tissues, and the role of heterogeneity in shaping neutrophil function has been an intense area of study (*155*, *156*). Neutrophil migration and trafficking turns out to be far more complex than once thought.

T CELLS

The T cell life cycle is one that is spatially dynamic. T cell progenitors originate in the bone marrow, and must migrate to the thymus for maturation, selection, and differentiation (*157*). Conventional T cells expressing αß TCR are released into the circulation. Naïve T cells circulate constantly between blood and SLOs, scanning for cognate antigen. T cell entry into lymph node is mediated by CCR7, CCL19, and CCL21 as they enter through the HEV (*158*). CCR7 signalling within the lymph node is an important chemokinetic factor for basal T cell motility (*159*). Intranodally, CCR7 promotes cortical actin flows and LFA-1 provides the substrate friction to generate naïve T cell motility (*160*). Within the lymph node, T cells were observed to migrate at a mean speed ~10 µm/min with peak velocities upwards of 25 µm/min (*161*). DCs in the lymph node migrate at half the speed of T cells, but their large surface area and dendritic shape allow them to scan up to 500 T cells per hour (*162*). T cells migrate in a random walk and each individual T cell will scan about 100 DCs per hour (*163*). Lymph nodes are also the location of a unique stromal cell type termed

fibroblastic reticular cells (FRCs). FRCs express CCL19 and CC21. The FRC secrete ECM that forms a conduit system that allows fluid flow and transport of molecules to and from the peripheral tissues (*164*). The FRC network also provides tracks along which naïve T cells migrate (*165*). In fact, it is this topology of this network that leads to the stop and go migratory behavior exhibited by T cells, where the velocity fluctuations are driven by the surrounding environmental features (*163*). T cell interactions with pMHC elicit brief pauses in migratory routes (*166*). Intrinsically, Myosin 1g promotes cell meandering and turning which is important for search and detection of the rare cognate antigens (*167*). Dwell time within the lymph node is around 12, 21, and 25 hours, respectively, for naïve CD4, CD8, and Tregs at steady state (*6*, *166*). T cell egress is mediated by sphingolipid S1P which is abundant in blood and lymph, but low within lymphoid organs, creating a S1P gradient across the lymphatic endothelium to draw T cells out (*168*). Ultimately, retention and egress is tuned by S1PR1, CCR7, and MHCII interactions (*158*). Activated T cells also downregulate CD62L and CCR7 and upregulate specific homing molecules for peripheral tissues.

T cells must undergo transendothelial migration to reach tissues, and this is mediated by the upregulation of receptors that are involved in this process, such as CD44, CD43, LFA-1, PGSL-1, and VLA-4. Additional priming by DCs and the anatomical location of the activating SLO elicits the upregulation of tissue-specific receptors to promote precise homing. For example, homing to skin is facilitated by upregulation of CCR4, CCR10, and CLA, whereas homing to gut is mediated by α4β7-integrin and CCR9. Though, these dependencies are not definitive, and there is a degree of promiscuity to the tissues into which T cells enter (*169*). Upon entry into the peripheral tissue, pMHC scanning will recommence. Effector T cells in peripheral tissues can migrate adhesively along ECM fibers or in an adhesion-independent manner between them. T cells tune their migration strategy based on the tissue architecture, where reliance on chemotactic signals or integrins depends on ECM density (*170*). Search strategies in peripheral tissues are tissue-specific, and depend

on the availability of haptokinetic cues, chemokinetic cues, and APC frequency. Resulting motility patterns can span from diffusive to ballistic (*171*).

Upon the contraction of the acute response, effector T cells mostly die, but some have the potential to differentiate into memory T cells. These memory T cells can be classified into different subsets defined partly by their surface molecules and circulatory properties. T_{EM} recirculate through the blood, SLOs, and peripheral tissues. T_{CM} also recirculate amongst the SLOs. T_{RM} are restricted to the peripheral tissue with little to no recirculation. T_{RM} within the peripheral tissues occupy specific anatomical niches such as in the epithelial layer of the skin, gut, and lungs where they are persistent and long-lived (*172*). Memory T cells express subset- and tissue-specific chemokine and adhesion receptors that mediate their surveillance and persistence. In peripheral tissues, the scanning speeds of T_{RM} differ, which may reflect the distinct anatomical structures of various tissues (*173*). Rarely stationary, T cells live a life of perpetual motion.

DENDRITIC CELLS

Dendritic cells are a critical link between innate and adaptive immunity. The life of a conventional DC consists of two distinct phases immature and mature, where various microbial or viral products trigger a rapid phenotypic switch (*174*). In tissues, immature DCs patrol the environment, sampling antigens and searching for inflammatory signals. DCs sample antigens by phagocytosis and macropinocytosis. Upon maturation, DCs quickly migrate towards the lymphatic organs (*175*). This process is driven by CCR7 upregulation and a haptotactic CCL21 gradient (*176*). With different fundamental roles, the state of the dendritic cell also dictates migratory behaviour. DCs must balance their migratory, phagocytic, and antigen-presenting functions, all of which require cytoskeletal remodelling. Immature DCs migrate in fast and slow phases. Fast and directional migration is driven by RhoA-mDia1 actin cables in the rear; a switch to Cdc42-Arp2/3 driven branched actin at the cell front considerably slows migration, the more optimal migration strategy for efficient search and antigen capture (*177*). In fact, in immature DCs, these two migration

strategies are antagonistic, controlled by MHC class II-associated invariant chain (Ii or CD74) at the cell front which drives local myosinIIA enrichment (*178*, *179*). One function of actomyosin recruitment in the front is to facilitate the formation of macropinosomes that immature DCs use to acquire environmental antigens. A surprising secondary effect is that micropinocytosis also helps immature DCs to overcome hydraulic resistance, allowing these DCs to explore a greater space (*180*). Once DCs sense microbial products, the upregulation of lysosomal genes promotes antigen processing into peptides for presentation on MHCII. Signaling of this lysosomal axis was identified as a trigger for DC switch into fast migration and for chemotaxis into the LN (*181*).

LPS-driven maturation will induce DCs to adopt the RhoA-mDia1 actin pool in the rear, increasing migration speed by about ~25% in a one-dimensional channel (*182*). One of the key functions of the mature DC is to stimulate T cells, and DCs lacking mDia1, in addition to slower migration, fail to home to lymph nodes effectively, and have reduced capacity to prime T cells (*183*). MyosinIIA and mDia1 are both particularly important for migration through smaller pores and constricted environments (*183*, *184*). DCs have a comparatively stiff nucleus due to LaminA/C expression, but overcome this by actively deforming the nucleus with actin-driven mechanisms. It has been shown that as DCs enter a constriction, an Arp2/3-dependent perinuclear actin accumulates, and acts to push the nucleus, and even transiently rupture it (*87*). Cofilin also promotes further nuclear deformation upon DC maturation through the formation of a contractile cofilin-actomyosin perinuclear ring (*185*). Despite their terminal differentiation, mature DCs have been shown to possess multiple centrosomes. Centrosomes serve as a nucleation site for microtubules, and DCs with more centrosomes display greater migration persistence towards chemotactic cues (*186*). Altogether, mature DCs exhibit a transcriptional program that promotes antigen presentation and tunes migratory strategy.

MIGRATION DEFECTS IN PRIMARY IMMUNODEFICIENCY

In humans, mutations in the genome can result in heritable immunodeficiencies. As of 2022, a total of 485 inborn errors of immunity have been discovered (*187*). Impaired immunity can arise from dysregulation in any step of immune cell motility, which commonly affects processes such as chemotactic response, adhesion, or cytoskeletal regulation. The study of these primary immunodeficiencies has significantly furthered our understanding of previously understudied genes.

CHEMOTAXIS DEFICIENCIES

Chemokines are the best-described mediators of immune cell migration. Breakdown in chemotactic signalling results in the failure of immune cells to traffic and localize correctly within tissues. One example is in mutation of the CXCR4 gene, which can result in WHIM (Warts, Hypogammaglobulinemia, Immunodeficiency, Myelokethexis) syndrome, which is characterized by the namesake symptoms. CXCR4 is a GPCR, and WHIM syndrome arises as a result of gain-of-function mutations in this receptor, which results in prolonged signalling in response to CXCL12 (or SDF-1) (*188*). Enhanced CXCR4 signalling leads to abnormal cellular retention in the bone marrow and impaired release into the bloodstream and peripheral tissues. The result is neutropenia, lymphopenia, and heightened susceptibility to infection, particularly HPV (*189*). Loss-of-function mutations in CXCR2 can also result in WHIM syndrome, as CXCR2 promotes egress from the bone marrow as a counter-regulator to CXCR4 (*190*, *191*). Together these mutations highlight the important role of chemokines in orchestrating leukocyte trafficking.

ADHESION DEFICIENCIES

Once egressed out of the bone marrow, leukocytes must gain entry into another tissue. Another group of well-characterized mutations in genes involved in leukocyte rolling, adhesion, and transendothelial migration are Leukocyte Adhesion Deficiencies (LADs), which are described as 3 different variants. LAD-II deficiencies affect the fucosylation of selectin ligands such as Sialyl Lewis X, resulting in defective

leukocyte rolling (*192*). LAD-I and LAD-II deficiencies interfere with proper integrin signaling, affecting adhesion and chemotaxis. LAD-I is caused by a mutation to ß2-integrin (CD18); LAD-III by a mutation in kindlin-3, which along with talin-1 functions to activate ß2-integrins from a dormant to a high avidity state (*193*). Neutrophils with these mutations ineffectively extravasate into tissues, and patients present with severe neutrophilia and recurrent infections (*193*). This group of immunodeficiencies demonstrates the critical role of proper interactions between leukocytes and the extracellular environment.

CYTOSKELETAL DEFICIENCIES

Finally, the largest group of known primary immunodeficiencies known to affect immune cell migration are the actin-related inborn errors of immunity. Actinopathies often have effects beyond just cell migration, since many critical cell processes such as cell division, phagocytosis, and synaptic formation all require specific actin structures (**Figure 6**). The first identified and best well-characterized of these actinopathies is Wiskott-Aldrich syndrome (WAS), caused by mutations in the *WAS* gene affecting the WAS protein (WASP), was mapped in 1994 (*194*). Since that time, more than 20 additional actin-related inborn errors of immunity have been identified, though WAS remains the archetype of how actin cytoskeletal defects impair immune responses (*48*, *195*). Clinical manifestation of the disease includes bleeding, eczema, recurrent infections, and autoimmunity (*196*, *197*). WASP is a hematopoietic-specific effector downstream of CDC42 (*198*).

Following the elucidation of WAS, many more mutations driving immune-related actin function have been identified, including in the gene encoding ß-actin itself, ACTB (*199*). Proteins modulating Arp2/3-dependent actin branching include WASP, WIP, PSTPIP1, HEM1, and ARPC1B. Proteins involved in actin filament elongation include the formin mDia. Conversely, mutations to negative regulators of actin growth also result in migration defects; these include proteins involved in actin capping- CARMIL2, and actin turnover via Cofilin- Coronin1A and WDR1. Further upstream, a number of mutations affect RhoGTPases, including Cdc42, Rac2, RhoG,

and RhoH. Further upstream still, regulators of RhoGTPases include DOCK2, DOCK8, DEF6, and ARHGEF1. Other indirect modulators of actin include a transcription factor of actin-related genes (MKL1), a Hippo pathway kinase (MST/STK4), a non-canonical NF-κB pathway component (NIK), and a GEF for RAS GTPase (RASGRP1). Most of these actin-related deficiencies have been discovered in the last decade, since the onset of next-generation sequencing to aid in their identification, so research into the molecular mechanisms of these actinopathies has expanded rapidly in recent years (*48*, *200*). Already, numerous insights into human immunology have been derived from the study of these diseases, and ongoing research will elucidate much more as it pertains to the hematopoietic-specific actin regulators.

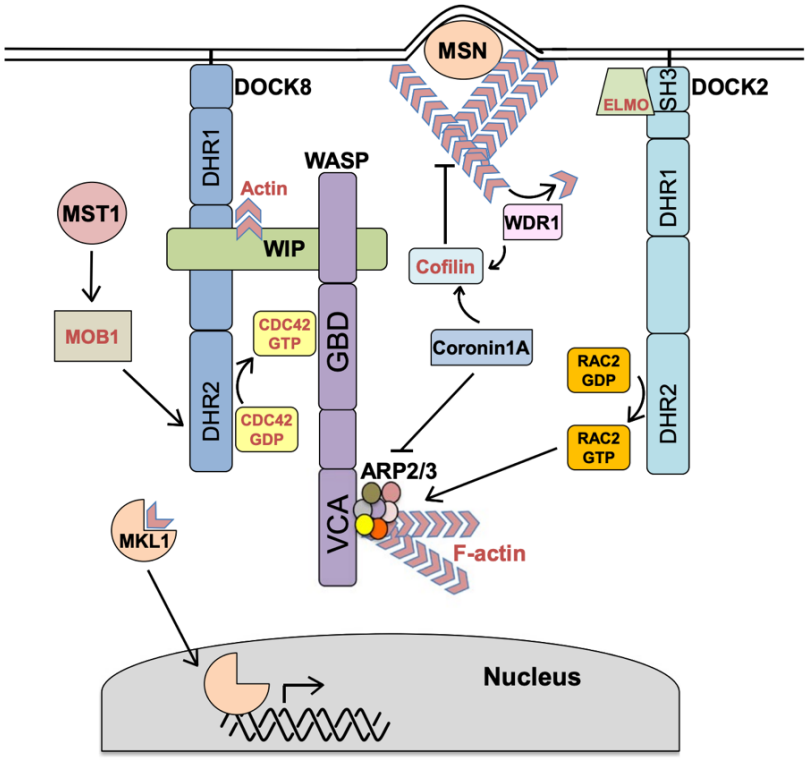

Figure 6. Actin regulatory proteins associated with primary immunodeficiencies. These are a sample of proteins mutated in actinopathies (in black) and how they interact. Dock8 and Dock2 activate CDC42 and RAC2 respectively. CDC42, RAC2, and WASP promote Arp2/3 actin polymerization. MST1 promotes Dock8 activation. Coronin1A and WDR1 promote actin depolymerization through cofilin. MSN links actin to the membrane. MKL1 is a transcription factor for actin-related genes. Adapted from (*200*).

DOCK8 DEFICIENCY

Dock8 deficiency was first described in 2009 and is characterized by excessive IgE, severe allergy, and recurrent infections. Patients also frequently have rashes and asthma (*201–203*). T cells from these patients are T_H2 biased at the expense of T_H1 and T_H17, which can explain many of the observed symptoms (*204*). The T_H2 bias likely contributes to the heightened susceptibility to viral, bacterial, and fungal infection (*205*, *206*). Dock8 is primarily expressed in cells of the immune compartment, thus these symptoms are entirely mediated by aberrant immune cell functions (*206*, *207*). Hematopoietic stem cell transplants are currently the only treatment option, but are effective in curing infection susceptibility– the primary cause of death (*208*).

Dock8 is an atypical guanine exchange factor (GEF) which binds and regulates Rho GTPases by facilitating the exchange of GDP for GTP (*209*). GEFs for RhoGTPases belong to two subfamilies: Dbl and DOCK. In mammals, there are at least 70 members of the Dbl family and 11 members of the DOCK family (*210*, *211*). RhoGEFs far outnumber RhoGTPases, so there is some redundancy in their function. Dock GEFs, lacking the Dbl domain are also referred to as 'atypical GEFs' (*212*). Dock8 GEFs are classified into four subfamilies: DOCK-A (Dock1/180, 2, 5), DOCK-B (Dock3 and 4), DOCK-C (Dock6, 7, and 8), and DOCK-D (Dock9, 10, and 11). Dock GEFs share a Dock homology region 1 (DHR-1) that directly binds PIP_3, localizing Dock8 proteins to the membrane (*212*). The DHR-2 domain is the catalytic domain with specificity for Rac or CDC42, but not Rho (*213*). Dock2 has an additional Src homology 3 (SH3) domain associated with ELMO. In lymphocytes, Dock2 is essential for migration, as it selectively activates Rac downstream of chemokine and S1P signaling (*214*). Dock8, in contrast, is specific for CDC42 and controls its activation at the leading edge (*215*). Beyond its GEF domain, additional Dock8 binding partners have been identified including MST1, LRAP35a, WIP, WASP, LRCH1, and septin 7 (*216*). Clinical deficiencies may be explained by either catalytic GEF activity or by other interactions mediated by Dock8.

Dock8 mutations result in lymphopenia, particularly of T cells, and to a lesser extent NK cells and B cells (*217*). Dock8 mutations hamper the humoral response, specifically affinity maturation of antibody-response which is T cell-dependent, resulting in defective antibody titers. The initial wave of T cell-independent antibody creation is preserved, but germinal center B cells failed to persist as a result of defective synaptic formation in the absence of Dock8. Dock8 functions at the B cell synapse to recruit LFA-1 and ICAM-1, as well as coordinate synaptic actin structures for optimal B cell-T cell contacts that promote survival (*218*, *219*). Mirroring synaptic defects in B cells, NK cells also have reduced cytotoxicity from impaired F-actin accumulation at the immunological synapse, and deficient LFA-1 recruitment due to Dock8 interactions with talin and WASP (*220*, *221*). The T cell compartment is the most severely lymphopenic. Dock8-deficient CD8 T cells are able to expand and mount normal immune responses to primary infection of acute influenza virus. Persistence of memory CD8 T cells is impaired due to reduced survival (*222*, *223*). One of the most striking phenotypes of Dock8-deficient T cells is the loss of cell shape integrity during migration in highly confined environments. Dock8 coordinates cell shape through CDC42 and PAK. Dock8-deficient T_{RM} poorly control HSV skin infection (*224*, *225*). Loss of this shape integrity leads to altered morphology and ultimately to cell death by cell shattering, termed 'cytothripsis' (*224*). Similarly, in dendritic cells (DCs), DOCK8 was found to be critical for DC migration through the interstitium through its activity as a Cdc42 activator (*215*). Previously, we showed that Dock8-deficient BMDCs would also shatter and die during migration. Consequent to shattering, IL-1β release would drive GM-CSF production by CD4 T cells, driving a feed-forward loop of GM-CSF production and T_H2 bias (*5*). Altogether, studies of Dock8 have provided insights into the regulation of immune cell migration and many other immune functions.

CONCLUSION

Immune cell migration is critical for mounting effective immune responses. The study of the genetic causes of human immune disease has provided insights into the

molecular and cellular underpinnings of disease pathogenesis. Research into primary immunodeficiencies has enabled advancements in the treatment of disease and bolstered our understanding of the immune system. In Chapter 3, we further examine the mechanisms by which Dock8 regulates immune cell motility in complex environments.

1.4 MECHANOSENSING DURING MIGRATION

Michael Abercrombie and Joan Heaysman, considered pioneers of cell migration, famously described in the 1950's their observations that migrating chicken fibroblasts influenced each other's movement, in a processed termed 'contact inhibition' (*226*). Interestingly, the first published observation of contact inhibition was actually by Leo Loeb, who documented the phenomena in Horseshoe crab hemocytes in the 1920's (*227*, *228*). The insight that immune cell motion is modulated by mechanical interactions with other cells and the environment dates back over a century, however modern tools have allowed for a revitalization of research into the question of exactly *how* this mechanosensing occurs. The existence of a typical immune cell involves resisting forces from bulk fluid flow, dense cellular crowds, and a labyrinth of interstitial matrix. Recent studies have begun to unravel the many pathways by which immune cells integrate these mechanical signals. Significant work has been done as it pertains to immune cell receptor activation but less understood is mechanosensing as it pertains to the physical environment. Here, I will describe the physical properties of tissues and the major pathways by which immune cells integrate mechanical signals, highlighting mechanical aspects that relate to migration. Finally, I will describe recent advancements in our understanding of how these mechanical signals influence immune cell function.

MECHANICAL PROPERTIES OF TISSUES

Every tissue has distinct mechanical properties. Different tissues will vary by a multitude of parameters including stiffness, viscoelasticity, composition, confinement, and architecture. I will review some key parameters which affect the mechanical microenvironment within tissues. All these tissue parameters combine to form a unique environment within each tissue, and varying one parameter will often modulate at least one other. Cells must be able to sense and adapt to these different tissue environments as they migrate and exert effector functions.

COMPOSITION

The composition of the tissue is also largely determined by the ECM. Biological tissues are comprised of ECM and cells, which themselves are the producers of the ECM. Fibrous ECM components include collagen, elastin, and fibronectin, of which, collagen is the most abundant. In humans there are 28 identified subtypes of collagen, with type I collagen comprising >90% of the collagen molecules (*229*). The mechanical properties of a tissue will depend on not only which ECM proteins are present, but also the types and strength of bonds and the crosslinks formed between enmeshed macromolecular chains (*230*). Different types of ECM components will also contain distinct chemical moieties with which cells can interact, directly influencing their migration behaviour. Thus, the biochemical ECM composition will affect the mechanical properties of tissues.

STIFFNESS

Stiffness is a structural property which describes a material's resistance to deformation. The stiffness, or elasticity, of a material is often measured as the Young's elastic modulus (E), derived from measures of the material under uniaxial stress (*231*). Biological tissues span a massive range of stiffness, with different organs having elastic moduli differing by orders of magnitude. On the low end, brains measure around just 1kPa, skin measures around 100 kPa, and the stiffest organ, bone, clocks in at about 20 GPa (*231*). Comparatively, a standard 2D *in vitro* environment such as a glass or plastic tissue culture dish measures around 10-100 GPa, which is vastly stiffer than the typical physiological environment a cell would encounter *in vivo* (*232*). It is worth noting that material properties of tissues are largely measured in bulk, and may differ from the forces measured at the microscale or nanoscale. Measurements at smaller scales are more difficult to obtain and the data is generally more sparse (*231*). Additionally, although stiffness measures are quantitative, measurements can vary greatly based on tissue preparation and technique used (*233*). Though precise measurements may vary amongst studies, it is clear that *in vitro* cell biology studies have largely been performed within

supraphysiologically stiff environments, raising the intriguing question of how cellular behavior may differ when substrate stiffness is within physiological range.

As a widely varied property amongst biological tissues, stiffness was also one of the first mechanical properties shown to drive cellular behaviour (*234*). In one striking example, substrate stiffness was sufficient in directing mesenchymal stem cell differentiation towards specific lineages. Stem cells grown on soft matrix (0.1-1kPa) developed into neurons, on moderately stiff matrix (8-17 kPa) developed into myoblasts, and on a rigid matrix (25-40 kPa) developed into osteoblasts (*235*). Effects of mechanical experiences can also last beyond the duration of the stimuli, indicating a mechanism for the retention of mechanical memory (*236*). In the context of migration, cells can actively move towards a specific substrate stiffness, termed durotaxis. On two-dimensional surfaces, this process is driven by force transmission via focal adhesions and stress fibers (*237*). Immune cell durotaxis studies are limited, but one study suggests that in a migration assay engineered to have a stiffness gradient but fixed confinement that T cells and neutrophils are able to durotax, though not through adhesion dependent mechanisms, but rather the NMIIA polarization (*238*). Additional mechanisms of immune cell stiffness sensing are reviewed in the next section.

VISCOELASTICITY

Every structural biological tissue is also viscoelastic, a mechanical property describing a material's ability to deform and recover over time. This viscoelasticity of tissue is a result of the mechanics of collagen fibers and its 3D composition, imbuing tissue elastic properties akin to mechanical springs (*239*). Similar to stiffness, tissue viscoelasticity is changed in aging and in tumours, and It is increasingly appreciated that cells can sense viscoelastic properties of their environment. Recent advancements in biomaterial engineering have allowed for the development of tunable substrates where viscoelastic properties can be modified independently of other mechanical features (*230*). These studies have indicated that the viscoelasticity

of a substrate can have profound effects on cellular growth, proliferation, and migration (*239*).

CONFINEMENT

Confinement is an important mechanical signal experienced by cells. The confinement of a tissue is determined by a combination of the matrix pore size, viscoelasticity, and degradability (*240*). In most physiological settings, cells are embedded in ECM networks and confined by the pressure of other cells. Confinement is another mechanical signal lacking from traditional 2D *in vitro* studies taking place in a cell culture dish. As discussed in Chapter 1.2, the shift from a 2D to 3D context will completely change the migration modality of immune cells from mesenchymal to amoeboid (*99*, *105*). Similarly, mechanisms of mechanostransduction also differ in the 2D and 3D context. For example, studies in the 2D context suggested YAP as a universal transducer of mechanical stiffness, but 3D contexts have revealed YAP-independent mechanical stiffness signal transduction (*239*, *241*). The porosity of a tissue presents a physical challenge to migrating cells. There is great variability in the porosity between tissues, where the spaces between collagen fibers can range from >100 μm^2 in looser tissues compared to <1 μm^2 in denser tissue (*242*). The porosity of the environment imposes limits on cell migration, dependent upon nuclear deformability (*98*, *243*). Confinement is a limiting factor for migration and a primary determinant of migration strategy.

ARCHITECTURE

The architecture, or organization of the matrix elements within the tissue also influences cell behaviour. Physical measures of tissues, such as stiffness and elasticity, are typically measured in bulk. However, 3D ECM networks are highly heterogeneous at the cellular scale. The local fiber stiffness of a collagen matrix will span two orders of magnitude (*244*). Mesenchymal cells tend to migrate in the direction of fibrillar collagen bundles (*105*). T cell migration is also sensitive to nanotopography, and will opt to migrate along the nanogrooves (*245*). The ECM of

disordered tissues, such as in fibrosis and cancer, become highly disordered, and this architecture may impact leukocyte migration.

DYNAMIC MECHANICAL PROPERTIES

Mechanical properties of tissues while relatively stable in the short term, can change drastically in different disease states. For example, tissue stiffness is well described as increasing with advanced age due to heightened ECM disposition and fibrosis. Changes in tissue viscoelasticity, where tissues lose their shape over time, is also characteristic of aging tissue (*239*). Fibrosis can be understood as a loss of mechanical homeostasis, and mechanosensing of fibrotic tissue by resident cells can result in a feed-forward loop of mechanical dysregulation (*246*). Another instance of ECM stiffening is in cancer– ECM alterations are considered a hallmark of the disease, and it has been well-described that matrix stiffness drives cancer progression (*247*). The tumour microenvironment often has an aberrantly high ECM disposition as well as increased solid stress arising from the increased pressure of tumour growth within a constrained volume (*231*). Cancer-associated fibroblasts (CAFs) generate matrix far higher in stiffness than normal fibroblasts, resulting in cancer tissues which have been reported to be ~2x stiffer in liver and pancreatic cancer, ~20x stiffer in breast and lung cancer, and ~100x stiffer in glioma (*248*). Tumor-associated macrophages also increase collagen production in response to stiffer ECM (*249*). For T cells, the physical constraints within a tumour can present significant challenges to their motility and thus hamper their anti-tumour response (*247*, *250*).

Mechanical changes to the tissues are characteristic of a proper immune response. Swelling, the accumulation of fluid at the site of inflammation, results in significant mechanical changes to the tissue environment. Swelling elicits loosening of ECM fibers which allows for more permissive cellular entry, but also exerts greater tensile stresses and hydrostatic pressure onto the cells contained within the tissue (*251*). In fact, the swelling itself can be a pro-inflammatory signal. Swelling results in hypotonicity which can boost inflammasome activity (*252*). Leukocytes detect osmotic hypotonicity at the site of inflammation which activates a cPLA2-dependent

promotion of leukocyte chemotaxis (*253*). During an infection, lymph nodes also massively swell while the FRC network proliferates and expands to accommodate lymphocyte proliferation. The whole lymph node increases in stiffness from about 4 kPa to 40 kPa upon inflammation (*254*, *255*). Over the course of 2 weeks, the lymph node undergoes a 10-fold increase in size, and a corresponding increase in effective resistance, viscosity, and elasticity compared to homeostatic conditions (*256*). Mechanical cues associated with inflammation are potent biomechanical signals for immune cell function.

Finally, cells themselves have mechanical properties, which can be modulated by the surrounding ECM and other biochemical cues. For example, tumour microenvironments often have increased rigidity as a result of fibrosis, and this increased stiffness is sensed by cancer cell focal adhesions to promote increased cytoskeletal tension and proliferation, and increased cytoskeletal tension then increases further oncogene activation in a positive feedback loop (*257*). Immune cells have mechanical properties that can also be modulated by environmental factors as well. Dendritic cells, but not macrophages, increase rigidity in response to inflammatory stimuli such as IFNγ or LPS treatment (*258*). This in turn can influence T cell responses, as it was found that DC cortex stiffening leads to stiffness-dependent priming in naïve T cells, particularly in CD4 T cells (*259*). T cells in particular are amongst the softest cells documented in the body at less than 0.1 kPa (*258*). Upon activation, T cells rapidly become stiffer and more viscous (*260*). Cytotoxic T cells themselves exert mechanical forces on other cells to enhance perforin pore formation (*261*). Force exertions and force sensing are an integral part of leukocyte function.

In summary, there is an ongoing conversation between the migrating cells and the tissue ECM. The influence of cells on ECM, and the ECM on cells, is a delicate dance where perturbations to either will lead to disruption of the balance and result in disease. This bi-directional relationship has been termed 'mechanoreciprocity' (*242*). Understanding the instances where these reciprocal relationships drive disease progression will be important to identify points of intervention.

MECHANOTRANSDUCTION PATHWAYS

Cells are constantly subject to physical forces. These include shear, osmotic, compression, and tension forces. Different forces exerted on the cell signal important mechanical information about the environment. In order for cells to integrate physical information, mechanical signals must be converted into biochemical signals in a process termed mechanotransduction. Mechanosensors are the proteins or cellular structures that are responsive to physical cues and initiate the signal propagation that ultimately lead to a cell response. In this section, I outline the primary mechanotransduction pathways in immune cells (**Figure 7**).

HIPPO PATHWAY

The Hippo pathway was initially characterized as a regulator of tissue growth, but has since been discovered to participate in many more biological functions. The mammalian Hippo pathway is highly conserved, and canonically includes MST1/2 and LATS1/2 and downstream coactivators YAP and TAZ (*262*). The signaling cascade is that MST1/2 phosphorylate and activate LATS1/2, which phosphorylate and inactivate YAP/TAZ, which are retained in the cytoplasm and degraded. YAP and TAZ are mechanoresponsive and translocate to the nucleus in response to mechanical stimuli such as stiff substrate, low cell density, disturbed flow, stiff ECM, and pressure. YAP/TAZ translocate into the nucleus to bind TEAD factors to enhance gene expression (*263*). In immune cells, Hippo pathway activation regulates substrate stiffness-dependent function and migration.

INTEGRINS

The first mechanotransduction pathways were primarily via adhesion complexes and force transmission via the cytoskeleton (*234*). The integrin adhesome is a multi-protein complex physically linking the extracellular environment to the intracellular actin network. Integrins directly bind ECM ligands and act as conduits of extracellular inputs for the cell. Integrins do not bind actin directly, but rather integrin binding to ECM ligands induces a conformational change which allows for

the attachment of nearly 30 different adaptor proteins, which can in turn directly bind to actin (*264*). Mechanical force on integrins can elicit Rho GEF activity, inducing actomyosin contractility via ROCK and MLC, and downstream activation of YAP/TAZ, NF-κB, and MAPK (*265*). In this model, termed the 'molecular clutch theory', the ECM is directly attached to the cytoskeletal actin fibers through adhesion complex adaptor proteins such as Talin and Vinculin. Force transmission occurs via direct pushing or pulling against the ECM by myosin contraction or actin polymerization (*266*). One example of cellular rigidity sensing is in fibroblasts which exhibit durotaxis, a migratory preference towards stiffer substrates mediated by stronger traction forces (*267*). This route of integrin-cytoskeletal mechanotransduction has also been implicated in morphogenesis and cancer cell migration. Migrating immune cells use integrin-based signaling for sensing the environment, particularly at integrin-driven processes such as transmigration or extravasation.

ION CHANNELS

Ion channels allow for the permeation of calcium and other ions into the cell. In general, channels are gated, and there are several mechanisms by which ion channels can be switched to the opened state. Ion channels can be voltage-gated, ligand-gated, and tension-gated. Ion channels that are important to mechanotransduction are tension-gated. In these channels, the probability of channel opening increases in response to lateral membrane tension, and their opening allows ions to flow down their electrochemical gradient. In this 'two-state' model, ion channels can be either open or closed, however, it is worth noting that ion channels can also be further regulated through desensitization or inactivation (*268*). Best described channels are the TRP and Piezo channels. Vertebrates have two Piezo proteins: Piezo1 and Piezo2 (*269*). TRP channels are widely implicated in mechanosensitive processes. Though, they likely function as secondary rather than primary mechanotransducers since TRP channels were found to be insensitive to membrane stretching (*270*). Both

PIEZO and TRP channels have been implicated in immune cell mechanosensation (*251*).

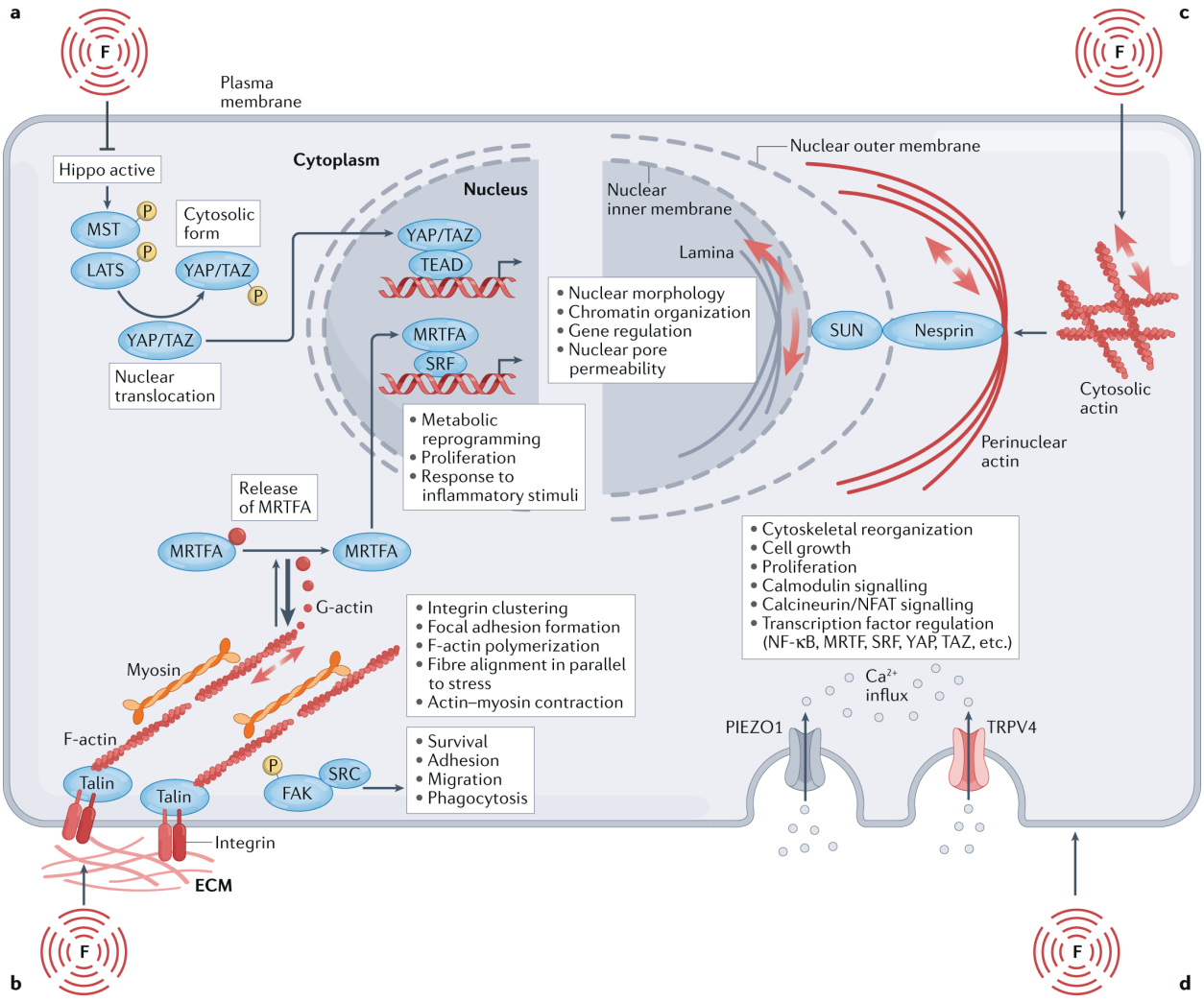

Figure 7. Mechanotransduction pathways. Diagram of major mechanotransduction pathways in cells: (a) Hippo pathway, (b) integrins, (c) nucleus, and (d) ion channels. Adapted from (*251*).

NUCLEUS

The nucleus has been shown to play a major role in mechanosensitive pathways, as a point of convergence for different signal transduction pathways, and as a mechanosensor in its own right. Some of the first mechanotransduction studies demonstrated that the stiffness of a matrix could direct mesenchymal stem cell

differentiation, thereby influencing cell fate. Lamin-A, a major intermediate filament of the nucleus contributing to nuclear stiffness (*71*), was identified as a "mechanostat", where levels of Lamin-A increased in response to increased matrix stiffness (*271*). Modulating Lamin-A expression alone was sufficient to recapitulate the phenotype of cells that had been cultured on either soft or stiff matrix (*271*). Lamin A has emerged as a key mechanosensitive protein. Lamin A is required not only for mechanical stiffness, but also chromatin organization, positioning of NPCs, and the localization of Emerin and other nuclear proteins (*97*).

The nucleus itself acts directly as a mechanosensor, particularly in 3D contexts. Nuclear deformation is a direct mechanism by which the nucleus can integrate external force to the cell. Force transmission to the nucleus can be mediated through the LINC complex, or through LINC-independent direct compression (*272*). The nucleus is typically in a wrinkled state, and forces on the nucleus will cause nuclear unfolding and increased nuclear membrane tension (*88*). Force from compression or swelling of the nucleus itself can induce conformation changes to proteins resulting in their phosphorylation or altered interaction. Lamin A and Emerin, proteins of the nuclear lamina and envelope respectively, have mechanotransductive functions (*273*). In a demonstration of this, isolated nuclei can respond directly to force, even absent any cytoskeletal mediators. Direct pulling on nesprin-1 will elicit nuclear stiffening through the phosphorylation of emerin, which recruits greater Lamin A/C to the site of deformation in a force response that takes just seconds (*274*). Increasing matrix stiffness will induce greater actomyosin tension in the cell which will exert forces on the nucleus via the LINC complex. The forces on the nuclear lamina will hide Lamin-A phosphorylation sites. Matrix softening will relieve tension on the nucleus, exposing the phosphorylation sites on Lamin-A that lead to a soluble form that can dissociate from the nuclear lamina and become nucleoplasmic and ultimately degraded, leading to a softer nucleus (*275*). Nuclear deformation induces changes to the spatial organization of the genome (*276*). Force can alter the chromatin state directly, resulting in chromatin stretching that will upregulate transcription (*277*).

Nuclear deformations alone can exert longer-lasting changes in cell behaviour and through epigenetic reprogramming (*278*).

Nuclear envelope stretching can open nuclear pore complexes (NPCs) or ion channels to allow the influx of transcription factors, calcium, and other mediators. Force application on the nucleus opens nuclear pores that allow for YAP entry into the nucleus (*279*). This may suggest that cells with nuclei which are highly wrinkled may not as easily nuclear import YAP as easily due to reduced nuclear membrane tension overall. Nuclear swelling results in increased nuclear tension can result in the translocation of $cPLA_2$ from the nucleoplasm to the inner nuclear envelope, triggering leukocyte recruitment in a zebrafish model (*253*). In cancer cells and DCs, it was shown that the nucleus can sense direct compression via increased membrane tension that releases internal Ca^{2+}, along with $cPLA_2$ relocalization into the nucleus, leading to $cPLA_2$ enzymatic activity and arachidonic acid (AA) release. Ca^{2+} and AA are potent second messengers stimulating actomyosin contractility via the Rho/ROCK pathway (*280*, *281*). Reducing nuclear stiffness by depleting Lamin A/C led to the loss of this signaling pathway (*281*). In DCs, this $cPLA_2$ pathway is an important signal for migration into lymph nodes. As the DC squeezes through constricted pores in peripheral tissues, perinuclear actin facilitates passage creating pressure on the nucleus and nuclear envelope unfolding. Nuclear $cPLA_2$ signaling leads to NF-κB activation and downstream CCR7 activation (*282*). Another mechanoresponsive protein is Ataxia Telangiectasia and Rad3-related protein (ATR), which has non-canonical function in maintenance of nuclear integrity. Loss of ATR results in deformed nuclei that collapse under compression, resulting in significant cell death when migrating through pores. Large nuclear deformations recruit ATR to the nuclear envelope and modulate chromatin tethering and condensation (*283*, *284*).

In migratory cells, the nucleus itself also displays front-rear polarity, and this is generated by force transmission through the cytoskeleton. The LINC complex is the primary mediator of nucleo-cytoskeletal force transmission. Loss of the LINC complex results in disrupted perinuclear actin and intermediate filament networks, defective

nuclear positioning, and diminished cell polarization resulting in impaired migration (*285*). Emerin has recently emerged as a key regulator of nuclear polarity. Many nuclear proteins are not evenly distributed around the nucleus, but are rather differentially localized. Loss of Emerin leads to mislocalization of SUN proteins, Nesprin proteins, Lamin proteins, nuclear actin, and chromatin (*286*). Emerin also regulates nuclear stiffness in confined environments by modulating Lamin A to promote nuclear stretching and cPLA2 signaling, facilitating optimal amoeboid migration (*287*). In migrating immune cells, the nucleus has distinct roles due to its unique properties and localization. The nucleus is positioned towards the cell front, and actually functions as a mechanical gauge for selecting the path of least resistance (*58*). The nucleus functions as an effective mechanosensor during migration.

MECHANOTRANSDUCTION IN IMMUNITY

Failure of mechanotransduction can lead to a spectrum of diseases ranging from deafness, to premature ageing, to cancer. Mechanotransduction disorders can result from mutations in proteins integral to mechanosensitive pathways, such as in ECM to actin filament linkages, cytoskeletal to nuclear linkages, ion channels, or downstream signaling pathways (*257*). Recent research has begun to unravel the ways in which mechanosensitive pathways are implicated at homeostasis and in inflammation. Furthermore, while mechanotransduction occurs on the timescale of seconds to minutes, downstream gene expression changes can last on the order of days to the entire lifespan of the cell, a mechanism by which mechanical cues received by a cell may have long-lasting impacts on cellular function and behaviour in immunity.

NEUTROPHILS

Neutrophils circulate in a relatively quiescent and un-primed state. Exposure to numerous chemical signals (ex. fMLF, GM-CSF, PAF, TNF, LPS) can elicit neutrophils to enter a state of heightened bactericidal capacity and increased lifespan. Primed neutrophils become polarized, upregulate integrins, and increase

the expression of molecules for reactive oxygen species (ROS) production. Primed neutrophils can become fully activated with exposure to additional stimuli, unleashing full capacity for phagocytosis, ROS generation, degranulation, and NETosis; or they can become de-primed, returning neutrophils to a quiescent and depolarized state (*288*). Increasingly, mechanical forces have been characterized as mediators of neutrophil priming. L-selectin (CD62L) mediates rolling on the endothelium, and priming requires the engagement of this receptor. Altering the mechanochemistry of the L-selectin catch bond modulates the inflammatory capacity of the neutrophil (*289*). The process of transendothelial migration is integrin-dependent. GPCRs can serve as mechnosensors of fluid shear stress (*290*), and integrin CD18 modulates neutrophil mechanosensitivity to shear stress (*291*). Once neutrophils are firmly attached to the endothelium, cells rapidly flatten and polarize to facilitate crawling. Neutrophil spreading and migration is increased on stiffer substrates, and this mechanosensing was dependent on PI3K (*292*). Accordingly, increasing endothelial cell substrate stiffness can increase neutrophil TEM (*293*). Neutrophils can integrate mechanical signals through a number of surface receptors.

Physical mechanical deformations alone can induce neutrophil priming. Neutrophils pushed through a small 3μm pore become polarized and activated (*294*). However, continuous mechanical deformations result in depolarization and depriming (*295*). These mechanical signals serve to prime neutrophils for immune defense, but also to avoid unnecessary activation (*291*). Neutrophil squeezing during transmigration increases membrane tension, activating Piezo1 to induce Ca^{2+} signaling which activates bactericidal function. Loss of mechanical signal integration via Piezo1 deletion leads to reduced bacterial clearance both *in vitro* and *in vivo* (*296*). Neutrophils, previously understood to be simple foot soldiers of the immune system, have recently burst onto the scene as phenotypically and functionally heterogenous tacticians (*297–299*). One major source of heterogeneity is the transcriptional differences acquired in peripheral tissues (*300*). This tissue-specific reprogramming may be a result of environmental adaptations, a response to tissue-derived signals

that remain undefined (*297*). It is intriguing to consider that tissue-specific mechanical signals may contribute to these phenotypic changes. How neutrophil function is modulated by the mechanical environment of interstitial tissues remains an open question.

T CELLS

T cells can mechanosense via integrins. This effect is most pertinent when cells transmigrate across endothelial barriers, an integrin-dependent process. T cells not only withstand shear forces, but actively migrate against them. In fact, T cell integrin-dependent migration requires shear flow in order for optimal adherence to their ligands and to actually cross the endothelial barrier (*301*). Shear-induced mechanical signals are integrated through LFA-1 and VLA-4, and provides a means for T cells to determine the correct migration strategy in a given environment (*302*). T cell migration via LFA-1 requires Piezo1 recruitment and activation at the leading edge (*303*). Shear stress is also a necessary signal for T cells to produce transient filapodial foci on the basal membrane (*304*). Engagement of LFA-1 mediates integrin-dependent crawling via integration of shear force, and also environmental elasticity, where the greater the substrate stiffness on which ICAM-1 was bound, the greater the actin polymerization (*305*). As T cells crawl, they form invasive protrusions that probe deep into the endothelial cell. These podosome-like protrusions function as dynamic probes to detect local endothelial stiffness in order to determine the path of least resistance through which to undergo diapedesis (*306*).

T cell activation is mechanoresponsive. Fluid shear stress as a mechanical force stretches the cell membrane and amplifies the magnitude of T cell activation through Piezo1 calcium signaling (*307*, *308*). To date, the best described T cell mechanosensor is the TCR complex. Greater substrate or APC rigidity during T cell activation leads to greater activation, proliferation, and cytokine production (*309*). The T cell and APC exert both pushing and pulling forces on each other at the immunological synapse via actin, and these mechanical forces contribute to TCR signaling (*310*). In fact, mechanical stimulation at the synapse is required for activation via TCR (*311*). One

study indicates that optimal TCR activation requires integration of mechanical force via Piezo1 potentiating Ca^{2+} influx and actin rearrangements (*312*). Though, the requirement of Piezo1 in T cell activation is conflicting (*313*). The mechanical environment in which a T cell is activated can have profound effects on cell function. On a 2D surface, T cell activation and proliferation is more robust on softer substrates (*314*). When 3D cultured in high density collagen matrix, compared to a low density collagen matrix or 2D culture on plastic, T cells proliferate less well and are less cytotoxic, and were consequently less effective at controlling cancer cells (*315*). T cells activated in a stiff matrix were biased towards an exhausted rather than cytotoxic phenotype, driven by integration of mechanical stress via Piezo1 and induction of transcription factor Osr2 which promoted epigenetic reprogramming towards exhaustion (*316*). Mechanosensing during T cell activation can be mediated directly through TCR as the mechanosensory or indirectly by environmental stiffness, and can have lasting effect on T cell function.

Environmental mechanosensing also impacts T cells post-activation. Effector and memory T cells can enter and adapt to most organs and tissues in the body. T cells are highly heterogenous, and circulating T cells are phenotypically distinct from tissue resident T cells. Depending on the tissue of residence, T_{RM} cells can exhibit location-specific transcriptional signatures (*317*). These phenotypic differences are shaped by the microenvironment, and the most well-described mediators of these differences are tissue-derived biochemical cues within the local milieu, such as TGFß and other cytokines (*172*). Less well described has been how the differing mechanical properties of peripheral tissues may also shape the T cell response. During the course of infection, mechanical stiffness of the matrix has been shown to control YAP entry into the nucleus, affecting T cell activation and fine-tuning the antiviral response (*255*). Adjusting just the viscoelastic properties of the ECM is sufficient to generate transcriptionally distinct T cell populations. Functionally, T cells cultured in slow-relaxing, rather than fast-relaxing, matrices were more activated and exhibited increased tumour killing *in vitro* (*318*). The finding that vast transcriptional changes

occur as a result of substrate mechanical properties has been demonstrated over several different model systems (*255*, *315*, *316*, *318*).

For T cells, mechanosensing informs migration. In Chapter 1.2, I covered how T cells incorporate biochemical and mechanical information about the environment to tune their migration strategy. In general, greater levels of confinement tilt the balance toward less adhesive and more protrusive migration. But aside from integrins, it is less clear what other mechanosensitive pathways may mediate the integration of environmental information during migration. T cell rapidly upregulate PIEZO1 upon activation. Mechanosensing by Piezo1 modulates F-actin dynamics. Blocking of Piezo1 in T cells strengthened their traction forces and improved their infiltration into tumors (*319*). In peripheral tissues, chemotactic and adhesive molecules promote motility. Some signals may be context-specific. T_{RM} residing in the salivary gland are able to efficiently scan for pMHC despite lacking chemoattractant or adhesive signals. Instead, their motility is triggered by physical confinement. Nuclear deformation and $cPLA_2$ release trigger actomyosin contractility and bleb-based migration to promote immune surveillance (*320*). The nucleus is a potent mechanosensor for migrating T cells. Septins, a relatively under-studied component of the cytoskeleton that can form filament bundles and ring structures (*321*), have also been identified as a novel mechanosensor in T cells. Located at the plasma membrane of T cells, septins are required for cortical integrity. Loss of septins results in excess blebbing and protrusions, lengthened uropod, and poor transmigration (*322*, *323*). During passage through pores, cortical indentations lead to the accumulation of septin at the site of membrane curvature, which assemble an F-actin ring. These rings are proposed to compartmentalize actomyosin contractility. In complex environments, septin curvature sensing of ECM fibers is required for motility and cell cohesion (*324*). T cells must constantly modify their migration to conform with the local microenvironment, a process which requires dynamic mechanosensing mechanisms.

MYELOID CELLS

Mechanical forces impact DC function. DCs can be activated by fluid shear stress, a force which has the capacity to open ion channels (*325*). Mechanical stiffness promotes DC function, metabolism, and activation through Mst1/2 kinases, TAZ signaling, and Ca^{2+} ion channels (*326*, *327*). DC stiffness sensing via PIEZO1 also informs T cell differentiation within tumours (*328*). Many mechanical cues contribute to the classical PRR stimulation of DCs. NLRP3, a PRR which can sense many PAMPs and DAMPs, is mechanically regulated by changes in shear stress, ECM stiffness, and osmotic tonicity. PIEZO1 serves as a primary mechanosensory controlling inflammasome activity, with implications for chronic inflammation if dysregulated (*252*). Mechanical cues can also shape DC migration. As previously discussed, DCs use their nuclei as a confinement mechanosensor to permit migration to lymph nodes via CCR7 upregulation (*282*). Even in 2D, conditioning on a stiffer substrate increases CCR7 expression, improving the chemotactic response towards CCL21 (*329*). Multiple mechanosensitive pathways converge to control DC migration.

Macrophages are embedded in dynamic tissue environments and mediate homeostatic and inflammatory functions. Tissue-resident macrophages are either embryonically-seeded or monocyte-derived at steady state. Upon inflammation, circulatory monocytes are recruited into tissue and differentiate into distinct monocyte-derived macrophages (*330*). Macrophages reside in tissues long-term, so unsurprisingly, macrophages have emerged as highly mechanosensitive cells. Macrophages and monocytes express Piezo1 several-fold higher than in other tissues, and accordingly, Piezo1 is required for response to mechanical stimulation (*331*). Macrophages plated on stiffer substrates have faster migration and proliferation rates (*332*). This stiffness sensitivity is dependent on Piezo1 Ca^{2+} influx. Piezo1 promotes F-actin polymerization, which in turn promotes a positive feedback loop of activation (*333*). Upon macrophage activation, Piezo1 is induced and associated with TLR4. Piezo1 then enhances macrophage bactericidal function by inducing Mst1/2-Rac1-driven F-actin reorganization (*334*). Piezo1 expression on monocytes and

macrophages is essential for sensing hydrostatic pressure in the lung and stimulating inflammatory responses. In the lung, loss of Piezo1 in monocytes leads to weakened protection against bacterial infection and reduced fibrotic autoinflammation (*335*). Piezo1 deletion in myeloid cells reduced the infiltration of immature myeloid cells, suppressing myeloid-derived suppressor cell expansion, and exerting protective effects in cancer and polymicrobial sepsis (*331*). Thus, depending on the context and the functional state of the macrophage, mechanosensitive pathways can lead to both favourable and unfavourable immunological outcomes. Emerging evidence indicates that macrophage polarization into pro-inflammatory versus wound healing phenotypes is mechanically regulated (*336*). Macrophages can sense ECM stiffness in an integrin-independent manner as they migrate. Macrophages in stiffer ECM-dense environments undergo cytoskeletal remodeling to repress genes related to tissue-repair, a regulatory circuit which may serve to protect tissue repair responses from evolving into pro-fibrotic ones (*337*). Altogether, immune cells possess the ability to sense their local mechanical environment in order to fine-tune their function.

CONCLUSION

Much remains to be understood about how immune cells sense and adapt to diverse tissue microenvironments. Mechanoimmunity, the interaction between tissue mechanics and immune cell function is becoming increasingly appreciated aspect of effective immune responses. Some mechanical signals change cell behaviour instantaneously, and some of these changes are retained longer term. More research is also investigating the extent to which signals influence cell behaviour longer term, after the cessation of the mechanical signal. There is evidence for mechanical memory, and research is just beginning to unravel the mechanisms by which this occurs. Similarly, mechanisms of mechano-adaptation *in vivo* are not well understood. Further understanding of these processes will provide insights into how immune cell migration is modulated by physical aspects of the environment, particularly in dysregulated tissue states where the mechanical landscape is altered, as is the case in inflammation, aging, and cancer.

CHAPTER 2: NUCLEAR SEGMENTATION FACILITATES NEUTROPHIL MIGRATION

2.1 ABSTRACT

Neutrophils are among the fastest-moving immune cells. Their speed is critical to their function as 'first responder' cells at sites of damage or infection and it has been postulated that the neutrophils' unique segmented nucleus functions to assist their rapid migration. Here, we tested this hypothesis by imaging primary human neutrophils traversing narrow channels using custom-designed microfluidic devices. Individuals were given intravenous low-dose endotoxin to elicit the recruitment of neutrophils into the blood with a high diversity of nuclear phenotypes, ranging from hypo- to hyper-segmented. Both by sorting on neutrophils from the blood using markers that correlate with lobularity, and by directly quantifying the migration of neutrophils with distinct lobe numbers, we found that neutrophils with 1-2 nuclear lobes were significantly slower to traverse narrower channels, compared to neutrophils with >2 nuclear lobes. Thus, our data show that in primary human neutrophils nuclear segmentation provides a speed advantage during migration through confined spaces.

2.2 INTRODUCTION

Neutrophils are rapidly mobilized from the bone marrow into the blood in response to infection or injury, and are usually the first leukocytes to arrive in tissues, extravasating from blood vessels and navigating diverse microenvironments to reach affected sites. Using an amoeboid migration mode defined by low traction forces and a lack of focal adhesions (*101*, *105*), neutrophils achieve speeds of up to 30µm/min, several-fold faster than other immune cells (*80*, *107*). Leukocyte mobility within confined spaces such as tissues requires frequent shape changes and is a tightly coordinated cytoskeletal process, with actin retrograde flow generating forward motion in concert with myosin motors and microtubule networks (*110*, *177*). An important impediment to immune cells passing through tissue structure-imposed obstacles is the nucleus, the largest and most rigid organelle in a cell. The relative stiffness of the nucleus, determined largely by the composition of the nuclear envelope lamina and the degree of chromatin condensation, can thus hamper the ability of cells to move quickly in complex environments. Among nuclear lamina proteins, laminA/C is regarded as a key determinant of nucleus stiffness, and compared to non-hematopoietic cells, fast-moving immune cells such as T cells and neutrophils in particular express laminA/C at very low levels (*82*, *243*). In some instances, the physical deformation of the nucleus that occurs during the passage through small pores such as in basement membranes or collagen-dense skin can even lead to nuclear envelope rupture (*45*, *87*, *338*, *339*). Additionally, recent work showing that the nucleus can act as a size gauge for migratory path selection (*340*), underscores that the bulky nucleus presents a challenge for mobile cells, particularly when cells must move rapidly.

One key feature that differentiates the neutrophil nucleus from that of other leukocytes is its unique shape. In human neutrophils, the nucleus can range from having a 'banded' horseshoe-shape to being hyper-segmented with 5 or more lobes. This nuclear segmentation is a feature common to both humans and mice, but in murine neutrophils the nucleus assumes a circular and in human neutrophils a linear

configuration (*341*). The current paradigm is that the smaller nuclear diameter and reduced steric hinderance of the multi-lobular 'pearls-on-a-string' arrangement allows for greater cell flexibility and thus enables faster migration, particularly though tight spaces (*80*, *137*, *243*). However, there currently exists only limited experimental evidence for this enduring hypothesis. Previous studies have demonstrated that human neutrophils can pass though smaller pores and migrate through dense collagen matrices with greater speed compared to tumor cells or even T cells (*243*). Work directly investigating the role of nuclear segmentation itself in neutrophil migration has relied on manipulating nuclear envelope composition. In one notable study, expression of lamin A/C and lamin B receptor (LBR) was altered in neutrophil-differentiated HL-60 cells *in vitro* to obtain neutrophils retaining a circular nucleus, mimicking the lamin A/C downregulation and LBR up-regulation that is necessary for nuclear segmentation during neutrophil development (*79*). Ultimately, the authors found that the multilobed nuclear shape was not necessary for passage through 5µm constrictions, or 3µm transwell pores (*79*). Similarly, in clinical observations of Pelger-Huët anomaly (PHA), a genetic disorder defined by mutations in LBR, the hypo-lobulated neutrophils from people with PHA did not show clear impairments in cell movement and chemotaxis (*342*). However, an important caveat of these studies is that nuclear envelope proteins have physiological roles that might impact migration directly, or indirectly through modified gene regulation, beyond their effects on nucleus lobularity (*343–345*). Furthermore, the *in vitro* differentiated HL-60 immortalized cells differ from peripheral blood neutrophils in their nuclear composition including in lamina content and heterochromatin density (*346*).

Here, we sought to determine whether nuclear lobulation facilitates the ability of neutrophil migratory capacity in small spaces in a physiological setting, comparing the migration of human neutrophils with varying degrees of nuclear segmentation in microfluidic devices. During homeostasis, circulating neutrophils are a relatively homogenous population of matured, differentiated cells with 2-4 nuclear lobes (*137*).

However, in response to inflammatory stimuli such as endotoxin, an additional pool of neutrophils is rapidly recruited to the circulation, and neutrophils released into the blood span a wide range of nuclear phenotypes ranging from banded to hyper-segmented (*347*). We obtained circulating neutrophils from individuals given low-dose endotoxin to induce a controlled emergency granulopoiesis response, and leveraged the increased diversity in neutrophil nuclear lobularity to directly address the question of whether nuclear phenotype influences migratory capacity. We found that greater lobularity led to increased cell velocity towards the chemokine gradient when neutrophils migrate through narrow paths.

Neutrophil subsets display differential migratory behaviour correlating with nuclear lobularity

We obtained circulating neutrophils from human donors given low-dose endotoxin to investigate the limits of the ability of neutrophils with different nuclear segmentation phenotypes to migrate through tightly constricted spaces. During the endotoxemia response, the neutrophils released into the blood can be sorted into subsets based on their CD16 (FcγRIII) and CD62L (L-Selectin) expression. The homeostatic pool of $CD16^{high}$ $CD62L^{high}$ neutrophils have standard segmented nuclei (2-3 lobes), the $CD16^{low}$ subset is enriched for neutrophils with banded nuclei (1 lobe), and the $CD16^{high}CD62L^{low}$ subset is enriched for hyper-segmented nuclei (4 or more lobes) (*348*). We FACS-sorted neutrophils into these three subsets based on CD16 and CD62L expression, and refer to these subsets as banded, segmented, or hypersegmented thereafter (**Figure 1A**). To observe the sorted neutrophils migrating in increasingly narrow spaces, we employed custom-fabricated microfluidic devices, which serve as a reductionist approach to studying complex 3D migration dynamics and allow for the tracking of single cell spatiotemporal patterns (*349*). The microfluidic devices are made of PDMS in a pillar-forest design, where the channels through which the cells migrate have a fixed height of 5µm, but reduce in width in a step-wise fashion from 6µm to 4µm to 3µm to 2µm and then step-wise back up to 6µm (**Figure 1B)**. The 6µm width is fairly permissive, whereas the 2µm width presents a significant challenge for cells to migrate through due to the width being smaller than the diameter of the nucleus (*87*, *243*). Neutrophils were seeded on one side of the microchannel and the chemoattractant f-Met-Leu-Phe (fMLF) added on the other to diffuse through the microchannels, creating a chemotactic gradient. The three sorted subsets were stained with 3 distinct fluorescent dyes (Hoechst, Calcein AM, or Draq5), mixed at equal ratios, and added to our fabricated pillar forest. Dye labels were rotated between different donors, and we confirmed that the dyes did not differentially affect migration speed by dye-labeling neutrophils from non-LPS-

treated donors (controls) and measuring cell speed (**Figure S1A**). As the neutrophils traversed from the 6µm region to the 2µm, the cells and their nuclei became increasingly constrained and elongated (**Figure 1C**). Of note, we have previously shown that the process of transmigration through small pores does not itself induce nuclear segmentation in neutrophils (*348*).

Next, we assessed differences between neutrophil subsets in their ability to move within the more constrained channels using two approaches: by taking a static image after 3 hours of migration in the microfluidic device (**Figure 1D, E**), and by dynamic imaging of cell behaviour over time (**Figure 1F-I**). Given that the 2µm section is the most challenging width for migrating cells to navigate through, we first quantified the total number of neutrophils that were able to successfully pass through the whole section as proxy for migration capacity. Compared to the segmented and hypersegmented subsets, a smaller proportion of the banded neutrophil subset crossed the 2µm section in 3 hours, even though the subsets are present in similar proportions prior to reaching the 2µm section (**Figure 1D**). Performing this analysis across six donors, we found a robust difference between the frequency of banded neutrophil subset that traversed the 2µm section compared to the segmented and hypersegmented subsets (**Figure 1E**). Second, we performed live cell imaging of the dynamic behaviour of neutrophils migrating through the channels (**Movie 1**). From our videos, we tracked individual cell behaviours by subset, including track length, speed, displacement, and velocity. We have defined the track length as the total distance travelled by the cell, the mean speed as the average rate of movement along the track, displacement as the total distance travelled towards the chemokine, and the velocity as the rate of movement towards the direction of the chemokine over the course of the cell track (**Figure 1F**). Overall, the banded subset had significantly lower mean cell speed and displacement length compared to the hypersegmented neutrophils (**Figure 1G,H**), without a reduction in track duration, length or straightness (**Figure S1B**). Analyzing each cell's migration distance towards the chemoattractant as a function of time, we observed that there were significant

differences in the speed at which each subset could traverse the pillar forest. The average velocities for the banded, segmented, and hypersegmented subsets were 8.5, 9.4, and 12 μm/min respectively (**Figure 1I**). Furthermore, the reduced speeds observed in the banded subset is attributable to the narrower paths since we observed similar speeds for all three subsets in the wider 6μm section (**Figure S1B**). While there was donor-to-donor variation in the average neutrophil cell speed, relative velocities amongst the neutrophil subsets nonetheless robustly demonstrated that the banded neutrophils had a migratory disadvantage compared to the other subsets (**Figure 1J,K**). Based on a previously published proteomics dataset (*350*), these differences were not explained by FPR1, LMNB1, LMNB2, or LBR expression, which did not differ significantly in protein expression levels between subsets (**Figure S1C,D**).

Single-lobed nuclei in neutrophils reduce their migratory capacity through narrow channels

One caveat of utilizing CD16 and CD62L as markers for neutrophil nucleus segmentation is that there is a substantial overlap in nucleus lobularity between subsets, even if the average number of nuclear lobes differs (**Figure S1E**). Moreover, there are other functional differences described between the subsets, including gene expression differences, that could impact cell migration (*350*–*352*). Therefore, we next investigated the relationship between the number of nucleus lobes and neutrophil migration more directly. Instead of sorting subsets based on surface marker expression, we labelled total blood neutrophils from endotoxin-treated donors with the fluorescent nuclear dye Hoechst and performed the same microchannel migration assay as before, manually annotating cells according to their number of nuclear lobes (**Figure 2A**). We were able to robustly discern neutrophils with 1-2, 3, and 4 or more nuclear lobes (**Figure 2**). Once annotated, cell movements were tracked (**Movie 2**), and the migratory tracks compared (**Figure 2B**). Our data revealed that 1-2 lobe neutrophils were less able to traverse the smallest 2μm section, as shown by the significantly reduced track displacement, greater percentage of time spent in the 4-

6µm section, and reduced mean speed of 11.3µm/min compared to the 3- and 4-lobe neutrophils which migrated at average speeds of 14.9µm/min and 17.9µm/min, respectively (**Figure 2C-E**). Thus, neutrophils with more segmented nuclei not only traveled faster, but also moved a greater distance despite having similar total track duration and track length (**Figure S2A-C**). Indeed, analyzing neutrophil migration distance towards the chemoattractant as a function of time, we observed that 3 and 4+ nucleus lobe neutrophils migrated across the channel with greater velocity towards the chemokine (8.4µm/min and 11.8µm/min, respectively) than the neutrophils with 1-2 nucleus lobes (4.6µm/min) (**Figure 2F**). Overall our results showed that the variation in migratory speeds observed among neutrophils could be explained by the extent of their nuclear segmentation, and this relationship was more pronounced when grouping neutrophils strictly by their nuclear lobularity, rather than by phenotype-defined subset.

Our study of the migratory behaviour of unmanipulated human neutrophils provides evidence supporting the theory that nuclear segmentation facilitates cell navigation of tight spaces. We previously reported non-segmented banded neutrophils were not restrained in 3D collagen matrices (*348*). However, these complex matrices have variable pore sizes (*243*) and neutrophils have been shown to probe for the widest path (*340*). Here, we precisely defined the environmental constraints imposed on neutrophils using custom-designed microfluidic devices to prevent them from choosing the widest path, and force them into ever tighter channels. In capturing the dynamics of individual neutrophils migrating through decreasing path widths, we observed that banded neutrophils were less able to traverse the smallest 2µm section than segmented and hypersegmented neutrophils. Moreover, we showed that the effect of nuclear lobularity on migratory behaviour is greater than that of neutrophil subtype defined by CD16 and CD62L expression. This supports the conclusion that neutrophil lobularity, rather than their functional subset plays a greater role in determining migration efficiency in this context. However, there may be gene expression changes that track with lobulation that we have not examined in the

present study, and we cannot rule out a role for an unidentified factor correlating with nuclear lobularity that is impacting neutrophil migratory differences. Nonetheless, our work gives credence to the idea that neutrophils may have evolved their nuclear shape to better navigate through narrow pores, enabling their function as 'first responders' in tissue upon insult or injury.

In cells containing classically round nuclei, this large rigid organelle is a hinderance to migration. Cells passing through small constrictions can experience nuclear blebbing, lamina rupture, and nuclear envelope rupture (*85–87*, *353*). If this is the case, the reduction of intranuclear pressure as well as lesser steric hinderance when the nucleus is segmented may explain the ability of neutrophils with greater number of nuclear lobes to pass through tighter constrictions with relative ease. It has also been described that the neutrophil nucleus, rather than deforming, can unfold to migrate through tight pores (*243*). Future investigations into the biophysical properties of the differentially segmented neutrophil nuclei, such as rigidity and flexibility, will better define the mechanism by which neutrophils migrate with such efficiency.

The notion that neutrophils are a short-lived, homogeneous population has been increasingly challenged in studies of neutrophils at homeostasis and in various pathological states such as infection and cancer (*154*, *298*, *299*, *354–357*). Indeed, the presence of neutrophils with different functional capabilities can have significant effects on disease outcome. Our data suggests that an important variable in characterizing neutrophil heterogeneity with regard to their migratory behaviour is the extent of nuclear lobulation. It will be interesting to investigate whether among neutrophils there are differences with regard to arrival time at a site of local tissue injury and infection, with hypersegmented neutrophils reaching sites in denser tissue first, and their subsequent inflammatory response rendering tissue more permissive for banded neutrophils and other mono-lobed leukocytes to infiltrate.

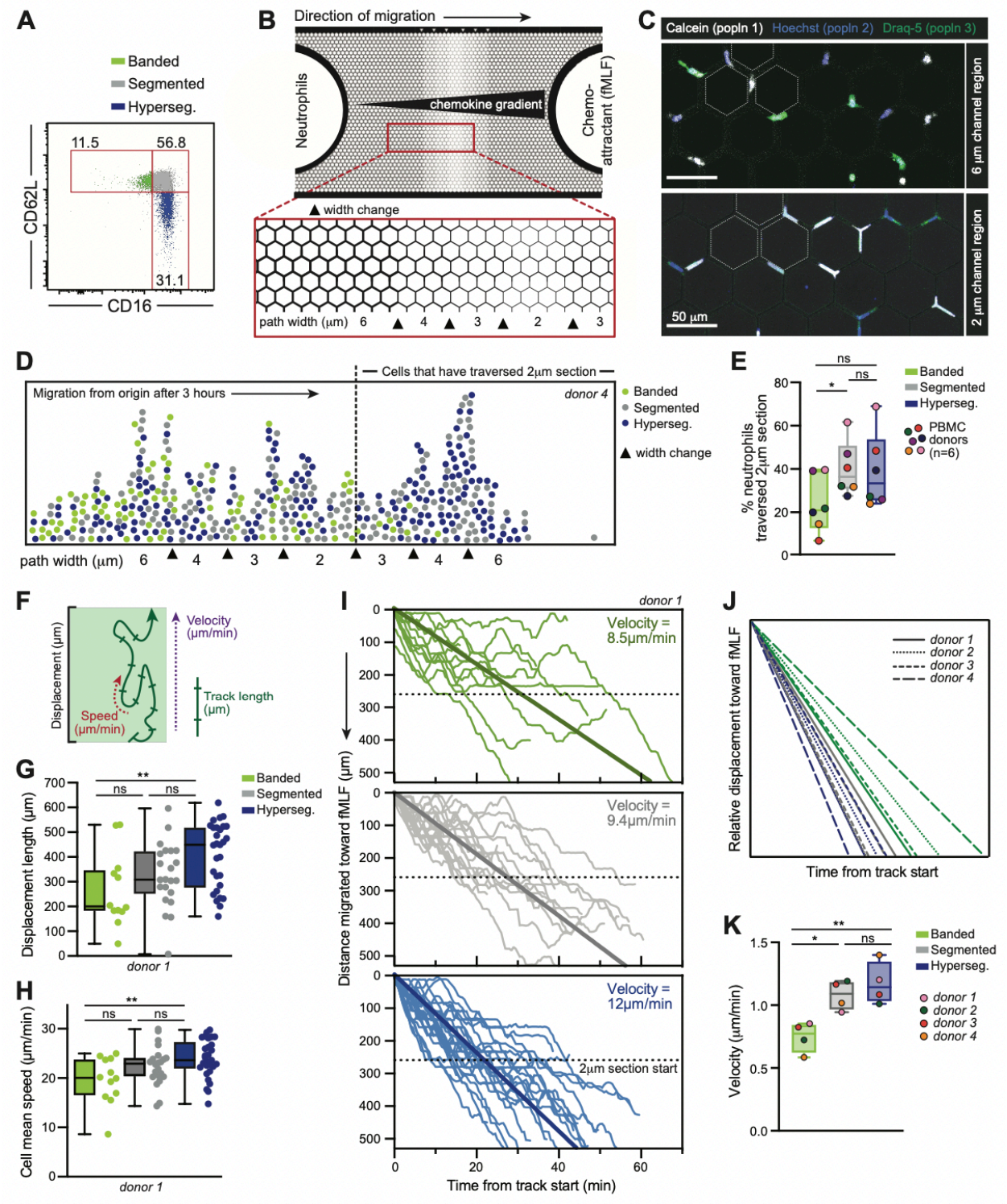
A
Banded
Segmented
Hyperseg.
11.5
56.8
31.1
CD62L
CD16
B
Direction of migration
Neutrophils
chemokine gradient
Chemo-attractant (fMLF)
width change
path width (μm) 6 4 3 2 3
C
Calcein (popln 1) Hoechst (popln 2) Draq-5 (popln 3)
6 μm channel region
2 μm channel region
50 μm
D
Cells that have traversed 2μm section
Migration from origin after 3 hours
donor 4
Banded
Segmented
Hyperseg.
width change
path width (μm) 6 4 3 2 3 4 6
E
ns
ns
*
Banded
Segmented
Hyperseg.
PBMC donors (n=6)
% neutrophils traversed 2μm section
F
Displacement (μm)
Velocity (μm/min)
Track length (μm)
Speed (μm/min)
G
**
ns
ns
Banded
Segmented
Hyperseg.
Displacement length (μm)
donor 1
H
**
ns
ns
Cell mean speed (μm/min)
donor 1
I
donor 1
Velocity = 8.5μm/min
Velocity = 9.4μm/min
Velocity = 12μm/min
2μm section start
Distance migrated toward fMLF (μm)
Time from track start (min)
J
donor 1
donor 2
donor 3
donor 4
Relative displacement toward fMLF
Time from track start
K
**
*
ns
Banded
Segmented
Hyperseg.
donor 1
donor 2
donor 3
donor 4
Velocity (μm/min)

Figure 1. Neutrophil subsets display differential ability to migrate through tight spaces.

(A) Representative FACS plot of CD16 and CD62L expression by neutrophils sorted from blood 3 hours after low-dose endotoxin administration. Numbers indicate percent of cells in each gate. (B) Schematic of pillar forest custom-made microfluidic device used in migration assays. Neutrophils were seeded on one side and 10^{-7}M fMLF chemoattractant added on the other side, such that cells migrate across the pillar forest in paths that decrease in width in a step-wise fashion from 6μm to 4μm to 3μm to 2μm along the chemokine gradient. (C) Example static image of three subsets of sorted neutrophils differentially stained with fluorescent dyes (Hoechst 33342, Calcein-AM, or Draq-5). Fluorescent neutrophils are visualized either by a static tile scan of the entire microchannel when at least 25% of cell pass through the 2μm section (D-E), or by time lapse microscopy (F-K). (D) Representative example from donor 4 of distance migrated by each neutrophil subset within pillar forest after 3 hours. Path width changes are indicated by triangular arrow heads; dotted line represents the point at which cells have traversed the 2μm section. (E) Quantification of % cells that have crossed the 2μm section (as shown in D). Data is from n=6 human donors, 150-450 cells analyzed per donor. P values from one-way ANOVA are shown; *$P \leq 0.05$. (F) Schematic illustrating the measured cell migration parameters: track length, speed, displacement, and velocity. Track length is the total distance the cell has travelled. Speed is the rate of movement along the track. Displacement is the total distance travelled towards the chemokine. Velocity is the rate of movement towards the direction of the chemokine over the course of the cell track. (G, H, I) Representative plots of total displacement length (G), and cell mean speed (H), calculated by neutrophil subset. P values from one-way ANOVA are shown; *$P \leq 0.05$. Normalized tracks (I) by subset shown from one donor (donor 1), total of n=63 cells. Tracks are displayed as distance migrated along the x-axis, towards chemoattractant, as a function of time. Velocities were calculated as an average of the simple linear regression of each track. Dotted lines indicate the start of the 2μm section. (J,K) Relative velocities were calculated as in (I) for n=4 different donors, 40-65 cells analyzed per donor. Velocities were normalized to the average velocity within each donor. Average velocities shown by subset (J) and bar graph showing normalized velocity as calculated per donor (K). P values from one-way ANOVA are shown; *$P \leq 0.05$, **$P \leq 0.01$.

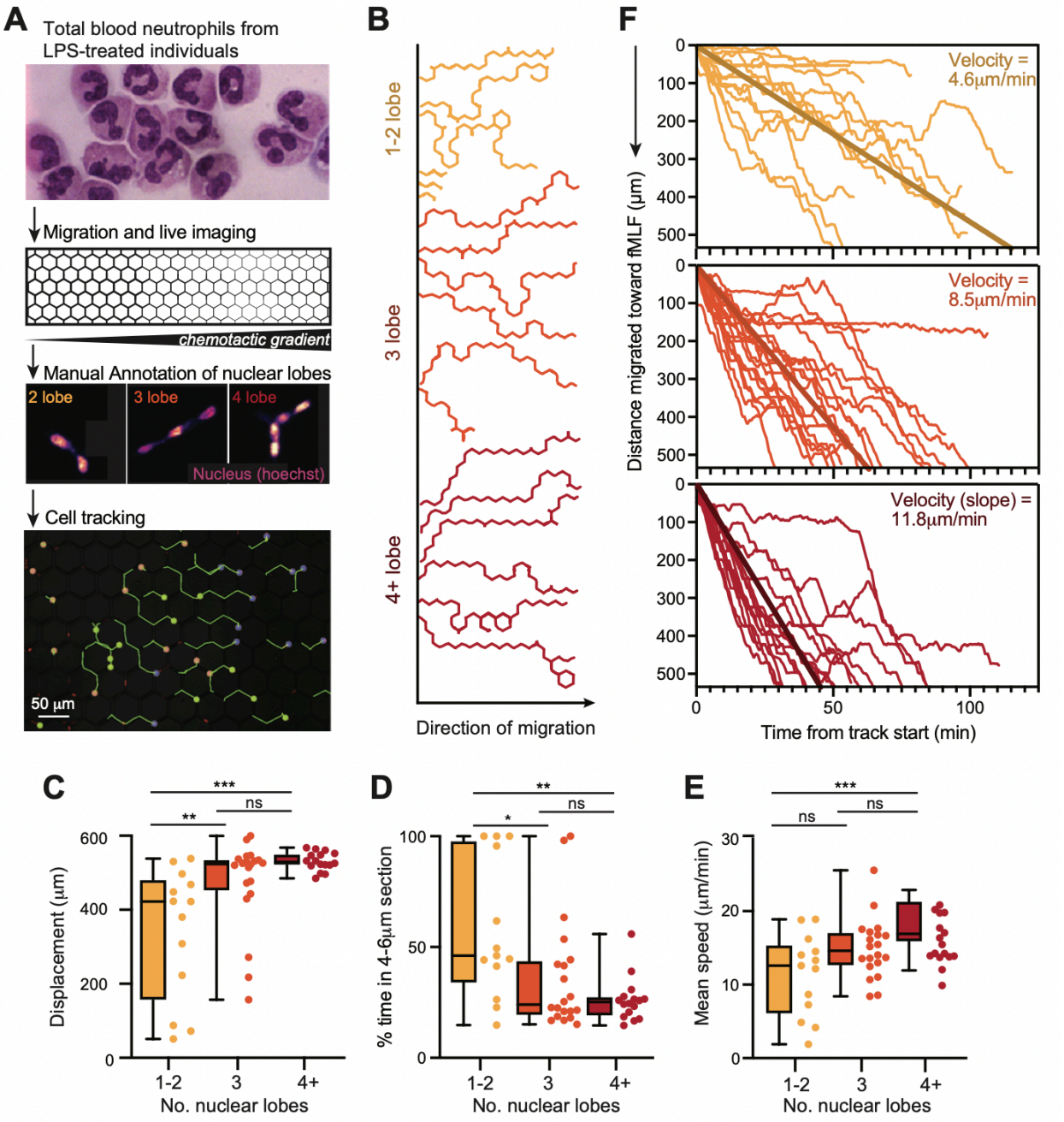
A
Total blood neutrophils from LPS-treated individuals
Migration and live imaging
chemotactic gradient
Manual Annotation of nuclear lobes
2 lobe
3 lobe
4 lobe
Nucleus (hoechst)
Cell tracking
50 µm
B
1-2 lobe
3 lobe
4+ lobe
Direction of migration
F
Velocity = 4.6µm/min
Velocity = 8.5µm/min
Velocity (slope) = 11.8µm/min
Distance migrated toward fMLF (µm)
Time from track start (min)
C
Displacement (µm)
No. nuclear lobes
D
% time in 4-6µm section
No. nuclear lobes
E
Mean speed (µm/min)
No. nuclear lobes
ns

Figure 2. Greater nuclear lobularity in neutrophils confers increased migratory capacity

(A) Schematic of work flow: after 3 hours of i.v. endotoxin administration, total blood neutrophils were stained with nuclear dye Hoechst, run through pillar forest migration assay, and cells visualized by time lapse microscopy. Videos were analyzed by cell tracking and manual nucleus lobule annotation into 1-2, 3, and 4+ lobes. Examples annotations and tracking data are shown. (B) Representative example of cell tracks, as relative X and Y coordinates, shown by nucleus lobularity group. (C,D,E) Total displacement length (C), % time spent in the 4-6μm section (D), and cell mean speed (E), calculated by nucleus lobularity group. P values from one-way ANOVA are shown; $*P \leq 0.05$, $**P \leq 0.01$, $***P \leq 0.001$. (F) Normalized tracks by subset shown from one donor, n=49 cells. All tracks are shown including those in (B). Tracks are displayed as distance migrated along the x-axis, towards chemoattractant, as a function of time. Slopes were calculated as an average simple linear regression of each track.

Human blood samples

For volunteers treated with endotoxin, blood samples were acquired from a random 17 out of 100 volunteers who participated in the 100LPS human endotoxemia study (NL68166.091.18, CMO: 2018-4983). All volunteers signed a written informed consent. The study was approved by the ethics review board of the Radboud University Medical Center. Participants were both male and female, aged 18-35, and were healthy as confirmed by physical examination, electrocardiography, medical history and multiple laboratory tests. Among the exclusion criteria were pregnancy, smoking and recent hospital admission.

On the day of the LPS challenge volunteers were hospitalized at the Radboud University Medical Center, and received a single intravenous administration of 1ng/kg LPS (Escherichia coli O:113, List Biological Laboratories Inc., Campbell, California, US), inducing controlled systemic inflammation. Participants were constantly monitored by a care physician for sepsis related symptoms such as high blood pressure, high heart rate, fever and more. Blood samples were collected three hours after LPS administration. For non-endotoxin treated controls, human blood samples were obtained from healthy volunteers both male and female, age 18-65. All donors signed an informed consent and sampling was approved by the Biobanks Review Committee of the University Medical Center Utrecht (approval code 18/774, approval date 25 June 2013).

Neutrophil isolation

Blood samples were collected in sodium heparin tubes. Cold (4°C) shock buffer (0.1 mM Na2EDTA, 10 mM KHCO3, and 150 mM NH4Cl in double distilled water with a pH adjusted to 7.4) was added to the blood to lyse erythrocytes. Next, white blood cells were washed once with PBS2+ (0.32% sodium citrate and 4g/L human albumin in phosphate-buffered saline) and stained with antibodies against CD16 (Beckman

Coulter, 3G8) and CD62L (Biolegend, DREG-56) at 1:100 dilution. After staining, neutrophil subsets were sorted using a BD FACSAria TM 3 Cell sorter (BD). First, singlets were selected based on forward scatter height (FSC-H) and forward scatter area (FSC-A). Neutrophils were gated by forward and side scatter area, whereafter neutrophil subsets were sorted on differential CD16 and CD62L expression levels (**Fig. 1**). Sorted subsets were acquired in FACS tubes containing PBS2+ buffer. For experiments using total neutrophils, these were isolated from blood by Ficoll density separation. In short, whole blood samples from healthy controls were diluted 1:1 in PBS2+ and layered on Ficoll-Paque Plus (GE Healthcare) followed by the red blood cell shocking procedure described above. Cells were washed with HEPES3+ buffer containing 20mM HEPES, 132mM NaCl, 6mM KCl, 1mM MgSO4, 1.2mM KH2PO4, 1.0mM CaCl2, 5mM glucose and 5 mg/ml human serum albumin (Albuman 200 g/l, Sanquin, Amsterdam, The Netherlands) at a pH adjusted to 7.4. This procedure yielded a purity of >90% neutrophils. Isolated neutrophils were stained with either Hoechst 33342 (AnaSpec Inc., 4µM), Calcein-AM (Molecular probes, 0.25µM) or Draq-5 (eBioscience, 20µM).

Cytospins and nuclear morphology

Neutrophils were seeded on a standard microscope slide (Menzel-Glaser, Thermo scientific) using a cytocentrifuge (Shandon cytospin 2, Block Scientific INC). May-Grünwald (Merck) and Giemsa (Merck) staining was applied and images were obtained with an Axioskop 40 microscope (Zeiss). Lobes were classified as separate when the connection between two adjacent lobes was smaller than 1/3 of the width of the adjacent nucleus.

Microfluidic channels

Microfluidic devices were prepared as previously described. Briefly, polydimethylsiloxane (PDMS) (Momentive performance materials, RTV615) was poured into our custom-design molds previously manufactured (4D Cell). Air bubbles were removed by vacuum chamber then incubated for 1 hour at 100°C or 24 hours at

room temperature. PDMS microfluidic devices were removed from the molds with isopropanol and cleaned with ethanol. The devices were plasma cleaned on high intensity for 2 minutes. PDMS molds were then irreversibly bound to a glass-bottomed dish (WPI FluoroDish). Prior to use, microchannels were plasma cleaned on high intensity for 3 minutes. Channels were coated with 10% human albumin (200g/L) in phosphate buffered saline for 1 hour at 37°C, 5% CO2. Thereafter, channels were incubated with HEPES3+ buffer. In between coating and incubation steps wells were washed with PBS2+.

Migration assays and microscope image acquisition

Fluorescently labeled neutrophils (Hoechst 33342, Calcein-AM, or Draq-5, as described above) were mixed together in a 1:1:1 ratio with a final concentration of $1x10^8$ neutrophils/mL and loaded into the seeding well of the microfluidic channel. The well on the other side of the microfluidic channel was loaded with 10^{-7}M fMLF chemoattractant (Sigma Aldrich). Microfluidic channels were imaged with a confocal microscope (Zeiss, LSM710) or a fluorescence microscope (Olympus, IX83). Time lapses of one focal plane were made with a 20x air objective and a 30 second interval per timepoint. Microfluidic channels were maintained at 37°C. To exclude the possibility of staining dyes influencing neutrophil migration, the dyes were rotated for the 3 subsets across experiments.

Analysis

Static images were processed and quantified with Fiji (ImageJ). Time lapses were processed and analyzed with Imaris (version 9.1) and Python (version 3.8). Data was graphed and statistics performed using Prism 8. $P < 0.05$ was considered significant and tests used are specified in figure legends.

2.5 ACKNOWLEDGEMENTS

We thank the team at Radboud who performed the endotoxemia study, as well as all our human volunteers for participating in the study and kindly donating blood samples. We would also like to acknowledge the input of Suus Bongers for performing some of the neutrophil subset sorts, Corneli Van Aalst for running FACS sorter, and Tanner Ducharme for custom Python scripts.

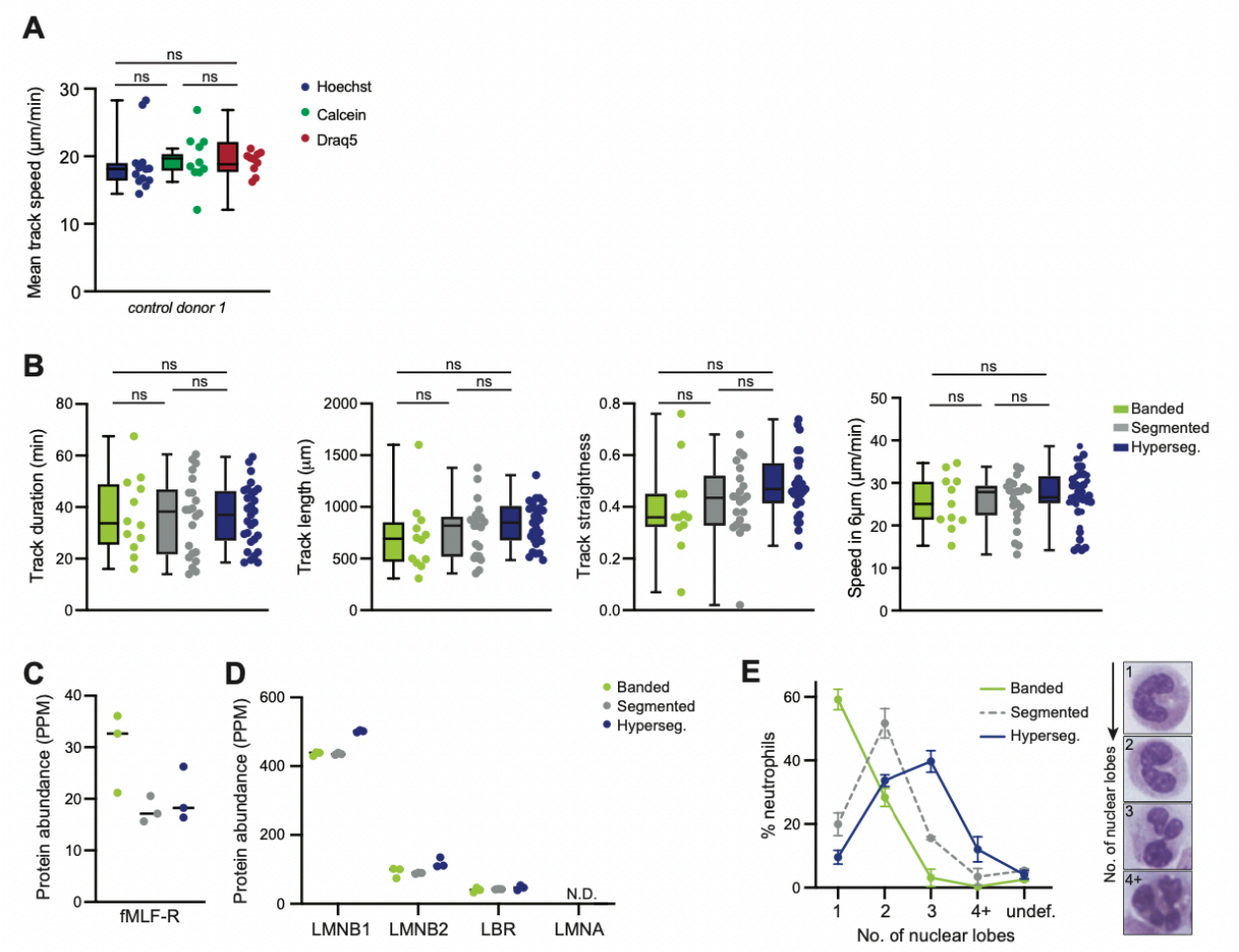

Figure S1. Differences in chemokine receptor expression, nuclear lamina composition and dye-labeling does not explain migration differences between neutrophil subsets.

(A) Total blood neutrophils from a non-endotoxin treated donor were isolated and differentially stained with fluorescent dyes (Hoechst 33342, Calcein-AM, or Draq-5). Mean track speeds are shown from n = 33 cells (**B**) Track duration, track length, track straightness, and cell speed in the 6µm section quantified by neutrophil subset for n=63 cells from one donor. Track duration is the total amount of time the cell is tracked; track length is the total distance the cell has travelled over the course of the track; track straightness is a calculation of the cell displacement / track length; cell speed in the 6µm section is the mean speed at the beginning of each track. P values from one-way ANOVA are shown; *$P \leq 0.05$. **(C, D)** Proteomics of FACS-sorted neutrophils based on CD16 and

CD62L expression from previously published dataset provided at ProteomeXchange Consortium via the PRIDE partner repository (data set identifier PXD001674; DOI: 10.6019/PXD001674). Protein levels for fMLF receptor (C), Lamin B1 (LMNB1), Lamin B2 (LMNB2), Lamin B receptor (LBR), and LaminA/C (D) are shown. N.D., not detectable. **(E)** Quantification of number of lobes per neutrophil in CD16/CD62L-expression sorted subsets from cytospins of May-Grünwald and Giemsa stained cells. Data is quantified from 3 donors, 100 cells per donor. Values shown are median and range.

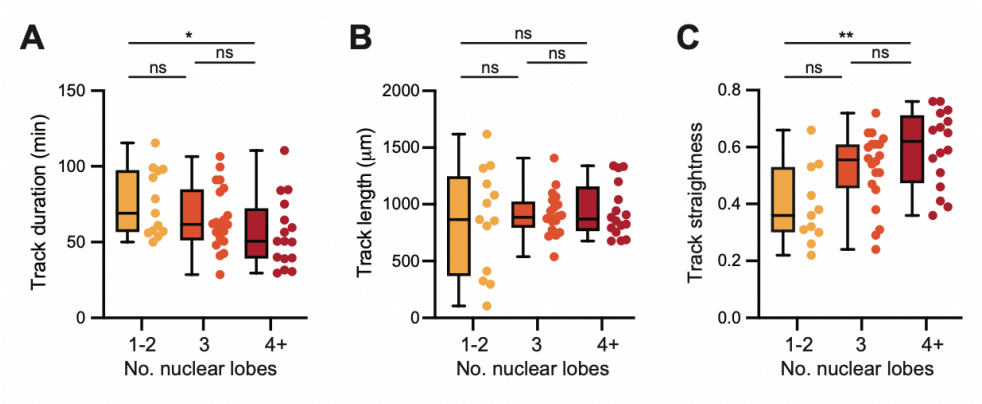

Figure S2. Cell track parameters in neutrophils with different nuclear lobe numbers.

(A) Track duration (total amount of time the cell is tracked), (B) track length (the total distance the cell has travelled over the course of the track), and (C) track straightness (cell displacement / track length) shown by nucleus lobularity group, n=49 cells. P values from one-way ANOVA are shown; *$P \leq 0.05$, **$P \leq 0.01$, ***$P \leq 0.001$.

CHAPTER 3: DOCK8 REGULATES A MECHANOSENSITIVE ACTIN REDISTRIBUTION THAT MAINTAINS IMMUNE CELL COHESION AND PROTECTS THE NUCLEUS DURING MIGRATION

3.1 ABSTRACT

Immune cells navigate through complex 3-dimensional tissue architectures, utilizing an amoeboid mode of migration, characterized by extensive cellular deformation, low adhesion, and high cell velocities. In the absence of expression of *Dedicator of Cytokinesis 8 (Dock8)*, a gene identified with loss-of-function mutations in immunodeficiency, cells become entangled during migration through dense, confined environments and consequently undergo catastrophic cell rupturing, while migration on 2D surfaces remains entirely intact. Here we investigated the specific cytoskeletal defect of *Dock8*-deficient activated T cells, showing that even prior to entanglement they display a striking difference in F-actin distribution compared to wild type (WT) cells. We describe a central pool of F-actin in WT murine and human T cells which is absent in *Dock8* KO T cells, and determine that the relocalization of F-actin is a mechanoresponsive circuit, emerging only when cells are very confined. Our works shows that the central actin pool is nucleo-protective, reducing nuclear deformation and DNA damage during confined migration. We identify the Hippo-pathway kinase Mst1 as a co-mediator of this mechanosensitive pathway in conjunction with Dock8, allowing for cell cohesion and survival during migration through complex environments.

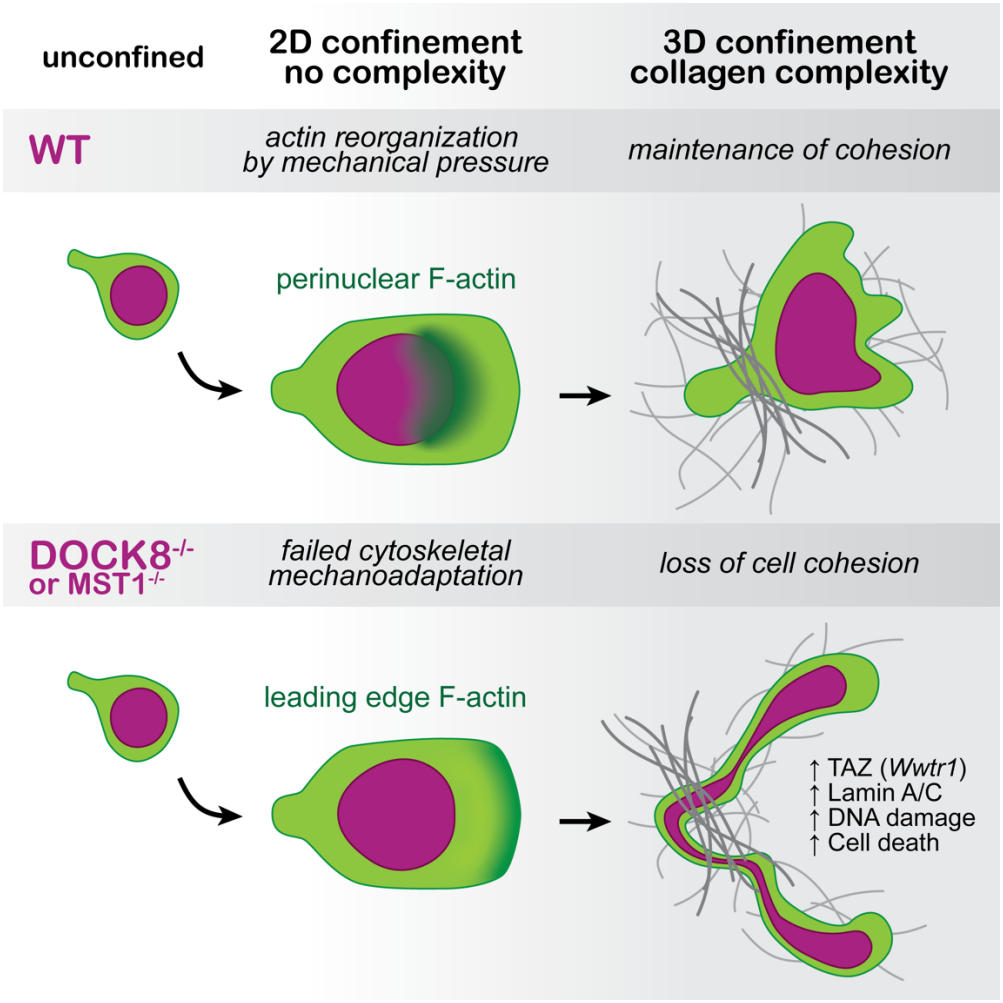
unconfined
2D confinement
no complexity
3D confinement
collagen complexity
WT
actin reorganization
by mechanical pressure
maintenance of cohesion
perinuclear F-actin
DOCK8-/-
or MST1-/-
failed cytoskeletal
mechanoadaptation
loss of cell cohesion
leading edge F-actin
↑ TAZ (Wwtr1)
↑ Lamin A/C
↑ DNA damage
↑ Cell death

3.3 INTRODUCTION

Cell migration is a cornerstone of any immune response. To exert their effector functions and participate in pathogen clearance or tissue homeostasis, leukocytes must be able to traffic throughout the body, transmigrate out of vessels, and traverse diverse tissues in the body which span many distinct architectures, topologies, and mechanical properties (*177*, *231*). How immune cells are able to navigate such a broad range of 3-dimensional (3D) microenvironments – from lymph nodes, to collagen-rich skin, or dense tumours – and the specific cytoskeletal processes that enable them to do so while keeping their cell shape integrity intact, remains incompletely understood.

Studies of cells migrating in 2D on coated glass *in vitro* have been essential in characterizing the fundamental principles which underlie cell motility (*19*). Such 2D studies have described the protrusive filamentous (F-)actin polymerization at the cell front that is driven by the Rho-GTPases Cdc42 and Rac1 and is coupled to actomyosin contractility in the cell rear dominated by RhoA and myosin-II (*358*, *359*). In this setting, integrin-mediated focal adhesions enable cells to pull themselves forward upon polarization (*177*, *359*). In contrast, in complex 3D environments encountered *in vivo,* leukocytes use an 'amoeboid' migration mode where the reliance on, and balance of, adhesive forces required for migration is much more context dependent(*99*, *105*, *106*). When migrating in tissue, leukocyte motion often does not require integrins; instead, cells utilize rapid shape changes to push against tissue topology, generating traction forces with little to no tissue remodelling (*110*, *112*, *360*, *361*). Notably, such pushing forces necessitate an interaction with, and response to, the surrounding substrates, including extracellular matrix (ECM) structures, presumably through mechanically-sensitive pathways (*29*, *362*). Yet, whether and how cell mechano-responses might enable leukocyte shape adaptations during migration even while moving rapidly through highly confined tissue terrains is still unclear.

Mechanical forces can be sensed and responded to by cells through multiple pathways, including through mechanosensitive ion channels, adhesion molecules, the Hippo pathway transcriptional regulators Yap/Taz, and direct effects on the cytoskeleton, which can in turn modify cell state and behavior (*240*, *363*). A major limiting factor for the shape changes required during immune cell migration, and of key importance to cell proprioception, is the nucleus, which is the stiffest and bulkiest organelle in the cell (*45*, *364*). Cells require contractile forces to push the nucleus through small pores (*87*), and use their nuclei as a mechanical gauge, allowing the cell to select the 'path of least resistance' (*58*). This nuclear path-sensing is one way in which immune cells can integrate mechanical information about the environment into effective locomotion. In addition, nuclear envelope deformation triggers actomyosin contractility via calcium dependent activation of the phospholipase $cPLA_2$ which leads to arachidonic acid release (*280*, *281*). Overall, the physical confinement experienced by immune cells when embedded in tissues, together with the extreme shape deformations they have to undergo to squeeze past obstacles, imposes challenges on the cell that may require additional or alternate molecular pathways to maintain their cohesion that are dispensable in 2D.

Inherited defects in immune cell migration provide an opportunity to probe the specific pathways required in navigating 3D tissue environments. Such is the case with the loss of expression of *dedicator of cytokinesis 8* (Dock8), which we and others have previously described to be critical for cell shape integrity during migration in highly confined 3D environments for T cells and dendritic cells (DCs) (*5*, *215*, *224*). *Dock8* KO cells display dysregulated morphology, loss of cell cohesion, and ultimately cell death by migration-induced shattering, termed 'cytothripsis' (*224*). Dock8 is an atypical guanine exchange factor (GEF) expressed only in immune cells which binds and regulates Rho GTPases by facilitating the exchange of GDP for GTP (*209*). Dock8 belongs to the 11-member family of DOCK180-related GEFs, a family that can interact with GTPases such as Rac, RhoA, and Cdc42, which are important for actin and cytoskeletal rearrangements implicated in cellular functions such as cell motility,

growth, survival, polarity, and differentiation (*212*, *365*). Rho GTPases modulate actin polymerization through actin binding proteins such as Arp2/3, via activation of nucleation promoting factors such as WASP and WAVE [5,6](*16*, *366*, *367*). Importantly, failure of *Dock8*-deficient leukocytes to migrate effectively in tissues leads to an immunodeficiency clinically characterized by disseminated cutaneous and systemic infections, hyper IgE syndrome, and allergic disease (*201*, *202*, *206*).

Here, we employed *in vitro* migration assays to understand the molecular underpinnings of how Dock8 regulates cell cohesion and nuclear integrity in T cells. We found that in the absence of environmental complexity, *Dock8*-deficient T cells display no detectable cytoskeletal defects, and in fact migrate at greater speeds and pass through narrow pores with greater ease than wild type (WT) T cells. However, in confined conditions, Dock8 is required for a redistribution of F-actin from the cell front to the cell center near the nucleus. Our data suggest that this central F-actin pool protects the nucleus, prevents force-mediated DNA damage, and is key to balancing the forward propulsion of the cell's leading edge with the necessity to maintain cohesion as the cell becomes stretched in confined spaces. We determined that this mechanosensitive actin redistribution response is dependent on both Dock8 and the Hippo-pathway kinase Mst1. Together, our data indicate that Dock8 is therefore a critical mediator of leukocyte mechanosensing during migration in 3D environments.

Loss of cell cohesion and consequent death of migrating *Dock8* KO T cells is collagen density-dependent

To investigate the impact of *Dock8*-deficiency on immune cell migration dynamics in 3D, we focused on activated T cells, which upon antigen encounter *in vivo* gain access to a variety of non-lymphoid tissue landscapes to curtail pathogen spread (*170*). As one of the softest immune cell types (*258*), T cells have the challenging task to maintain cell cohesion even as they deform to traverse tight gaps in the ECM or between other cells. We activated WT or *Dock8* KO murine T cells *in vitro* using anti-CD3/CD28 for 4 days and then embedded them in bovine collagen gels, previously used to mimic complex 3D tissue structure *in vitro* (*368*), and in which T cells move spontaneously without the addition of chemokine. Characteristic of their amoeboid migration in these gels, WT T cells frequently and rapidly modulated their shape to navigate past collagen fibers, but *Dock8* KO T cells displayed much greater shape distortions, including extreme elongations (**Fig. 1a** and **Video S1**). Such cell elongation and entanglement of *Dock8* KO T cells was not necessarily permanent in all instances, as some cells recovered to resume motility (**Fig. 1a,** bottom example). Notably, as shown previously, the addition of CCL19 to one side of the collagen gel to generate a gradient showed that chemotaxis by *Dock8* KO T cells in 3D collagen remained intact, although cell speed was slightly decreased, as was track straightness (**Fig. S1a-c**).

Next, we examined microtubule and F-actin arrangement in fixed WT and *Dock8* KO T cells migrating in collagen. Motile WT T cells had a polarized morphology with the microtubule organizing center (MTOC) in the uropod, the actin-rich cell front probing into the environment, and the nucleus deforming to fit through the constraints imposed by the collagen matrix (**Fig. 1b,** examples 1 and 2). In *Dock8* KO T cells migrating normally, the gross morphology observed in WT T cells was conserved, with no defect in cell polarization (**Fig. 1b,** examples 3 and 4). However, in entangled

Dock8 KO T cells, both the tubulin and F-actin organization was substantially dysregulated, with the nucleus stretched throughout the entire cell body. Most commonly, entangled *Dock8* KO cells had two competing cellular fronts at opposite ends, with more diffuse tubulin throughout the cell, and a centrally located MTOC (**Fig. 1b**, examples 6 and 7, and **S1d**). Less commonly, *Dock8* KO cell rears were 'stuck' in the matrix with the cell front continuing to advance (**Fig. 1b**, example 5 and 8). Overall, entangled *Dock8* KO T cells were exclusively bipolar (**Video S2**), different to what was observed in *Dock8* KO DCs (*5*).

Importantly, the collagen-rich and highly cross-linked ECM structure of the skin may explain the inability of *Dock8* KO T cells to control skin viral and bacterial infections in particular, hence leading to the characteristic cutaneous manifestations of Dock8-deficiency (*205*, *224*). Thus, we next explored the relationship between collagen density and the dependence of T cells on *Dock8* expression for cell shape integrity in 3D by comparing cell morphology in 1.5, 2 or 4 mg/ml collagen which differed in fiber density, pore size, and scaffold stiffness (**Fig. S1e,f**) (*243*). To systematically quantify cell shape integrity in WT and *Dock8* KO T cells at low or high collagen concentrations, we fixed cells after 4 hours of migration when the majority of both WT and *Dock8* KO cells were still viable, extracted cell shape outlines which we parameterized with 20 cell morphology descriptors (**Table S1**), and performed a principal component analysis (PCA). We found that entangled *Dock8* KO cells reliably segregated from the majority of cells along PC1 based on cell shape alone (**Fig. 1c**). The cell aspect ratio (the length of the major cell axis divided by the minor axis) was one of the best predictors of cell entanglement (increased by ~3-fold in *Dock8* KO cells that had lost their shape integrity), corroborating the consistently elongated shape characteristic of entangled T cells (**Fig. 1b**). While staining for F-actin showed that WT T cells became increasingly constrained as the collagen concentration increased, most evident from the increasingly irregularly shaped cell front as cells were probing tighter paths, they nonetheless maintained shape integrity (**Fig. S1g**). In contrast, *Dock8* KO T cells became entangled at all collagen densities tested, but the fraction

of entangled cells increased with greater collagen density (**Fig. 1e** and **S1g**). Moreover, *Dock8* KO T cell viability after 24 hours of migrating in collagen decreased as collagen density was increased, correlating with the fraction of cells that lost cohesion (**Fig. 1f**). Together, our data showed that *Dock8* KO T cells have a defect in 3D migration whereby cells became increasingly entangled, lost cell shape integrity, and died as collagen concentration, and thus environmental complexity, was increased.

Dock8 KO T cells navigate simple environments and tight constrictions with no impairment

To better understand the migration defect observed in *Dock8* KO T cells, we next investigated their motility in simplified environments where we could precisely control the specific constraints or obstacles encountered (without chemokine added). For this, we turned to fibronectin-coated microfluidic devices fabricated from polydimethylsiloxane (PDMS) (**Fig. 2a**)(*369*). First, we characterized cell migration speeds in one-dimensional straight channels wide and high enough (6mm x 5mm) for activated T cells to traverse easily without deformation. Surprisingly, we found that *Dock8* KO T cells were considerably (~1.6 fold) faster on average than WT T cells (**Fig. 2b,c** and **Video S3**). The greater migration speed of *Dock8* KO T cells was maintained in pillar forests (~1.5 fold fast than WT T cells), in which cells had to navigate obstacles and bifurcating paths but channel widths and heights were the same as for the straight channels (**Fig. 2d,e**). Notably, we did not observe the loss of cell cohesion of *Dock8* KO T cells in the simple lattice structure of the pillar forests (**Fig. 2e** and **Video S4**).

As the loss of cell shape integrity of *Dock8* KO T cells in collagen matrices appeared to be triggered by becoming stuck in the collagen fiber mesh, we next asked whether *Dock8* KO T cells had difficulty traversing narrow constrictions. To address this, we used straight channels as before, but incorporated constrictions 15 μm in length, ranging from 1.5 to 4 μm in width. Surprisingly, we found that *Dock8* KO T cells

successfully passed through even the smallest constrictions at a greater frequency compared to WT T cells, and of T cells able to pass through constrictions, the passage time of *Dock8* KO cells was consistently shorter than that of WT counterparts (**Fig. 2f-h** and **Video S5**). A rate-limiting step in the ability of cells to squeeze through tight spaces is the rigidity of the nucleus (*45*), the largest organelle in the cell, and transient nuclear envelope rupture has been shown to occur in some cell types to facilitate passage of constrictions (*85*, *86*). Thus, the greater ease with which *Dock8* KO T cells traversed narrow constrictions could indicate either that *Dock8* KO T cells (and their nuclei) are inherently more deformable, or that their nuclear envelope is more prone to rupture, enabling passage through constrictions. Our observation that the nucleus in entangled *Dock8* KO cells was stretched could be compatible with either explanation, given that we used the DNA intercalating agent Hoechst to visualize the nucleus in collagen (**Fig. 1b**). To date, it has not been investigated whether nuclear envelope rupture could impact T cell migration through small pores. To probe this further, we isolated T cells from mice expressing tdTomato fluorescent protein with a nuclear localization signal (NLS-nTnG) and examined whether *Dock8* KO T cells underwent nuclear rupture when passing through constrictions. We found that in both WT and *Dock8* KO T cells passing through even the smallest 1.5 μm widths, nuclear envelope rupture was a rare occurrence, accounting for fewer than 1% of all observed passing events (data not shown). When nuclear envelope ruptures did occur, the fluorescent reporter leaked into the cell body and could be detected in the cell cytoplasm (**Fig. S2a** and **Video S6**). Similarly, we found that although the nucleus of *Dock8* KO T cells entangled in collagen matrices lost its shape integrity, the nuclear envelope remained intact (**Fig. S2b** and **Video S7**). These results indicate that *Dock8* KO T cells are inherently faster than WT T cells when migrating in simple environments, and that KO cells have more deformable nuclei without increased susceptibility to nuclear envelope rupture.

Dock8 is necessary for a mechanoresponsive, integrin-independent redistribution of F-actin

Because we observed that simple environmental obstacles such as pillars or constrictions did not lead to loss of cell shape cohesion in *Dock8* KO T cells, we next asked whether confinement in the absence of obstacles would present a challenge, and whether a dysregulation of the organization of intracellular compartments or organelles in *Dock8* KO T cells might play a role in the migration defect. To do so, we utilized an under-agarose assay, where cells migrated freely in 2D, compressed between a fibronectin-coated glass slide and a pad of agarose, towards the chemokine CCL19 (*370*). We found no difference in the arrangement or levels of acetylated tubulin or α-tubulin, the location of the MTOC, levels or location of G-actin, mitochondria, lysosomes or vimentin between migrating WT or *Dock8* KO T cells (**Fig. S3a-e)**. However, we observed a striking difference in the localization of F-actin stained in fixed cells (using phalloidin) between confined WT and *Dock8* KO T cells (**Fig. 3a**). Without confinement, both WT and *Dock8* KO T cells migrating in 2D had the expected enrichment of F-actin at the leading edge with little actin polymerization occurring at the cell centroid (**Fig. 3a,b**). In contrast, in confined WT T cells, a distinct pool of F-actin appeared in the cell center which was entirely absent across all *Dock8* KO T cells analysed (**Fig. 3a,b**). This difference in F-actin localization reflected a change in distribution, as the total F-actin levels were similar between WT and *Dock8* KO T cells (**Fig. S3f,g**). Notably, when *Dock8* KO T cells encountered other cells under agarose, this was sufficient to lead to an entangled phenotype as observed in the collagen gels (**Fig. S3h** and **Fig. 1**). The phenotype of cells with a loss in shape integrity had a quite distinct organization from *Dock8* KO T cells undergoing cell division (**Fig. S3i**).

To further characterize the confinement-dependent central F-actin pool, we tracked the dynamics of cortical actin in direct contact with the fibronectin-coated glass in LifeAct-GFP expressing T cells, using total internal reflection fluorescence (TIRF) microscopy. In WT T cells we observed the transient appearance of many small actin patches throughout the cell, which existed on the time scale of seconds (**Fig. 3c**), as were noted also in confined DCs (*362*). In *Dock8* KO T cells, these transient actin

patches were reduced in number, and the majority of F-actin was distributed more uniformly at the cell front (**Fig. 3c** and **Video S8**). Examining the entirety of LifeAct-GFP T cells by widefield microscopy, we again observed a clear F-actin pool in the center of the WT T cells that, while dynamic in shape and intensity, was stable in its location at the mid-zone of the cell, and which was completely absent in *Dock8* KO T cells (**Fig. 3d** and **Video S9**). As the appearance of the central F-actin cloud was only seen under confinement, we next asked whether this mechanosensitive F-actin response would be modulated by the rigidity of confining agar. To address this, we titrated the percent agarose from 0.5 to 2% to increase the degree of mechanical load (*320*). Indeed, the fluorescence intensity at the cell centroid of F-actin scaled with the percent agarose in WT T cells (**Fig. 3e,f**). Moreover, even at the highest agarose percent and thus the greatest level of confinement, *Dock8* KO T cells did not redistribute F-actin to the cell center (**Fig. 3e,f**).

Although dispensable for T cell motility under confinement (*112*), integrins are a well-described mediator of mechanotransduction (*240*), and in NK cells Dock8 was found to be part of a multi-protein complex that included talin1, a required cytosolic adaptor protein for integrin-mediated signaling (*221*). Thus, we next tested whether the mechanosensitive F-actin rearrangement in WT T cells was dependent on integrin signaling by confining talin1-deficient (*Tln1* KO) T cells under agarose. *Tln1* KO T cells were previously shown to be unable to adhere to 2D surfaces (*112*). We found that *Tln1* KO T cells remained similarly able to rearrange the F-actin to the cell center in response to mechanical force as WT T cells, indicating that the appearance of the mechanosensitive F-actin pool did not require integrin signaling (**Fig. 3g**). These data indicated that T cells redistribute cellular actin in direct response to mechanical load and that this mechanosensitive cytoskeletal response requires Dock8 expression but is integrin signaling-independent.

The confinement-induced central actin pool is located at the nucleus front in human and murine T cells

We next sought to understand whether the central F-actin pool was located in a specific region of the cell, particularly in relation to cellular organelles. We hypothesized that its appearance in the cell center might be tied to the location of the nucleus. T cells migrating under-agarose were fixed and stained with both phalloidin and Hoechst, to examine the distribution of F-actin per cell from rear to front. One example T cell of each of WT and *Dock8* KO (**Fig. 4a,b**), as well as across n = 50 cells per genotype (**Fig. 4c**) were analysed. While in confined migrating WT T cells there was a consistent peak in F-actin fluorescence intensity located towards the front of the nucleus, in *Dock8* KO T cells the fluorescence intensity of F-actin was lowest in proximity to the nucleus (**Fig. 4a-c**). Moreover, during migration under confinement, the F-actin cloud in WT T cells, while dynamic alongside cellular shape changes, maintained its position towards the nucleus front in the direction of migration (**Fig. 4d** and **Video S10**). Importantly, we confirmed that the presence and positioning of the confinement-dependent central F-actin pool was similar for migrating activated human T cells (**Fig. 4e**).

Our data thus far suggest that the intensity of the F-actin pool in WT T cells scaled with greater mechanical force imposed by increasing agarose concentrations. To better define the extent of confinement required to elicit the cytoskeletal actin rearrangement, we next used microchannels with variable widths from 8μm to 3μm but constant heights of 5μm, or variable heights of 5μm or 2.5μm but constant widths of 8μm. We showed that only when cells were confined in either widths or heights below 3 μm the F-actin redistribution was triggered in WT T cells (**Fig. 4f,g**). We confirmed that also during migration through confined microchannels *Dock8* KO T cells did not relocate F-actin to the nuclear region (**Fig. 4f,g**). Thus, in both murine and human activated WT T cells, migration under confinement triggers a redistribution of polymerizing actin to a nucleus-proximal central region within cells.

Cytoskeletal response and cell shape cohesion under confinement is Dock8-dependent in dendritic cells, but not neutrophils

Given that we and others have previously described that DCs exhibited migration defects when they lacked Dock8 expression (*5*, *215*), we next investigated whether we also observed a central F-actin pool in bone marrow derived DCs (BMDC) under confinement, and whether it was similarly Dock8-dependent as in T cells. In an under-agarose migration assay, we found that WT BMDCs had a large increase in centrally located actin polymerization that was absent in *Dock8* KO BMDCs (**Fig. S4a**). Compared to WT T cells, the central actin pool in WT BMDCs occupied a much smaller proportion of the cell (**Fig. S4a,b**). We also examined the F-actin distribution within neutrophils migrating under agarose, and unexpectedly detected no centrally relocated F-actin pool in either WT or *Dock8* KO neutrophils (**Fig. S4c**). In both WT and *Dock8* KO cells, the F-actin distribution in confined neutrophils remained largely localized towards the front of the cell, particularly in the protrusive regions (**Fig. S4c**). The absence of the mechanically-induced central F-actin pool in neutrophils suggested the possibility that, unlike T cells and BMDCs, cell shape cohesion during 3D migration of neutrophils might be independent of Dock8 expression. To test this, we embedded LifeAct-GFP and NLS-nTnG-expressing WT and *Dock8* KO neutrophils in 2 mg/ml collagen and followed their morphology over time. Interestingly, *Dock8* KO neutrophils did not lose cell cohesion, become entangled or abnormally stretched during migration (**Fig. S4d,e**). Taken together, BMDCs and T cells, but not neutrophils, rely on a Dock8-dependent mechanosensitive pathway to redistribute actin towards the center of the cell. Moreover, the loss of the central F-actin in Dock8-deficiency leads to a migration defect in 3D in BMDCs and T cells, but is dispensable for cell shape integrity in confined environments in neutrophils.

Dock8-dependent F-actin redistribution in migrating T cells is nucleo-protective

Our data from distinct leukocyte types suggested that the redistribution of F-actin was associated with the maintenance of cell cohesion during 3D migration. We next investigated whether the confinement-induced central F-actin pool might have an additional functional role in migrating cells. To do so, we asked whether *Dock8*-deficiency in T cells led to differences in gene expression. We performed RNA sequencing on WT or *Dock8* KO activated $CD8^+$ T cells after 24 hours of migration in collagen matrices or incubation in media (non-migrating). Interestingly, we found that the majority of gene expression differences appeared in migrating WT compared to KO cells. Only 19 differentially expressed genes (DEG) were identified in the media condition, one of which was *Dock8* itself, compared to 925 DEG identified in collagen-embedded WT versus KO cells (**Fig. 5a**). Examining the pathways which were most perturbed during migration in *Dock8* KO T cells using gene ontology analysis, we found an enrichment of genes related to cell motility, cell death, adhesion, and actomyosin organization, in line with the observed cytoskeletal defect and migration-induced death of *Dock8* KO T cells (**Fig. 5b**). We also found that a number of genes in the 'p53 signaling' pathway, as well as in the 'response to virus' pathway were significantly enriched in migrating *Dock8* KO T cells. This suggested the possibility that *Dock8* KO T cells were accruing DNA damage and activating p53 as a result, with associated type I interferon signaling due to a DNA damage-related response downstream of DNA sensors. Indeed, among upregulated genes in *Dock8* KO T cells was *Aim2* (DNA sensor triggering inflammasome activation), *Oasl1, Oasl2,* and *Mx1* (classic type I IFN response genes), as well as p53 target or DNA damage response-related genes such as *Aen, Cdkn1a, Epha2, Phlda3, Pmaip1* (**Fig. 5c**).

In addition to several cytokine or cytokine receptor genes upregulated in migrating *Dock8* KO T cells compared to their WT counterparts, genes encoding nuclear envelope proteins were differentially regulated (**Fig. 5c**). This included *Lmna*, which encodes for lamin A/C – a component of the meshwork of structural fibrous proteins

protecting the cell's genomic material and a key determinant of nuclear stiffness (*71*, *75*). In our RNA sequencing data, *lmna* expression was comparable between WT T cells in media or collagen and *Dock8* KO T cells in media, but significantly upregulated (~3 fold) in *Dock8* KO T cells migrating in collagen (**Fig. 5d**). When we measured lamin A/C protein levels by flow cytometry, we found that there was a slightly greater level of lamin A/C in *Dock8* KO T cells compared to WT T cells when kept in media, but that this difference increased between KO and WT T cells migrating in collagen (**Fig. 5e,f**). Nuclear stiffening through the increase of lamin A/C has been shown to be a cellular response to mechanical cues (*271*, *275*). This suggests that *Dock8* KO T cells might be experiencing greater mechanical force transmitted onto the nucleus than WT T cells during migration as a result of the loss of the central, nucleus-proximal F-actin cloud, accounting for the DNA damage response signature at the gene level.

To test this idea, we used light sheet microscopy to measure the extent of nuclear compression in WT compared to *Dock8* KO T cells migrating under agarose, hypothesizing that the central F-actin in WT T cells plays a role in protecting the nucleus from force-mediated deformation. Indeed, we found the nuclei of *Dock8* KO T cells were significantly more compressed, and thus had a decreased height under agar than did the nuclei in WT T cells (**Fig. 5g,h**). To connect this observation with the gene expression results, we then asked whether the greater nucleus compression led to DNA damage by allowing WT and *Dock8* KO T cells to migrate in collagen for 12 hours and performing an alkaline comet assay, a method to detect double-stranded DNA breaks. Even with the exclusion of likely apoptotic cells (score 4, comparison with etoposide control which is a DNA damaging agent), we found a substantial increase in the frequency of cells with DNA breaks (scores 1-3) in migrating *Dock8* KO T cells (~38%) compared to WT T cells (~21%) (**Fig. 5i**). Taken together, our data suggest that Dock8 has a nucleo-protective role in migrating T cells, maintaining nuclear shape integrity and thus reducing mechanical force-induced genomic stress.

Mst1 is required for the nucleo-protective central actin pool during migration

Interestingly, individuals with mutations in the serine-threonine protein kinase 4 (*Stk4*) gene, encoding for the mammalian sterile 20-like (Mst1) protein, present with an immunodeficiency that, while not entirely overlapping in clinical presentation, is reminiscent of Dock8-deficiency(*200*). Like for Dock8, loss of Mst1 results in T cell lymphopenia and recurrent cutaneous viral and bacterial infections in particular, as well as eczema and atopic dermatitis (*371–375*). Naïve *Stk4* KO T cells have a defect in egressing the thymus and in trafficking to secondary lymphoid organs, and display reduced motility in 2D migration assays as well as within the lymph node(*376*, *377*). A direct link between Mst1 and Dock8 was suggested by studies showing that Dock8 can bind Mst1 through its N-terminal region(*216*, *378*), and that Mst1 regulates Dock8 via phosphorylation of Mps one binder 1 (Mob1), a Hippo pathway scaffold protein that can then interact with and activate Dock8 to promote Rac1 activity(*376*).

Thus, we next asked whether Mst1 was involved in the Dock8-dependent and confinement-induced redistribution of F-actin in activated T cells. We isolated T cells from *Stk4* KO mice, activated them *in vitro* as before and confined them under agarose. Strikingly, we observed that *Stk4* KO T cells had a similar complete abrogation of the central F-actin pool under confinement as *Dock8* KO T cells, while being indistinguishable from WT T cells when migrating in 2D without confinement (**Fig. 6a**). The loss of the mechanically regulated redistribution of F-actin in *Stk4* KO T cells also led to their entanglement and death in 3D collagen matrices (**Fig. 6b-d**). The phenotype of *Stk4* KO T cells that had lost cell shape cohesion was near-identical to that of *Dock8* KO T cells (**Fig. 6b**), and *Stk4* KO T cells also had increased lamin A/C protein expression, scaling with the density of collagen they were embedded in (**Fig. 6e**). This suggested that *Stk4* KO T cells were experiencing increased mechanical stress similar to *Dock8* KO T cells.

The Hippo pathway, of which Mst1/2 are core components in mammals, ultimately leads to the nuclear translocation of the transcriptional regulators Yap (yes-associated protein) and Taz (WW-domain-containing transcription regulator 1), encoded by *Yap* and *Wwtr1* respectively, which bind to DNA together with TEAD (transcriptional enhanced associated domain) transcription factors (*379*, *380*). Among other functions, Yap/Taz signaling has been shown to be critical in translating mechanical cues, including cell tension, ECM stiffness, cell density, and shear flow forces, into gene expression changes, including the upregulation of *Yap* and *Wwtr1* themselves (*263*). To corroborate the hypothesis that the change in lamin A/C expression was a result of increased mechanosensing in *Dock8* KO and *Stk4* KO T cells, we measured *Wwtr1* expression by qPCR in cells incubated in media, or migrating in 1.5, 2, or 4mg/ml collagen for 24 hours. In WT T cells, *Wwtr1* expression was increasingly upregulated with greater collagen density compared to cells in media (**Fig. 6f**). Interestingly, the titrated response in *Wwtr1* was maintained in both *Dock8* KO and *Stk4* KO T cells, but the upregulation in *Wwtr1* was substantially greater even at low collagen densities compared to WT T cells (**Fig. 6f**). Given this result, we asked whether *Dock8* expression itself might also be mechanically regulated. Indeed, in both WT and *Stk4* KO T cells, *Dock8* transcripts increased with greater collagen density, also confirming that Dock8 expression was intact in Mst1-deficient cells (**Fig. 6g**). These data suggest that together, Mst1 and Dock8 are co-requisite for the mechanosensitive actin redistribution in T cells that is important for cell cohesion, survival, and nuclear protection during migration through confined spaces. Thus, *Dock8* and *Stk4*-deficiency results in cells experiencing greater mechanical forces, and responding with transcriptional changes accordingly, than WT T cells in the same environments.

3.5 DISCUSSION

In most physiological contexts, immune cell migration occurs in highly confined settings, constrained by tissue architecture, ECM structure, and cell density. Here, we report a mechanosensitive cytoskeletal response axis in migrating T cells and DCs. Our data show that Dock8, whose expression is restricted to hematopoietic cells, is required for the redistribution of F-actin under confinement, localizing actin polymerization to the cell center near the nucleus front. Moreover, we found that in addition to Dock8, F-actin rearrangement in confined migrating T cells is dependent on Mst1, a member of the Hippo signaling pathway known to transmit mechanical input into biochemical changes. Importantly, our data suggest that the redistribution of F-actin serves two important functions. One role of the F-actin relocalization is in the maintenance of cell shape integrity during the navigation of tight interstitial spaces. The second function of the central F-actin pool is in preventing DNA damage by shielding the nucleus from mechanical forces. Thus, we have identified a novel mechanism by which cells rapidly integrate mechanical cues as they move through environments that necessitate cell deformation, both in balancing speed with exploration, and in protecting the cell's genomic material.

As leukocytes migrate in increasingly confined environments, the reduction of actin polymerization at the leading edge, with a concomitant increase in the cell center, appears to play a role in ensuring the maintenance of cell shape integrity while rapidly exploring interstitial space. The Arp2/3 and WAVE complex-dependent lamellipodial pool of F-actin is critical for cellular extrusion into the environment and hence promotes exploration (*8*, *30*), but this has to be balanced by actomyosin contractility in the cell rear (*116*, *119*). In *Dock8*-deficient T cells, increased actin polymerization at the lamellipodia results in the leading edge moving faster than the cell rear. This explains both why *Dock8* KO cells become elongated in collagen matrices, and why *Dock8* KO cells attain higher speeds in simple channels and pillar forests. When *Dock8* KO cells are navigating an obstacle while under confinement, they are unable to reconcile the opposing forces of two leading edges and the result is

conflicting cell fronts that can ultimately rip cells apart. The role of Dock8 in reining in actin protrusions only becomes critical under confinement, because in obstacle-free settings the cell rear is able to 'keep up' with the cell front. This is in line with prior studies which establish that rear contraction is dispensable in less constrained environments (*110*). Intriguingly, we found that unlike T cells and DCs, neutrophils did not exhibit the same F-actin rearrangement in response to mechanical pressure, and *Dock8* KO neutrophils did not lose cell cohesion while migrating in confined environments. One major difference between neutrophils and other leukocytes is their unique multi-lobulated nucleus, which allows for greater deformability (*1*). Perhaps neutrophils, with a more malleable nucleus, and a reduced need to protect genomic material due to their terminal differentiation and shorter life span (*156*), do not have the same requirement for a perinuclear F-actin structure when confined. Different immune cell types may thus have a differential dependence on Dock8 expression, and other mechanosensitive mechanisms by which neutrophils maintain cell cohesion during 3D migration independent of Dock8 will have to be further investigated.

The precise molecular machinery by which Dock8 relocalizes F-actin remains to be elucidated. Dock8 contains a DHR-1 domain, which binds PI(3,4,5)P3 (phosphatidylinositol 3,4,5-trisphosphate) in the membrane (*381*). One hypothesis is that Dock8 actin regulation is mediated by PIP(3,4,5)P3, a lipid involved in promoting actin polymerization at specific regions of the cellular cortex (*134*). Alternatively, the interaction of Dock8 with Cdc42 via its DHR-2 domain, which has specific catalytic activity as a GEF (*215*), could play a role. In T cells, Dock8 exists in complex with WIP and WASp to promote Cdc42 activity (*382*). In migrating DCs in 2D, loss of Cdc42 leads to the presence of multiple leading edges, and in 3D their motility is almost completely abrogated (*383*). Interestingly, in T cells loss of Cdc42 or PAK1/2 led to a similar cellular elongation and loss of shape integrity as observed in Dock8-deficiency, but neither inhibition of Rac1 or WASp impacted cell shape during migration (*224*). Dock8 interaction with WASp is therefore unlikely the mechanism

of cytoskeletal coordination observed under confinement, but the localization or activation of Cdc42 within the cell may contribute. It was recently shown that WASp regulates the formation of small mechanosensitive actin foci which push outwards against the environment orthogonally to cellular movement (*362*), and using TIRF microscopy we observed a reduction, albeit not a complete abrogation, of such foci in Dock8-deficient T cells. Thus, to what extent the central F-actin pool we describe, and the WASp-dependent actin foci that are also a response to compressive forces, are mediated by the same cytoskeletal circuitry remains to be defined.

Concurrent with the loss of cell cohesion in *Dock8* KO cells was the loss of nuclear shape integrity. Given our findings that *Dock8*-deficient T cells passed through narrow constrictions at both higher rates and faster passage times than WT T cells, it is possible that the central F-actin pool limits entry into very small constrictions. This is in contrast with an Arp2/3-dependent perinuclear actin pool that was found to transiently appear during DC passage through constrictions hypothesized to facilitate passage of the rigid nucleus (*87*). A key difference could be the relatively softer nucleus of T cells, at least in part due to much lower lamin A/C levels which are an important determinant of nucleus rigidity (*75*, *81*). Importantly, whereas nuclear envelope rupture has been documented in DCs and cancer cells (*85*, *86*), it was unknown whether nuclear envelope ruptures occur in migrating T cells. Here we showed that such ruptures were rare in both WT and *Dock8* KO T cells, and that even in severely entangled *Dock8* KO cells the nuclear envelope remained intact. Indeed, mechanical strain has been shown to induce DNA damage also in absence of nuclear envelope rupture (*91*), in line with the greater number of DNA breaks we observed in migrating *Dock8* KO T cells using a comet assay. That the *Dock8* KO T cells experience greater mechanical forces was also supported by the much more flattened nucleus under confinement compared to WT T cells, as well as the changes in gene expression observed only in migrating *Dock8* KO T cells, at least some of which are likely responses to greater DNA damage on the one hand, or increased mechanosensing on the other. Indeed, one read-out of the increased

mechanosensitivity of *Dock8* KO cells was lamin A/C expression itself, which was higher in the KO cells both at the mRNA and the protein level compared to WT T cells. Lamin A/C expression has been shown to be upregulated in response to mechanical force, and this upregulation plays a protective role in mesenchymal cells, macrophages, and others (*90*, *271*, *275*). In *Dock8* KO T cells, upregulation of lamin A/C was insufficient to prevent force-mediated DNA damage, but the phosphorylation state of lamins and other nuclear envelope proteins including emerin (*384*), which we found was downregulated at the transcript level in KO T cells, may also play a role. Finally, consistent with an increase in mechanical force experienced by *Dock8* or *Stk4* KO T cells, we also detected an upregulation of *Wwtr1* expression with increased collagen density that was greater in both *Dock8* and *Stk4* KO T cells.

It is worth noting that while *Dock8* or *Stk4* KO T cells had a complete loss of the central actin structure under confinement in all cells examined, only a fraction of KO T cells became entangled in collagen at any given time. We do not address here whether there is heterogeneity between cells that contributes to differences in survival, but given that cell death increases as a function of collagen density, it is likely that chance encounters with specific environmental constraints account for at least some of the variability in loss of cell cohesion. To this point, we observed that in under agarose assays, cell confinement was not sufficient to elicit entanglement, but when cells encountered obstacles such as other cells or debris, this led to a stretched cell phenotype. This aspect of Dock8-dependent F-actin regulation may relate to the clinical phenotypes observed, as cellular survival defects in *Dock8*-deficiency have been described in T cells (*222*–*224*), B cells (*218*), NKT cells (*385*), innate lymphoid cells (*386*, *387*), and DCs (*5*). It is possible that in addition to migration-induced shattering of cell, sustained DNA damage resulting from nuclear stress during migration may also play a role in reducing cell viability over time. While in Mst1 immunodeficiency, contributors to the lymphopenia observed have been described to be severely reduced thymic egress and increased FAS-mediated apoptosis (*371*), we describe for the first time that Mst1 is also required for cell cohesion during 3D

migration via a mechanosensitive regulatory network with Dock8 and actin, which may explain some of the overlapping features of Mst1 and Dock8 immunodeficiencies.

The mechanobiology of immune cells is a rapidly developing field, and previous to this work, most of our understanding of T cell mechanosensing was with respect to synapse formation during priming or target cell killing. Much less is known about whether and how T cells, or immune cells more generally, adapt to confined 3D interstitial migration and to what extent mechanosensing in 2D compared to 3D differ (*240*, *388*). It was recently shown that mechanical input leads to transcriptional changes in T cells (*255*, *318*). Moreover, stiffness sensing by effector T cells is a critical driver of the differentiation of tissue resident memory T cells, and confinement-induced motility plays a role in antigen surveillance by T cells in the salivary gland (*320*, *389*). Overall, defining the signaling axes which impact the ability of T cells to migrate through and establish residence in confined tissue environments may provide a therapeutic opportunity to modulate the migration to, and survival within, tissues where T cell surveillance is undesirable, for instance in autoimmunity. Alternatively, this work may ultimately enable the design of antigen-specific T cells for therapeutic settings where withstanding large mechanical forces is key to their effector function, as might be the case in anti-tumor responses. Overall, this work highlights how studying instances where cell migration goes wrong can shed light on the molecular mechanisms at play in effective migration through tissues.

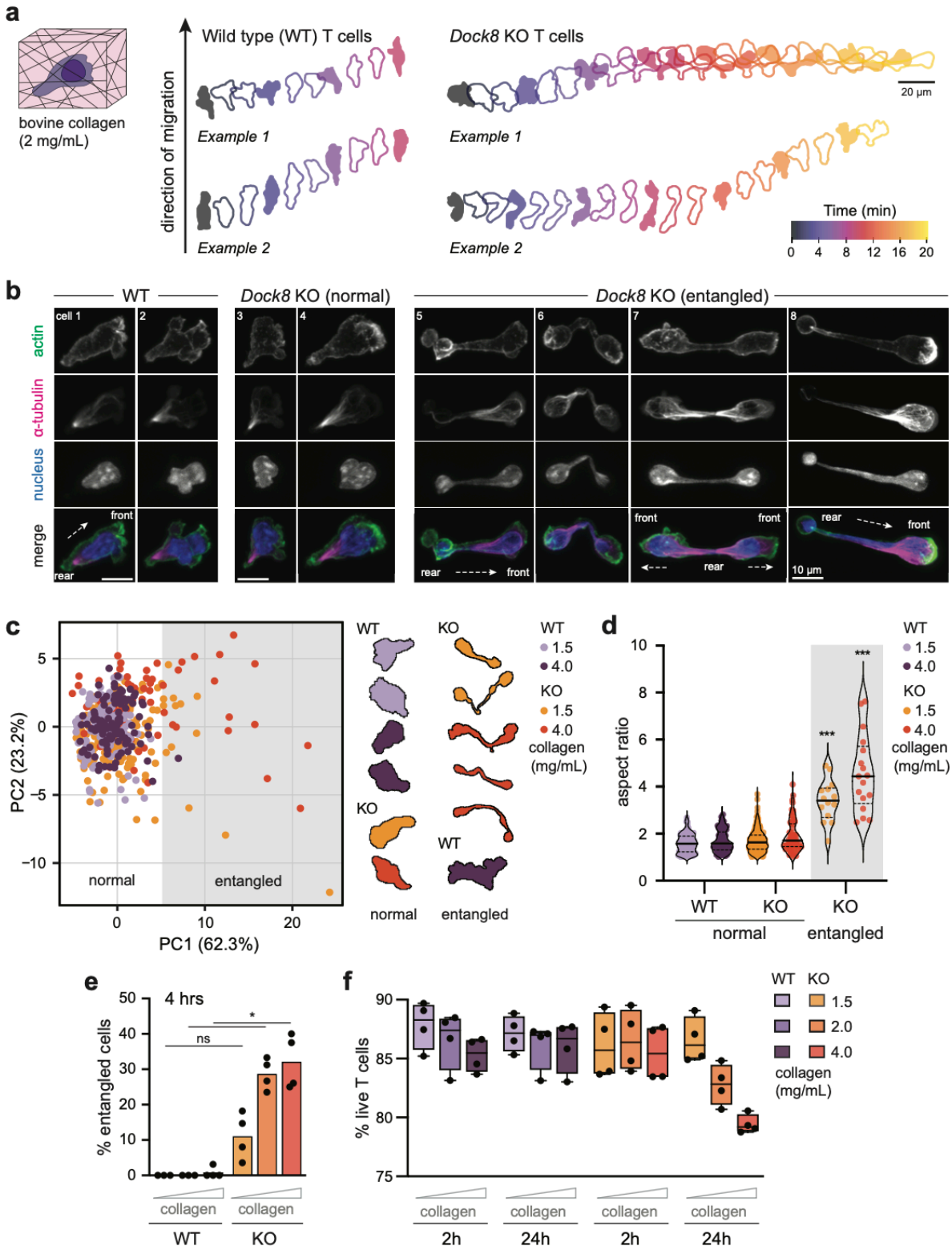
a
bovine collagen
(2 mg/mL)
direction of migration
Wild type (WT) T cells
Example 1
Example 2
Dock8 KO T cells
Example 1
Example 2
20 µm
Time (min)
0 4 8 12 16 20
b
WT
Dock8 KO (normal)
Dock8 KO (entangled)
actin
α-tubulin
nucleus
merge
cell 1
2
3
4
5
6
7
8
front
rear
10 µm
c
PC2 (23.2%)
PC1 (62.3%)
normal
entangled
WT
KO
WT
1.5
4.0
KO
1.5
4.0
collagen
(mg/mL)
d
aspect ratio
***
WT
KO
KO
normal
entangled
e
4 hrs
% entangled cells
ns
*
collagen
collagen
WT
KO
f
% live T cells
WT KO
1.5
2.0
4.0
collagen
(mg/mL)
collagen
collagen
collagen
collagen
2h
24h
2h
24h

Figure 1. Loss of cell cohesion and death of migrating *Dock8* KO T cells is collagen-density dependent.

(a) Two representative cell outlines of activated WT and *Dock8* KO T cells spontaneously migrating through a collagen matrix made of 2 mg/mL bovine type I collagen (no chemokine added), colour-coded by time with the direction of migration indicated (arrow). **(b)** Representative confocal microscopy images (max projection of z-stacks) of T cells migrating through collagen matrix as in (a). Examples of WT and *Dock8* KO T cells (entangled or not) are shown with cell front and rear indicated. Fixed cells were stained for F-actin (phalloidin), tubulin (**α**-tubulin antibody), and nucleus (Hoechst). **(c)** Principal component analysis (PCA) of 20 extracted cell shape parameters from $n = 211$ WT and $n = 293$ KO T cells migrating in low and high collagen densities (1.5 and 4 mg/mL) after 4 hours. Data points are individual cells; example cell outlines of T cells classified as normal or entangled by PCA are shown. **(d)** Summary violin plots of the aspect ratio of cells analysed in (c) for each category. Data points: individual cells; solid lines: median; dotted lines: quartiles. **(e)** Summary plot of percent WT and *Dock8* KO T cells entangled in collagen matrix (2 mg/mL) after 4 hours of migration. Data points: replicate T cell cultures from $n = 4$ mice; means are indicated. **(f)** Summary plot of percent live WT and *Dock8* KO T cells in collagen matrix (1.5, 2, or 4 mg/mL) after 2 or 24 hours of migration. Data points: replicate T cell cultures from $n = 4$ mice; medians are indicated with quartiles (box) and min to max ranges (error bars). Statistical tests: Kruskal-Wallis ANOVA with Dunn's multiple comparison test (d, e). $*P < 0.05$; $***P < 0.001$; ns, non-significant.

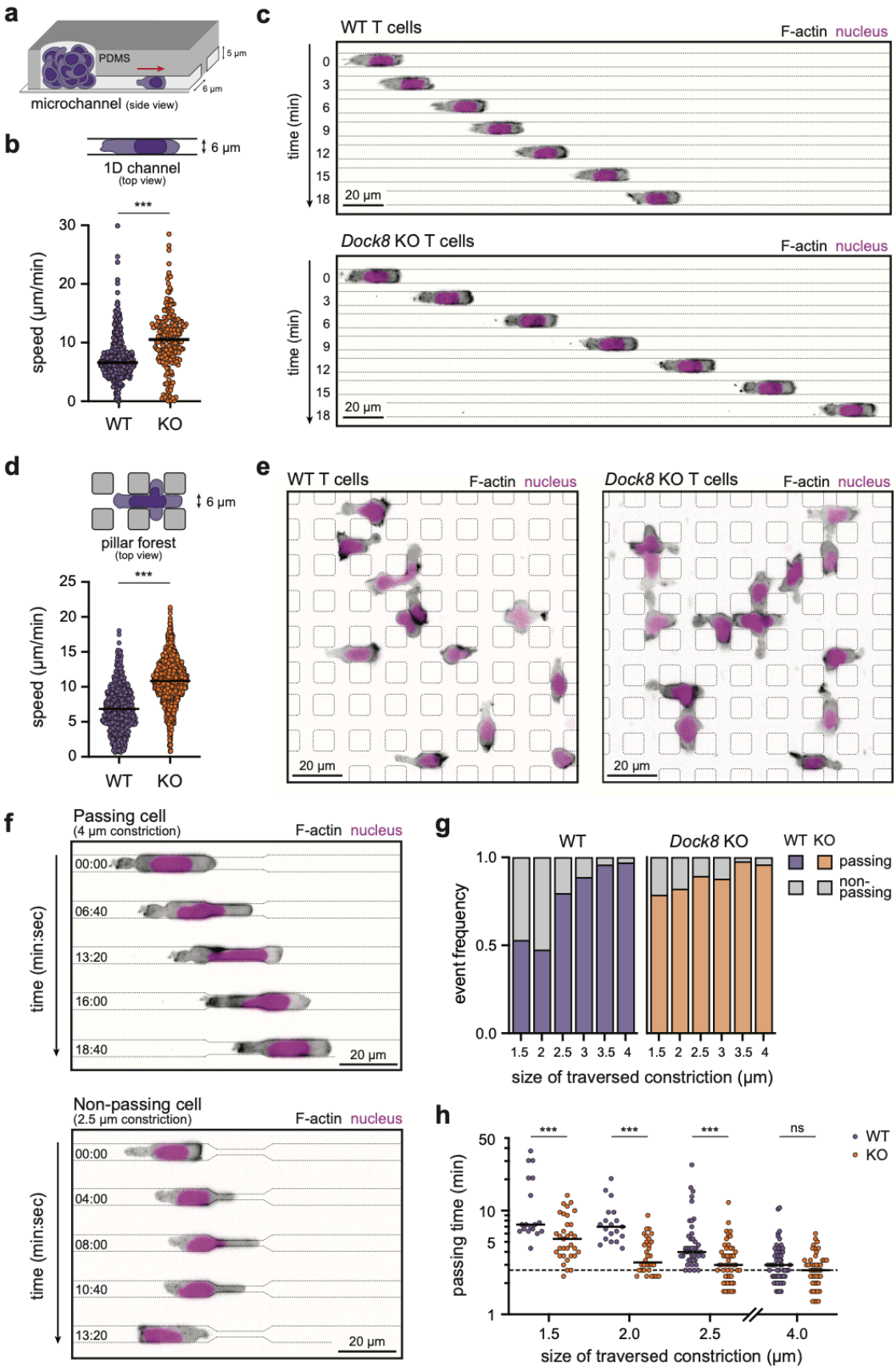
a
PDMS
5 µm
6 µm
microchannel (side view)
b
6 µm
1D channel
(top view)
***
speed (µm/min)
WT
KO
c
WT T cells
F-actin nucleus
time (min)
20 µm
Dock8 KO T cells
d
pillar forest
e
f
Passing cell
(4 µm constriction)
time (min:sec)
Non-passing cell
(2.5 µm constriction)
g
WT
Dock8 KO
WT KO
passing
non-passing
event frequency
size of traversed constriction (µm)
h
ns
passing time (min)

Figure 2. *Dock8* KO T cells navigate simple environments and small constrictions with no impairment.

(a, b, c) Activated WT and *Dock8* KO T cells expressing LifeAct-GFP and NLS-nTnG migrating in straight microchannels (width of 6 μm and height of 5 μm) coated with fibronectin, no chemokine added. Summary of individual cell mean speed (b), and representative examples acquired by epifluorescence microscope shown over time (c). Data is from 2 independent experiments, n = 361 (WT) and n = 179 (KO) cells; line: median. **(d, e)** Activated WT and *Dock8* KO T cells expressing LifeAct-GFP and NLS-nTnG migrating through pillar forest microchannels (channel width of 6 μm, height of 5 μm, pillars of 8 μm x 8 μm) coated with fibronectin, no chemokine added. Summary of individual cell mean velocities (d), and representative examples acquired by epifluorescence microscope (e). Data is n = 572 (WT) and n = 1385 (KO) cells; line: median. **(f, g, h)** Activated WT and *Dock8* KO T cells expressing LifeAct-GFP and NLS-nTnG migrating through microchannels with constrictions (channel width of 6 μm, height of 5 μm, constriction sizes 1.5–4 μm) coated with fibronectin, no chemokine added. Representative examples of cell retreating and cell passing acquired by epifluorescence microscope (f). Percent of cells passing through or retreating at constrictions (g), and summary of time spent passing through constrictions of different sizes, data points are individual cells, n = 18–57 cells per constriction size; line: median; dotted line at average passing time through 4 μm constrictions (h). Statistical tests: Mann-Whitney test (b, d); 2-way ANOVA (h). $^{**}P < 0.01$; $^{***}P < 0.001$; ns, non-significant.

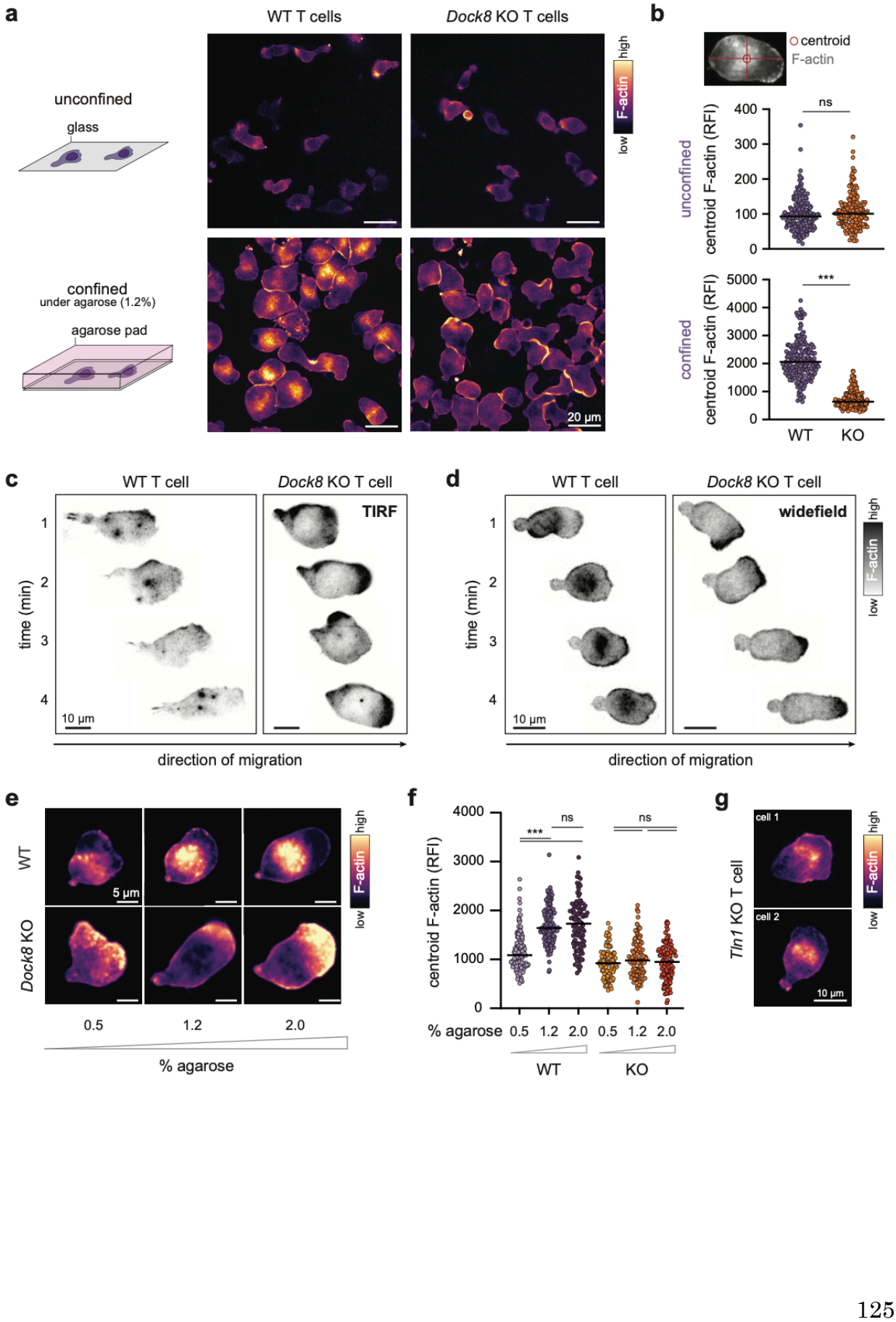
a
WT T cells
Dock8 KO T cells
unconfined
glass
confined
under agarose (1.2%)
agarose pad
high
F-actin
low
20 µm
b
centroid
F-actin
unconfined
centroid F-actin (RFI)
ns
confined
***
WT
KO
c
WT T cell
Dock8 KO T cell
TIRF
time (min)
10 µm
direction of migration
d
widefield
e
WT
Dock8 KO
5 µm
0.5
1.2
2.0
% agarose
f
ns
% agarose
g
Tln1 KO T cell
cell 1
cell 2

Figure 3. Confinement-induced redistribution of F-actin is absent in *Dock8* KO T cells.

(a) Fluorescence intensity of F-actin (phalloidin) in WT or Dock8 KO T cells migrating on fibronectin-coated glass either in absence of (unconfined) or under 1.2% agarose (confined). Representative images (epifluorescence microscope) are shown. **(b)** Summary plot of F-actin relative fluorescence intensity (RFI) measured at the cell centroid as indicated (top). Data points, individual cells (n = 166-210 cells); lines, medians. **(c, d)** Representative WT and *Dock8* KO T cells expressing LifeAct-GFP (grey scale, fluorescence intensity) migrating under 1.2% agarose over time acquired by TIRF (c), or widefield microscopy (d). **(e, f)** Fluorescence intensity of F-actin (phalloidin) in WT and *Dock8* KO T cells migrating under 0.5, 1.2 or 2% agarose. Representative examples (epifluorescence microscope) (e), and summary plots (f). Data points, individual cells (n = 109-140 cells); lines, medians. **(g)** Two representative example images of F-actin fluorescence intensity in talin1 (*Tln1*)-deficient murine T cells migrating under 1.2% agarose. Statistical tests: Mann-Whitney tests (b); Kruskal-Wallis ANOVA with Dunn's multiple comparison test (f). ***$P < 0.001$; ns, non-significant.

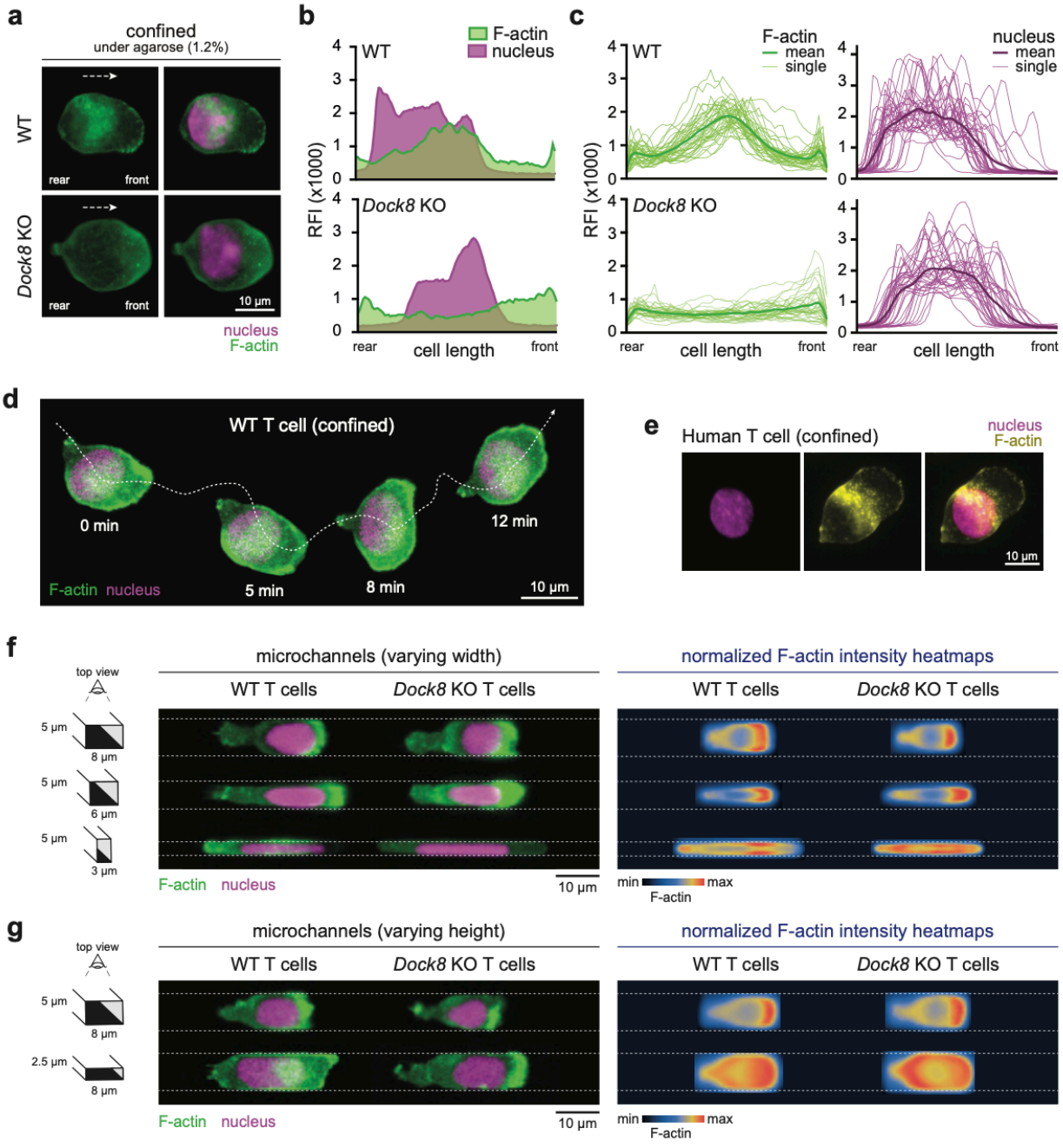
a
confined
under agarose (1.2%)
WT
Dock8 KO
rear
front
10 μm
nucleus
F-actin
b
F-actin
nucleus
WT
Dock8 KO
RFI (x1000)
rear
cell length
front
c
F-actin
mean
single
nucleus
mean
single
WT
Dock8 KO
RFI (x1000)
rear
cell length
front
d
WT T cell (confined)
0 min
5 min
8 min
12 min
F-actin nucleus
10 μm
e
Human T cell (confined)
nucleus
F-actin
10 μm
f
top view
5 μm
8 μm
5 μm
6 μm
5 μm
3 μm
microchannels (varying width)
WT T cells
Dock8 KO T cells
normalized F-actin intensity heatmaps
WT T cells
Dock8 KO T cells
F-actin nucleus
10 μm
min
max
F-actin
g
top view
5 μm
8 μm
2.5 μm
8 μm
microchannels (varying height)
WT T cells
Dock8 KO T cells
normalized F-actin intensity heatmaps
WT T cells
Dock8 KO T cells
F-actin nucleus
10 μm
min
max
F-actin

Figure 4. The confinement-induced central actin pool is located at the nucleus front in migrating human and murine T cells.

(a) Representative images of WT and *Dock8* KO T cells migrating under 1.2% agarose. Cells were fixed and stained for F-actin (phalloidin) and nucleus (Hoechst), and images were acquired by epifluorescence microscopy. **(b)** Histograms of RFI for both F-actin and nucleus from cells shown in (a) taken cross-sectionally across the cell from rear to front. **(c)** Aggregated histograms of F-actin (phalloidin) and nucleus (Hoechst) RFI of individual T cells (n = 35 per genotype) normalized over cell length by linear interpolation. Lines for individual cells and means are shown. **(d)** Representative timelapse images of WT T cells expressing LifeAct-GFP and NLS-nTnG migrating under 1.2% agarose acquired by epifluorescence microscopy. **(e)** Representative human T cell migrating under 1.2% agarose, fixed and stained for F-actin (phalloidin) and nucleus (Hoechst). **(f, g)** Representative images (left) and normalized F-actin intensity heatmaps of n = 12-31 cells (right) of WT and *Dock 8* KO T cells expressing LifeAct-GFP and NLS-nTnG migrating in straight microchannels with either fixed heights of 5 μm and variable widths of 3, 6 or 8 μm (f), or variable heights of 2.5 or 5 μm and fixed widths of 8 μm (g).

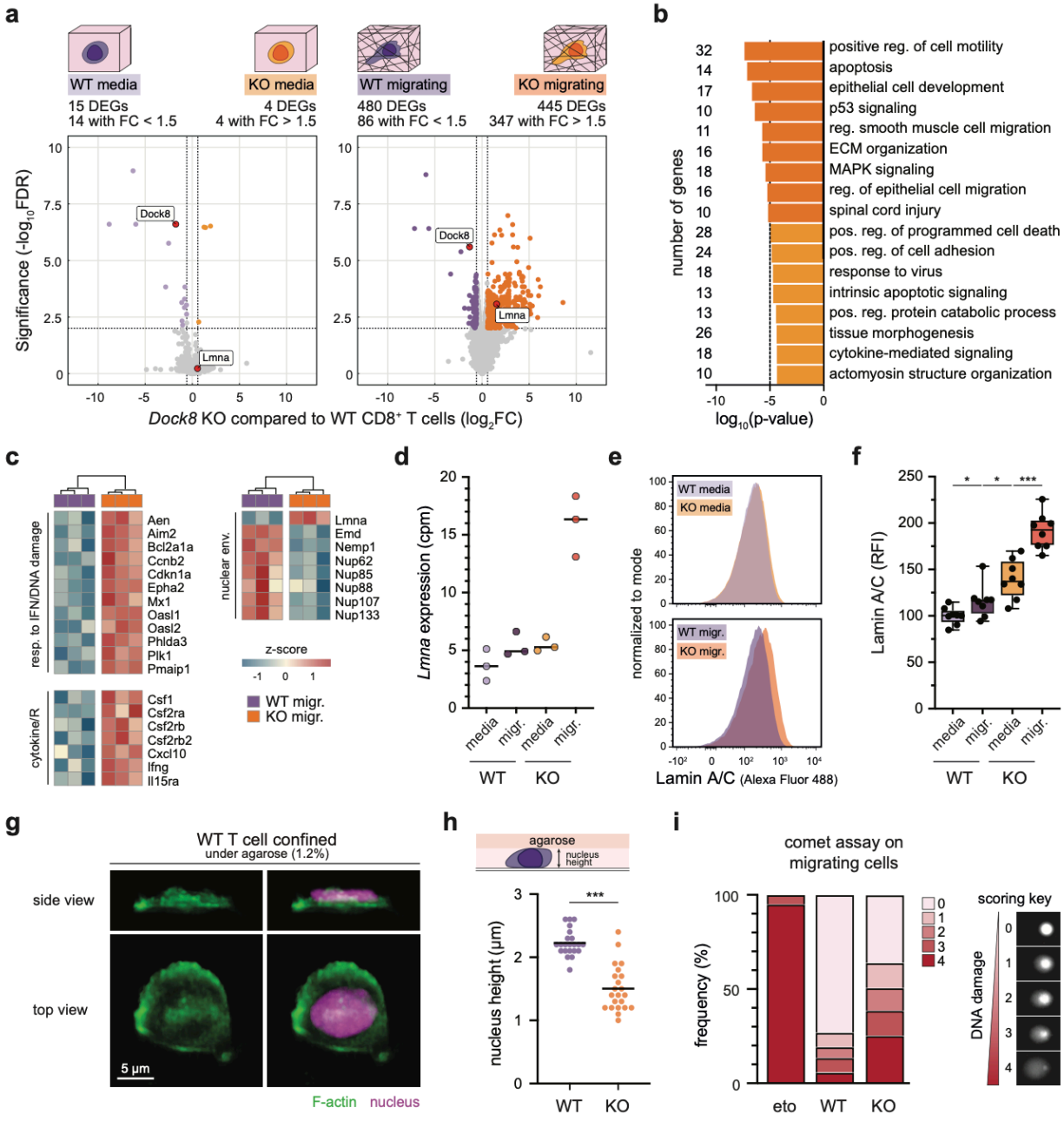
a
WT media
KO media
WT migrating
KO migrating
15 DEGs
14 with FC < 1.5
4 DEGs
4 with FC > 1.5
480 DEGs
86 with FC < 1.5
445 DEGs
347 with FC > 1.5
Significance (-log10 FDR)
Dock8
Lmna
Dock8 KO compared to WT CD8+ T cells (log2FC)
b
positive reg. of cell motility
apoptosis
epithelial cell development
p53 signaling
reg. smooth muscle cell migration
ECM organization
MAPK signaling
reg. of epithelial cell migration
spinal cord injury
pos. reg. of programmed cell death
pos. reg. of cell adhesion
response to virus
intrinsic apoptotic signaling
pos. reg. protein catabolic process
tissue morphogenesis
cytokine-mediated signaling
actomyosin structure organization
number of genes
log10(p-value)
c
resp. to IFN/DNA damage
Aen
Aim2
Bcl2a1a
Ccnb2
Cdkn1a
Epha2
Mx1
Oasl1
Oasl2
Phlda3
Plk1
Pmaip1
cytokine/R
Csf1
Csf2ra
Csf2rb
Csf2rb2
Cxcl10
Ifng
Il15ra
nuclear env.
Lmna
Emd
Nemp1
Nup62
Nup85
Nup88
Nup107
Nup133
z-score
WT migr.
KO migr.
d
Lmna expression (cpm)
media
migr.
WT
KO
e
WT media
KO media
WT migr.
KO migr.
normalized to mode
Lamin A/C (Alexa Fluor 488)
f
Lamin A/C (RFI)
media
migr.
WT
KO
g
WT T cell confined
under agarose (1.2%)
side view
top view
5 µm
F-actin
nucleus
h
agarose
nucleus height
nucleus height (µm)
WT
KO
i
comet assay on migrating cells
frequency (%)
eto
WT
KO
scoring key
DNA damage

Figure 5. The DOCK8-dependent F-actin redistribution in migrating T cells is nucleo-protective.

(a) Volcano plots of significant differentially expressed genes (DEG) identified by RNA-seq between WT and *Dock8* KO $CD8^+$ T cells activated *in vitro* and cultured in either media or migrating in collagen (2 mg/ml) for 24 hours with 3 biological replicates per genotype (*FDR* < 0.01). FC, fold change. Specific genes of interest (red data points) are labeled. **(b)** Gene ontology analysis of significant DEGs (445 genes) upregulated in *Dock8* KO compared to WT T cells from (a) at FC > 1.5. Bar graph showing gene numbers per category of the top non-redundant enrichment clusters identified with at least 10 genes. Reg., regulation; pos., positive. **(c)** Heatmap of expression (z-score) of selected genes in WT and *Dock8* KO T cells identified among DEGs from (a). **(d)** *Lmna* gene expression from RNA-seq data. cpm, counts per million. Data points are independent *in vitro* activated $CD8^+$ T cell cultures from *n* = 3 mice per genotype; lines represent medians. **(e,f)** Lamin A/C expression quantified by flow cytometry in WT or *Dock8* KO $CD8^+$ T cells cultured in either media or migrating in collagen (2 mg/ml) for 24 hours. Representative flow cytometry histograms (g), and data summarized from *n* = 8 mice per genotype and 3 independent experiments (h); lines represent medians; boxes are quartiles; error bars represent the min to max range; RFI are normalized to the mean of WT T cells in media. **(g,h)** LifeAct-GFP and NLS-nTnG WT and *Dock8* KO T cells migrating under 1.2% agarose and imaged using lattice light sheet microscopy. Representative image of a WT T cell shown both from a top view and a side view (g). Summary plot of nuclear height measurements taken from cells that were polarized and not in contact with more than one other cell (h). Data points, *n* = 22 cells per genotype; lines, means. **(i)** Alkaline comet assay of WT T cells treated with etoposide (n = 61 cells), or WT (n = 75 cells) and *Dock8* KO (n = 52 cells) T cells migrating in collagen (2 mg/ml) for 12 hours. Representative images of visual scoring of double-stranded DNA breaks (score 1 – 4) are shown (right). Statistical tests: one-way ANOVA with Holm-Šídák's multiple comparisons test (f); Mann-Whitney test (h); **P* < 0.05; ****P* < 0.001; ns, non-significant.

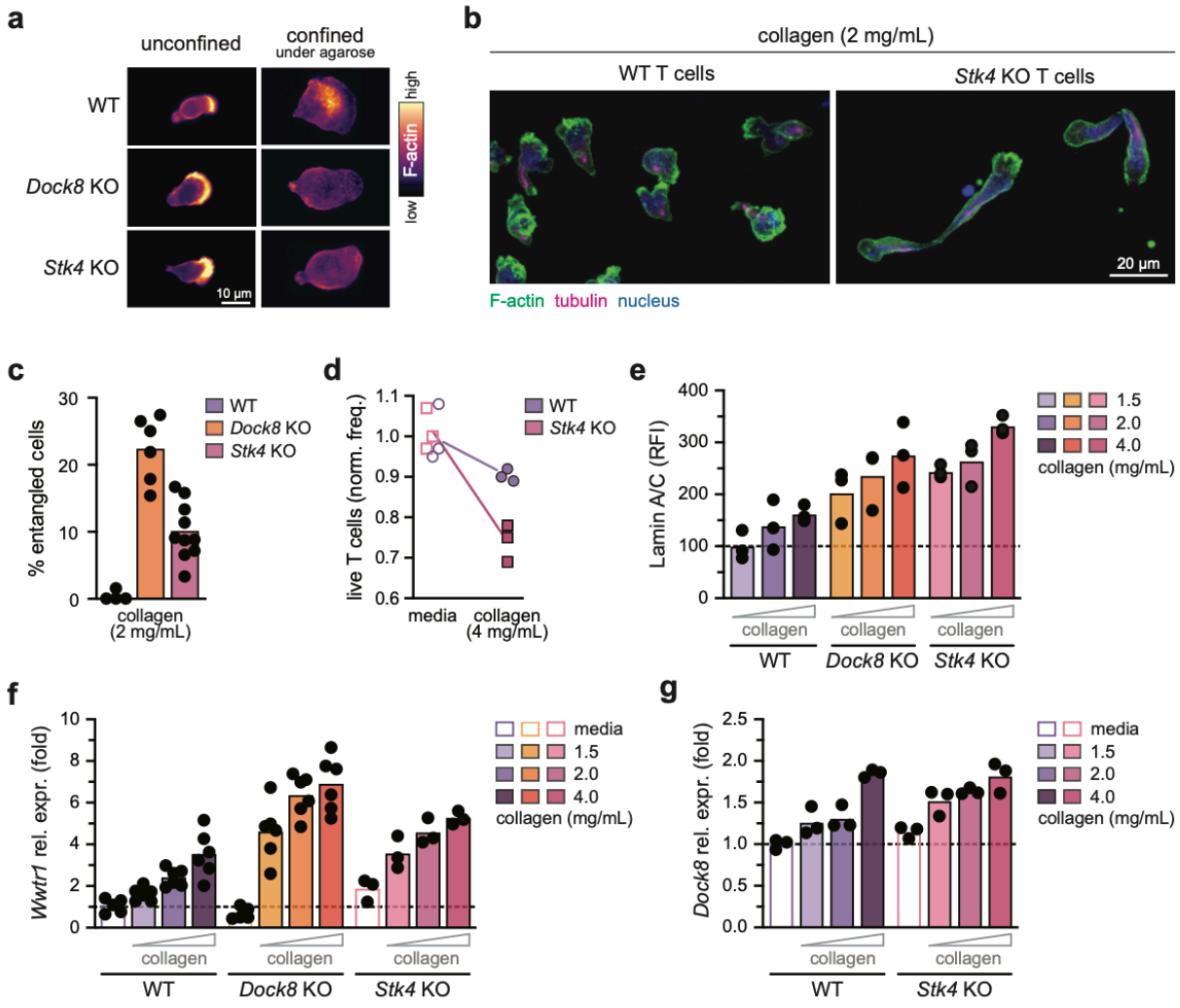
a
unconfined
confined
under agarose
WT
Dock8 KO
Stk4 KO
high
F-actin
low
10 μm
b
collagen (2 mg/mL)
WT T cells
Stk4 KO T cells
20 μm
F-actin tubulin nucleus
c
% entangled cells
WT
Dock8 KO
Stk4 KO
collagen
(2 mg/mL)
d
live T cells (norm. freq.)
WT
Stk4 KO
media
collagen
(4 mg/mL)
e
Lamin A/C (RFI)
1.5
2.0
4.0
collagen (mg/mL)
collagen
WT
Dock8 KO
Stk4 KO
f
Wwtr1 rel. expr. (fold)
media
1.5
2.0
4.0
collagen (mg/mL)
collagen
WT
Dock8 KO
Stk4 KO
g
Dock8 rel. expr. (fold)
media
1.5
2.0
4.0
collagen (mg/mL)
collagen
WT
Stk4 KO

Figure 6. Mst1 is required for the nucleo-protective central actin pool during migration.

(a) Fluorescence intensity of F-actin (phalloidin) in WT, *Dock8* KO, or *Stk4* KO T cells migrating on fibronectin-coated glass either in absence of (unconfined) or under 1.2% agarose (confined). Representative images (epifluorescence microscope) are shown. **(b)** Representative confocal microscopy images (max projection of z-stacks) of WT and *Stk4* KO T cells migrating through collagen (2 mg/ml). Fixed cells were stained for F-actin (phalloidin), tubulin (**α**-tubulin antibody), and nucleus (Hoechst). **(c)** Summary plot of percent WT, *Dock8* KO, and *Stk4* KO T cells entangled in collagen matrix (2 mg/ml) after 4 hours of migration. Data points, replicate T cell cultures from $n = 4$ mice per genotype; means are indicated. **(d)** Summary plot of the frequency of live WT or *Dock8* KO T cells either resting in media or after 24 hours of migration in 2mg/ml collagen matrices. Data summarized from $n = 3$ mice per genotype; frequency is normalized to the mean viability of WT T cells in media. **(e)** Lamin A/C expression quantified by flow cytometry in WT, *Dock8* KO, or Mst1 KO activated $CD8^+$ T cells migrating in 1.5, 2, or 4 mg/ml collagen for 24 hours. Data summarized from $n = 3$ mice per genotype; lines, means; RFI is normalized to the mean of WT T cells in 1.5 mg/ml collagen. Dotted line at RFI = 100. **(f)** Gene expression of *Wwtr1* (Taz) assessed by quantitative RT-PCR in WT, *Dock*8 KO, or Mst1 KO activated $CD8^+$ T cells cultured in media or migrating in 1.5, 2, or 4 mg/ml collagen for 24 hours. Expression was normalized to housekeeping gene Tbp and shown as fold change compared to WT T cells in media. Dotted line at fold = 1; data summarized from $n = 3$-6 mice per genotype from 1-2 independent experiment; lines, means. **(f)** Gene expression of *Dock8* assessed by quantitative RT-PCR in WT or Mst1 KO activated $CD8^+$ T cells cultured in media or migrating in 1.5, 2, or 4 mg/ml collagen for 24 hours. Expression was normalized to a housekeeping gene and shown as fold change compared to the WT T cells in media. Dotted line at fold = 1; data summarized from $n = 3$ mice per genotype from 1 experiment; lines, means.

Human samples

Participants were enrolled and informed consent obtained at the Center for Innovative Medicine (CIM), Research Institute of the McGill University Health Center (RI-MUHC), as approved by the McGill University Health Center Research Ethics Board (human ethics protocol #2023-8829). Volunteers included both males and females, in the age range of 21 - 45 years, and were sampled by venipuncture.

Mice

C57BL/6J, B6 CD45.1 (jax #002014), and NLS-nTnG (jax #023537) (*390*) mice were obtained from The Jackson Laboratory. LifeAct-GFP (*391*) mice were kindly shared by Janis Burkhardt (University of Pennsylvania). *Dock8* KO mice were generated by genOway and shared by Helen Su (NIH) (*5*). *Stk4* KO mice (*392*) were shared by Dae-Sik Lim (Korea Advanced Institute of Science and Technology). *Tln1*$^{flox/flox}$ mice (*393*)were shared by Irah King (McGill University). All mouse strains were bred in-house and studies were performed in accordance with the Guide for the Care and Use of Laboratory Animals, with approval by the McGill University Facility Animal Care Committee. Mice were housed in the CMARC animal facility at McGill University at a temperature of 18-24°C, 30-70% humidity, and 12h/12h light-dark cycles. Mice were used for experiments at 6-12 weeks of age. Both male and female mice were used and sex-matched where possible.

Cell isolation and culture

Murine T cells: Inguinal, axillary, brachial, and cervical lymph nodes were harvested and crushed through a 70 µm filter. T cells were isolated with the EasySep Mouse Total T Cell Isolation Kit (StemCell) following the manufacturer instructions. Isolated T cells were resuspended in RPMI 1640 supplemented with 10% heat-inactivated FBS, 2 mM L-glutamine, 100 U/mL penicillin, 100 ng/mL streptomycin, 1 mM sodium pyruvate, 10 mM HEPES, 1% non-essential amino acids, and 5 µM 2-

mercaptoethanol (complete RPMI) at 2.5×10^6 cells/mL. For activation, T cells were supplemented with 2 μg/mL anti-CD28 (37.51; Biolegend), seeded in a F-bottom 96-well plate precoated with 3 μg/mL anti-CD3 (145-2C11; Biolegend) using 5×10^5 cells (200 μl) per well, and incubated at 37°C, 5% CO_2. Two days after seeding, cells were centrifuged at 300 *g* for 5 min at 4°C and cultured in flasks at 10^6 cells/mL in complete RMPI with 20 ng/mL recombinant mouse IL-2 (rmIL-2; Biolegend). To generate talin-deficient T cells, T cells were incubated with 2 μM TAT-CRE Recombinase (Sigma) for 1 h, to excise the transgene flanked by *loxP* sites, before stimulation with rmIL-2. Activated T cells were used for experiments on day 4.

Human T cells: Lymphocytes were isolated from whole blood collected in sodium heparin tubes using Ficoll-Paque PLUS Density Gradient Media (Cytiva) following manufacturer instructions. $CD8^+$ T cells were isolated with the EasySep Human $CD8^+$ T Cell Isolation Kit (StemCell) using the manufacturer protocol. Isolated $CD8^+$ T cells were resuspended at 2×10^6 cells/mL in RPMI 1640 supplemented with 10% heat-inactivated FBS, 2 mM L-glutamine, 100 U/mL penicillin, 100 ng/mL streptomycin, 1 mM sodium pyruvate, 10 mM HEPES, 1% non-essential amino acids, and 5 μM 2-mercaptoethanol (complete RPMI). For activation, cells were supplemented with 25 μl/mL ImmunoCult Human CD3/CD28 T Cell Activator (StemCell) and 20 ng/mL Recombinant Human IL-2 (rhIL-2; Biolegend), seeded in a F-bottom 96-well plate using 4×10^5 cells (200 μl) per well, and incubated at 37°C, 5% CO_2. Complete RPMI supplemented rhIL-2 was added to the cells to reach a concentration of 2×10^6 cells/mL on day 3 and 6 post-activation. Activated T cells were used for experiments on day 8.

Murine BMDC: Bone marrow from femurs and tibias was harvested by flushing bones with RPMI and passed through a 70 μm filter. Isolated bone marrow cells were resuspended in complete RPMI at 2.66×10^5 cells/mL. For differentiation, cells were supplemented with 20 ng/ml GM-CSF (Biolegend), seeded into 6-well plates using 8×10^5 cells (3 mL) per well, and incubated at 37°C, 5% CO_2. 3 days later, 3 mL of complete RPMI supplemented with 20 ng/ml GM-CSF was gently added to each well.

3 days later, 3 mL of media was gently replaced from each well with fresh complete RPMI supplemented with 20 ng/ml GM-CSF. 2 days later, on day 8, the supernatant containing the BMDCs was harvested, centrifuged at 300 *g* for 5 min at 4°C, and the cells were resuspended in complete RPMI supplemented with 10 ng/ml GM-CSF at 10^7 cells/mL. BMDCs were pulsed with 1 μg/ml LPS (InvivoGen) for 30 minutes, then washed with media prior to use in migration assays.

Murine neutrophils: Bone marrow from femurs and tibias was harvested by flushing bones with RPMI and passed through a 70 μm filter. Neutrophils were isolated from bone marrow cells using the EasySep Mouse Neutrophil Enrichment Kit (StemCell) following manufacturer instructions. Neutrophils were resuspended in complete RPMI supplemented with 20 ng/ml GM-CSF at 1×10^7 cells/mL. Neutrophils were pulsed with 1 μg/ml LPS (InvivoGen) for 30 minutes, then washed with media prior to use in migration assays.

Flow cytometry

Cells were distributed in a U-bottom 96-well plate prior to centrifugation at 300 *g* for 5 min at 4°C. Cells were stained in FACS buffer (PBS supplemented with 2% FBS and 5 mM EDTA) for 30 min at 4°C using the following antibodies: eFluor450 anti-mouse CD4 (GK1.5; Invitrogen), BV605 anti-mouse CD8 (53-6.7; Biolegend), anti-mouse TCR-ß BV711 (H57-597; Biolegend), PE anti-mouse CD44 (IM7; Biolegend), and the Fixable Viability Dye eFluor 780 (eBioscience) for the exclusion of dead cells. After extracellular staining, the cells were fixed in 4% PFA in PBS at 4°C for 15 minutes. For the intracellular staining, cells were stained and permeabilized in FACS buffer supplemented with 0.3% Triton X-100 at 4°C for 1 hour using the following antibodies/probes: Alexa Fluor 488 or PE anti-mouse/human Lamin A/C (4C11; Cell Signaling Technology), Alexa Fluor 647 phalloidin (Invitrogen). Flow cytometry was performed on an LSR Fortessa (BD Biosciences). Files were analyzed using FlowJo (BD Biosciences).

RNA extraction for sequencing and RT-qPCR

RNA extraction: RNA extraction was performed using the PureLink RNA Mini Kit (Invitrogen). 2 to 4×10^6 $CD8^+$ T cells were lysed in the lysis buffer provided and passed through a homogenizer (Invitrogen) before RNA purification following manufacturer instructions. RNA concentration was quantified using a NanoDrop (Thermo Scientific). Isolated RNA was stored at -80°C (for bulk RNA sequencing) or immediately converted to cDNA using the High-Capacity cDNA Reverse Transcription Kit (Applied Biosystems) following manufacturer instructions, using 1000 ng RNA per 20 µL mix and stored at -20°C until used.

Two-step RT-qPCR: qPCR was performed on a StepOnePlus Real-Time PCR System (Applied Biosystems) using 2 µL of cDNA per well combined with TaqMan Fast Advanced Master Mix, the TaqMan probe Mm01277042_m1 (*Tbp*) in VIC (endogenous control), and one of the following TaqMan probes, in FAM: Mm00613802_m1 (*Dock8*), Mm01289583_m1 (*Wwtr1*) (all reagents from Applied Biosystems).

RNA sequencing

Purified RNA was provided to the Institut de recherches cliniques de Montréal sequencing core facility (QC, Canada). RNA quality control was performed by Pico assay with a bioanalyzer (Agilent). RNA-seq libraries were prepared from 150 ng RNA per condition using the following kits: RiboCop rRNA Depletion Kit HMR (Lexogen), KAPA RNA HyperPrep Kit (Roche), and TruSeq DNA UDI 96 Indexes (Illumina). Libraries were sequenced on a NovaSeq 6000 System (Illumina) using a Flow Cell S2 (Illumina) and a paired end run. More than 60 million paired-end reads were generated per sample. Reads were provided by the sequencing core facility as FASTQ files, quality checked using FastQC and MultiQC, and mapped to GRCm38/mm10 *Mus musculus* genome using HISAT2. Alignment quality checks were performed using Samtools Flagstat, FastQC, Picard Tools, and MultiQC. Sequencing reads overlapping exons were counted using featureCounts. Differential gene expression analysis was performed using EdgeR in R project, filtering out low

expression genes using the filterByExpr function, and normalizing the read counts (calcNormFactors function). The p values were corrected using the Benjamini-Hochberg method and only genes with an FDR < 0.01 were considered statistically significant. No fold change threshold was set unless stated otherwise. Volcano plots were generated using the ggplot2 package in R project. Heatmaps were built from CPM values using the R pheatmap function. CPM values were centered and scaled in the row direction. Gene ontology analysis was performed using Metascape (*394*). Only genes that were significantly upregulated (FDR < 0.01 and fold change > 2) were included. Enriched clusters identified with less than 10 genes were filtered out from the analysis.

Comet assay

An alkaline comet assay (capturing both single and double stranded DNA breaks) was performed using the Comet Assay Kit (Abcam) following the manufacturers protocol. Prior to the assay, a sample of activated T cells were treated with 10 μM etoposide for 1 hour at 37°C to generate a positive control. The comet tails were captured by epifluorescence and resulting images were manually scored as indicated in the figure.

Collagen gel migration assay

Gel preparation: Collagen gels were prepared using type 1 bovine atelocollagen (Nutragen; Advanced Biomatrix) at concentrations of 1.5, 2, and 4 mg/mL as indicated in the figure legends. Collagen gels were prepared and mixed on ice in 12-well plates by sequentially mixing water, neutralization buffer, collagen, concentrated RPMI and cells (in FBS) to reach a final concentration 1X RPMI, 2 g/L $NaHCO_3$, 25 mM HEPES, 2 mM L-glutamine, 20 ng/mL rmIL-2, and 12.5% FBS, pH = 7.2. Neutralization buffer consisted in 0.13N NaOH and was added at a ratio of 1 μl per 10 μl Nutragen. Concentrated RPMI consisted of 10X RPMI supplemented with 14 g/mL $NaHCO_3$, 175 mM HEPES, 14 mM L-glutamine, 140 ng/mL rmIL-2, and NaOH to reach pH = 7.2. Cells were seeded at a final concentration of 2×10^6 cells/mL.

Gels were allowed to polymerize at 37°C, 5% CO_2 for at least 2 h before individual assays. Gels were either fixed for staining or digested to extract the cells for downstream applications such as flow cytometry or RNA extraction.

Fluorescently labeled collagen: Fluorescent type I bovine atelocollagen was prepared by labelling Nutragen (Advanced Biomatrix) with Alexa Fluor 647 following a previously published protocol for labelling rat tail type I collagen (*395*), with the following modification: the collagen gel was prepared using the recipe above without L-glutamine, rmIL-2 and FBS instead of the protocol recipe using DMEM and RB.

Gel digestion: Collagen gels were dissociated using pipette tips and digested at 37°C for 45 minutes using 2 mg/mL Collagenase D (Sigma) in combination with gentle agitation. Cells were collected in microtubes and centrifuged at 300 *g* for 5 min.

Gel fixation and staining: Collagen gels were submerged in ice-cold 4% PFA in PBS for 30 minutes at room temperature and then cells permeabilized using 0.5% Triton-X 100 in PBS for 30 minutes at room temperature. Gels were stained overnight in PBS supplemented with 2% BSA and 0.1% Triton-X 100 in PBS using the following antibodies/probes: Alexa Flour 647 phalloidin (Invitrogen), Hoechst 33342 or 34580 (Invitrogen), Alexa Fluor 488 anti-mouse/human α-tubulin (B-5-1-2; Invitrogen). Collagen gels were rinsed with PBS prior to imaging by confocal microscopy.

Under agarose migration assay

Agarose preparation: The under agarose migration assay was adapted from (*370*). In brief, 35 mm glass-bottom dishes (Ibidi) were functionalized using a plasma cleaner (Harrick) and coated with 10 µg/ml fibronectin (Sigma) for 30 minutes at 37°C. Agarose gels were prepared by combining a solution made of 9 mL RPMI without phenol red, 10 µl 7.5% $NaHCO_3$, 1 mL 10X HBSS, 1 mL FBS, and 20 µl 50 mM ascorbic acid, maintained at 56°C, to a solution of agarose made of 0.1 to 0.4 g of UltraPure Agarose (Invitrogen) melted in 9 mL of sterile water. A concentration of 1.2% agarose was used unless otherwise indicated. Fibronectin-coated dishes were

rinsed with PBS, and 3 mL of agarose gel were poured per dish. Once solidified, agarose gel loading ports were made using a 2 mm UniCore punch spaced 2 mm apart. Cells were seeded in the first access port, at a concentration of 10^6 to 10^7 cells/mL in complete RPMI without phenol red. CCL19 was added to the second access port, at a concentration of 2 µg/ml. Cells were incubated at least 2 hours at 37°C and 5% CO_2 prior to performing live imaging by epifluorescence microscopy or fixing the cells for staining.

Cell fixation and staining: To fix the cells and retain their morphology, entry ports were flooded with 1 mL of ice-cold 4% PFA for exactly 5 min at room temperature before gently lifting off the agarose pad. Fixation was prolonged without the agarose pad for 10 min at room temperature. After fixation, samples were permeabilized with 0.2% Triton X-100 for 10 minutes at room temperature, then blocked with PBS supplemented with 1% BSA (blocking buffer). Cells were stained overnight at 4°C in blocking buffer using the following antibodies/probes: Alexa Fluor 488 or Alexa Fluor 647 phalloidin (Invitrogen), Hoechst 33342 or 34580 (Invitrogen), anti-α-tubulin (B-5-1-2; Invitrogen), Alexa Fluor 488 anti-acetylated tubulin (6-11B-1; Sigma), Alexa Fluor 488 DNAse 1 (Invitrogen), Mitotracker Deep Red (Invitrogen), Wheat Germ Agglutinin Alexa Fluor 594 (Invitrogen), Alexa Flour 647 anti-vimentin (D21H3; Cell Signaling Technologies). Samples were rinsed with PBS and imaged by epifluorescence microscopy as described below.

Microfluidic devices

Microchannels were prepared from PDMS as previously described[67, 89] (*1*, *349*) from custom-designed molds obtained from 4DCell. Prior to use for migration assays, microchannels were functionalized using a plasma cleaner (Harrick) and coated with 10 µg/ml fibronectin (Sigma) for 1 h at 37°C. Microchannels were rinsed multiple times with complete RPMI without phenol red prior to seeding the cells in the access ports at 10^8 cells/mL. Cells were incubated for at least 2 h at 37°C and 5% CO_2 before imaging their dynamic behavior by epifluorescence microscopy as described below.

Microscopy

Epifluorescence microscopy was performed with a ZEISS Axio Observer Fully Automated Inverted Microscope equipped with a Plan-Apochromat 20×/0.8 NA objective for all assays, except for the comet assay where a Plan-Neofluar 10×/0.3 NA objective was used. Confocal microscopy was performed with a ZEISS LSM880 equipped with a Plan-Apochromat 20×/1.0 NA water immersion objective. Total internal reflection fluorescence (TIRF) microscopy was performed with a (TIRF)-Spinning Disk Spectral Diskovery System (Spectral Applied Research) coupled to a DMI6000B Leica microscope equipped with a Plan-Apochromat 63×/1.47 NA oil immersion DIC objective. TIRF imaging depth was set to 120 nm. Lattice light-sheet microscopy was performed using a Zeiss Lattice Lightsheet 7 equipped with a 13.3×/0.4 NA objective for illumination, a 44.83×/1.0 NA objective for detection, and using a Sinc3 100 × 1800 lattice light sheet for acquisition. All live imaging was performed at 37°C with 5% CO_2 using a top-stage incubator (Live Cell Instrument).

Image analyses

Dynamic shape plots: Dynamic shape plots were generated from maximum intensity z-projections of time-lapse microscopy image sequences converted to evenly spaced sub-stacks of 10 to 20 frames to visualize cell morphology changes on a 1-minute scale. Sub-stacks were binarized in Fiji using Triangle thresholding. Cell outlines were extracted from the binary image sequence using the polygon selection tool.

Principle component analysis (PCA): T cells embedded in collagen gels were fixed and imaged in 3D by confocal microscopy. Cells were segmented using the Surface tool in Imaris Image Visualization and Analysis software v. 10.1.1 (Oxford Instruments). Surfaces corresponding to cell debris, diving cells, dead cells, and cells partially contained in the imaging area were excluded. Remaining surfaces were used to create a mask of viable single cells. Any (partially) overlapping cells were separated into different channels to ensure the most accurate shape analysis. 3D masked images were converted to 2D images by maximum intensity z-projection in Fiji. The 2D

projections were binarized by *Triangle* thresholding. Cell shape parameters were extracted using the built-in Analyze Particles function and the MorphoLibJ plugin. A PCA was performed using the prcomp function from the R statistical computing package. ggplot2 and factoextra packages were used for data visualization. PC1 > 5 was considered as a threshold above which cells were entangled/had lost cell cohesion in the collagen.

Heat maps: Actin distribution heat maps were generated from time-lapse widefield epifluorescence images, based on protocol outlined in (*181*). Cells were binarized by Triangle thresholding in Fiji. 2D average intensity z-projections were generated for each cell to yield an average cell shape over time. The 2D projections of all cells for each condition were combined into a single image stack and normalized to ensure a 30%-pixel saturation in each image. To account for differences in size between cells, the combined image stack was scaled to the smallest cell in the sequence. 2D average intensity z-projections were generated from the combined image sequence for each condition.

Centroid RFI: Cell centroid measurements were extracted with Fiji from widefield images of phalloidin-stained T cells. Centroid points were manually defined as the intersection of one axis along the direction of migration, and its perpendicular axis. Non-polarized, clumped, or dead cells were excluded from the analysis.

Intensity histograms: Fluorescence intensity histograms were generated by manually defining a line along the axis of migration. Non-polarized, clumped, or dead cells were excluded from the analysis. Intensity values along the line were extracted using the line profile tool in Fiji. A Python script was used to normalize x-axis values and perform linear interpolations.

Nuclear height measurement: Nuclear heights were extracted from the NLS-nTnG signal of T cells migrating under agarose as acquired by lattice light sheet microscopy. Non-polarized, clumped, or dead cells were excluded from the analysis. The thickness

of the center of the nucleus in the Z-direction was measured in Imaris Image Visualization and Analysis software v. 10.1.1 (Oxford Instruments).

Statistics

For analyses, statistical differences between groups were evaluated by the two-sided tests reported in figure legends. Comparisons were considered significant when $P \leq 0.05$. All statistical tests were performed using Prism 10 (GraphPad). *P*-values are indicated in figures as falling into one of 4 categories: ns, nonsignificant, $*P < 0.05$, $**P < 0.01$, or $***P < 0.001$, and statistical tests performed are indicated in legends.

Data Availability

RNA sequencing dataset is available through Gene Expression Omnibus (GEO) study GSE272197. All other data from this study are available from the corresponding author upon request.

3.7 ACKNOWLEDGEMENTS

We thank all the volunteers who kindly donated blood samples for our experiments. We thank Karel Prud'homme, Genvieve Perreault, and CMARC for their excellent care of our mice. The work was made possible by the McGill University Flow Cytometry Core Facility (FCCF) and Advanced Bioimaging Facility (ABIF). We particularly thank Nelly Vuillemin (ABIF) for her lattice light sheet expertise, and Tanner Ducharme for custom Python scripts. We thank all past and present Mandl lab members, especially Maryl Harris, Dakota Rogers, Angela Mingarelli, and Sam Jamaleddine for their contributions, as well as Reza Sharif-Naeini (McGill University), Johannes Textor (Radboud University, The Netherlands), and Stephanie Eisenbarth (Northwestern University) for their feedback. We are especially grateful to Michael Sixt, Patricia Reis-Rodrigues, and Alba Juanes Garcia at IST Austria for all their input and collaborative spirit in discussions we have had over the years this work was done.

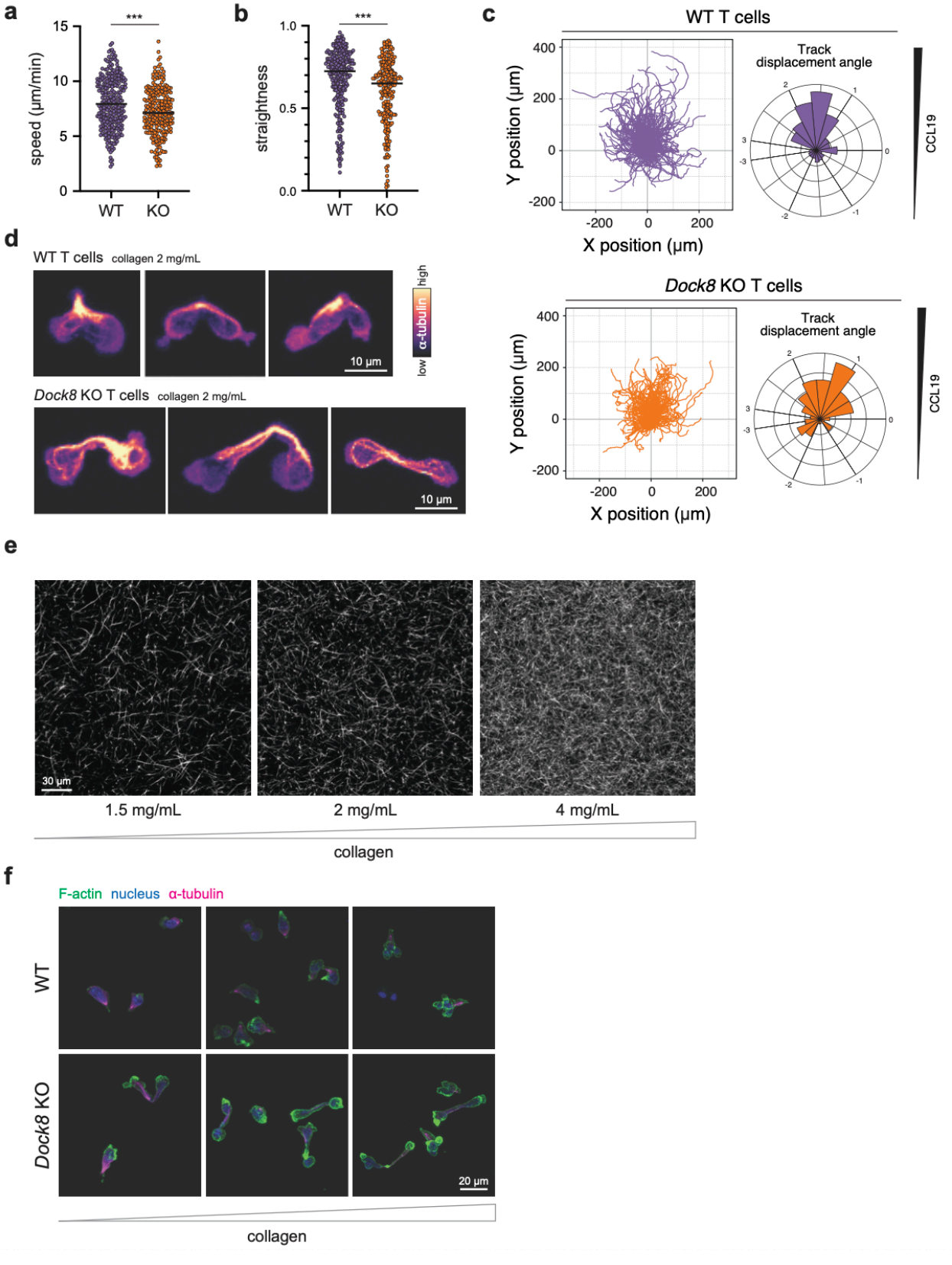
a
speed (μm/min)
15
10
5
0
***
WT
KO
b
straightness
1.0
0.5
0.0
***
WT
KO
c
WT T cells
Y position (μm)
X position (μm)
400
200
0
-200
-200
0
200
Track displacement angle
CCL19
Dock8 KO T cells
d
WT T cells collagen 2 mg/mL
high
α-tubulin
low
10 μm
Dock8 KO T cells collagen 2 mg/mL
10 μm
e
30 μm
1.5 mg/mL
2 mg/mL
4 mg/mL
collagen
f
F-actin nucleus α-tubulin
WT
Dock8 KO
20 μm
collagen

Figure S1. *Dock8* KO T cells are chemotactic but lose cell cohesion in collagen matrices.

(a,b,c) Summary plots of mean track speed (a), track straightness (b), track displacement (c), and track displacement angle (c) for WT and *Dock8* KO T cell migrating through 2 mg/mL collagen matrix towards a chemotactic gradient of 2 µg/ml CCL19. Data is n = 278 (WT) and n = 242 (KO) cells. **(d)** Examples of WT and *Dock8* KO T cells migrating through decision points in 2 mg/mL collagen matrix. Fixed cells were stained for tubulin (**α**-tubulin antibody). **(e,f)** Collagen matrices at various densities (1.5, 2.0, and 4.0 mg/ml) were imaged by confocal microscopy (e) and elastic modulus was measured by nanoindentation (f). Data is n = 4 technical replicates; lines: means; error bars: SD. **(g)** Representative z-stack projections of WT and *Dock8* KO T cells migrating in varying collagen densities (1.5, 2, and 4 mg/ml). Fixed cells were stained for F-actin (phalloidin), tubulin (**α**-tubulin antibody), and nucleus (Hoechst). Statistical tests: Mann-Whitney tests (a,b); Two-way ANOVA with Tukey's multiple comparison test (f). ***$P < 0.001$; ns, non-significant.

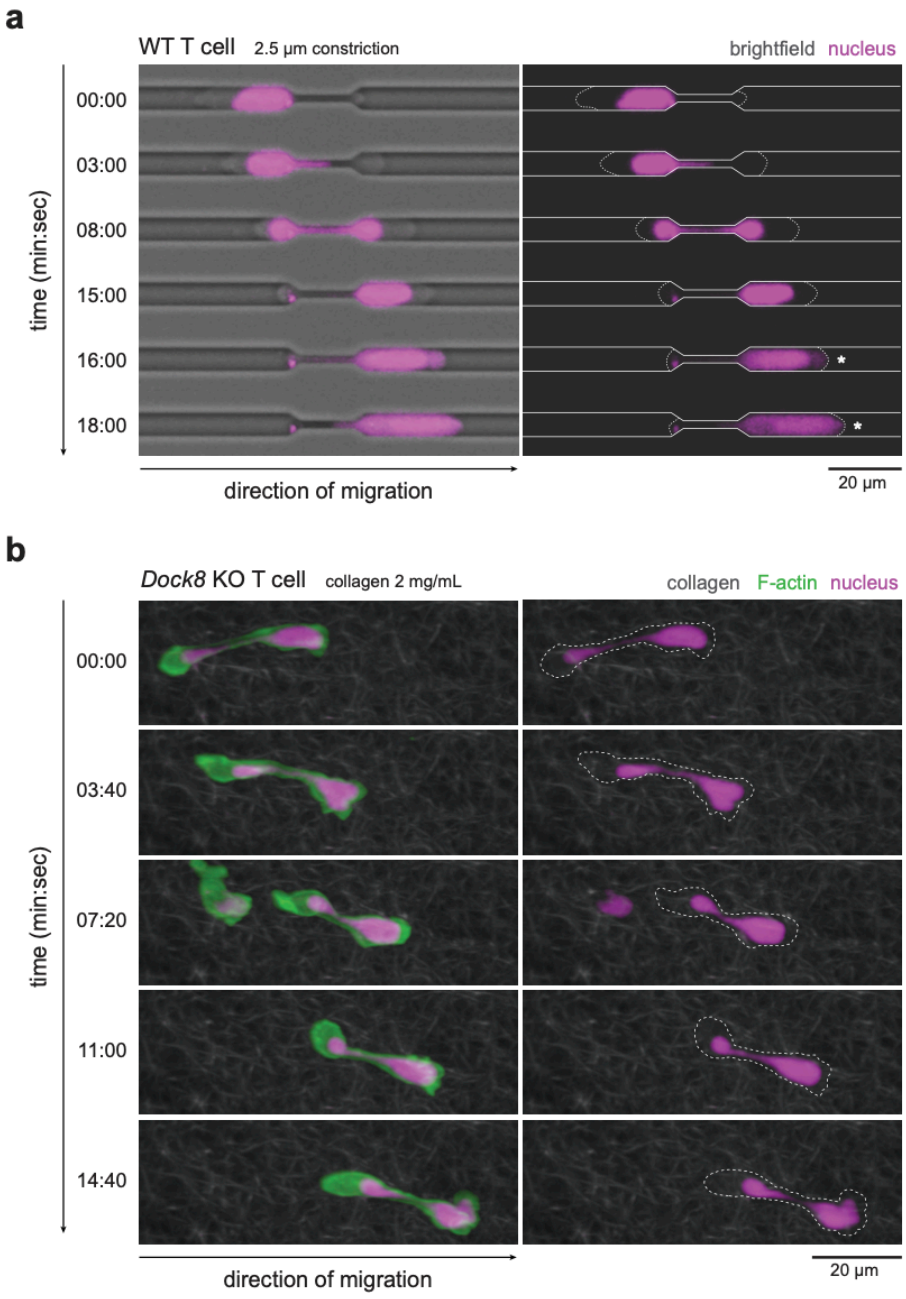

Figure S2. Perturbed nuclei of entangled *Dock8* KO T cells are stretched but do not rupture.

(a) Timelapse example of WT T cell passing through a 2.5 µm constriction with fluorescent nuclear reporter NLS-nTnG. Point of nuclear rupture is indicated by *. **(b)** Timelapse example of *Dock8* KO T cell expressing LifeAct-GFP and NLS-nTnG migrating in 2 mg/ml fluorescent collagen matrix acquired by lattice light sheet microscope and shown as a z-projection.

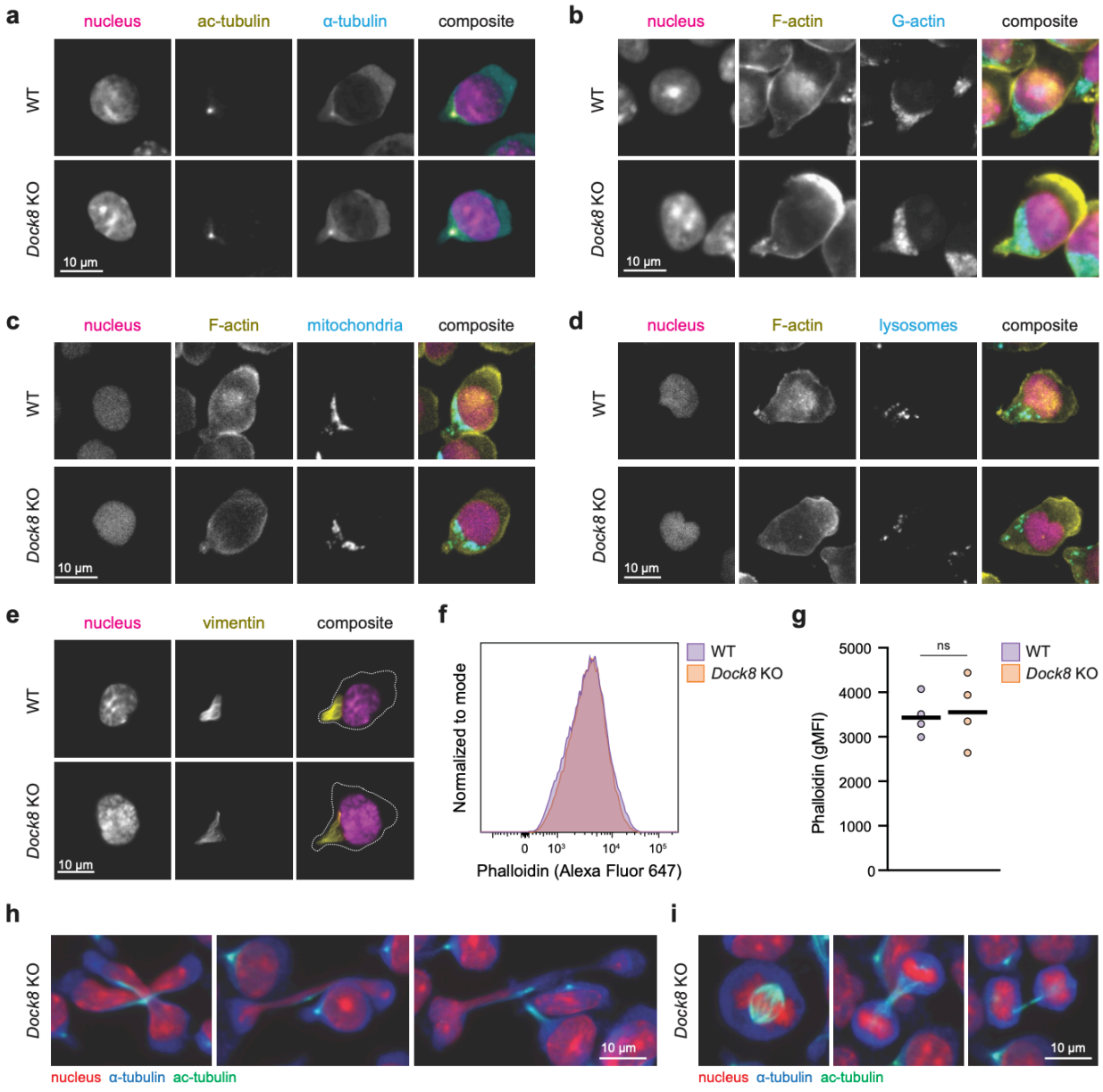
a
nucleus
ac-tubulin
α-tubulin
composite
WT
Dock8 KO
10 μm
b
nucleus
F-actin
G-actin
composite
c
nucleus
F-actin
mitochondria
composite
d
nucleus
F-actin
lysosomes
composite
e
nucleus
vimentin
composite
f
Normalized to mode
Phalloidin (Alexa Fluor 647)
WT
Dock8 KO
g
ns
Phalloidin (gMFI)
5000
4000
3000
2000
1000
0
h
i
nucleus α-tubulin ac-tubulin

Figure S3. *Dock8* KO T cells display normal cell cytoskeleton, organelle organization, total F-actin, and cell division under confinement.

(a-e) Examples of WT and *Dock8* KO T cells migrating under 1.2% agarose. Fixed cells were stained for nucleus (Hoechst) (a-e), acetyl-tubulin (ac-tubulin antibody) (a), tubulin (**α**-tubulin antibody) (a), F-actin (phalloidin) (b-d), G-actin (DNAseI) (b), mitochondria (Mitotracker) (c), lysosomes (wheat germ agglutinin) (d), and/or vimentin (vimentin antibody) with cell outline from brightfield (e). **(f,g)** Total cellular F-actin of activated T cells (TCR-**β**+ CD44+) embedded in 2mg/mL collagen for 2 hours prior to digestion and stained with phalloidin for flow cytometry. Representative histogram (f) and data summarized from $n = 4$ mice per genotype (g). **(h,i)** Examples of *Dock8* KO T cells under 1.2% agarose that are stretching (h) or dividing (i). Fixed cells were stained for acetyl-tubulin (ac-tubulin antibody), tubulin (**α**-tubulin antibody), and nucleus (Hoechst).

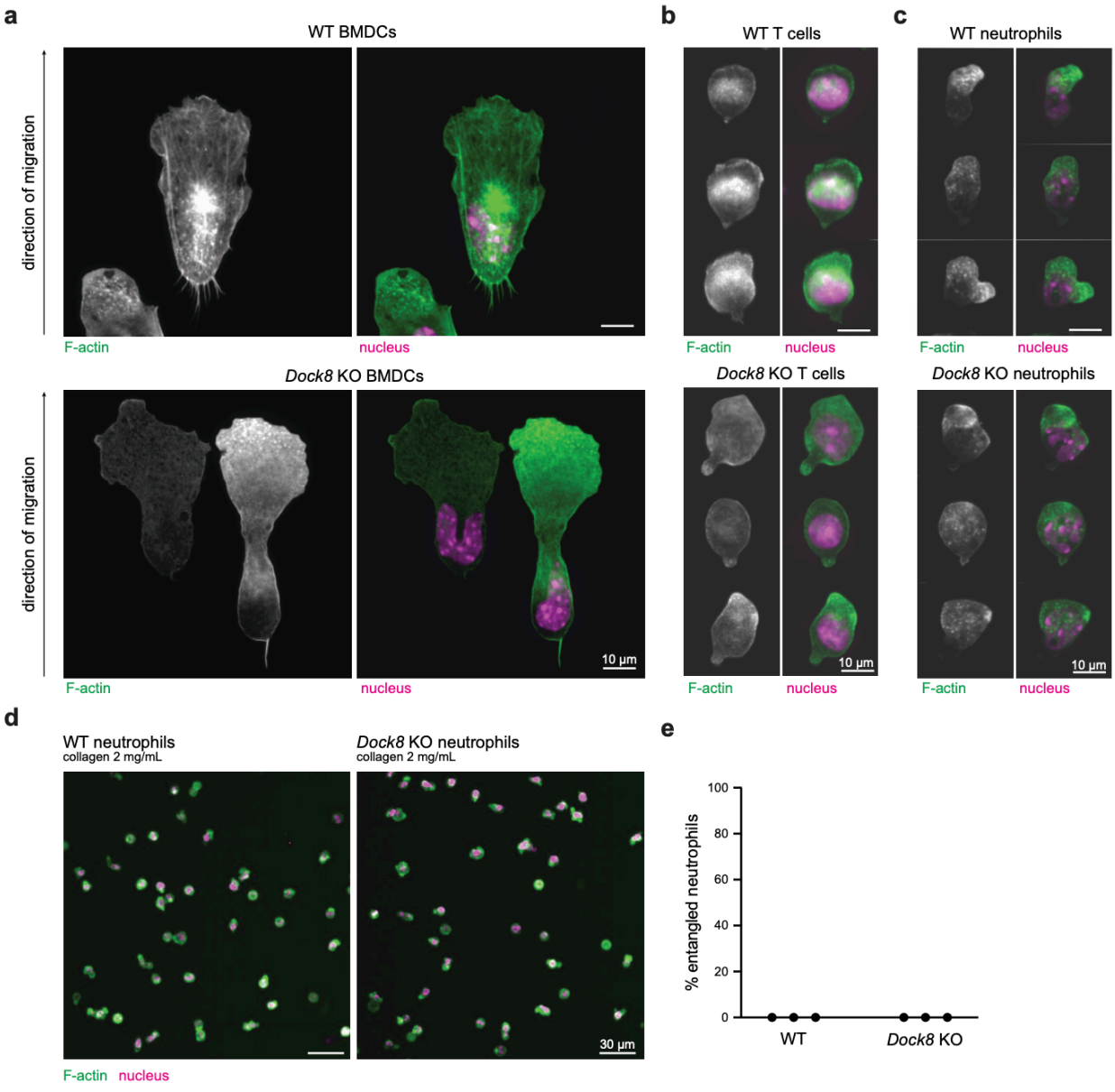
a
WT BMDCs
direction of migration
F-actin
nucleus
Dock8 KO BMDCs
direction of migration
10 µm
F-actin
nucleus
b
WT T cells
F-actin
nucleus
Dock8 KO T cells
10 µm
F-actin
nucleus
c
WT neutrophils
F-actin
nucleus
Dock8 KO neutrophils
10 µm
F-actin
nucleus
d
WT neutrophils
collagen 2 mg/mL
Dock8 KO neutrophils
collagen 2 mg/mL
30 µm
F-actin nucleus
e
% entangled neutrophils
100
80
60
40
20
0
WT
Dock8 KO

Figure S4. Confinement-dependent central actin pool is present in dendritic cells, but not in entanglement-resistant neutrophils.

(a-c) Representative examples of WT and *Dock8* KO BMDCs (a), T cells (b), and neutrophils (c) migrating under 1.2% agarose with a chemokine gradient (CCL19 for BDMC and T cells, fMLF for neutrophils). Fixed cells were stained for F-actin (phalloidin) and the nucleus (Hoechst). **(d)** LifeAct-GFP and NLS-nTnG WT and *Dock8* KO neutrophils spontaneously migrating through a 2mg/ml bovine collagen matrix (no chemokine added). **(e)** Summary plot of neutrophil entanglement frequency during migration in collagen matrix (d) from $n = 3$ mice per genotype, 2 independent experiments.

Supplemental tables

Table S1. List of summary cell shape parameters used in the PCA with their relative contribution to variance per column.

Table S2. List of DEGs identified by RNA-sequencing comparing WT and *Dock8* KO T cells in either media or collagen for 24 hours.

Supplemental movies

Video S1. Examples of LifeAct-GFP and NLS-nTnG WT and *Dock8* KO T cells moving in collagen gels, corresponding to Figure 1a.

Video S2. Examples of LifeAct-GFP and NLS-nTnG *Dock8* KO T cells entangled in collagen matrices.

Video S3. Examples of LifeAct-GFP NLS-nTnG WT and *Dock8* KO T cells migrating in 6 μm straight microchannels, corresponding to Figure 2b. Scale bar is 10μm.

Video S4. Examples of LifeAct-GFP NLS-nTnG WT and *Dock8* KO T cells migrating in pillar forest microchannel, corresponding to Figure 2d. Scale bar is 20μm.

Video S5. Examples of passing and non-passing LifeAct-GFP NLS-nTnG WT T cells in constriction microchannels, corresponding to Figure 2f. Scale bar is 10μm.

Video S6. Example of nuclear rupture in LifeAct-GFP NLS-nTnG WT T cell during passage through constriction microchannel, corresponding to Figure S2a.

Video S7. Example of LifeAct-GFP NLS-nTnG *Dock8* KO T cell migrating through fluorescent collagen imaged by lattice light sheet, corresponding to Figure S2b.

Video S8. Examples of LifeAct-GFP WT and *Dock8* KO T cells migrating under agarose imaged by TIRF, corresponding to Figure 3c.

Video S9. Examples of LifeAct-GFP WT and *Dock8* KO T cells migrating under agarose imaged by widefield microscopy, corresponding to Figure 3d.

Video S10. Example of LifeAct-GFP NLS-nTnG WT T cell migrating under agarose imaged by widefield microscopy, corresponding to Figure 4d.

CHAPTER 4: DISCUSSION

SUMMARY OF RESEARCH FINDINGS

In this thesis, I describe two mechanisms that control immune cell migration. In Chapter 2, we provide experimental evidence for the long-held hypothesis that the uniquely lobulated neutrophil nucleus serves to facilitate migration through small pores, allowing for fast migration. We show this using a physiologically relevant model, a phenotypically heterogeneous population of human neutrophils. In Chapter 3, we demonstrate a mechanosensitive function for Dock8 in mediating the production of a central actin structure that appears only under confinement. We further implicate Hippo pathway Mst1 as a co-mediator of this mechanosensitive circuit.

AVENUES FOR FUTURE RESEARCH

LEUKOCYTE HETEROGENEITY

There is a general framework for the amoeboid mode of migration employed by immune cells. Fast. Dynamic. Adhesion-free. Amazingly agile, immune cells are uniquely suited for vast surveillance and expeditious capture of pathogens. However, not all immune cells are speedy shape-shifters, and the flavor of amoeboid migration differs both between immune cell types, and depending on cell state. Form follows function, and the morphological differences between leukocytes is enormous. Leukocytes vary in their size, nucleus, and spatial organization. Take for example cell size: though macrophages comprise just 10% of immune cells, they are so large that they account for nearly 50% of the cellular mass (*396*). These morphological differences between white blood cells were apparent at the advent of immunology, and most famously phenotyped in landmark observations made by Paul Ehrlich in 1870s (*397*). Since then, immunologists have uncovered a multitude of new cells that were unknowable at the time, and these morphological differences and how their structure relates to function have not been systematically characterized.

Leukocytes vary in their migratory capacity. Peak velocities for neutrophils are the fastest at 30 µm/min, lymphocytes reach 25 µm/min, DCs 10 µm/min, and monocytes just 5 µm/min (*107*). Many other immune cell subsets are simply unstudied in the context of migration. Particularly at the cellular level, DCs, neutrophils, and T cells are among the most thoroughly studied, and their regulation mechanisms may not be broadly applicable. For example, innate lymphoid cells (ILCs), though arising from the same lymphoid lineage as T cells, are phenotypically distinct (*unpublished observations*). Even though mast cells were among the first ones described by Ehrlich, understanding of their migration has remained elusive until just this past year. While immune cell interstitial movement is generally characterized as amoeboid and integrin-independent, tissue-resident mast cells are found to migrate in a slow and integrin-dependent manner. Furthermore, mast cells completely lack the migratory plasticity of other immune cells (*398*). These data raise considerations about the generalizability of migration mechanisms across leukocytes.

Nuclear morphology is another major difference between different immune cells. Nuclei differ in shape, size, location, and composition. Immune cells have the most diverse nuclear phenotypes of any cells in the body, ranging from flexible and multilobulated granulocyte nuclei, to soft yet round lymphocyte nuclei, to kidney-shaped monocyte nuclei that mature into round and rigid macrophage and DC nuclei. Determinants of cell shape are not well understood. Lamin B receptor upregulation is required for nuclear lobulation (*399*). More recently, it was identified that halting DNA loop extrusion contributes to the development of the neutrophil nucleus and neutrophil-specific gene program (*400*). Nuclear morphology will also impact the mechanosensing mechanisms available to the cell. Neutrophil nuclei are wrinkled and nuclear membranes are under low tension. Tension-driven protein translocation therefore would be less likely to occur in these cells, and proteins such as $cPLA_2$ will remain in the nucleus (*88*, *353*). Cells of the hematopoietic lineage have vastly different nuclear lamina compositions and accordingly different mechanical properties (*401*). DCs and macrophages have high levels of Lamin A/C, compared to

T cells, B cells, and neutrophils that have barely detectable amounts (*402*). So whereas DCs require an Arp2/3-dependent perinuclear actin network to pass through small pores, neutrophils have no such dependency. In fact, the formation of perinuclear actin filaments does not occur absent Lamin A/C (*87*). Nuclear composition may also dictate its connection to the rest of the cell. Monocytes and macrophages express LINC complex proteins, yet neutrophils are deficient in several LINC complex proteins (*403*). The nucleus is now understood to be an organelle that is not simply a passive container for genomic information, but an active driver of cell behaviour.

Nuclear morphology heterogeneity within a cell type also has implications for cellular function. We described how greater nuclear segmentation in neutrophils is associated with a greater ability to pass through narrow constrictions (*1*). Naïve T cells also display nuclear diversity, where some are stereotypically round and some possess prominent nuclear envelope invaginations. The subpopulation of T cells with deformed nuclei had a higher propensity to polarize upon TCR stimulation, resulting in greater cell proliferation and effector differentiation (*404*). Emerging research is clarifying the link between nuclear shape and chromatin topology, suggesting a direct axis of genomic regulation by nuclear morphology (*405*). Nuclear phenotype is inextricably linked to cellular function, and a greater understanding of nuclear mechanics may ultimately provide greater insights into cellular function.

Prior to our study, a surprising finding was made that DCs induce small nuclear ruptures to pass through constrictions (*86*, *87*). In our study, we did not observe T cells routinely undergoing nuclear rupture in even our smallest constrictions. We did occasionally observe ruptures, but those occurrences were seldom. Perhaps, because T cells have lower Lamin A/C levels than DCs, the nucleus is already more deformable and does not require nuclear membrane breakage to pass through constrictions. We also found that neutrophils, which have even lower Lamin A/C and even greater nuclear flexibility, did not exhibit a Dock8-mediated actin cloud in response to confinement. Neutrophils do express Dock8 protein, so this observation is not due to

lack of expression (*406*). We surmise that neutrophil nuclei may not require the same protection as T cells because they are terminally differentiated and relatively short-lived. Whereas both T cells and DCs become entangled in 3D matrices absent Dock8, neutrophils do not require the Dock8 mechanosensing axis to maintain cell cohesion during migration. Thus, the differential reliance on Dock8 across cell types is indicative of divergent methods of mechanosensing during migration.

The overall blueprint of each leukocyte, though roughly amoeboid, is different. As just discussed, leukocyte nuclei have various shapes. But, nuclei can also have different positions within the cell relative to other cellular structures and occupy a different amount of cellular volume. For example, naïve T cells have a cellular volume of which half is occupied by the nucleus, and half by cytoplasm. Activated T cells expand their cytoplasm 8-fold, approximately doubling their cytoplasm-to-nucleus ratio (*407*). However, even upon activation, the amount of cytoplasm a T cell possesses is meagre compared to a DC. It is then perhaps unsurprising that DCs, with massively higher cytoplasm-to-nucleus ratio and very large surface-to-volume ratio due to their ruffled morphology, have differentially regulated cytoskeletal structures. In our studies, we have demonstrated that though both T cells and DC become entangled in 3D matrices, their entangled morphology is distinct. T cells were only ever entangled in a bipolar configuration, with a maximum of two competing cell fronts. In stark contrast, DCs entanglement was always multipolar. This may be because smaller cells such as T cells and neutrophils utilize membrane tension to communicate between protrusions, but larger ramified cells utilize the microtubule network for protrusion coordination (*57*). Microtubules bestow the ability to generate multiple protrusions. In DCs, microtubules are necessary for the retraction of protrusions, and destabilizing them results in entanglement and impaired migration (*59*). In T cells, microtubule destabilization and release of GEF-H1 leads to heightened Rho-mediated contractility, but unlike DCs actually improves intratumoral infiltration and migration (*125*). Interestingly, T_{RM}s residing in the skin curiously take on a more dendritic morphology, and in this case, microtubule destabilization will result in

cellular elongation more similar to the DCs (*408*, *409*). All this indicates that immune cells have fundamentally different mechanisms of cell cohesion that depend not only on cell type but also cell state and location. Intriguingly, cell entanglement phenotypes that arise from microtubule deregulation and Dock8-deficiency look similar and it remains to be determined whether Dock8 has a direct role in regulating microtubules, or whether resulting morphologies overlap due to similar downstream effects on contractility or actin polymerization.

The mechanisms governing immune cell migration, mechanosensing, and function cover the whole spectrum of universality to specificity. Another consideration of specificity is the divergence of certain structures and functions between murine and human leukocytes. This is most obvious from the gross morphology of neutrophil nuclei which are linear in humans but circular in mice. Human and murine neutrophils further differ in receptor expression, signaling pathways, secreted molecules, and metabolism (*410*). So too, do model cell lines differ from their primary counterparts. Differentiated HL-60 cells differ nuclei differ from primary neutrophils in their nuclear composition (*346*). Jurkat cells have distinct actin architectures from primary T cells (*411*). These cell lines have been the source of many fundamental insights into leukocyte biology due to their ease of manipulation. The fidelity of these models may vary. Nonetheless, the extrapolation of regulatory mechanisms in these systems and the design of future experiments should be made with these considerations in mind.

CONTEXT IS EVERYTHING

We now understand the specific mechanisms that drive this migration are highly context-dependent. One theme this thesis addresses is understanding how two-dimensional versus three-dimensional migration differs fundamentally. Differences in these migratory modes include the use of adhesive structures, the primary molecular drivers, and mechanisms of force generation. Beyond 2D vs 3D, we now understand more than ever how the environmental context affects immune cell migration. Future work can be done on how immune cells integrate biomechanical

information such as level of confinement. This also has implications for future cell migration research as it is becoming more apparent that selecting the correct migration assay to match the research question is paramount. For example, the first widely used migration assay was the transwell migration assay. This assay measures chemotactic responsiveness more than true migration. Microfluidic devices provide excellent control of environmental geometries, but are limited in mimicking physiological stiffness. Under agarose assays recapitulate confinement and allow for excellent resolution, but lack other elements of environmental complexity. 3D matrices mirror environmental complexity, but heterogeneity can be a challenge. Finally, visualization of migration *in vivo* is the most physiologically faithful, but can be technically challenging and difficult to perturb mechanistically.

In general, the selection of migration assays involves a tradeoff between molecular resolution and biological context. On one end, advances in super-resolution microscopy and molecular probes allow us to visualize the molecules of movement in greater detail than ever before, but often in only specific *in vitro* contexts, such as TIRF or lattice light sheet microscopy. On the other end, techniques such as intravital allow for the visualization of cell migration *in situ*, but limit what we can visualize in terms of cellular detail and environmental interactions. Experimental approaches to understanding cell function should consider the mechanical context in which they would physiologically occur. There may be shortcomings in the interpretability of results which arise from two-dimensional highly stiff cell culture plates. Techniques and assays should be selected to best probe the specific aspect of migration in question.

BALANCING ACTIN FORCES

Concurrent with our study into the role of Dock8 in T cells, a separate study by the Sixt group characterized the function of Dock8 in DCs (*412*). In both studies, a Dock8-dependent central actin pool was generated under confinement. In our study, we observed under the confinement of 1.2% agarose that both T cells and DCs produced a prominent actin cloud towards the front of the nucleus. Unlike the T cells in our

study which maintained the same actin positioning at both higher and lower agarose concentrations, Reis-Rodrigues and colleagues find that under softer agarose (0.5%), DCs were more likely to have the central actin pool present at the rear of the nucleus. The authors describe this as an 'amoeboid to mesenchymal transition' that occurs as cells move from permissive to constrained environments. Another prominent difference that emerged between these cell types is the actin cloud association with other organelles and cytoskeletal structures. In T cells, the MTOC was always located in the uropod of the cell behind the nucleus, and the actin cloud was always positioned to the front; these two structures never overlapped. In contrast, the central actin cloud of DCs was always observed to be associated with the MTOC as well as with organelles such as the Golgi and lysosomes. Their study expands on the differences we observed between DCs and T cells in our study and further illustrates the gaps in our knowledge of how different immune cells regulate their migratory strategies in various environments.

Using pushing force microscopy both under agarose and in collagen gel, the Sixt group identified a function for the actin cloud in pushing out on the environment ahead of the nucleus. When under confinement, the central actin structure deforms the environment preceding the nucleus to make the environment more permissive for passage. In Dock8-deficient DCs which lack this actin structure, the primary pushing force is exerted by the nucleus. This complements our observation of greater nuclear deformation and DNA damage in Dock8-deficient T cells. Together, these data suggest the central actin structure may exert nucleoprotective capacity under confinement by reducing environmental pressure on the nucleus.

In both studies, the presence of the central actin structure is completely dependent on Dock8 expression. Loss of the central actin structure results in a redistribution of F-actin to the leading edge. In Dock8-deficiency, both T cells and DCs develop a hyperstabilized leading edge which propels the cell forward. This leads to the observation in both cell types where migration in simple 1D channels is actually faster without Dock8, whereas migration speed in 3D collagen matrices is reduced.

Speed reduction in both cases is likely due to a combination of the nucleus becoming more of an obstacle without actin to clear the way, and as a result of cell entanglement which occurs when leading edges split and compete. These results indicate two distinct actin pools present in immune cells: one central structure and one at the leading edge. These two actin pools may regulate each other. As one is reduced, the other one increases, conserving total F-actin levels. G-actin supply is typically not considered to be limiting (*11*). However, there is evidence that suggests F-actin structures may have to compete for a homeostatic supply of G-actin (*413*). Perhaps, the two actin pools present in immune cells are in communication in a mechanism which requires Dock8 to integrate mechanical signals about environmental confinement to properly allocate F-actin for optimal migration. These findings also suggest that during migration through complex environments, there is a trade-off between cell speed and persistence on one end, and cell cohesion and integrity on the other. Without Dock8, cells lose the mechanosensitive switch to modulate the balance of these actin pools.

CONCLUDING REMARKS

Ultimately, cell migration mechanisms fall on a spectrum from highly context- and cell-specific processes, to entirely universal phenomena. This thesis represents my contribution to unravelling the mechanisms of cell migration in different immune cell types in complex environments. We identify a relationship between nuclear morphology and migratory capacity in neutrophils, and a novel confinement-responsive mechanosensitive circuit in T-cells and DCs. Understanding the full range of regulation will help inform our broader knowledge of immune networks and more precisely target specific functions for modulation in the context of disease.

REFERENCES

1. C. Shen, E. Mulder, W. Buitenwerf, J. Postat, A. Jansen, M. Kox, J. N. Mandl, N. Vrisekoop, Nuclear segmentation facilitates neutrophil migration. *Journal of Cell Science* **136**, jcs260768 (2023).

2. C. Shen, J. Postat, A. Cerf, M. Merino, A. Bhagrath, D. Patel, V. Luo, A. Abu-Thuraia, C. Schneider, A. Sharma, W.-K. Suh, A. Ehrlicher, J.-F. Côté, J. N. Mandl, DOCK8 regulates a mechanosensitive actin redistribution that maintains immune cell cohesion and protects the nucleus during migration. bioRxiv [Preprint] (2024). https://doi.org/10.1101/2024.07.26.605273.

3. V. M. Luo, C. Shen, S. Worme, A. Bhagrath, E. Simo-Cheyou, S. Findlay, S. Hébert, W. Wai Lam Poon, Z. Aryanpour, T. Zhang, R. P. Zahedi, J. Boulais, Z. S. Buchwald, C. H. Borchers, J.-F. Côté, C. L. Kleinman, J. N. Mandl, A. Orthwein, The Deubiquitylase Otub1 Regulates the Chemotactic Response of Splenic B Cells by Modulating the Stability of the γ-Subunit Gng2. *Molecular and Cellular Biology* **44**, 1–16 (2024).

4. D. Rogers, A. Sood, H. Wang, J. J. P. van Beek, T. J. Rademaker, P. Artusa, C. Schneider, C. Shen, D. C. Wong, A. Bhagrath, M.-È. Lebel, S. A. Condotta, M. J. Richer, A. J. Martins, J. S. Tsang, L. B. Barreiro, P. François, D. Langlais, H. J. Melichar, J. Textor, J. N. Mandl, Pre-existing chromatin accessibility and gene expression differences among naive CD4+ T cells influence effector potential. *Cell Reports* **37** (2021).

5. C. Schneider, C. Shen, A. A. Gopal, T. Douglas, B. Forestell, K. D. Kauffman, D. Rogers, P. Artusa, Q. Zhang, H. Jing, A. F. Freeman, D. L. Barber, I. L. King, M. Saleh, P. W. Wiseman, H. C. Su, J. N. Mandl, Migration-induced cell shattering due to DOCK8 deficiency causes a type 2–biased helper T cell response. *Nature Immunology* **21**, 1528–1539 (2020).

6. A. A. Tong, B. Forestell, D. V. Murphy, A. Nair, F. Allen, J. Myers, F. Klauschen, C. Shen, A. A. Gopal, A. Y. Huang, J. N. Mandl, Regulatory T cells differ from conventional CD4+ T cells in their recirculatory behavior and lymph node transit times. *Immunology & Cell Biology* **97**, 787–798 (2019).

7. T. D. Pollard, J. A. Cooper, Actin, a Central Player in Cell Shape and Movement. *Science* **326**, 1208–1212 (2009).

8. L. K. Fritz-Laylin, M. Riel-Mehan, B.-C. Chen, S. J. Lord, T. D. Goddard, T. E. Ferrin, S. M. Nicholson-Dykstra, H. Higgs, G. T. Johnson, E. Betzig, R. D. Mullins, Actin-based protrusions of migrating neutrophils are intrinsically lamellar and facilitate direction changes. *eLife* **6**, e26990 (2017).

9. F. Huber, A. Boire, M. P. López, G. H. Koenderink, Cytoskeletal crosstalk: when three different personalities team up. *Current Opinion in Cell Biology* **32**, 39–47 (2015).

10. K. Skruber, T.-A. Read, E. A. Vitriol, Reconsidering an active role for G-actin in cytoskeletal regulation. *J Cell Sci* **131**, jcs203760 (2018).

11. T. D. Pollard, G. G. Borisy, Cellular Motility Driven by Assembly and Disassembly of Actin Filaments. *Cell* **112**, 453–465 (2003).

12. R. D. Mullins, J. A. Heuser, T. D. Pollard, The interaction of Arp2/3 complex with actin: Nucleation, high affinity pointed end capping, and formation of branching networks of filaments. *Proc Natl Acad Sci U S A* **95**, 6181–6186 (1998).

13. D. A. Valencia, M. E. Quinlan, Formins. *Current Biology* **31**, R517–R522 (2021).

14. D. Breitsprecher, B. L. Goode, Formins at a glance. *J Cell Sci* **126**, 1–7 (2013).

15. M. E. Quinlan, J. E. Heuser, E. Kerkhoff, R. Dyche Mullins, Drosophila Spire is an actin nucleation factor. *Nature* **433**, 382–388 (2005).

16. P. Lappalainen, T. Kotila, A. Jégou, G. Romet-Lemonne, Biochemical and mechanical regulation of actin dynamics. *Nat Rev Mol Cell Biol* **23**, 836–852 (2022).

17. C. D. Nobes, A. Hall, Rho, Rac, and Cdc42 GTPases regulate the assembly of multimolecular focal complexes associated with actin stress fibers, lamellipodia, and filopodia. *Cell* **81**, 53–62 (1995).

18. R. El Masri, J. Delon, RHO GTPases: from new partners to complex immune syndromes. *Nature Reviews Immunology*, 1–15 (2021).

19. A. J. Ridley, M. A. Schwartz, K. Burridge, R. A. Firtel, M. H. Ginsberg, G. Borisy, J. T. Parsons, A. R. Horwitz, Cell Migration: Integrating Signals from Front to Back. *Science* **302**, 1704–1709 (2003).

20. M. Edwards, A. Zwolak, D. A. Schafer, D. Sept, R. Dominguez, J. A. Cooper, Capping protein regulators fine-tune actin assembly dynamics. *Nat Rev Mol Cell Biol* **15**, 677–689 (2014).

21. M. R. Mejillano, S. Kojima, D. A. Applewhite, F. B. Gertler, T. M. Svitkina, G. G. Borisy, Lamellipodial Versus Filopodial Mode of the Actin Nanomachinery: Pivotal Role of the Filament Barbed End. *Cell* **118**, 363–373 (2004).

22. P. Maiuri, J.-F. Rupprecht, S. Wieser, V. Ruprecht, O. Bénichou, N. Carpi, M. Coppey, S. De Beco, N. Gov, C.-P. Heisenberg, C. Lage Crespo, F. Lautenschlaeger, M. Le Berre, A.-M. Lennon-Dumenil, M. Raab, H.-R. Thiam,

M. Piel, M. Sixt, R. Voituriez, Actin Flows Mediate a Universal Coupling between Cell Speed and Cell Persistence. *Cell* **161**, 374–386 (2015).

23. A. J. Ridley, Life at the Leading Edge. *Cell* **145**, 1012–1022 (2011).

24. M. L. Gardel, I. C. Schneider, Y. Aratyn-Schaus, C. M. Waterman, Mechanical Integration of Actin and Adhesion Dynamics in Cell Migration. *Annual Review of Cell and Developmental Biology* **26**, 315–333 (2010).

25. D. A. Murphy, S. A. Courtneidge, The "ins" and "outs" of podosomes and invadopodia: characteristics, formation and function. *Nat Rev Mol Cell Biol* **12**, 413–426 (2011).

26. S. Linder, P. Cervero, R. Eddy, J. Condeelis, Mechanisms and roles of podosomes and invadopodia. *Nat Rev Mol Cell Biol* **24**, 86–106 (2023).

27. H. Schachtner, S. D. J. Calaminus, S. G. Thomas, L. M. Machesky, Podosomes in adhesion, migration, mechanosensing and matrix remodeling. *Cytoskeleton* **70**, 572–589 (2013).

28. J. M. García-Arcos, A. Jha, C. M. Waterman, M. Piel, Blebology: principles of bleb-based migration. *Trends in Cell Biology*, doi: 10.1016/j.tcb.2024.02.009 (2024).

29. D. A. Fletcher, R. D. Mullins, Cell mechanics and the cytoskeleton. *Nature* **463**, 485–492 (2010).

30. A. Leithner, A. Eichner, J. Müller, A. Reversat, M. Brown, J. Schwarz, J. Merrin, D. J. J. de Gorter, F. Schur, J. Bayerl, I. de Vries, S. Wieser, R. Hauschild, F. P. L. Lai, M. Moser, D. Kerjaschki, K. Rottner, J. V. Small, T. E. B. Stradal, M. Sixt, Diversified actin protrusions promote environmental exploration but are dispensable for locomotion of leukocytes. *Nat Cell Biol* **18**, 1253–1259 (2016).

31. A. Diz-Muñoz, M. Krieg, M. Bergert, I. Ibarlucea-Benitez, D. J. Muller, E. Paluch, C.-P. Heisenberg, Control of Directed Cell Migration In Vivo by Membrane-to-Cortex Attachment. *PLOS Biology* **8**, e1000544 (2010).

32. A. Bisaria, A. Hayer, D. Garbett, D. Cohen, T. Meyer, Membrane-proximal F-actin restricts local membrane protrusions and directs cell migration. *Science* **368**, 1205–1210 (2020).

33. J. M. García-Arcos, J. Ziegler, S. Grigolon, L. Reymond, G. Shajepal, C. J. Cattin, A. Lomakin, D. J. Müller, V. Ruprecht, S. Wieser, R. Voituriez, M. Piel, Rigidity percolation and active advection synergize in the actomyosin cortex to drive amoeboid cell motility. *Developmental Cell*, doi: 10.1016/j.devcel.2024.06.023 (2024).

34. P. Chugh, A. G. Clark, M. B. Smith, D. A. D. Cassani, K. Dierkes, A. Ragab, P. P. Roux, G. Charras, G. Salbreux, E. K. Paluch, Actin cortex architecture regulates cell surface tension. *Nat Cell Biol* **19**, 689–697 (2017).

35. H. D. Belly, S. Yan, H. B. da Rocha, S. Ichbiah, J. P. Town, P. J. Zager, D. C. Estrada, K. Meyer, H. Turlier, C. Bustamante, O. D. Weiner, Cell protrusions and contractions generate long-range membrane tension propagation. *Cell* **186**, 3049-3061.e15 (2023).

36. H. De Belly, O. D. Weiner, Follow the flow: Actin and membrane act as an integrated system to globally coordinate cell shape and movement. *Current Opinion in Cell Biology* **89**, 102392 (2024).

37. A. R. Houk, A. Jilkine, C. O. Mejean, R. Boltyanskiy, E. R. Dufresne, S. B. Angenent, S. J. Altschuler, L. F. Wu, O. D. Weiner, Membrane tension maintains cell polarity by confining signals to the leading edge during neutrophil migration. *Cell* **148**, 175–188 (2012).

38. R. G. Fehon, A. I. McClatchey, A. Bretscher, Organizing the cell cortex: the role of ERM proteins. *Nat Rev Mol Cell Biol* **11**, 276–287 (2010).

39. M. Arpin, D. Chirivino, A. Naba, I. Zwaenepoel, Emerging role for ERM proteins in cell adhesion and migration. *Cell Adh Migr* **5**, 199–206 (2011).

40. Y. Liu, N. V. Belkina, C. Park, R. Nambiar, S. M. Loughhead, G. Patino-Lopez, K. Ben-Aissa, J.-J. Hao, M. J. Kruhlak, H. Qi, U. H. von Andrian, J. H. Kehrl, M. J. Tyska, S. Shaw, Constitutively active ezrin increases membrane tension, slows migration, and impedes endothelial transmigration of lymphocytes in vivo in mice. *Blood* **119**, 445–453 (2012).

41. F. Sánchez-Madrid, J. M. Serrador, Bringing up the rear: defining the roles of the uropod. *Nat Rev Mol Cell Biol* **10**, 353–359 (2009).

42. T. F. Robertson, P. Chengappa, D. Gomez Atria, C. F. Wu, L. Avery, N. H. Roy, I. Maillard, R. J. Petrie, J. K. Burkhardt, Lymphocyte egress signal sphingosine-1-phosphate promotes ERM-guided, bleb-based migration. *J Cell Biol* **220**, e202007182 (2021).

43. J. A. Virtanen, M. K. Vartiainen, Diverse functions for different forms of nuclear actin. *Current Opinion in Cell Biology* **46**, 33–38 (2017).

44. C. P. Caridi, C. D'Agostino, T. Ryu, G. Zapotoczny, L. Delabaere, X. Li, V. Y. Khodaverdian, N. Amaral, E. Lin, A. R. Rau, I. Chiolo, Nuclear F-actin and myosins drive relocalization of heterochromatic breaks. *Nature* **559**, 54–60 (2018).

45. P. Friedl, K. Wolf, J. Lammerding, Nuclear mechanics during cell migration. *Curr Opin Cell Biol* **23**, 55–64 (2011).

46. S. Ulferts, M. Lopes, K. Miyamoto, R. Grosse, Nuclear actin dynamics and functions at a glance. *Journal of Cell Science* **137**, jcs261630 (2024).

47. C. P. Caridi, M. Plessner, R. Grosse, I. Chiolo, Nuclear actin filaments in DNA repair dynamics. *Nat Cell Biol* **21**, 1068–1077 (2019).

48. L. Dupré, G. Prunier, Deciphering actin remodelling in immune cells through the prism of actin-related inborn errors of immunity. *European Journal of Cell Biology* **102**, 151283 (2023).

49. H. V. Goodson, E. M. Jonasson, Microtubules and Microtubule-Associated Proteins. *Cold Spring Harb Perspect Biol* **10**, a022608 (2018).

50. A. Akhmanova, L. C. Kapitein, Mechanisms of microtubule organization in differentiated animal cells. *Nat Rev Mol Cell Biol* **23**, 541–558 (2022).

51. N. B. Gudimchuk, J. R. McIntosh, Regulation of microtubule dynamics, mechanics and function through the growing tip. *Nat Rev Mol Cell Biol* **22**, 777–795 (2021).

52. A. Akhmanova, M. O. Steinmetz, Microtubule minus-end regulation at a glance. *J Cell Sci* **132** (2019).

53. C. Janke, J. Chloë Bulinski, Post-translational regulation of the microtubule cytoskeleton: mechanisms and functions. *Nat Rev Mol Cell Biol* **12**, 773–786 (2011).

54. D. Portran, L. Schaedel, Z. Xu, M. Théry, M. V. Nachury, Tubulin acetylation protects long-lived microtubules against mechanical ageing. *Nat Cell Biol* **19**, 391–398 (2017).

55. S. Etienne-Manneville, Microtubules in Cell Migration. *Annual Review of Cell and Developmental Biology* **29**, 471–499 (2013).

56. P. J. Hooikaas, H. G. Damstra, O. J. Gros, W. E. van Riel, M. Martin, Y. T. Smits, J. van Loosdregt, L. C. Kapitein, F. Berger, A. Akhmanova, Kinesin-4 KIF21B limits microtubule growth to allow rapid centrosome polarization in T cells. *eLife* **9**, e62876 (2020).

57. A. Kopf, E. Kiermaier, Dynamic Microtubule Arrays in Leukocytes and Their Role in Cell Migration and Immune Synapse Formation. *Frontiers in Cell and Developmental Biology* **9**, 158 (2021).

58. J. Renkawitz, A. Kopf, J. Stopp, I. de Vries, M. K. Driscoll, J. Merrin, R. Hauschild, E. S. Welf, G. Danuser, R. Fiolka, M. Sixt, Nuclear positioning facilitates amoeboid migration along the path of least resistance. *Nature* **568**, 546–550 (2019).

59. A. Kopf, J. Renkawitz, R. Hauschild, I. Girkontaite, K. Tedford, J. Merrin, O. Thorn-Seshold, D. Trauner, H. Häcker, K.-D. Fischer, E. Kiermaier, M. Sixt, Microtubules control cellular shape and coherence in amoeboid migrating cells. *J Cell Biol* **219** (2020).

60. G. Dutour-Provenzano, S. Etienne-Manneville, Intermediate filaments. *Current Biology* **31**, R522–R529 (2021).

61. S. Etienne-Manneville, Cytoplasmic Intermediate Filaments in Cell Biology. *Annual Review of Cell and Developmental Biology* **34**, 1–28 (2018).

62. B.-M. Chung, J. D. Rotty, P. A. Coulombe, Networking galore: intermediate filaments and cell migration. *Current Opinion in Cell Biology* **25**, 600–612 (2013).

63. L. M. Godsel, R. P. Hobbs, K. J. Green, Intermediate filament assembly: dynamics to disease. *Trends in Cell Biology* **18**, 28–37 (2008).

64. K. M. Ridge, J. E. Eriksson, M. Pekny, R. D. Goldman, Roles of vimentin in health and disease. *Genes Dev.* **36**, 391–407 (2022).

65. E. Infante, S. Etienne-Manneville, Intermediate filaments: Integration of cell mechanical properties during migration. *Front. Cell Dev. Biol.* **10** (2022).

66. A. E. Patteson, A. Vahabikashi, K. Pogoda, S. A. Adam, K. Mandal, M. Kittisopikul, S. Sivagurunathan, A. Goldman, R. D. Goldman, P. A. Janmey, Vimentin protects cells against nuclear rupture and DNA damage during migration. *J Cell Biol* **218**, 4079–4092 (2019).

67. M. J. Brown, J. A. Hallam, E. Colucci-Guyon, S. Shaw, Rigidity of Circulating Lymphocytes Is Primarily Conferred by Vimentin Intermediate Filaments. *The Journal of Immunology* **166**, 6640–6646 (2001).

68. M. Nieminen, T. Henttinen, M. Merinen, F. Marttila–Ichihara, J. E. Eriksson, S. Jalkanen, Vimentin function in lymphocyte adhesion and transcellular migration. *Nat Cell Biol* **8**, 156–162 (2006).

69. M. R. Shaebani, L. Stankevicins, D. Vesperini, M. Urbanska, D. A. D. Flormann, E. Terriac, A. K. B. Gad, F. Cheng, J. E. Eriksson, F. Lautenschläger, Effects of vimentin on the migration, search efficiency, and mechanical resilience of dendritic cells. *Biophysical Journal* **121**, 3950–3961 (2022).

70. B. Burke, C. L. Stewart, The nuclear lamins: flexibility in function. *Nat Rev Mol Cell Biol* **14**, 13–24 (2013).

71. J. Lammerding, L. G. Fong, J. Y. Ji, K. Reue, C. L. Stewart, S. G. Young, R. T. Lee, Lamins A and C but Not Lamin B1 Regulate Nuclear Mechanics *. *Journal of Biological Chemistry* **281**, 25768–25780 (2006).

72. T. P. Lele, R. B. Dickinson, G. G. Gundersen, Mechanical principles of nuclear shaping and positioning. *Journal of Cell Biology* **217**, 3330–3342 (2018).

73. S. M. Schreiner, P. K. Koo, Y. Zhao, S. G. J. Mochrie, M. C. King, The tethering of chromatin to the nuclear envelope supports nuclear mechanics. *Nat Commun* **6**, 7159 (2015).

74. A. D. Stephens, E. J. Banigan, S. A. Adam, R. D. Goldman, J. F. Marko, Chromatin and lamin A determine two different mechanical response regimes of the cell nucleus. *Mol Biol Cell* **28**, 1984–1996 (2017).

75. Y. Kalukula, A. D. Stephens, J. Lammerding, S. Gabriele, Mechanics and functional consequences of nuclear deformations. *Nat Rev Mol Cell Biol* **23**, 583–602 (2022).

76. L. Guelen, L. Pagie, E. Brasset, W. Meuleman, M. B. Faza, W. Talhout, B. H. Eussen, A. de Klein, L. Wessels, W. de Laat, B. van Steensel, Domain organization of human chromosomes revealed by mapping of nuclear lamina interactions. *Nature* **453**, 948–951 (2008).

77. A. Buchwalter, J. M. Kaneshiro, M. W. Hetzer, Coaching from the sidelines: the nuclear periphery in genome regulation. *Nat Rev Genet* **20**, 39–50 (2019).

78. S. K. Yadav, S. W. Feigelson, F. Roncato, M. Antman-Passig, O. Shefi, J. Lammerding, R. Alon, Elevated nuclear lamin A is permissive for granulocyte transendothelial migration but not for motility through collagen I barriers. *J Leukoc Biol* **104**, 239–251 (2018).

79. A. C. Rowat, D. E. Jaalouk, M. Zwerger, W. L. Ung, I. A. Eydelnant, D. E. Olins, A. L. Olins, H. Herrmann, D. A. Weitz, J. Lammerding, Nuclear Envelope Composition Determines the Ability of Neutrophil-type Cells to Passage through Micron-scale Constrictions. *J Biol Chem* **288**, 8610–8618 (2013).

80. H. R. Manley, M. C. Keightley, G. J. Lieschke, The Neutrophil Nucleus: An Important Influence on Neutrophil Migration and Function. *Front Immunol* **9** (2018).

81. J. M. González-Granado, C. Silvestre-Roig, V. Rocha-Perugini, L. Trigueros-Motos, D. Cibrián, G. Morlino, M. Blanco-Berrocal, F. G. Osorio, J. M. P. Freije,

C. López-Otín, F. Sánchez-Madrid, V. Andrés, Nuclear Envelope Lamin-A Couples Actin Dynamics with Immunological Synapse Architecture and T Cell Activation. *Science Signaling* **7**, ra37–ra37 (2014).

82. T. Harada, J. Swift, J. Irianto, J.-W. Shin, K. R. Spinler, A. Athirasala, R. Diegmiller, P. C. D. P. Dingal, I. L. Ivanovska, D. E. Discher, Nuclear lamin stiffness is a barrier to 3D migration, but softness can limit survival. *J Cell Biol* **204**, 669–682 (2014).

83. C. R. Pfeifer, M. Vashisth, Y. Xia, D. E. Discher, Nuclear failure, DNA damage, and cell cycle disruption after migration through small pores: a brief review. *Essays in Biochemistry* **63**, 569–577 (2019).

84. P. Shah, K. Wolf, J. Lammerding, Bursting the Bubble – Nuclear Envelope Rupture as a Path to Genomic Instability? *Trends in Cell Biology* **27**, 546–555 (2017).

85. C. M. Denais, R. M. Gilbert, P. Isermann, A. L. McGregor, M. te Lindert, B. Weigelin, P. M. Davidson, P. Friedl, K. Wolf, J. Lammerding, Nuclear envelope rupture and repair during cancer cell migration. *Science* **352**, 353–358 (2016).

86. M. Raab, M. Gentili, H. de Belly, H.-R. Thiam, P. Vargas, A. J. Jimenez, F. Lautenschlaeger, R. Voituriez, A.-M. Lennon-Duménil, N. Manel, M. Piel, ESCRT III repairs nuclear envelope ruptures during cell migration to limit DNA damage and cell death. *Science* **352**, 359–362 (2016).

87. H.-R. Thiam, P. Vargas, N. Carpi, C. L. Crespo, M. Raab, E. Terriac, M. C. King, J. Jacobelli, A. S. Alberts, T. Stradal, A.-M. Lennon-Dumenil, M. Piel, Perinuclear Arp2/3-driven actin polymerization enables nuclear deformation to facilitate cell migration through complex environments. *Nature Communications* **7**, 10997 (2016).

88. G. P. de F. Nader, A. Williart, M. Piel, Nuclear deformations, from signaling to perturbation and damage. *Current Opinion in Cell Biology* **72**, 137–145 (2021).

89. C. T. Halfmann, R. M. Sears, A. Katiyar, B. W. Busselman, L. K. Aman, Q. Zhang, C. S. O'Bryan, T. E. Angelini, T. P. Lele, K. J. Roux, Repair of nuclear ruptures requires barrier-to-autointegration factor. *J Cell Biol* **218**, 2136–2149 (2019).

90. N. S. De Silva, J. Siewiera, C. Alkhoury, G. P. F. Nader, F. Nadalin, K. de Azevedo, M. Couty, H. M. Izquierdo, A. Bhargava, C. Conrad, M. Maurin, K. Antoniadou, C. Fouillade, A. Londono-Vallejo, R. Behrendt, K. Bertotti, C. Serdjebi, F. Lanthiez, L. Gallwitz, P. Saftig, B. Herrero-Fernández, A. Saez, J. M. González-Granado, G. van Niel, A. Boissonnas, M. Piel, N. Manel, Nuclear

envelope disruption triggers hallmarks of aging in lung alveolar macrophages. *Nat Aging* **3**, 1251–1268 (2023).

91. P. Shah, C. M. Hobson, S. Cheng, M. J. Colville, M. J. Paszek, R. Superfine, J. Lammerding, Nuclear Deformation Causes DNA Damage by Increasing Replication Stress. *Current Biology* **31**, 753-765.e6 (2021).

92. M. Guo, A. J. Ehrlicher, S. Mahammad, H. Fabich, M. H. Jensen, J. R. Moore, J. J. Fredberg, R. D. Goldman, D. A. Weitz, The Role of Vimentin Intermediate Filaments in Cortical and Cytoplasmic Mechanics. *Biophysical Journal* **105**, 1562–1568 (2013).

93. C. P. Brangwynne, F. C. MacKintosh, S. Kumar, N. A. Geisse, J. Talbot, L. Mahadevan, K. K. Parker, D. E. Ingber, D. A. Weitz, Microtubules can bear enhanced compressive loads in living cells because of lateral reinforcement. *Journal of Cell Biology* **173**, 733–741 (2006).

94. C. Leduc, S. Etienne-Manneville, Regulation of microtubule-associated motors drives intermediate filament network polarization. *J Cell Biol* **216**, 1689–1703 (2017).

95. S. Seetharaman, S. Etienne-Manneville, Cytoskeletal Crosstalk in Cell Migration. *Trends in Cell Biology* **30**, 720–735 (2020).

96. C. M. Waterman-Storer, R. A. Worthylake, B. P. Liu, K. Burridge, E. D. Salmon, Microtubule growth activates Rac1 to promote lamellipodial protrusion in fibroblasts. *Nat Cell Biol* **1**, 45–50 (1999).

97. M. Maurer, J. Lammerding, The Driving Force: Nuclear Mechanotransduction in Cellular Function, Fate, and Disease. *Annual Review of Biomedical Engineering* **21**, 443–468 (2019).

98. A. L. McGregor, C.-R. Hsia, J. Lammerding, Squish and squeeze – the nucleus as a physical barrier during migration in confining environments. *Curr Opin Cell Biol* **40**, 32–40 (2016).

99. P.-H. Wu, D. M. Gilkes, D. Wirtz, The Biophysics of 3D Cell Migration. *Annual Review of Biophysics* **47**, 549–567 (2018).

100. J. Kroll, J. Renkawitz, Principles of organelle positioning in motile and non-motile cells. *EMBO reports* **25**, 2172–2187 (2024).

101. P. Kameritsch, J. Renkawitz, Principles of Leukocyte Migration Strategies. *Trends in Cell Biology*, doi: 10.1016/j.tcb.2020.06.007 (2020).

102. A. V. Burakov, E. S. Nadezhdina, Association of nucleus and centrosome: magnet or velcro? *Cell Biol Int* **37**, 95–104 (2013).

103. D. Obino, F. Farina, O. Malbec, P. J. Sáez, M. Maurin, J. Gaillard, F. Dingli, D. Loew, A. Gautreau, M.-I. Yuseff, L. Blanchoin, M. Théry, A.-M. Lennon-Duménil, Actin nucleation at the centrosome controls lymphocyte polarity. *Nat Commun* **7**, 10969 (2016).

104. J. Kroll, R. Hauschild, A. Kuznetcov, K. Stefanowski, M. D. Hermann, J. Merrin, L. Shafeek, A. Müller-Taubenberger, J. Renkawitz, Adaptive pathfinding by nucleokinesis during amoeboid migration. *The EMBO Journal* **42**, e114557 (2023).

105. K. M. Yamada, M. Sixt, Mechanisms of 3D cell migration. *Nature Reviews Molecular Cell Biology* **20**, 738–752 (2019).

106. T. Lämmermann, M. Sixt, Mechanical modes of 'amoeboid' cell migration. *Current Opinion in Cell Biology* **21**, 636–644 (2009).

107. P. Friedl, B. Weigelin, Interstitial leukocyte migration and immune function. *Nature Immunology* **9**, 960–969 (2008).

108. T. Lämmermann, R. N. Germain, The multiple faces of leukocyte interstitial migration. *Semin Immunopathol* **36**, 227–251 (2014).

109. P. Friedl, F. Entschladen, C. Conrad, B. Niggemann, K. S. Zänker, CD4+ T lymphocytes migrating in three-dimensional collagen lattices lack focal adhesions and utilize β1 integrin-independent strategies for polarization, interaction with collagen fibers and locomotion. *European Journal of Immunology* **28**, 2331–2343 (1998).

110. T. Lämmermann, B. L. Bader, S. J. Monkley, T. Worbs, R. Wedlich-Söldner, K. Hirsch, M. Keller, R. Förster, D. R. Critchley, R. Fässler, M. Sixt, Rapid leukocyte migration by integrin-independent flowing and squeezing. *Nature* **453**, 51–55 (2008).

111. M. L. Heuzé, P. Vargas, M. Chabaud, M. Le Berre, Y.-J. Liu, O. Collin, P. Solanes, R. Voituriez, M. Piel, A.-M. Lennon-Duménil, Migration of dendritic cells: physical principles, molecular mechanisms, and functional implications. *Immunological Reviews* **256**, 240–254 (2013).

112. A. Reversat, F. Gaertner, J. Merrin, J. Stopp, S. Tasciyan, J. Aguilera, I. de Vries, R. Hauschild, M. Hons, M. Piel, A. Callan-Jones, R. Voituriez, M. Sixt, Cellular locomotion using environmental topography. *Nature* **582**, 582–585 (2020).

113. J. Jacobelli, R. S. Friedman, M. A. Conti, A.-M. Lennon-Dumenil, M. Piel, C. M. Sorensen, R. S. Adelstein, M. F. Krummel, Confinement-Optimized 3-Dimensional T cell Amoeboid Motility is Modulated via Myosin IIA-Regulated Adhesions. *Nat Immunol* **11**, 953–961 (2010).

114. J. Jacobelli, S. A. Chmura, D. B. Buxton, M. M. Davis, M. F. Krummel, A single class II myosin modulates T cell motility and stopping, but not synapse formation. *Nat Immunol* **5**, 531–538 (2004).

115. C. A. Wilson, M. A. Tsuchida, G. M. Allen, E. L. Barnhart, K. T. Applegate, P. T. Yam, L. Ji, K. Keren, G. Danuser, J. A. Theriot, Myosin II contributes to cell-scale actin network treadmilling through network disassembly. *Nature* **465**, 373–377 (2010).

116. T. Y.-C. Tsai, S. R. Collins, C. K. Chan, A. Hadjitheodorou, P.-Y. Lam, S. S. Lou, H. W. Yang, J. Jorgensen, F. Ellett, D. Irimia, M. W. Davidson, R. S. Fischer, A. Huttenlocher, T. Meyer, J. E. Ferrell, J. A. Theriot, Efficient Front-Rear Coupling in Neutrophil Chemotaxis by Dynamic Myosin II Localization. *Developmental Cell* **49**, 189-205.e6 (2019).

117. Y.-J. Liu, M. Le Berre, F. Lautenschlaeger, P. Maiuri, A. Callan-Jones, M. Heuzé, T. Takaki, R. Voituriez, M. Piel, Confinement and Low Adhesion Induce Fast Amoeboid Migration of Slow Mesenchymal Cells. *Cell* **160**, 659–672 (2015).

118. R. J. Petrie, H. Koo, K. M. Yamada, Generation of compartmentalized pressure by a nuclear piston governs cell motility in a 3D matrix. *Science* **345**, 1062–1065 (2014).

119. V. Ruprecht, S. Wieser, A. Callan-Jones, M. Smutny, H. Morita, K. Sako, V. Barone, M. Ritsch-Marte, M. Sixt, R. Voituriez, C.-P. Heisenberg, Cortical Contractility Triggers a Stochastic Switch to Fast Amoeboid Cell Motility. *Cell* **160**, 673–685 (2015).

120. J. Keys, B. C. H. Cheung, M. A. Elpers, M. Wu, J. Lammerding, Rear cortex contraction aids in nuclear transit during confined migration by increasing pressure in the cell posterior. *Journal of Cell Science* **137**, jcs260623 (2024).

121. P. Friedl, K. Wolf, Plasticity of cell migration: a multiscale tuning model. *Journal of Cell Biology* **188**, 11–19 (2009).

122. R. J. Petrie, K. M. Yamada, Multiple Mechanisms of 3D Migration: The Origins of Plasticity. *Curr Opin Cell Biol* **42**, 7–12 (2016).

123. J. Renkawitz, K. Schumann, M. Weber, T. Lämmermann, H. Pflicke, M. Piel, J. Polleux, J. P. Spatz, M. Sixt, Adaptive force transmission in amoeboid cell migration. *Nat Cell Biol* **11**, 1438–1443 (2009).

124. M. F. Krummel, R. S. Friedman, J. Jacobelli, Modes and Mechanisms of T cell Motility: Roles for Confinement and Myosin-IIA. *Curr Opin Cell Biol* **0**, 9–16 (2014).

125. E. D. Tabdanov, N. J. Rodríguez-Merced, A. X. Cartagena-Rivera, V. V. Puram, M. K. Callaway, E. A. Ensminger, E. J. Pomeroy, K. Yamamoto, W. S. Lahr, B. R. Webber, B. S. Moriarity, A. S. Zhovmer, P. P. Provenzano, Engineering T cells to enhance 3D migration through structurally and mechanically complex tumor microenvironments. *Nat Commun* **12**, 2815 (2021).

126. A. B. Kay, The early history of the eosinophil. *Clinical & Experimental Allergy* **45**, 575–582 (2015).

127. D. B. Brewer, Max Schultze and the living, moving, phagocytosing leucocytes: 1865. *Med Hist* **38**, 91–101 (1994).

128. M. Schultze, Ein heizbarer Objecttisch und seine Verwendung bei Untersuchungen des Blutes. *Archiv f. mikrosk. Anatomie* **1**, 1–42 (1865).

129. B. A. Zabel, A. Rott, E. C. Butcher, Leukocyte Chemoattractant Receptors in Human Disease Pathogenesis. *Annu. Rev. Pathol. Mech. Dis.* **10**, 51–81 (2015).

130. T. Lämmermann, W. Kastenmüller, Concepts of GPCR-controlled navigation in the immune system. *Immunol Rev* **289**, 205–231 (2019).

131. S. SenGupta, C. A. Parent, J. E. Bear, The principles of directed cell migration. *Nat Rev Mol Cell Biol* **22**, 529–547 (2021).

132. A. Zlotnik, O. Yoshie, Chemokines: A New Classification System and Their Role in Immunity. *Immunity* **12**, 121–127 (2000).

133. H. Xu, S. Lin, Z. Zhou, D. Li, X. Zhang, M. Yu, R. Zhao, Y. Wang, J. Qian, X. Li, B. Li, C. Wei, K. Chen, T. Yoshimura, J. M. Wang, J. Huang, New genetic and epigenetic insights into the chemokine system: the latest discoveries aiding progression toward precision medicine. *Cell Mol Immunol* **20**, 739–776 (2023).

134. R. H. Insall, O. D. Weiner, PIP3, PIP2, and Cell Movement—Similar Messages, Different Meanings? *Developmental Cell* **1**, 743–747 (2001).

135. L. Tweedy, P. A. Thomason, P. I. Paschke, K. Martin, L. M. Machesky, M. Zagnoni, R. H. Insall, Seeing around corners: Cells solve mazes and respond at a distance using attractant breakdown. *Science* **369** (2020).

136. J. Alanko, M. C. Uçar, N. Canigova, J. Stopp, J. Schwarz, J. Merrin, E. Hannezo, M. Sixt, CCR7 acts as both a sensor and a sink for CCL19 to coordinate collective leukocyte migration. *Science Immunology* **8**, eadc9584 (2023).

137. P. X. Liew, P. Kubes, The Neutrophil's Role During Health and Disease. *Physiological Reviews* **99**, 1223–1248 (2019).

138. T. N. Mayadas, X. Cullere, C. A. Lowell, The Multifaceted Functions of Neutrophils. *Annu Rev Pathol* **9**, 181–218 (2014).

139. S. Nourshargh, R. Alon, Leukocyte Migration into Inflamed Tissues. *Immunity* **41**, 694–707 (2014).

140. M. Phillipson, B. Heit, S. A. Parsons, B. Petri, S. C. Mullaly, P. Colarusso, R. M. Gower, G. Neely, S. I. Simon, P. Kubes, Vav1 is Essential for Mechanotactic Crawling and Migration of Neutrophils out of the Inflamed Microvasculature. *J Immunol* **182**, 6870–6878 (2009).

141. M.-D. Filippi, Neutrophil transendothelial migration: updates and new perspectives. *Blood* **133**, 2149–2158 (2019).

142. C. V. Carman, P. T. Sage, T. E. Sciuto, M. A. de la Fuente, R. S. Geha, H. D. Ochs, H. F. Dvorak, A. M. Dvorak, T. A. Springer, Transcellular Diapedesis Is Initiated by Invasive Podosomes. *Immunity* **26**, 784–797 (2007).

143. S. Barzilai, S. K. Yadav, S. Morrell, F. Roncato, E. Klein, L. Stoler-Barak, O. Golani, S. W. Feigelson, A. Zemel, S. Nourshargh, R. Alon, Leukocytes Breach Endothelial Barriers by Insertion of Nuclear Lobes and Disassembly of Endothelial Actin Filaments. *Cell Reports* **18**, 685–699 (2017).

144. E. Kolaczkowska, P. Kubes, Neutrophil recruitment and function in health and inflammation. *Nat Rev Immunol* **13**, 159–175 (2013).

145. T. Chtanova, M. Schaeffer, S.-J. Han, G. G. van Dooren, M. Nollmann, P. Herzmark, S. W. Chan, H. Satija, K. Camfield, H. Aaron, B. Striepen, E. A. Robey, Dynamics of Neutrophil Migration in Lymph Nodes during Infection. *Immunity* **29**, 487–496 (2008).

146. N. C. Peters, J. G. Egen, N. Secundino, A. Debrabant, N. Kimblin, S. Kamhawi, P. Lawyer, M. P. Fay, R. N. Germain, D. Sacks, In Vivo Imaging Reveals an Essential Role for Neutrophils in Leishmaniasis Transmitted by Sand Flies. *Science* **321**, 970–974 (2008).

147. K. Kienle, T. Lämmermann, Neutrophil swarming: an essential process of the neutrophil tissue response. *Immunol Rev* **273**, 76–93 (2016).

148. K. Kienle, K. M. Glaser, S. Eickhoff, M. Mihlan, K. Knöpper, E. Reátegui, M. W. Epple, M. Gunzer, R. Baumeister, T. K. Tarrant, R. N. Germain, D. Irimia, W. Kastenmüller, T. Lämmermann, Neutrophils self-limit swarming to contain bacterial growth in vivo. *Science* **372**, eabe7729 (2021).

149. S. Uderhardt, A. J. Martins, J. S. Tsang, T. Lämmermann, R. N. Germain, Resident Macrophages Cloak Tissue Microlesions to Prevent Neutrophil-Driven Inflammatory Damage. *Cell* **177**, 541-555.e17 (2019).

150. S. de Oliveira, E. E. Rosowski, A. Huttenlocher, Neutrophil migration in infection and wound repair: going forward in reverse. *Nature Reviews Immunology* **16**, 378–391 (2016).

151. J. Wang, M. Hossain, A. Thanabalasuriar, M. Gunzer, C. Meininger, P. Kubes, Visualizing the function and fate of neutrophils in sterile injury and repair. *Science* **358**, 111–116 (2017).

152. M. Casanova-Acebes, J. A. Nicolás-Ávila, J. L. Li, S. García-Silva, A. Balachander, A. Rubio-Ponce, L. A. Weiss, J. M. Adrover, K. Burrows, N. A-González, I. Ballesteros, S. Devi, J. A. Quintana, G. Crainiciuc, M. Leiva, M. Gunzer, C. Weber, T. Nagasawa, O. Soehnlein, M. Merad, A. Mortha, L. G. Ng, H. Peinado, A. Hidalgo, Neutrophils instruct homeostatic and pathological states in naive tissues. *Journal of Experimental Medicine* **215**, 2778–2795 (2018).

153. L. S. C. Lok, T. W. Dennison, K. M. Mahbubani, K. Saeb-Parsy, E. R. Chilvers, M. R. Clatworthy, Phenotypically distinct neutrophils patrol uninfected human and mouse lymph nodes. *Proc Natl Acad Sci U S A* **116**, 19083–19089 (2019).

154. M. Voisin, S. Nourshargh, Neutrophil trafficking to lymphoid tissues: physiological and pathological implications. *J Pathol* **247**, 662–671 (2019).

155. K. Ley, H. M. Hoffman, P. Kubes, M. A. Cassatella, A. Zychlinsky, C. C. Hedrick, S. D. Catz, Neutrophils: New insights and open questions. *Sci. Immunol.* **3**, eaat4579 (2018).

156. A. Aroca-Crevillén, T. Vicanolo, S. Ovadia, A. Hidalgo, Neutrophils in Physiology and Pathology. *Annual Review of Pathology: Mechanisms of Disease* **19**, 227–259 (2024).

157. B. V. Kumar, T. Connors, D. L. Farber, Human T cell development, localization, and function throughout life. *Immunity* **48**, 202–213 (2018).

158. J. N. Mandl, P. Torabi-Parizi, R. N. Germain, Visualization and dynamic analysis of host–pathogen interactions. *Current Opinion in Immunology* **29**, 8–15 (2014).

159. T. Worbs, T. R. Mempel, J. Bölter, U. H. von Andrian, R. Förster, CCR7 ligands stimulate the intranodal motility of T lymphocytes in vivo. *J Exp Med* **204**, 489–495 (2007).

160. M. Hons, A. Kopf, R. Hauschild, A. Leithner, F. Gaertner, J. Abe, J. Renkawitz, J. V. Stein, M. Sixt, Chemokines and integrins independently tune actin flow and substrate friction during intranodal migration of T cells. *Nat Immunol* **19**, 606–616 (2018).

161. M. J. Miller, S. H. Wei, I. Parker, M. D. Cahalan, Two-Photon Imaging of Lymphocyte Motility and Antigen Response in Intact Lymph Node. *Science* **296**, 1869–1873 (2002).

162. P. Bousso, E. Robey, Dynamics of CD8+ T cell priming by dendritic cells in intact lymph nodes. *Nat Immunol* **4**, 579–585 (2003).

163. J. B. Beltman, A. F. M. Marée, J. N. Lynch, M. J. Miller, R. J. de Boer, Lymph node topology dictates T cell migration behavior. *J Exp Med* **204**, 771–780 (2007).

164. S. E. Acton, L. Onder, M. Novkovic, V. G. Martinez, B. Ludewig, Communication, construction, and fluid control: lymphoid organ fibroblastic reticular cell and conduit networks. *Trends in Immunology* **42**, 782–794 (2021).

165. M. Bajénoff, J. Egen, L. Y. Koo, J. P. Laugier, F. Brau, N. Glaichenhaus, R. N. Germain, Stromal Cell Networks Regulate Lymphocyte Entry, Migration, and Territoriality in Lymph Nodes. *Immunity* **25**, 989–1001 (2006).

166. J. N. Mandl, R. Liou, F. Klauschen, N. Vrisekoop, J. P. Monteiro, A. J. Yates, A. Y. Huang, R. N. Germain, Quantification of lymph node transit times reveals differences in antigen surveillance strategies of naïve CD4 $^{+}$ and CD8 $^{+}$ T cells. *Proc. Natl. Acad. Sci. U.S.A.* **109**, 18036–18041 (2012).

167. A. Gérard, G. Patino-Lopez, P. Beemiller, R. Nambiar, K. Ben-Aissa, Y. Liu, F. J. Totah, M. J. Tyska, S. Shaw, M. F. Krummel, Detection of Rare Antigen Presenting Cells through T cell-intrinsic meandering motility, mediated by Myo1g. *Cell* **158**, 492–505 (2014).

168. J. G. Cyster, S. R. Schwab, Sphingosine-1-Phosphate and Lymphocyte Egress from Lymphoid Organs. *Annual Review of Immunology* **30**, 69–94 (2012).

169. D. Masopust, J. M. Schenkel, The integration of T cell migration, differentiation and function. *Nat Rev Immunol* **13**, 309–320 (2013).

170. D. J. Fowell, M. Kim, The spatio-temporal control of effector T cell migration. *Nature Reviews Immunology*, 1–15 (2021).

171. M. F. Krummel, F. Bartumeus, A. Gérard, T cell migration, search strategies and mechanisms. *Nat Rev Immunol* **16**, 193–201 (2016).

172. S. N. Mueller, L. K. Mackay, Tissue-resident memory T cells: local specialists in immune defence. *Nat Rev Immunol* **16**, 79–89 (2016).

173. J. V. Stein, N. Ruef, Regulation of global CD8+ T-cell positioning by the actomyosin cytoskeleton. *Immunological Reviews* **289**, 232–249 (2019).

174. I. Mellman, R. M. Steinman, Dendritic Cells: Specialized and Regulated Antigen Processing Machines. *Cell* **106**, 255–258 (2001).

175. T. Worbs, S. I. Hammerschmidt, R. Förster, Dendritic cell migration in health and disease. *Nat Rev Immunol* **17**, 30–48 (2017).

176. K. Schumann, T. Lämmermann, M. Bruckner, D. F. Legler, J. Polleux, J. P. Spatz, G. Schuler, R. Förster, M. B. Lutz, L. Sorokin, M. Sixt, Immobilized Chemokine Fields and Soluble Chemokine Gradients Cooperatively Shape Migration Patterns of Dendritic Cells. *Immunity* **32**, 703–713 (2010).

177. H. D. Moreau, M. Piel, R. Voituriez, A.-M. Lennon-Duménil, Integrating Physical and Molecular Insights on Immune Cell Migration. *Trends in Immunology* **39**, 632–643 (2018).

178. M. Chabaud, M. L. Heuzé, M. Bretou, P. Vargas, P. Maiuri, P. Solanes, M. Maurin, E. Terriac, M. Le Berre, D. Lankar, T. Piolot, R. S. Adelstein, Y. Zhang, M. Sixt, J. Jacobelli, O. Bénichou, R. Voituriez, M. Piel, A.-M. Lennon-Duménil, Cell migration and antigen capture are antagonistic processes coupled by myosin II in dendritic cells. *Nat Commun* **6**, 7526 (2015).

179. G. Faure-André, P. Vargas, M.-I. Yuseff, M. Heuzé, J. Diaz, D. Lankar, V. Steri, J. Manry, S. Hugues, F. Vascotto, J. Boulanger, G. Raposo, M.-R. Bono, M. Rosemblatt, M. Piel, A.-M. Lennon-Duménil, Regulation of Dendritic Cell Migration by CD74, the MHC Class II-Associated Invariant Chain. *Science* **322**, 1705–1710 (2008).

180. H. D. Moreau, C. Blanch-Mercader, R. Attia, M. Maurin, Z. Alraies, D. Sanséau, O. Malbec, M.-G. Delgado, P. Bousso, J.-F. Joanny, R. Voituriez, M. Piel, A.-M. Lennon-Duménil, Macropinocytosis Overcomes Directional Bias in Dendritic Cells Due to Hydraulic Resistance and Facilitates Space Exploration. *Developmental Cell* **49**, 171-188.e5 (2019).

181. M. Bretou, P. J. Sáez, D. Sanséau, M. Maurin, D. Lankar, M. Chabaud, C. Spampanato, O. Malbec, L. Barbier, S. Muallem, P. Maiuri, A. Ballabio, J. Helft, M. Piel, P. Vargas, A.-M. Lennon-Duménil, Lysosome signaling controls the migration of dendritic cells. *Science Immunology* **2**, eaak9573 (2017).

182. P. Vargas, P. Maiuri, M. Bretou, P. J. Sáez, P. Pierobon, M. Maurin, M. Chabaud, D. Lankar, D. Obino, E. Terriac, M. Raab, H.-R. Thiam, T. Brocker,

S. M. Kitchen-Goosen, A. S. Alberts, P. Sunareni, S. Xia, R. Li, R. Voituriez, M. Piel, A.-M. Lennon-Duménil, Innate control of actin nucleation determines two distinct migration behaviours in dendritic cells. *Nat Cell Biol* **18**, 43–53 (2016).

183. H. Tanizaki, G. Egawa, K. Inaba, T. Honda, S. Nakajima, C. S. Moniaga, A. Otsuka, T. Ishizaki, M. Tomura, T. Watanabe, Y. Miyachi, S. Narumiya, T. Okada, K. Kabashima, Rho-mDia1 pathway is required for adhesion, migration, and T-cell stimulation in dendritic cells. *Blood* **116**, 5875–5884 (2010).

184. L. Barbier, P. J. Sáez, R. Attia, A.-M. Lennon-Duménil, I. Lavi, M. Piel, P. Vargas, Myosin II Activity Is Selectively Needed for Migration in Highly Confined Microenvironments in Mature Dendritic Cells. *Front Immunol* **10**, 747 (2019).

185. H. Warner, G. Franciosa, G. van der Borg, B. Coenen, F. Faas, C. Koenig, R. de Boer, R. Classens, S. Maassen, M. V. Baranov, S. Mahajan, D. Dabral, F. Bianchi, N. van Hilten, H. J. Risselada, W. H. Roos, J. V. Olsen, L. Q. Cano, G. van den Bogaart, Atypical cofilin signaling drives dendritic cell migration through the extracellular matrix via nuclear deformation. *Cell Reports* **43** (2024).

186. A.-K. Weier, M. Homrich, S. Ebbinghaus, P. Juda, E. Miková, R. Hauschild, L. Zhang, T. Quast, E. Mass, A. Schlitzer, W. Kolanus, S. Burgdorf, O. J. Gruß, M. Hons, S. Wieser, E. Kiermaier, Multiple centrosomes enhance migration and immune cell effector functions of mature dendritic cells. *J Cell Biol* **221**, e202107134 (2022).

187. S. G. Tangye, W. Al-Herz, A. Bousfiha, C. Cunningham-Rundles, J. L. Franco, S. M. Holland, C. Klein, T. Morio, E. Oksenhendler, C. Picard, A. Puel, J. Puck, M. R. J. Seppänen, R. Somech, H. C. Su, K. E. Sullivan, T. R. Torgerson, I. Meyts, Human Inborn Errors of Immunity: 2022 Update on the Classification from the International Union of Immunological Societies Expert Committee. *J Clin Immunol* **42**, 1473–1507 (2022).

188. L. E. Heusinkveld, S. Majumdar, J.-L. Gao, D. H. McDermott, WHIM Syndrome: from Pathogenesis towards Personalized Medicine and Cure. *J Clin Immunol* **39**, 532–556 (2019).

189. T. Kawai, H. L. Malech, WHIM Syndrome: Congenital Immune Deficiency Disease. *Curr Opin Hematol* **16**, 20–26 (2009).

190. P. L. Auer, A. Teumer, U. Schick, A. O'Shaughnessy, K. S. Lo, N. Chami, C. Carlson, S. de Denus, M.-P. Dubé, J. Haessler, R. D. Jackson, C. Kooperberg, L.-P. L. Perreault, M. Nauck, U. Peters, J. D. Rioux, F. Schmidt, V. Turcot, U. Völker, H. Völzke, A. Greinacher, L. Hsu, J.-C. Tardif, G. A. Diaz, A. P. Reiner,

G. Lettre, Rare and low-frequency coding variants in CXCR2 and other genes are associated with hematological traits. *Nat Genet* **46**, 629–634 (2014).

191. C. Martin, P. C. E. Burdon, G. Bridger, J.-C. Gutierrez-Ramos, T. J. Williams, S. M. Rankin, Chemokines Acting via CXCR2 and CXCR4 Control the Release of Neutrophils from the Bone Marrow and Their Return following Senescence. *Immunity* **19**, 583–593 (2003).

192. R. Badolato, Defects of leukocyte migration in primary immunodeficiencies. *European Journal of Immunology* **43**, 1436–1440 (2013).

193. E. G. G. Sprenkeler, S. D. S. Webbers, T. W. Kuijpers, When Actin is Not Actin' Like It Should: A New Category of Distinct Primary Immunodeficiency Disorders. *J Innate Immun* **13**, 3–25 (2021).

194. J. M. J. Derry, H. D. Ochs, U. Francke, Isolation of a novel gene mutated in Wiskott-Aldrich syndrome. *Cell* **78**, 635–644 (1994).

195. A. Kamnev, C. Lacouture, M. Fusaro, L. Dupré, Molecular Tuning of Actin Dynamics in Leukocyte Migration as Revealed by Immune-Related Actinopathies. *Front Immunol* **12**, 750537 (2021).

196. H. Ochs, A. Thrasher, The Wiskott-Aldrich syndrome. *Journal of Allergy and Clinical Immunology* **117**, 725–738 (2006).

197. M. Bosticardo, F. Marangoni, A. Aiuti, A. Villa, M. Grazia Roncarolo, Recent advances in understanding the pathophysiology of Wiskott-Aldrich syndrome. *Blood* **113**, 6288–6295 (2009).

198. M. Symons, J. M. J. Derry, B. Karlak, S. Jiang, V. Lemahieu, F. McCormick, U. Francke, A. Abo, Wiskott–Aldrich Syndrome Protein, a Novel Effector for the GTPase CDC42Hs, Is Implicated in Actin Polymerization. *Cell* **84**, 723–734 (1996).

199. H. Nunoi, T. Yamazaki, H. Tsuchiya, S. Kato, H. L. Malech, I. Matsuda, S. Kanegasaki, A heterozygous mutation of ß-actin associated with neutrophil dysfunction and recurrent infection. *Proceedings of the National Academy of Sciences* **96**, 8693–8698 (1999).

200. E. Janssen, R. S. Geha, Primary immunodeficiencies caused by mutations in actin regulatory proteins. *Immunological Reviews* **287**, 121–134 (2019).

201. Q. Zhang, J. C. Davis, I. T. Lamborn, A. F. Freeman, H. Jing, A. J. Favreau, H. F. Matthews, J. Davis, M. L. Turner, G. Uzel, S. M. Holland, H. C. Su, Combined Immunodeficiency Associated with DOCK8 Mutations. *N Engl J Med* **361**, 2046–2055 (2009).

202. S. E. Aydin, S. S. Kilic, C. Aytekin, A. Kumar, O. Porras, L. Kainulainen, L. Kostyuchenko, F. Genel, N. Kütükcüler, N. Karaca, L. Gonzalez-Granado, J. Abbott, D. Al-Zahrani, N. Rezaei, Z. Baz, J. Thiel, S. Ehl, L. Marodi, J. S. Orange, J. Sawalle-Belohradsky, S. Keles, S. M. Holland, Ö. Sanal, D. C. Ayvaz, I. Tezcan, H. Al-Mousa, Z. Alsum, A. Hawwari, A. Metin, S. Matthes-Martin, M. Hönig, A. Schulz, C. Picard, V. Barlogis, A. Gennery, M. Ifversen, J. van Montfrans, T. Kuijpers, R. Bredius, G. Dückers, W. Al-Herz, S.-Y. Pai, R. Geha, G. Notheis, C.-P. Schwarze, B. Tavil, F. Azik, K. Bienemann, B. Grimbacher, V. Heinz, H. B. Gaspar, R. Aydin, B. Hagl, B. Gathmann, B. H. Belohradsky, H. D. Ochs, T. Chatila, E. D. Renner, H. Su, A. F. Freeman, K. Engelhardt, M. H. Albert, On behalf of the inborn errors working party of EBMT, DOCK8 Deficiency: Clinical and Immunological Phenotype and Treatment Options - a Review of 136 Patients. *J Clin Immunol* **35**, 189–198 (2015).

203. K. R. Engelhardt, S. McGhee, S. Winkler, A. Sassi, C. Woellner, G. Lopez-Herrera, A. Chen, H. S. Kim, M. G. Lloret, I. Schulze, S. Ehl, J. Thiel, D. Pfeifer, H. Veelken, T. Niehues, K. Siepermann, S. Weinspach, I. Reisli, S. Keles, F. Genel, N. Kütükçüler, Y. Camcioğlu, A. Somer, E. K. Aydiner, I. Barlan, A. Gennery, A. Metin, A. Degerliyurt, M. C. Pietrogrande, M. Yeganeh, Z. Baz, S. Al-Tamemi, C. Klein, J. M. Puck, S. M. Holland, E. R. B. McCabe, B. Grimbacher, T. Chatila, Large Deletions and Point Mutations Involving DOCK8 in the Autosomal Recessive Form of the Hyper-IgE Syndrome. *J Allergy Clin Immunol* **124**, 1289 (2009).

204. S. G. Tangye, B. Pillay, K. L. Randall, D. T. Avery, T. G. Phan, P. Gray, J. B. Ziegler, J. M. Smart, J. Peake, P. D. Arkwright, S. Hambleton, J. Orange, C. C. Goodnow, G. Uzel, J.-L. Casanova, S. O. L. Reyes, A. F. Freeman, H. C. Su, C. S. Ma, Dedicator of cytokinesis 8–deficient CD4+ T cells are biased to a TH2 effector fate at the expense of TH1 and TH17 cells. *Journal of Allergy and Clinical Immunology* **139**, 933–949 (2017).

205. O. Tirosh, S. Conlan, C. Deming, S.-Q. Lee-Lin, X. Huang, H. C. Su, A. F. Freeman, J. A. Segre, H. H. Kong, Expanded skin virome in DOCK8-deficient patients. *Nat Med* **24**, 1815–1821 (2018).

206. H. C. Su, H. Jing, P. Angelus, A. F. Freeman, Insights into immunity from clinical and basic science studies of DOCK8 immunodeficiency syndrome. *Immunological Reviews* **287**, 9–19 (2019).

207. H. C. Su, H. Jing, Q. Zhang, DOCK8 deficiency. *Annals of the New York Academy of Sciences* **1246**, 26–33 (2011).

208. B. A. Pillay, D. T. Avery, J. M. Smart, T. Cole, S. Choo, D. Chan, P. E. Gray, K. Frith, R. Mitchell, T. G. Phan, M. Wong, D. E. Campbell, P. Hsu, J. B. Ziegler, J. Peake, F. Alvaro, C. Picard, J. Bustamante, B. Neven, A. J. Cant, G. Uzel, P.

D. Arkwright, J.-L. Casanova, H. C. Su, A. F. Freeman, N. Shah, D. D. Hickstein, S. G. Tangye, C. S. Ma, Hematopoietic stem cell transplant effectively rescues lymphocyte differentiation and function in DOCK8-deficient patients. *JCI Insight* **4**, e127527 (2019).

209. A. Ruusala, P. Aspenström, Isolation and characterisation of DOCK8, a member of the DOCK180-related regulators of cell morphology. *FEBS Letters* **572**, 159–166 (2004).

210. J. Cherfils, M. Zeghouf, Regulation of Small GTPases by GEFs, GAPs, and GDIs. *Physiological Reviews* **93**, 269–309 (2013).

211. J.-F. Côté, K. Vuori, GEF what? Dock180 and related proteins help Rac to polarize cells in new ways. *Trends Cell Biol* **17**, 383–393 (2007).

212. M. Laurin, J.-F. Côté, Insights into the biological functions of Dock family guanine nucleotide exchange factors. *Genes Dev* **28**, 533–547 (2014).

213. J.-F. Côté, K. Vuori, Identification of an evolutionarily conserved superfamily of DOCK180-related proteins with guanine nucleotide exchange activity. *Journal of Cell Science* **115**, 4901–4913 (2002).

214. A. Nishikimi, M. Kukimoto-Niino, S. Yokoyama, Y. Fukui, Immune regulatory functions of DOCK family proteins in health and disease. *Experimental Cell Research* **319**, 2343–2349 (2013).

215. Y. Harada, Y. Tanaka, M. Terasawa, M. Pieczyk, K. Habiro, T. Katakai, K. Hanawa-Suetsugu, M. Kukimoto-Niino, T. Nishizaki, M. Shirouzu, X. Duan, T. Uruno, A. Nishikimi, F. Sanematsu, S. Yokoyama, J. V. Stein, T. Kinashi, Y. Fukui, DOCK8 is a Cdc42 activator critical for interstitial dendritic cell migration during immune responses. *Blood* **119**, 4451–4461 (2012).

216. K. Kunimura, T. Uruno, Y. Fukui, DOCK family proteins: key players in immune surveillance mechanisms. *Int Immunol* **32**, 5–15 (2019).

217. H. C. Su, Dedicator of cytokinesis 8 (DOCK8) deficiency. *Current Opinion in Allergy and Clinical Immunology* **10**, 515 (2010).

218. K. L. Randall, T. Lambe, A. L. Johnson, B. Treanor, E. Kucharska, H. Domaschenz, B. Whittle, L. E. Tze, A. Enders, T. L. Crockford, T. Bouriez-Jones, D. Alston, J. G. Cyster, M. J. Lenardo, F. Mackay, E. K. Deenick, S. G. Tangye, T. D. Chan, T. Camidge, R. Brink, C. G. Vinuesa, F. D. Batista, R. J. Cornall, C. C. Goodnow, Dock8 mutations cripple B cell immunological synapses, germinal centers and long-lived antibody production. *Nat Immunol* **10**, 1283–1291 (2009).

219. M. Deobagkar-Lele, G. Crawford, T. L. Crockford, J. Back, R. Hodgson, A. Bhandari, K. R. Bull, R. J. Cornall, B cells require DOCK8 to elicit and integrate T cell help when antigen is limiting. *Science Immunology* **9**, eadd4874 (2024).

220. M. C. Mizesko, P. P. Banerjee, L. Monaco-Shawver, E. M. Mace, W. E. Bernal, J. Sawalle-Belohradsky, B. H. Belohradsky, V. Heinz, A. F. Freeman, K. E. Sullivan, S. M. Holland, T. R. Torgerson, W. Al-Herz, J. Chou, I. C. Hanson, M. H. Albert, R. S. Geha, E. D. Renner, J. S. Orange, Defective actin accumulation impairs human natural killer cell function in DOCK8 deficiency. *J Allergy Clin Immunol* **131**, 840–848 (2013).

221. H. Ham, S. Guerrier, J. Kim, R. A. Schoon, E. L. Anderson, M. J. Hamann, Z. Lou, D. D. Billadeau, DOCK8 Interacts with Talin and WASPto Regulate Natural Killer Cell Cytotoxicity. *J Immunol* **190**, 10.4049/jimmunol.1202792 (2013).

222. T. Lambe, G. Crawford, A. L. Johnson, T. L. Crockford, T. Bouriez-Jones, A. M. Smyth, T. H. M. Pham, Q. Zhang, A. F. Freeman, J. G. Cyster, H. C. Su, R. J. Cornall, DOCK8 is essential for T-cell survival and the maintenance of CD8+ T-cell memory. *Eur J Immunol* **41**, 3423–3435 (2011).

223. K. L. Randall, S. S.-Y. Chan, C. S. Ma, I. Fung, Y. Mei, M. Yabas, A. Tan, P. D. Arkwright, W. Al Suwairi, S. O. Lugo Reyes, M. A. Yamazaki-Nakashimada, M. de la Luz Garcia-Cruz, J. M. Smart, C. Picard, S. Okada, E. Jouanguy, J.-L. Casanova, T. Lambe, R. J. Cornall, S. Russell, J. Oliaro, S. G. Tangye, E. M. Bertram, C. C. Goodnow, DOCK8 deficiency impairs CD8 T cell survival and function in humans and mice. *J Exp Med* **208**, 2305–2320 (2011).

224. Q. Zhang, C. G. Dove, J. L. Hor, H. M. Murdock, D. M. Strauss-Albee, J. A. Garcia, J. N. Mandl, R. A. Grodick, H. Jing, D. B. Chandler-Brown, T. E. Lenardo, G. Crawford, H. F. Matthews, A. F. Freeman, R. J. Cornall, R. N. Germain, S. N. Mueller, H. C. Su, DOCK8 regulates lymphocyte shape integrity for skin antiviral immunity. *Journal of Experimental Medicine* **211**, 2549–2566 (2014).

225. Q. Zhang, H. Jing, H. C. Su, Recent Advances in DOCK8 Immunodeficiency Syndrome. *J Clin Immunol* **36**, 441–449 (2016).

226. M. Abercrombie, J. E. M. Heaysman, Observations on the social behaviour of cells in tissue culture: I. Speed of movement of chick heart fibroblasts in relation to their mutual contacts. *Experimental Cell Research* **5**, 111–131 (1953).

227. L. Loeb, Amœboid Movement, Tissue Formation and Consistency of Protoplasm. *Science* **53**, 261–262 (1921).

228. A. Roycroft, R. Mayor, Michael Abercrombie: contact inhibition of locomotion and more. *Int. J. Dev. Biol.* **62**, 5–13 (2018).

229. B. Sun, The mechanics of fibrillar collagen extracellular matrix. *Cell Rep Phys Sci* **2**, 100515 (2021).

230. H. Atcha, Y. S. Choi, O. Chaudhuri, A. J. Engler, Getting physical: Material mechanics is an intrinsic cell cue. *Cell Stem Cell* **30**, 750–765 (2023).

231. C. F. Guimarães, L. Gasperini, A. P. Marques, R. L. Reis, The stiffness of living tissues and its implications for tissue engineering. *Nat Rev Mater* **5**, 351–370 (2020).

232. M. Akhmanova, E. Osidak, S. Domogatsky, S. Rodin, A. Domogatskaya, Physical, Spatial, and Molecular Aspects of Extracellular Matrix of In Vivo Niches and Artificial Scaffolds Relevant to Stem Cells Research. *Stem Cells Int* **2015**, 167025 (2015).

233. P. A. Janmey, D. A. Fletcher, C. A. Reinhart-King, Stiffness Sensing by Cells. *Physiol Rev* **100**, 695–724 (2020).

234. D. E. Discher, P. Janmey, Y. Wang, Tissue Cells Feel and Respond to the Stiffness of Their Substrate. *Science* **310**, 1139–1143 (2005).

235. A. J. Engler, S. Sen, H. L. Sweeney, D. E. Discher, Matrix Elasticity Directs Stem Cell Lineage Specification. *Cell* **126**, 677–689 (2006).

236. C. Yang, M. W. Tibbitt, L. Basta, K. S. Anseth, Mechanical memory and dosing influence stem cell fate. *Nature Mater* **13**, 645–652 (2014).

237. L. Trichet, J. Le Digabel, R. J. Hawkins, S. R. K. Vedula, M. Gupta, C. Ribrault, P. Hersen, R. Voituriez, B. Ladoux, Evidence of a large-scale mechanosensing mechanism for cellular adaptation to substrate stiffness. *Proceedings of the National Academy of Sciences* **109**, 6933–6938 (2012).

238. C. Kang, P. Chen, X. Yi, D. Li, Y. Hu, Y. Yang, H. Cai, B. Li, C. Wu, Amoeboid cells undergo durotaxis with soft end polarized NMIIA. *eLife* **13** (2024).

239. O. Chaudhuri, J. Cooper-White, P. A. Janmey, D. J. Mooney, V. B. Shenoy, Effects of extracellular matrix viscoelasticity on cellular behaviour. *Nature* **584**, 535–546 (2020).

240. A. Saraswathibhatla, D. Indana, O. Chaudhuri, Cell–extracellular matrix mechanotransduction in 3D. *Nat Rev Mol Cell Biol* **24**, 495–516 (2023).

241. J. Y. Lee, J. K. Chang, A. A. Dominguez, H. Lee, S. Nam, J. Chang, S. Varma, L. S. Qi, R. B. West, O. Chaudhuri, YAP-independent mechanotransduction drives breast cancer progression. *Nat Commun* **10**, 1848 (2019).

242. S. van Helvert, C. Storm, P. Friedl, Mechanoreciprocity in cell migration. *Nat Cell Biol* **20**, 8–20 (2018).

243. K. Wolf, M. te Lindert, M. Krause, S. Alexander, J. te Riet, A. L. Willis, R. M. Hoffman, C. G. Figdor, S. J. Weiss, P. Friedl, Physical limits of cell migration: Control by ECM space and nuclear deformation and tuning by proteolysis and traction force. *J Cell Biol* **201**, 1069–1084 (2013).

244. F. Beroz, L. M. Jawerth, S. Münster, D. A. Weitz, C. P. Broedersz, N. S. Wingreen, Physical limits to biomechanical sensing in disordered fibre networks. *Nat Commun* **8**, 16096 (2017).

245. K. W. Kwon, H. Park, K. H. Song, J.-C. Choi, H. Ahn, M. J. Park, K.-Y. Suh, J. Doh, Nanotopography-Guided Migration of T Cells. *The Journal of Immunology* **189**, 2266–2273 (2012).

246. D. J. Tschumperlin, G. Ligresti, M. B. Hilscher, V. H. Shah, Mechanosensing and fibrosis. *J Clin Invest* **128**, 74–84 (2018).

247. Z. Mai, Y. Lin, P. Lin, X. Zhao, L. Cui, Modulating extracellular matrix stiffness: a strategic approach to boost cancer immunotherapy. *Cell Death Dis* **15**, 1–16 (2024).

248. S. Ishihara, H. Haga, Matrix Stiffness Contributes to Cancer Progression by Regulating Transcription Factors. *Cancers (Basel)* **14**, 1049 (2022).

249. K. M. Tharp, K. Kersten, O. Maller, G. A. Timblin, C. Stashko, F. P. Canale, R. E. Menjivar, M.-K. Hayward, I. Berestjuk, J. ten Hoeve, B. Samad, A. J. Ironside, M. P. di Magliano, A. Muir, R. Geiger, A. J. Combes, V. M. Weaver, Tumor-associated macrophages restrict CD8+ T cell function through collagen deposition and metabolic reprogramming of the breast cancer microenvironment. *Nat Cancer* **5**, 1045–1062 (2024).

250. J. M. Schenkel, K. E. Pauken, Localization, tissue biology and T cell state — implications for cancer immunotherapy. *Nat Rev Immunol* **23**, 807–823 (2023).

251. H. Du, J. M. Bartleson, S. Butenko, V. Alonso, W. F. Liu, D. A. Winer, M. J. Butte, Tuning immunity through tissue mechanotransduction. *Nat Rev Immunol*, 1–15 (2022).

252. J. S. Bezbradica, C. E. Bryant, Inflammasomes as regulators of mechano-immunity. *EMBO reports* **25**, 21–30 (2024).

253. B. Enyedi, S. Kala, T. Nikolich-Zugich, P. Niethammer, Tissue damage detection by osmotic surveillance. *Nat Cell Biol* **15**, 1123–1130 (2013).

254. M. Lee, H. Du, D. A. Winer, X. Clemente-Casares, S. Tsai, Mechanosensing in macrophages and dendritic cells in steady-state and disease. *Front. Cell Dev. Biol.* **10** (2022).

255. K. P. Meng, F. S. Majedi, T. J. Thauland, M. J. Butte, Mechanosensing through YAP controls T cell activation and metabolism. *J Exp Med* **217**, e20200053 (2020).

256. F. P. Assen, J. Abe, M. Hons, R. Hauschild, S. Shamipour, W. A. Kaufmann, T. Costanzo, G. Krens, M. Brown, B. Ludewig, S. Hippenmeyer, C.-P. Heisenberg, W. Weninger, E. Hannezo, S. A. Luther, J. V. Stein, M. Sixt, Multitier mechanics control stromal adaptations in the swelling lymph node. *Nat Immunol* **23**, 1246–1255 (2022).

257. D. E. Jaalouk, J. Lammerding, Mechanotransduction gone awry. *Nat Rev Mol Cell Biol* **10**, 63–73 (2009).

258. N. Bufi, M. Saitakis, S. Dogniaux, O. Buschinger, A. Bohineust, A. Richert, M. Maurin, C. Hivroz, A. Asnacios, Human Primary Immune Cells Exhibit Distinct Mechanical Properties that Are Modified by Inflammation. *Biophys J* **108**, 2181–2190 (2015).

259. D. Blumenthal, V. Chandra, L. Avery, J. K. Burkhardt, Mouse T cell priming is enhanced by maturation-dependent stiffening of the dendritic cell cortex. *eLife* **9**, e55995.

260. A. Zak, S. V. Merino-Cortés, A. Sadoun, F. Mustapha, A. Babataheri, S. Dogniaux, S. Dupré-Crochet, E. Hudik, H.-T. He, A. I. Barakat, Y. R. Carrasco, Y. Hamon, P.-H. Puech, C. Hivroz, O. Nüsse, J. Husson, Rapid viscoelastic changes are a hallmark of early leukocyte activation. *Biophysical Journal* **120**, 1692–1704 (2021).

261. R. Basu, B. M. Whitlock, J. Husson, A. L. Floc'h, W. Jin, A. Oyler-Yaniv, F. Dotiwala, G. Giannone, C. Hivroz, N. Biais, J. Lieberman, L. C. Kam, M. Huse, Cytotoxic T Cells Use Mechanical Force to Potentiate Target Cell Killing. *Cell* **165**, 100–110 (2016).

262. S. Ma, Z. Meng, R. Chen, K.-L. Guan, The Hippo Pathway: Biology and Pathophysiology. *Annu. Rev. Biochem.* **88**, 577–604 (2019).

263. T. Panciera, L. Azzolin, M. Cordenonsi, S. Piccolo, Mechanobiology of YAP and TAZ in physiology and disease. *Nat Rev Mol Cell Biol* **18**, 758–770 (2017).

264. H. Wolfenson, I. Lavelin, B. Geiger, Dynamic Regulation of the Structure and Functions of Integrin Adhesions. *Developmental Cell* **24**, 447–458 (2013).

265. M. C. Lampi, C. A. Reinhart-King, Targeting extracellular matrix stiffness to attenuate disease: From molecular mechanisms to clinical trials. *Science Translational Medicine* **10**, eaao0475 (2018).

266. J. Z. Kechagia, J. Ivaska, P. Roca-Cusachs, Integrins as biomechanical sensors of the microenvironment. *Nat Rev Mol Cell Biol* **20**, 457–473 (2019).

267. C. M. Lo, H. B. Wang, M. Dembo, Y. L. Wang, Cell movement is guided by the rigidity of the substrate. *Biophys J* **79**, 144–152 (2000).

268. J. M. Kefauver, A. B. Ward, A. Patapoutian, Discoveries in structure and physiology of mechanically activated ion channels. *Nature* **587**, 567–576 (2020).

269. B. Coste, J. Mathur, M. Schmidt, T. J. Earley, S. Ranade, M. J. Petrus, A. E. Dubin, A. Patapoutian, Piezo1 and Piezo2 Are Essential Components of Distinct Mechanically Activated Cation Channels. *Science* **330**, 55–60 (2010).

270. Y. A. Nikolaev, C. D. Cox, P. Ridone, P. R. Rohde, J. F. Cordero-Morales, V. Vásquez, D. R. Laver, B. Martinac, Mammalian TRP ion channels are insensitive to membrane stretch. *Journal of Cell Science* **132**, jcs238360 (2019).

271. J. Swift, I. L. Ivanovska, A. Buxboim, T. Harada, P. C. D. P. Dingal, J. Pinter, J. D. Pajerowski, K. R. Spinler, J.-W. Shin, M. Tewari, F. Rehfeldt, D. W. Speicher, D. E. Discher, Nuclear Lamin-A Scales with Tissue Stiffness and Enhances Matrix-Directed Differentiation. *Science* **341**, 1240104 (2013).

272. P. Mistriotis, E. O. Wisniewski, B. R. Si, P. Kalab, K. Konstantopoulos, Coordinated in confined migration: crosstalk between the nucleus and ion channel-mediated mechanosensation. *Trends in Cell Biology*, doi: 10.1016/j.tcb.2024.01.001 (2024).

273. J. Lammerding, J. Hsiao, P. C. Schulze, S. Kozlov, C. L. Stewart, R. T. Lee, Abnormal nuclear shape and impaired mechanotransduction in emerin-deficient cells. *The Journal of Cell Biology* **170**, 781 (2005).

274. C. Guilluy, L. D. Osborne, L. Van Landeghem, L. Sharek, R. Superfine, R. Garcia-Mata, K. Burridge, Isolated nuclei adapt to force and reveal a mechanotransduction pathway in the nucleus. *Nat Cell Biol* **16**, 376–381 (2014).

275. S. Cho, M. Vashisth, A. Abbas, S. Majkut, K. Vogel, Y. Xia, I. L. Ivanovska, J. Irianto, M. Tewari, K. Zhu, E. D. Tichy, F. Mourkioti, H.-Y. Tang, R. A. Greenberg, B. L. Prosser, D. E. Discher, Mechanosensing by the Lamina

Protects against Nuclear Rupture, DNA Damage, and Cell-Cycle Arrest. *Dev Cell* **49**, 920-935.e5 (2019).

276. C. Uhler, G. V. Shivashankar, Regulation of genome organization and gene expression by nuclear mechanotransduction. *Nat Rev Mol Cell Biol* **18**, 717–727 (2017).

277. A. Tajik, Y. Zhang, F. Wei, J. Sun, Q. Jia, W. Zhou, R. Singh, N. Khanna, A. S. Belmont, N. Wang, Transcription upregulation via force-induced direct stretching of chromatin. *Nature Mater* **15**, 1287–1296 (2016).

278. Y. Song, J. Soto, B. Chen, T. Hoffman, W. Zhao, N. Zhu, Q. Peng, L. Liu, C. Ly, P. K. Wong, Y. Wang, A. C. Rowat, S. K. Kurdistani, S. Li, Transient nuclear deformation primes epigenetic state and promotes cell reprogramming. *Nat. Mater.* **21**, 1191–1199 (2022).

279. A. Elosegui-Artola, I. Andreu, A. E. M. Beedle, A. Lezamiz, M. Uroz, A. J. Kosmalska, R. Oria, J. Z. Kechagia, P. Rico-Lastres, A.-L. L. Roux, C. M. Shanahan, X. Trepat, D. Navajas, S. Garcia-Manyes, P. Roca-Cusachs, Force Triggers YAP Nuclear Entry by Regulating Transport across Nuclear Pores. *Cell* **171**, 1397-1410.e14 (2017).

280. V. Venturini, F. Pezzano, F. Català Castro, H.-M. Häkkinen, S. Jiménez-Delgado, M. Colomer-Rosell, M. Marro, Q. Tolosa-Ramon, S. Paz-López, M. A. Valverde, J. Weghuber, P. Loza-Alvarez, M. Krieg, S. Wieser, V. Ruprecht, The nucleus measures shape changes for cellular proprioception to control dynamic cell behavior. *Science* **370**, eaba2644 (2020).

281. A. J. Lomakin, C. J. Cattin, D. Cuvelier, Z. Alraies, M. Molina, G. P. F. Nader, N. Srivastava, P. J. Sáez, J. M. Garcia-Arcos, I. Y. Zhitnyak, A. Bhargava, M. K. Driscoll, E. S. Welf, R. Fiolka, R. J. Petrie, N. S. De Silva, J. M. González-Granado, N. Manel, A. M. Lennon-Duménil, D. J. Müller, M. Piel, The nucleus acts as a ruler tailoring cell responses to spatial constraints. *Science* **370**, eaba2894 (2020).

282. Z. Alraies, C. A. Rivera, M.-G. Delgado, D. Sanséau, M. Maurin, R. Amadio, G. Maria Piperno, G. Dunsmore, A. Yatim, L. Lacerda Mariano, A. Kniazeva, V. Calmettes, P. J. Sáez, A. Williart, H. Popard, M. Gratia, O. Lamiable, A. Moreau, Z. Fusilier, L. Crestey, B. Albaud, P. Legoix, A. S. Dejean, A.-L. Le Dorze, H. Nakano, D. N. Cook, T. Lawrence, N. Manel, F. Benvenuti, F. Ginhoux, H. D. Moreau, G. P. F. Nader, M. Piel, A.-M. Lennon-Duménil, Cell shape sensing licenses dendritic cells for homeostatic migration to lymph nodes. *Nat Immunol* **25**, 1193–1206 (2024).

283. A. Kumar, M. Mazzanti, M. Mistrik, M. Kosar, G. V. Beznoussenko, A. A. Mironov, M. Garrè, D. Parazzoli, G. V. Shivashankar, G. Scita, J. Bartek, M.

Foiani, ATR Mediates a Checkpoint at the Nuclear Envelope in Response to Mechanical Stress. *Cell* **158**, 633–646 (2014).

284. G. R. Kidiyoor, Q. Li, G. Bastianello, C. Bruhn, I. Giovannetti, A. Mohamood, G. V. Beznoussenko, A. Mironov, M. Raab, M. Piel, U. Restuccia, V. Matafora, A. Bachi, S. Barozzi, D. Parazzoli, E. Frittoli, A. Palamidessi, T. Panciera, S. Piccolo, G. Scita, P. Maiuri, K. M. Havas, Z.-W. Zhou, A. Kumar, J. Bartek, Z.-Q. Wang, M. Foiani, ATR is essential for preservation of cell mechanics and nuclear integrity during interstitial migration. *Nat Commun* **11**, 4828 (2020).

285. M. L. Lombardi, D. E. Jaalouk, C. M. Shanahan, B. Burke, K. J. Roux, J. Lammerding, The Interaction between Nesprins and Sun Proteins at the Nuclear Envelope Is Critical for Force Transmission between the Nucleus and Cytoskeleton *. *Journal of Biological Chemistry* **286**, 26743–26753 (2011).

286. P. Nastały, D. Purushothaman, S. Marchesi, A. Poli, T. Lendenmann, G. R. Kidiyoor, G. V. Beznoussenko, S. Lavore, O. M. Romano, D. Poulikakos, M. C. Lagomarsino, A. A. Mironov, A. Ferrari, P. Maiuri, Role of the nuclear membrane protein Emerin in front-rear polarity of the nucleus. *Nat Commun* **11**, 2122 (2020).

287. S. B. Lavenus, K. W. Vosatka, A. P. Caruso, M. F. Ullo, A. Khan, J. S. Logue, Emerin regulation of nuclear stiffness is required for fast amoeboid migration in confined environments. *Journal of Cell Science* **135**, jcs259493 (2022).

288. K. L. Vogt, C. Summers, E. R. Chilvers, A. M. Condliffe, Priming and de-priming of neutrophil responses in vitro and in vivo. *European Journal of Clinical Investigation* **48**, e12967 (2018).

289. Z. Liu, T. Yago, N. Zhang, S. R. Panicker, Y. Wang, L. Yao, P. Mehta-D'souza, L. Xia, C. Zhu, R. P. McEver, L-selectin mechanochemistry restricts neutrophil priming in vivo. *Nat Commun* **8**, 15196 (2017).

290. A. Makino, E. R. Prossnitz, M. Bünemann, J. M. Wang, W. Yao, G. W. Schmid-Schönbein, G protein-coupled receptors serve as mechanosensors for fluid shear stress in neutrophils. *American Journal of Physiology-Cell Physiology* **290**, C1633–C1639 (2006).

291. A. E. Ekpenyong, N. Toepfner, E. R. Chilvers, J. Guck, Mechanotransduction in neutrophil activation and deactivation. *Biochimica et Biophysica Acta (BBA) - Molecular Cell Research* **1853**, 3105–3116 (2015).

292. P. W. Oakes, D. C. Patel, N. A. Morin, D. P. Zitterbart, B. Fabry, J. S. Reichner, J. X. Tang, Neutrophil morphology and migration are affected by substrate elasticity. *Blood* **114**, 1387–1395 (2009).

293. K. M. Stroka, H. Aranda-Espinoza, Endothelial cell substrate stiffness influences neutrophil transmigration via myosin light chain kinase-dependent cell contraction. *Blood* **118**, 1632–1640 (2011).

294. B. Yap, R. D. Kamm, Cytoskeletal remodeling and cellular activation during deformation of neutrophils into narrow channels. *Journal of Applied Physiology* **99**, 2323–2330 (2005).

295. A. E. Ekpenyong, N. Toepfner, C. Fiddler, M. Herbig, W. Li, G. Cojoc, C. Summers, J. Guck, E. R. Chilvers, Mechanical deformation induces depolarization of neutrophils. *Sci Adv* **3**, e1602536 (2017).

296. A. Mukhopadhyay, Y. Tsukasaki, W. C. Chan, J. P. Le, M. L. Kwok, J. Zhou, V. Natarajan, N. Mostafazadeh, M. Maienschein-Cline, I. Papautsky, C. Tiruppathi, Z. Peng, J. Rehman, B. Ganesh, Y. Komarova, A. B. Malik, trans-Endothelial neutrophil migration activates bactericidal function via Piezo1 mechanosensing. *Immunity* **57**, 52-67.e10 (2024).

297. M. Palomino-Segura, J. Sicilia, I. Ballesteros, A. Hidalgo, Strategies of neutrophil diversification. *Nat Immunol* **24**, 575–584 (2023).

298. C. Silvestre-Roig, Z. G. Fridlender, M. Glogauer, P. Scapini, Neutrophil Diversity in Health and Disease. *Trends in Immunology* **40**, 565–583 (2019).

299. D. F. Quail, B. Amulic, M. Aziz, B. J. Barnes, E. Eruslanov, Z. G. Fridlender, H. S. Goodridge, Z. Granot, A. Hidalgo, A. Huttenlocher, M. J. Kaplan, I. Malanchi, T. Merghoub, E. Meylan, V. Mittal, M. J. Pittet, A. Rubio-Ponce, I. A. Udalova, T. K. van den Berg, D. D. Wagner, P. Wang, A. Zychlinsky, K. E. de Visser, M. Egeblad, P. Kubes, Neutrophil phenotypes and functions in cancer: A consensus statement. *Journal of Experimental Medicine* **219**, e20220011 (2022).

300. I. Ballesteros, A. Rubio-Ponce, M. Genua, E. Lusito, I. Kwok, G. Fernández-Calvo, T. E. Khoyratty, E. van Grinsven, S. González-Hernández, J. Á. Nicolás-Ávila, T. Vicanolo, A. Maccataio, A. Benguría, J. L. Li, J. M. Adrover, A. Aroca-Crevillen, J. A. Quintana, S. Martín-Salamanca, F. Mayo, S. Ascher, G. Barbiera, O. Soehnlein, M. Gunzer, F. Ginhoux, F. Sánchez-Cabo, E. Nistal-Villán, C. Schulz, A. Dopazo, C. Reinhardt, I. A. Udalova, L. G. Ng, R. Ostuni, A. Hidalgo, Co-option of Neutrophil Fates by Tissue Environments. *Cell* **183**, 1282-1297.e18 (2020).

301. G. Cinamon, V. Shinder, R. Alon, Shear forces promote lymphocyte migration across vascular endothelium bearing apical chemokines. *Nat Immunol* **2**, 515–522 (2001).

302. E. Woolf, I. Grigorova, A. Sagiv, V. Grabovsky, S. W. Feigelson, Z. Shulman, T. Hartmann, M. Sixt, J. G. Cyster, R. Alon, Lymph node chemokines promote

sustained T lymphocyte motility without triggering stable integrin adhesiveness in the absence of shear forces. *Nat Immunol* **8**, 1076–1085 (2007).

303. C. S. C. Liu, T. Mandal, P. Biswas, M. A. Hoque, P. Bandopadhyay, B. P. Sinha, J. Sarif, R. D'Rozario, D. K. Sinha, B. Sinha, D. Ganguly, Piezo1 mechanosensing regulates integrin-dependent chemotactic migration in human T cells. *eLife* **12**, RP91903 (2024).

304. Z. Shulman, V. Shinder, E. Klein, V. Grabovsky, O. Yeger, E. Geron, A. Montresor, M. Bolomini-Vittori, S. W. Feigelson, T. Kirchhausen, C. Laudanna, G. Shakhar, R. Alon, Lymphocyte Crawling and Transendothelial Migration Require Chemokine Triggering of High-Affinity LFA-1 Integrin. *Immunity* **30**, 384–396 (2009).

305. N. H. Roy, J. L. MacKay, T. F. Robertson, D. A. Hammer, J. K. Burkhardt, Crk adaptor proteins mediate actin-dependent T cell migration and mechanosensing induced by the integrin LFA-1. *Science Signaling* **11**, eaat3178 (2018).

306. R. Martinelli, A. S. Zeiger, M. Whitfield, T. E. Sciuto, A. Dvorak, K. J. Van Vliet, J. Greenwood, C. V. Carman, Probing the biomechanical contribution of the endothelium to lymphocyte migration: diapedesis by the path of least resistance. *Journal of Cell Science* **127**, 3720–3734 (2014).

307. N. S. Sarna, S. H. Desai, B. G. Kaufman, N. M. Curry, A. M. Hanna, M. R. King, Enhanced and sustained T cell activation in response to fluid shear stress. *iScience* **27** (2024).

308. J. M. Hope, J. A. Dombroski, R. S. Pereles, M. Lopez-Cavestany, J. D. Greenlee, S. C. Schwager, C. A. Reinhart-King, M. R. King, Fluid shear stress enhances T cell activation through Piezo1. *BMC Biol* **20**, 61 (2022).

309. M. Saitakis, S. Dogniaux, C. Goudot, N. Bufi, S. Asnacios, M. Maurin, C. Randriamampita, A. Asnacios, C. Hivroz, Different TCR-induced T lymphocyte responses are potentiated by stiffness with variable sensitivity. *eLife* **6**, e23190 (2017).

310. D. Blumenthal, J. K. Burkhardt, Multiple actin networks coordinate mechanotransduction at the immunological synapse. *Journal of Cell Biology* **219**, e201911058 (2020).

311. K. H. Hu, M. J. Butte, T cell activation requires force generation. *Journal of Cell Biology* **213**, 535–542 (2016).

312. C. S. C. Liu, D. Raychaudhuri, B. Paul, Y. Chakrabarty, A. R. Ghosh, O. Rahaman, A. Talukdar, D. Ganguly, Cutting Edge: Piezo1 Mechanosensors

Optimize Human T Cell Activation. *The Journal of Immunology* **200**, 1255–1260 (2018).

313. A. Jairaman, S. Othy, J. L. Dynes, A. V. Yeromin, A. Zavala, M. L. Greenberg, J. L. Nourse, J. R. Holt, S. M. Cahalan, F. Marangoni, I. Parker, M. M. Pathak, M. D. Cahalan, Piezo1 channels restrain regulatory T cells but are dispensable for effector CD4+ T cell responses. *Science Advances* **7**, eabg5859 (2021).

314. R. S. O'Connor, X. Hao, K. Shen, K. Bashour, T. Akimova, W. W. Hancock, L. Kam, M. C. Milone, Substrate rigidity regulates human T cell activation and proliferation. *J Immunol* **189**, 1330–1339 (2012).

315. D. E. Kuczek, A. M. H. Larsen, M.-L. Thorseth, M. Carretta, A. Kalvisa, M. S. Siersbæk, A. M. C. Simões, A. Roslind, L. H. Engelholm, E. Noessner, M. Donia, I. M. Svane, P. thor Straten, L. Grøntved, D. H. Madsen, Collagen density regulates the activity of tumor-infiltrating T cells. *j. immunotherapy cancer* **7**, 68 (2019).

316. J. Zhang, J. Li, Y. Hou, Y. Lin, H. Zhao, Y. Shi, K. Chen, C. Nian, J. Tang, L. Pan, Y. Xing, H. Gao, B. Yang, Z. Song, Y. Cheng, Y. Liu, M. Sun, Y. Linghu, J. Li, H. Huang, Z. Lai, Z. Zhou, Z. Li, X. Sun, Q. Chen, D. Su, W. Li, Z. Peng, P. Liu, W. Chen, H. Huang, Y. Chen, B. Xiao, L. Ye, L. Chen, D. Zhou, Osr2 functions as a biomechanical checkpoint to aggravate CD8+ T cell exhaustion in tumor. *Cell* **187**, 3409-3426.e24 (2024).

317. S. N. Christo, M. Evrard, S. L. Park, L. C. Gandolfo, T. N. Burn, R. Fonseca, D. M. Newman, Y. O. Alexandre, N. Collins, N. M. Zamudio, F. Souza-Fonseca-Guimaraes, D. G. Pellicci, D. Chisanga, W. Shi, L. Bartholin, G. T. Belz, N. D. Huntington, A. Lucas, M. Lucas, S. N. Mueller, W. R. Heath, F. Ginhoux, T. P. Speed, F. R. Carbone, A. Kallies, L. K. Mackay, Discrete tissue microenvironments instruct diversity in resident memory T cell function and plasticity. *Nat Immunol* **22**, 1140–1151 (2021).

318. K. Adu-Berchie, Y. Liu, D. K. Y. Zhang, B. R. Freedman, J. M. Brockman, K. H. Vining, B. A. Nerger, A. Garmilla, D. J. Mooney, Generation of functionally distinct T-cell populations by altering the viscoelasticity of their extracellular matrix. *Nat. Biomed. Eng* **7**, 1374–1391 (2023).

319. R. Pang, W. Sun, Y. Yang, D. Wen, F. Lin, D. Wang, K. Li, N. Zhang, J. Liang, C. Xiong, Y. Liu, PIEZO1 mechanically regulates the antitumour cytotoxicity of T lymphocytes. *Nat. Biomed. Eng*, 1–15 (2024).

320. N. Ruef, J. Martínez Magdaleno, X. Ficht, V. Purvanov, M. Palayret, S. Wissmann, P. Pfenninger, B. Stolp, F. Thelen, J. Barreto de Albuquerque, P. Germann, J. Sharpe, J. Abe, D. F. Legler, J. V. Stein, Exocrine gland–resident

memory CD8+ T cells use mechanosensing for tissue surveillance. *Science Immunology* **8**, eadd5724 (2023).

321. S. Mostowy, P. Cossart, Septins: the fourth component of the cytoskeleton. *Nat Rev Mol Cell Biol* **13**, 183–194 (2012).

322. A. J. Tooley, J. Gilden, J. Jacobelli, P. Beemiller, W. S. Trimble, M. Kinoshita, M. F. Krummel, Amoeboid T lymphocytes Require the Septin Cytoskeleton for Cortical Integrity and Persistent Motility. *Nat Cell Biol* **11**, 17–26 (2009).

323. J. K. Gilden, S. Peck, Y.-C. M. Chen, M. F. Krummel, The septin cytoskeleton facilitates membrane retraction during motility and blebbing. *J Cell Biol* **196**, 103–114 (2012).

324. A. S. Zhovmer, A. Manning, C. Smith, A. Nguyen, O. Prince, P. J. Sáez, X. Ma, D. Tsygankov, A. X. Cartagena-Rivera, N. A. Singh, R. K. Singh, E. D. Tabdanov, Septins provide microenvironment sensing and cortical actomyosin partitioning in motile amoeboid T lymphocytes. *Science Advances* **10**, eadi1788 (2024).

325. J. A. Dombroski, S. J. Rowland, A. R. Fabiano, S. V. Knoblauch, J. M. Hope, M. R. King, Fluid shear stress enhances dendritic cell activation. *Immunobiology* **228**, 152744 (2023).

326. M. Chakraborty, K. Chu, A. Shrestha, X. S. Revelo, X. Zhang, M. J. Gold, S. Khan, M. Lee, C. Huang, M. Akbari, F. Barrow, Y. T. Chan, H. Lei, N. K. Kotoulas, J. Jovel, C. Pastrello, M. Kotlyar, C. Goh, E. Michelakis, X. Clemente-Casares, P. S. Ohashi, E. G. Engleman, S. Winer, I. Jurisica, S. Tsai, D. A. Winer, Mechanical Stiffness Controls Dendritic Cell Metabolism and Function. *Cell Reports* **34** (2021).

327. X. Du, J. Wen, Y. Wang, P. W. F. Karmaus, A. Khatamian, H. Tan, Y. Li, C. Guy, T.-L. M. Nguyen, Y. Dhungana, G. Neale, J. Peng, J. Yu, H. Chi, Hippo/Mst signalling couples metabolic state and immune function of CD8α+ dendritic cells. *Nature* **558**, 141–145 (2018).

328. Y. Wang, H. Yang, A. Jia, Y. Wang, Q. Yang, Y. Dong, Y. Hou, Y. Cao, L. Dong, Y. Bi, G. Liu, Dendritic cell Piezo1 directs the differentiation of TH1 and Treg cells in cancer. *eLife* **11**, e79957 (2022).

329. S. F. B. Mennens, M. Bolomini-Vittori, J. Weiden, B. Joosten, A. Cambi, K. van den Dries, Substrate stiffness influences phenotype and function of human antigen-presenting dendritic cells. *Sci Rep* **7**, 17511 (2017).

330. M. D. Park, A. Silvin, F. Ginhoux, M. Merad, Macrophages in health and disease. *Cell* **185**, 4259–4279 (2022).

331. B. Aykut, R. Chen, J. I. Kim, D. Wu, S. A. A. Shadaloey, R. Abengozar, P. Preiss, A. Saxena, S. Pushalkar, J. Leinwand, B. Diskin, W. Wang, G. Werba, M. Berman, S. K. B. Lee, A. Khodadadi-Jamayran, D. Saxena, W. A. Coetzee, G. Miller, Targeting Piezo1 unleashes innate immunity against cancer and infectious disease. *Science Immunology* **5**, eabb5168 (2020).

332. K. M. Adlerz, H. Aranda-Espinoza, H. N. Hayenga, Substrate elasticity regulates the behavior of human monocyte-derived macrophages. *Eur Biophys J* **45**, 301–309 (2016).

333. H. Atcha, A. Jairaman, J. R. Holt, V. S. Meli, R. R. Nagalla, P. K. Veerasubramanian, K. T. Brumm, H. E. Lim, S. Othy, M. D. Cahalan, M. M. Pathak, W. F. Liu, Mechanically activated ion channel Piezo1 modulates macrophage polarization and stiffness sensing. *Nat Commun* **12**, 3256 (2021).

334. J. Geng, Y. Shi, J. Zhang, B. Yang, P. Wang, W. Yuan, H. Zhao, J. Li, F. Qin, L. Hong, C. Xie, X. Deng, Y. Sun, C. Wu, L. Chen, D. Zhou, TLR4 signalling via Piezo1 engages and enhances the macrophage mediated host response during bacterial infection. *Nat Commun* **12**, 3519 (2021).

335. A. G. Solis, P. Bielecki, H. R. Steach, L. Sharma, C. C. D. Harman, S. Yun, M. R. de Zoete, J. N. Warnock, S. D. F. To, A. G. York, M. Mack, M. A. Schwartz, C. S. Dela Cruz, N. W. Palm, R. Jackson, R. A. Flavell, Mechanosensation of cyclical force by PIEZO1 is essential for innate immunity. *Nature* **573**, 69–74 (2019).

336. N. Jain, J. Moeller, V. Vogel, Mechanobiology of Macrophages: How Physical Factors Coregulate Macrophage Plasticity and Phagocytosis. *Annu. Rev. Biomed. Eng.* **21**, 267–297 (2019).

337. M. L. Meizlish, Y. Kimura, S. D. Pope, R. Matta, C. Kim, N. H. Philip, L. Meyaard, A. Gonzalez, R. Medzhitov, Mechanosensing regulates tissue repair program in macrophages. *Science Advances* **10**, eadk6906 (2024).

338. P. M. Davidson, C. Denais, M. C. Bakshi, J. Lammerding, Nuclear deformability constitutes a rate-limiting step during cell migration in 3-D environments. *Cell Mol Bioeng* **7**, 293–306 (2014).

339. M. Salvermoser, D. Begandt, R. Alon, B. Walzog, Nuclear Deformation During Neutrophil Migration at Sites of Inflammation. *Front. Immunol.* **9** (2018).

340. J. Renkawitz, A. Kopf, J. Stopp, I. de Vries, M. K. Driscoll, J. Merrin, R. Hauschild, E. S. Welf, G. Danuser, R. Fiolka, M. Sixt, Nuclear positioning facilitates amoeboid migration along the path of least resistance. *Nature* **568**, 546–550 (2019).

341. L. O. Carvalho, E. N. Aquino, A. C. D. Neves, W. Fontes, The Neutrophil Nucleus and Its Role in Neutrophilic Function. *Journal of Cellular Biochemistry* **116**, 1831–1836 (2015).

342. M. M. Speeckaert, C. Verhelst, A. Koch, R. Speeckaert, F. Lacquet, Pelger-Huët Anomaly: A Critical Review of the Literature. *AHA* **121**, 202–206 (2009).

343. P. M. Davidson, J. Lammerding, Broken nuclei – lamins, nuclear mechanics, and disease. *Trends in Cell Biology* **24**, 247–256 (2014).

344. K. Szymczak, M. G. H. Pelletier, K. Malu, A. M. Barbeau, R. M. Giadone, S. C. Babroudi, P. C. W. Gaines, Expression Levels of Lamin A or C Are Critical to Nuclear Maturation, Functional Responses, and Gene Expression Profiles in Differentiating Mouse Neutrophils. *ImmunoHorizons* **6**, 16–35 (2022).

345. P. Gaines, C. W. Tien, A. L. Olins, D. E. Olins, L. D. Shultz, L. Carney, N. Berliner, Mouse neutrophils lacking lamin B-receptor expression exhibit aberrant development and lack critical functional responses. *Experimental Hematology* **36**, 965–976 (2008).

346. A. L. Olins, M. Zwerger, H. Herrmann, H. Zentgraf, A. J. Simon, M. Monestier, D. E. Olins, The human granulocyte nucleus: Unusual nuclear envelope and heterochromatin composition. *European Journal of Cell Biology* **87**, 279–290 (2008).

347. M. G. Manz, S. Boettcher, Emergency granulopoiesis. *Nature Reviews Immunology* **14**, 302–314 (2014).

348. E. van Grinsven, J. Textor, L. S. P. Hustin, K. Wolf, L. Koenderman, N. Vrisekoop, Immature Neutrophils Released in Acute Inflammation Exhibit Efficient Migration despite Incomplete Segmentation of the Nucleus. *The Journal of Immunology* **202**, 207–217 (2019).

349. M. L. Heuzé, O. Collin, E. Terriac, A.-M. Lennon-Duménil, M. Piel, "Cell Migration in Confinement: A Micro-Channel-Based Assay" in *Cell Migration: Developmental Methods and Protocols*, C. M. Wells, M. Parsons, Eds. (Humana Press, Totowa, NJ, 2011; https://doi.org/10.1007/978-1-61779-207-6_28)*Methods in Molecular Biology*, pp. 415–434.

350. T. Tak, P. Wijten, M. Heeres, P. Pickkers, A. Scholten, A. J. R. Heck, N. Vrisekoop, L. P. Leenen, J. A. M. Borghans, K. Tesselaar, L. Koenderman, Human CD62Ldim neutrophils identified as a separate subset by proteome profiling and in vivo pulse-chase labeling. *Blood* **129**, 3476–3485 (2017).

351. J. Pillay, V. M. Kamp, E. van Hoffen, T. Visser, T. Tak, J.-W. Lammers, L. H. Ulfman, L. P. Leenen, P. Pickkers, L. Koenderman, A subset of neutrophils in

human systemic inflammation inhibits T cell responses through Mac-1. *J Clin Invest* **122**, 327–336 (2012).

352. J. Pillay, B. P. Ramakers, V. M. Kamp, A. L. T. Loi, S. W. Lam, F. Hietbrink, L. P. Leenen, A. T. Tool, P. Pickkers, L. Koenderman, Functional heterogeneity and differential priming of circulating neutrophils in human experimental endotoxemia. *Journal of Leukocyte Biology* **88**, 211–220 (2010).

353. N. Srivastava, G. P. de F. Nader, A. Williart, R. Rollin, D. Cuvelier, A. Lomakin, M. Piel, Nuclear fragility, blaming the blebs. *Current Opinion in Cell Biology* **70**, 100–108 (2021).

354. L. G. Ng, R. Ostuni, A. Hidalgo, Heterogeneity of neutrophils. *Nat Rev Immunol* **19**, 255–265 (2019).

355. P. L. B. Bruijnzeel, M. Uddin, L. Koenderman, Targeting neutrophilic inflammation in severe neutrophilic asthma: can we target the disease-relevant neutrophil phenotype? *Journal of Leukocyte Biology* **98**, 549–556 (2015).

356. P. Hellebrekers, N. Vrisekoop, L. Koenderman, Neutrophil phenotypes in health and disease. *European Journal of Clinical Investigation* **48** (2018).

357. X. Xie, Q. Shi, P. Wu, X. Zhang, H. Kambara, J. Su, H. Yu, S.-Y. Park, R. Guo, Q. Ren, S. Zhang, Y. Xu, L. E. Silberstein, T. Cheng, F. Ma, C. Li, H. R. Luo, Single-cell transcriptome profiling reveals neutrophil heterogeneity in homeostasis and infection. *Nat Immunol* **21**, 1119–1133 (2020).

358. M. Fukata, M. Nakagawa, K. Kaibuchi, Roles of Rho-family GTPases in cell polarisation and directional migration. *Current Opinion in Cell Biology* **15**, 590–597 (2003).

359. A. J. Ridley, Rho GTPase signalling in cell migration. *Curr Opin Cell Biol* **36**, 103–112 (2015).

360. K. Wolf, R. Müller, S. Borgmann, Eva.-B. Bröcker, P. Friedl, Amoeboid shape change and contact guidance: T-lymphocyte crawling through fibrillar collagen is independent of matrix remodeling by MMPs and other proteases. *Blood* **102**, 3262–3269 (2003).

361. E. K. Paluch, I. M. Aspalter, M. Sixt, Focal Adhesion-Independent Cell Migration. *Annu Rev Cell Dev Biol* **32**, 469–490 (2016).

362. F. Gaertner, P. Reis-Rodrigues, I. de Vries, M. Hons, J. Aguilera, M. Riedl, A. Leithner, S. Tasciyan, A. Kopf, J. Merrin, V. Zheden, W. A. Kaufmann, R. Hauschild, M. Sixt, WASp triggers mechanosensitive actin patches to facilitate immune cell migration in dense tissues. *Developmental Cell* **57**, 47-62.e9 (2022).

363. H. De Belly, E. K. Paluch, K. J. Chalut, Interplay between mechanics and signalling in regulating cell fate. *Nat Rev Mol Cell Biol* **23**, 465–480 (2022).

364. T. J. Kirby, J. Lammerding, Emerging views of the nucleus as a cellular mechanosensor. *Nature Cell Biology* **20**, 373–381 (2018).

365. H. Bagci, N. Sriskandarajah, A. Robert, J. Boulais, I. E. Elkholi, V. Tran, Z.-Y. Lin, M.-P. Thibault, N. Dubé, D. Faubert, D. R. Hipfner, A.-C. Gingras, J.-F. Côté, Mapping the proximity interaction network of the Rho-family GTPases reveals signalling pathways and regulatory mechanisms. *Nature Cell Biology* **22**, 120–134 (2020).

366. J. D. Rotty, C. Wu, J. E. Bear, New insights into the regulation and cellular functions of the ARP2/3 complex. *Nat Rev Mol Cell Biol* **14**, 7–12 (2013).

367. S. Buracco, S. Claydon, R. Insall, Control of actin dynamics during cell motility. *F1000Res* **8**, F1000 Faculty Rev-1977 (2019).

368. K. Wolf, S. Alexander, V. Schacht, L. M. Coussens, U. H. von Andrian, J. van Rheenen, E. Deryugina, P. Friedl, Collagen-based cell migration models in vitro and in vivo. *Seminars in Cell & Developmental Biology* **20**, 931–941 (2009).

369. P. Vargas, E. Terriac, A.-M. Lennon-Duménil, M. Piel, Study of Cell Migration in Microfabricated Channels. *J Vis Exp*, 51099 (2014).

370. B. Heit, P. Kubes, Measuring Chemotaxis and Chemokinesis: The Under-Agarose Cell Migration Assay. *Science's STKE* **2003**, pl5–pl5 (2003).

371. N. T. Nehme, J. P. Schmid, F. Debeurme, I. André-Schmutz, A. Lim, P. Nitschke, F. Rieux-Laucat, P. Lutz, C. Picard, N. Mahlaoui, A. Fischer, G. de Saint Basile, MST1 mutations in autosomal recessive primary immunodeficiency characterized by defective naive T-cell survival. *Blood* **119**, 3458–3468 (2012).

372. H. Abdollahpour, G. Appaswamy, D. Kotlarz, J. Diestelhorst, R. Beier, A. A. Schäffer, E. M. Gertz, A. Schambach, H. H. Kreipe, D. Pfeifer, K. R. Engelhardt, N. Rezaei, B. Grimbacher, S. Lohrmann, R. Sherkat, C. Klein, The phenotype of human STK4 deficiency. *Blood* **119**, 3450–3457 (2012).

373. S. O. Halacli, D. C. Ayvaz, C. Sun-Tan, B. Erman, E. Uz, D. Y. Yilmaz, K. Ozgul, İ. Tezcan, O. Sanal, STK4 (MST1) deficiency in two siblings with autoimmune cytopenias: A novel mutation. *Clinical Immunology* **161**, 316–323 (2015).

374. T. S. Dang, J. D. Willet, H. R. Griffin, N. V. Morgan, G. O'Boyle, P. D. Arkwright, S. M. Hughes, M. Abinun, L. J. Tee, D. Barge, K. R. Engelhardt, M. Jackson, A. J. Cant, E. R. Maher, M. S. Koref, L. N. Reynard, S. Ali, S. Hambleton, Defective

Leukocyte Adhesion and Chemotaxis Contributes to Combined Immunodeficiency in Humans with Autosomal Recessive MST1 Deficiency. *J Clin Immunol* **36**, 117–122 (2016).

375. A. Crequer, C. Picard, E. Patin, A. D'Amico, A. Abhyankar, M. Munzer, M. Debré, S.-Y. Zhang, G. de Saint-Basile, A. Fischer, L. Abel, G. Orth, J.-L. Casanova, E. Jouanguy, Inherited MST1 Deficiency Underlies Susceptibility to EV-HPV Infections. *PLOS ONE* **7**, e44010 (2012).

376. F. Mou, M. Praskova, F. Xia, D. Van Buren, H. Hock, J. Avruch, D. Zhou, The Mst1 and Mst2 kinases control activation of rho family GTPases and thymic egress of mature thymocytes. *J Exp Med* **209**, 741–759 (2012).

377. K. Katagiri, T. Katakai, Y. Ebisuno, Y. Ueda, T. Okada, T. Kinashi, Mst1 controls lymphocyte trafficking and interstitial motility within lymph nodes. *The EMBO Journal* **28**, 1319–1331 (2009).

378. K. Yamamura, T. Uruno, A. Shiraishi, Y. Tanaka, M. Ushijima, T. Nakahara, M. Watanabe, M. Kido-Nakahara, I. Tsuge, M. Furue, Y. Fukui, The transcription factor EPAS1 links DOCK8 deficiency to atopic skin inflammation via IL-31 induction. *Nature Communications* **8**, 13946 (2017).

379. V. Rausch, C. G. Hansen, The Hippo Pathway, YAP/TAZ, and the Plasma Membrane. *Trends in Cell Biology* **30**, 32–48 (2020).

380. A. Bouchard, M. Witalis, J. Chang, V. Panneton, J. Li, Y. Bouklouch, W.-K. Suh, Hippo Signal Transduction Mechanisms in T Cell Immunity. *Immune Network* **20** (2020).

381. J.-F. Côté, A. B. Motoyama, J. A. Bush, K. Vuori, A novel and evolutionarily conserved PtdIns(3,4,5)P3-binding domain is necessary for DOCK180 signalling. *Nat Cell Biol* **7**, 797–807 (2005).

382. E. Janssen, M. Tohme, M. Hedayat, M. Leick, S. Kumari, N. Ramesh, M. J. Massaad, S. Ullas, V. Azcutia, C. C. Goodnow, K. L. Randall, Q. Qiao, H. Wu, W. Al-Herz, D. Cox, J. Hartwig, D. J. Irvine, F. W. Luscinskas, R. S. Geha, A DOCK8-WIP-WASp complex links T cell receptors to the actin cytoskeleton. *J Clin Invest* **126**, 3837–3851.

383. T. Lämmermann, J. Renkawitz, X. Wu, K. Hirsch, C. Brakebusch, M. Sixt, Cdc42-dependent leading edge coordination is essential for interstitial dendritic cell migration. *Blood* **113**, 5703–5710 (2009).

384. S. Cho, J. Irianto, D. E. Discher, Mechanosensing by the nucleus: From pathways to scaling relationships. *J Cell Biol* **216**, 305–315 (2017).

385. G. Crawford, A. Enders, U. Gileadi, S. Stankovic, Q. Zhang, T. Lambe, T. L. Crockford, H. E. Lockstone, A. Freeman, P. D. Arkwright, J. M. Smart, C. S. Ma, S. G. Tangye, C. C. Goodnow, V. Cerundolo, D. I. Godfrey, H. C. Su, K. L. Randall, R. J. Cornall, DOCK8 is critical for the survival and function of NKT cells. *Blood* **122**, 2052–2061 (2013).

386. A. K. Singh, A. Eken, M. Fry, E. Bettelli, M. Oukka, DOCK8 regulates protective immunity by controlling the function and survival of RORγt+ ILCs. *Nat Commun* **5**, 4603 (2014).

387. R. Aihara, K. Kunimura, M. Watanabe, T. Uruno, N. Yamane, T. Sakurai, D. Sakata, F. Nishimura, Y. Fukui, DOCK8 controls survival of group 3 innate lymphoid cells in the gut through Cdc42 activation. *Int Immunol* **33**, 149–160 (2021).

388. M. Huse, Mechanical forces in the immune system. *Nature Reviews Immunology* **17**, 679–690 (2017).

389. J. Postat, A. Bhagrath, C. Shen, J. Brodbeck, P. Tirgar, A. Cerf, D. Rogers, T. Jeyakumar, A. R. Mingarelli, C. Schneider, S. Coley, N. Gianetti, J. Textor, A. Sharma, A. Ehrlicher, R. Sharif-Naeni, J. N. Mandl, Stiffness sensing by T cells promotes tissue-resident memory T cell differentiation. *Under Review* (2024).

390. J. R. Prigge, J. A. Wiley, E. A. Talago, E. M. Young, L. L. Johns, J. A. Kundert, K. M. Sonsteng, W. P. Halford, M. R. Capecchi, E. E. Schmidt, Nuclear double-fluorescent reporter for in vivo and ex vivo analyses of biological transitions in mouse nuclei. *Mamm Genome*, 10.1007/s00335-013-9469–8 (2013).

391. J. Riedl, K. C. Flynn, A. Raducanu, F. Gärtner, G. Beck, M. Bösl, F. Bradke, S. Massberg, A. Aszodi, M. Sixt, R. Wedlich-Söldner, Lifeact mice for studying F-actin dynamics. *Nat Methods* **7**, 168–169 (2010).

392. J. Choi, S. Oh, D. Lee, H. J. Oh, J. Y. Park, S. B. Lee, D.-S. Lim, Mst1-FoxO Signaling Protects Naïve T Lymphocytes from Cellular Oxidative Stress in Mice. *PLoS One* **4**, e8011 (2009).

393. B. G. Petrich, P. Marchese, Z. M. Ruggeri, S. Spiess, R. A. M. Weichert, F. Ye, R. Tiedt, R. C. Skoda, S. J. Monkley, D. R. Critchley, M. H. Ginsberg, Talin is required for integrin-mediated platelet function in hemostasis and thrombosis. *J Exp Med* **204**, 3103–3111 (2007).

394. Y. Zhou, B. Zhou, L. Pache, M. Chang, A. H. Khodabakhshi, O. Tanaseichuk, C. Benner, S. K. Chanda, Metascape provides a biologist-oriented resource for the analysis of systems-level datasets. *Nat Commun* **10**, 1523 (2019).

395. A. D. Doyle, Fluorescent Labeling of Rat-tail Collagen for 3D Fluorescence Imaging. *Bio Protoc* **8**, e2919 (2018).

396. R. Sender, Y. Weiss, Y. Navon, I. Milo, N. Azulay, L. Keren, S. Fuchs, D. Ben-Zvi, E. Noor, R. Milo, The total mass, number, and distribution of immune cells in the human body. *Proceedings of the National Academy of Sciences* **120**, e2308511120 (2023).

397. A. B. Kay, Paul Ehrlich and the Early History of Granulocytes. *Microbiology Spectrum* **4**, 10.1128/microbiolspec.mchd-0032–2016 (2016).

398. L. Kaltenbach, P. Martzloff, S. K. Bambach, N. Aizarani, M. Mihlan, A. Gavrilov, K. M. Glaser, M. Stecher, R. Thünauer, A. Thiriot, K. Heger, K. Kierdorf, S. Wienert, U. H. von Andrian, M. Schmidt-Supprian, C. Nerlov, F. Klauschen, A. Roers, M. Bajénoff, D. Grün, T. Lämmermann, Slow integrin-dependent migration organizes networks of tissue-resident mast cells. *Nat Immunol* **24**, 915–924 (2023).

399. K. Hoffmann, C. K. Dreger, A. L. Olins, D. E. Olins, L. D. Shultz, B. Lucke, H. Karl, R. Kaps, D. Müller, A. Vayá, J. Aznar, R. E. Ware, N. S. Cruz, T. H. Lindner, H. Herrmann, A. Reis, K. Sperling, Mutations in the gene encoding the lamin B receptor produce an altered nuclear morphology in granulocytes (Pelger–Huët anomaly). *Nat Genet* **31**, 410–414 (2002).

400. I. Patta, M. Zand, L. Lee, S. Mishra, A. Bortnick, H. Lu, A. Prusty, S. McArdle, Z. Mikulski, H.-Y. Wang, C. S. Cheng, K. M. Fisch, M. Hu, C. Murre, Nuclear morphology is shaped by loop-extrusion programs. *Nature* **627**, 196–203 (2024).

401. J.-W. Shin, K. R. Spinler, J. Swift, J. A. Chasis, N. Mohandas, D. E. Discher, Lamins regulate cell trafficking and lineage maturation of adult human hematopoietic cells. *Proceedings of the National Academy of Sciences* **110**, 18892–18897 (2013).

402. A. Saez, B. Herrero-Fernandez, R. Gomez-Bris, B. Somovilla-Crespo, C. Rius, J. M. Gonzalez-Granado, Lamin A/C and the Immune System: One Intermediate Filament, Many Faces. *Int J Mol Sci* **21**, 6109 (2020).

403. A. L. Olins, T. V. Hoang, M. Zwerger, H. Herrmann, H. Zentgraf, A. A. Noegel, I. Karakesisoglou, D. Hodzic, D. E. Olins, The LINC-less granulocyte nucleus. *European Journal of Cell Biology* **88**, 203–214 (2009).

404. B. D. Hale, Y. Severin, F. Graebnitz, D. Stark, D. Guignard, J. Mena, Y. Festl, S. Lee, J. Hanimann, N. S. Zangger, M. Meier, D. Goslings, O. Lamprecht, B. M. Frey, A. Oxenius, B. Snijder, Cellular architecture shapes the naïve T cell response. *Science* **384**, eadh8697 (2024).

405. J. Salafranca, J. K. Ko, A. K. Mukherjee, M. Fritzsche, E. van Grinsven, I. A. Udalova, Neutrophil nucleus: shaping the past and the future. *Journal of Leukocyte Biology* **114**, 585–594 (2023).

406. A. B. Mandola, J. Levy, A. Nahum, N. Hadad, R. Levy, A. Rylova, A. J. Simon, A. Lev, R. Somech, A. Broides, Neutrophil Functions in Immunodeficiency Due to DOCK8 Deficiency. *Immunological Investigations* (2019).

407. T. Wolf, W. Jin, G. Zoppi, I. A. Vogel, M. Akhmedov, C. K. E. Bleck, T. Beltraminelli, J. C. Rieckmann, N. J. Ramirez, M. Benevento, S. Notarbartolo, D. Bumann, F. Meissner, B. Grimbacher, M. Mann, A. Lanzavecchia, F. Sallusto, I. Kwee, R. Geiger, Dynamics in protein translation sustaining T cell preparedness. *Nat Immunol* **21**, 927–937 (2020).

408. A. Zaid, L. K. Mackay, A. Rahimpour, A. Braun, M. Veldhoen, F. R. Carbone, J. H. Manton, W. R. Heath, S. N. Mueller, Persistence of skin-resident memory T cells within an epidermal niche. *Proc Natl Acad Sci U S A* **111**, 5307–5312 (2014).

409. A. Zaid, J. L. Hor, S. N. Christo, J. R. Groom, W. R. Heath, L. K. Mackay, S. N. Mueller, Chemokine Receptor–Dependent Control of Skin Tissue–Resident Memory T Cell Formation. *The Journal of Immunology* **199**, 2451–2459 (2017).

410. W. M. Nauseef, Human neutrophils ≠ murine neutrophils: does it matter? *Immunological reviews* **314**, 442 (2023).

411. H. Colin-York, S. Kumari, L. Barbieri, L. Cords, M. Fritzsche, Distinct actin cytoskeleton behaviour in primary and immortalised T-cells. *Journal of Cell Science* **133**, jcs232322 (2019).

412. P. Reis-Rodrigues, N. Canigova, M. J. Avellaneda, F. Gaertner, K. Vaahtomeri, M. Riedl, J. Merrin, R. Hauschild, Y. Fukui, A. J. Garcia, M. Sixt, Global coordination of protrusive forces in migrating immune cells. bioRxiv [Preprint] (2024). https://doi.org/10.1101/2024.07.26.605242.

413. T. A. Burke, J. R. Christensen, E. Barone, C. Suarez, V. Sirotkin, D. R. Kovar, Homeostatic Actin Cytoskeleton Networks Are Regulated by Assembly Factor Competition for Monomers. *Current Biology* **24**, 579–585 (2014).